

**BORYL PARTICIPATION IN THE BOND ACTIVATION REACTIONS BY PBP TYPE
IRIDIUM AND RHODIUM COMPLEXES AND APPLICATION IN SELECTIVE C-H
ALKYLATION OF PYRIDINES**

A Dissertation

by

YIHAN CAO

Submitted to the Graduate and Professional School of
Texas A&M University
in partial fulfillment of the requirements for the degree of

DOCTOR OF PHILOSOPHY

Chair of Committee,	Oleg V. Ozerov
Committee Members,	Marcetta Y. Darensbourg
	Michael Nippe
	Perla B. Balbuena
Head of Department,	Simon W. North

December 2021

Major Subject: Chemistry

Copyright 2021 Yihan Cao

ABSTRACT

Pincer ligands are commonly utilized in the design of transition metal catalysts. Our group recently reported the synthesis of diarylboryl-based Ir and Rh complexes, which feature an X-type boryl ligand that is Lewis acidic. Herein, we explored the properties and reactivity of Ag, Ir and Rh metal complexes that feature boryl or borane ligand.

In Chapter II, silver halide complexes of a borane/bis(phosphine) ligand were prepared and characterized. With AgF, the borane abstracts fluoride, resulting in a zwitterionic complex. With AgCl, AgBr, and AgI, the halide stays coordinated to Ag, with little to no Ag–B interaction.

In Chapter III, H–X bond addition across the Ir–B unit of the previously reported (PBP)Ir(CO)₂ were examined. Water, methanol, ethanol, cyclohexanol, phenols, benzoic acid, and triethylamine trihydrofluoride added the O–H and F–H units across the Ir–B bond, resulting in dicarbonyl complexes with Ir–H and B–O/F bonds. Thermolysis of (PBP)Ir(CO)₂ with *n*-butylamine resulted in a monocarbonyl product of N–H addition. Two possible mechanisms were proposed, and mechanistic experiments were conducted to study this system.

In Chapter IV, reactions of (PBP)Ir complexes with ethylene were examined. (PBP)IrH₄, (PBP)IrH₂(CO), and (PBP)Ir(CO)₂ activated the C–H bond in ethylene to form unique products that have the elements of ethylene incorporated into the molecules and resulted in B–C bonds. These reactions demonstrate that the boryl donor is not merely an

electronically unique central donor with Lewis acidic properties. It also participates in the activation of C–H bonds by the metal center and forms B–C bond in the product.

In Chapter V, we examined selective C–H activation of pyridines with (PBP)Rh and (PBP)Ir complexes. We observed the isomerism derived from the 2-pyridyl fragment connecting either via B-N/C-M bonds or via B-C/N-M bonds. This M-C/M-N isomerism was systematically examined for four structural Types, totaling 16 compounds. Several of these compounds were isolated or observed in solution by experimental methods, in addition to a few 2-quinolyl variants. The DFT predictions concerning the thermodynamic preference within each M-C/M-N isomeric match the experimental findings very well.

In Chapter VI, we utilized (PBP)Rh complexes synthesized in Chapter V to catalyze norbornylation of substrates containing pyridyl groups. For substrates such as pyridine, quinoline, 4-tert-butylpyridine, 4-dimethylaminopyridine, and 3-ethylpyridine, the norbornylation happened at the pyridine ortho position. However, for 2-tolylpyridine, the norbornylation happened on the tolyl group.

DEDICATION

To my parents.

ACKNOWLEDGEMENTS

I would like to thank my committee chair and research advisor, Dr. Oleg V. Ozerov. I appreciate his time and effort throughout the course of this research. His guidance and support over the past five years motivated me to become a better chemist. I would also like to thank my committee members, Dr. Marcetta Y. Darensbourg, Dr. Michael Nippe, and Dr. Perla B. Balbuena.

Thanks also go to my colleagues and the department faculty and staff for making my time at Texas A&M University a great experience. I would like to thank Dr. Wei-Chun Shih, who mentored me, introduced me to PBP chemistry, and trained me on experiment skills. Dr. Nattamai Bhuvanesh, a professional crystallographer, helped me solve the crystal structures. Dr. Jia Zhou provided DFT calculations for the PBP system. Ozerov group members that I have a good time working with, especially Ming-Uei Hung and S. Olivia Gunther.

Finally, thanks to my parents, who always support me when I am curious about the world. My best friend, Yuezhu Chen, who always be there to encourage me through those difficulties. My roommate Tian Qiao, you can also get through it and have a bright future.

CONTRIBUTORS AND FUNDING SOURCES

Contributors

This work was supervised by a dissertation committee consisting of Professors Oleg V. Ozerov and Marcetta Y. Darensbourg, Michael Nippe of the Department of Chemistry and Professor Perla B. Balbuena of the Department of Chemical Engineering.

In Chapter II, the synthesis and crystal structure of **201** has been developed and solved by our former group member Dr. Wei-Chun Shih. The crystal structure of **204** was solved by crystallographer Dr. Nattamai Bhuvanesh. The work was published in 2019. In Chapter III, the synthesis and crystal structure of **309a** and **316b** has been developed and solved by our former group member Dr. Wei-Chun Shih. The work was published in 2019. In Chapter IV, the synthesis and crystal structure of **401**, **403** has been developed and solved by our former group member Dr. Wei-Chun Shih. The crystal structure of **402** was solved by crystallographer Dr. Nattamai Bhuvanesh. The work was published in 2020. In Chapter V, the crystal structure of **V-1RhN**, **V-1RhNq**, **V-1IrCq**, **V-2RhC**, **V-3RhN** were solved by crystallographer Dr. Nattamai Bhuvanesh. All the DFT calculations were accomplished by Professor Jia Zhou from Harbin Institute of Technology.

All other work conducted for the dissertation was completed by the student independently.

Funding Sources

Graduate study was supported by a fellowship from Texas A&M University. This work was also made possible in part by the support of this research by the US National

Science Foundation (grants CHE-1565923 and CHE-2102324 to O. V. O.), and the Welch Foundation (grant A-1717). The computational work by Dr. Jia Zhou was also supported by Open Project of State Key Laboratory of Urban Water Resource and Environment, Harbin Institute of Technology (No. QA202009). Computer time made available by the National Supercomputing Center of China in Shenzhen (Shenzhen Cloud Computing Center) is gratefully acknowledged.

NOMENCLATURE

COD	1,5-Cyclooctadiene
COE	Cyclooctene
^t Bu	tert-Butyl
ⁱ Pr	isopropyl
Mes	Mesityl
Me	Methyl
Et	Ethyl
Ph	Phenyl
L	Ligand
NCS	N-Chlorosuccinimide
NBS	N-Bromosuccinimide
NMR	Nuclear Magnetic Resonance
OAc	Acetate
OPiv	Pivalate
OTf	Triflate
Py	pyridine
nbd	2,5-norbornadiene
DMAP	4-Dimethylaminopyridine
DME	1,2-Dimethoxyethane
BAr ^F ₄	tetrakis[3,5-bis(trifluoromethyl)phenyl]borate)

TPB	borane/tris(phosphine) ligand
DPB	borane/bis(phosphine) ligand
mt	2-sulfanyl-1-methylimidazole
NLMO	Natural localized molecular orbital
THF	Tetrahydrofuran
NaHMDS	Sodium bis(trimethylsilyl)amide
TBE	<i>Tert</i> -Butylethylene

TABLE OF CONTENTS

	Page
ABSTRACT	ii
DEDICATION	iv
ACKNOWLEDGEMENTS	v
CONTRIBUTORS AND FUNDING SOURCES.....	vi
NOMENCLATURE.....	viii
TABLE OF CONTENTS	x
LIST OF FIGURES.....	xiv
LIST OF SCHEMES.....	xxi
LIST OF TABLES	xxiii
CHAPTER I INTRODUCTION AND LITERATURE REVIEW	1
1.1 General Introduction for Pincer Ligands.....	1
1.2 Versatile Binding Modes of Boron for Borane/tris(phosphine) TPB and Borane/bis(phosphine) DPB Ligands.....	3
1.2.1 General Considerations on Metal Boron Interactions	3
1.2.2 Metallaboratranes with Borane/tris(phosphine) Ligand.....	6
1.2.3 Metallaboratranes with Borane/bis(phosphine) Ligand	9
1.3 Pincer Complexes with Boryl Center Donor.....	14
1.3.1 Diaminoboryl PBP Complexes	15
1.3.2 Diarylboryl PBP Complexes	17
1.4 Rhodium Catalyzed Alkylation of Pyridines with Inactivated Alkenes	20
1.4.1 Pyridyl as An Intact Directing Group.....	21
1.4.2 C–H Alkylation of the Pyridyl Groups.....	22
CHAPTER II SILVER HALIDE COMPLEXES OF A BORANE/BIS(PHOSPHINE) LIGAND.....	25
2.1 Introduction	25
2.2 Result and Discussion	26

2.2.1 Synthesis of Silver Complexes with Borane Ligand.....	26
2.2.2 Spectroscopic Characterization	27
2.2.3 X-ray Diffraction Studies	29
2.3 Conclusion.....	34
2.4 Experimental Section	34
2.4.1 General Considerations	34
2.4.2 Physical Methods	35
2.4.3 Synthesis and Characterization of Silver Complexes.....	35
2.4.4 X-Ray Structural Determination Details.	39
CHAPTER III ADDITION OF O-H, N-H AND F-H BONDS ACROSS A BORYL- IRIDIUM UNIT	42
3.1 Introduction	42
3.2 Result and Discussion	44
3.2.1 O-H and F-H Cleavage Reactions	44
3.2.2 N-H Cleavage Studies.	45
3.2.3 Spectroscopic Characterization	47
3.2.4 X-ray Diffraction Studies	49
3.2.5 Mechanistic Considerations	52
3.3 Conclusion.....	56
3.4 Experimental Section	56
3.4.1 General Considerations	56
3.4.2 Physical Methods	56
3.4.3 Synthesis and Characterization of Iridium Complexes	57
3.4.4 X-Ray Structural Determination Details	89
CHAPTER IV REVERSIBLE ADDITION OF ETHYLENE TO A PINCER-BASED BORYL-IRIDIUM UNIT WITH THE FORMATION OF A BRIDGING ETHYLIDENE.....	92
4.1 Introduction	92
4.2 Result and Discussion	94
4.2.1 Reaction of Ethylene with (PBP)Ir Complexes.....	94
4.2.2 Structural Characterization.....	96
4.2.3 Mechanistic Analysis	100
4.3 Conclusion.....	103
4.4 Experimental Section	103
4.4.1 General Considerations	103
4.4.2 Physical Methods	104
4.4.3 Synthesis and Characterization of Iridium Complexes	104
4.4.4 In Situ NMR Study of Ethylene Addition	110
4.4.5 X-Ray Structural Determination Details.	117

CHAPTER V COOPERATIVE C-H ACTIVATION OF PYRIDINE BY PBP COMPLEXES OF RH AND IR CAN LEAD TO BRIDGING 2-PYRIDYLS WITH DIFFERENT CONNECTIVITY TO THE B-M UNIT	122
5.1 Introduction	122
5.2 Result and Discussion	124
5.2.1 Compounds under Consideration and Nomenclature.....	124
5.2.2 Synthesis of Rh and Ir Complexes	125
5.2.3 Spectroscopic Characterization	129
5.2.4 XRD Structural Characterization	130
5.2.5 DFT Studies.....	132
5.3 Conclusion.....	137
5.4 Experimental Section	138
5.4.1 General Considerations	138
5.4.2 Physical Methods	138
5.4.3 Synthesis and Characterization of Rhodium and Iridium Complexes	139
5.4.4 X-Ray Structural Determination Details.....	150
5.4.5 DFT Calculations.....	156
CHAPTER VI ORTHO-SELECTIVE C-H NORBORNYLATION OF PYRIDINES.....	164
6.1 Introduction	164
6.2 Result and Discussion.....	165
6.3 Conclusion.....	170
6.4 Experimental Section	170
6.4.1 General Considerations	170
6.4.2 Physical Methods	171
6.4.3 In Situ Observation of Ortho-selective Quinoline Ethylation and Nobornylation.....	171
6.4.4 Details for Condition Optimization.....	174
6.4.5 Substrate Scopes.....	174
6.4.6 Unsuccessful Substrates and Side Reactions Analysis.....	185
CHAPTER VII SUMMARY	191
REFERENCES.....	194
APPENDIX A OTHER RELATED (PBP)IR AND (PBP)RH COMPLEXES	211
APPENDIX B THIOPHENE BORYLATION REACTIONS AND SOME RELATED TESTS	214
APPENDIX C SYNTHESIS OF BINOL LIGAND AND ATTEMPTED METALATIONS WITH NIOBIUM AND TANTALUM	217

APPENDIX D LIST OF PUBLICATIONS RESULTING FROM THE WORK
DESCRIBED IN THE DISSERTATION222

LIST OF FIGURES

	Page
Figure I-1. General design of pincer type metal complexes and the first reported (PCP)NiCl.....	1
Figure I-2. L-type ligands, X-type ligands, and Z-type ligands	2
Figure I-3. Pincer complexes with different center atoms and phosphine outer donors	2
Figure I-4. Interaction between boron and metal center	4
Figure I-5. TPB 4, 5 and DPB 6, 7, 8.....	6
Figure I-6. Metallaboratranes synthesized based on 4 and 5	7
Figure I-7. Reported structures given unusual M–B distance and boron pyramidalization.	8
Figure I-8. Metallaboratranes bearing DPB ligand	10
Figure I-9. Pincer metal complexes with a central boryl X-type donor	14
Figure I-10. Diaminoboryl-based Pincer Ligands.....	15
Figure I-11. Diamino-based (PBP)M complexes	16
Figure I-12. Boryl pincer complexes generated by B–Ph insertion	18
Figure II-1. Generic depiction of complexes of borane/tris(phosphine) and borane/bis(phosphine) ligands emphasizing the Z-type interactions of the metal with the central borane unit	26
Figure II-2. $^{31}\text{P}\{^1\text{H}\}$ NMR spectrum of 201 in C_6D_6 at RT measured on a 500 MHz Varian NMR	28
Figure II-3. Top: POV-Ray rendition of the ORTEP drawing (50% thermal ellipsoids) of 201 showing selected atom labelling. Hydrogen atoms and isopropyl groups are omitted for clarity. Selected bond distances (Å) and angles (°) for 201: Ag1-P1, 2.4342(6); Ag1-P3, 2.4425(8); Ag2-P2, 2.4323(8); Ag2-P4, 2.4255(7); Ag681, 2.928(1); Ag682, 2.667(1); Ag2-F1, 2.735(1); Ag2-F2, 2.960(1); Ag1-C48, 2.901(2); Ag1-C43, 2.850(2); Ag2-C18, 2.720(2); Ag2-C13, 2.820(2); F1-B1, 1.464(2); F2-B2, 1.463(2); P1-Ag1-P3, 153.03(2); P2-Ag2-P4, 151.12(2). Bottom: POV-Ray rendition of the ORTEP drawing	

(50% thermal ellipsoids) of truncated 201 showing selected atom labelling and selected interatomic distances rounded to 0.01 Å.....	31
Figure II-4. POV-Ray rendition of the ORTEP drawing (50% thermal ellipsoids) of 204, (DPB)AuCl and (DPB)CuCl. Top: Front view showing selected atom labelling and M-B Distance. Hydrogen atoms and isopropyl groups are omitted for clarity. Middle: Truncated molecules with metal center and atoms around metal. Bottom: Truncated molecules with boron center and atoms around boron.....	33
Figure II-5. ¹ H NMR stacked spectrum (500 MHz, C ₆ D ₆) of 204/203/202 in C ₆ D ₆ . Red, 204; Green, 203; Blue, 202.....	38
Figure III-1. POV-Ray rendition of the ORTEP drawing (50% thermal ellipsoids) of 309a and 316b showing selected atom labeling. Hydrogen atoms are omitted except Ir-H for clarity. Selected bond distances (Å) and angles (°) for 309a: Ir-C1, 1.978(8); Ir-C2, 1.883(7); Ir-B1, 2.479(8); Ir-P1, 2.330(2); Ir-P2, 2.307(2); Ir-H1, 1.4350(8); B1-O3, 1.466(8); C1-O1, 1.15(1); P1-Ir-P2, 150.04(6); C3-B1-Ir, 108.0(4); C3-B1-C4, 114.9(5); C4-B1-Ir, 104.2(4). Selected bond distances (Å) and angles (°) for 316b: Ir-C1, 1.906(4); Ir-P1, 2.2907(8); Ir-P2, 2.2714(8); Ir-H1, 1.31(3); Ir-B1, 2.272(4); Ir-N1, 2.176(2); C1-O1, 1.146(5); B1-N1, 1.516(4); P1-Ir-P2, 138.47(3); Ir-B1-C3, 115.8(13); Ir-B1-C4, 113.4(2); C3-B1-C4, 122.0(3).....	49
Figure III-2. Comparison of B–O bond distances	50
Figure III-3. Comparison of B–N bond distances	51
Figure III-4. Plausible representations of the structure of 316b.....	52
Figure III-5. ³¹ P{ ¹ H} NMR spectra recorded for 74 (0.040 M), cyclohexanol (0.20 M), and 1,4 dioxane (0.040 M) mixture after a certain period of time at room temperature	60
Figure III-6. In <i>situ</i> ³¹ P{ ¹ H} NMR spectra of 74 and <i>tert</i> -butyl alcohol mixture	61
Figure III-7. ³¹ P{ ¹ H} NMR spectra of 314a and 314b mixture after certain periods of time	64
Figure III-8. Bottom: ³¹ P{ ¹ H} NMR spectrum of pure 74 (0.044M, 202 M Hz, C ₆ D ₆). Middle: ³¹ P{ ¹ H} NMR (202 M Hz, C ₆ D ₆) spectrum of Sample III-2 recorded 5 min after addition of <i>n</i> BuNH ₂ to 74. Sample contains a mixture of 74/316c. Top: ³¹ P{ ¹ H} NMR (202 M Hz, C ₆ D ₆) spectrum of Sample III-2 recorded after 16 h heating at 50 °C and dynamic vacuum to remove volatiles. Sample contains 95% 316b.....	69

Figure III-9. $^{31}\text{P}\{^1\text{H}\}$ NMR spectra of 74 and diethylamine mixture after certain periods of time	71
Figure III-10. $^{31}\text{P}\{^1\text{H}\}$ NMR spectrum of 74 and tert-butylamine mixture after certain periods of time	72
Figure III-11. $^{31}\text{P}\{^1\text{H}\}$ NMR spectrum of 74 and aniline mixture after certain periods of time	73
Figure III-12. $^{31}\text{P}\{^1\text{H}\}$ NMR spectrum of 74 and p-anisidine mixture after certain periods of time	74
Figure III-13. $^{31}\text{P}\{^1\text{H}\}$ NMR spectrum of 74 and pyrrole mixture after certain periods of time	75
Figure III-14. $^{11}\text{B}\{^1\text{H}\}$ NMR spectrum of 317a in THF measured on a 500 MHz Varian NMR	77
Figure III-15. Bottom: $^{31}\text{P}\{^1\text{H}\}$ NMR spectrum of 317a in THF; Middle: $^{31}\text{P}\{^1\text{H}\}$ NMR spectrum of 317a mixed with NEt_3 after 12 h of stirring. The sample contains 2% of 74 and 98% of 317a; Top: $^{31}\text{P}\{^1\text{H}\}$ NMR spectrum of 317a mixed with $^i\text{Pr}_2\text{NEt}_3$ after 12 h of stirring. The sample contains 5% of 74 and 95% of 317a	78
Figure III-16. Bottom: ^1H NMR spectrum of 317a in $\text{CD}_3\text{OD}/\text{C}_6\text{D}_6$ (5 : 1) after stirring at r. t. for 1 h; Top: ^1H NMR spectrum of 317a in $\text{CD}_3\text{OD}/\text{C}_6\text{D}_6$ (5 : 1) after stirring at r. t. for 12 h.....	79
Figure III-17. A. Top: ^1H NMR spectrum of 308a- d_4 in $\text{C}_6\text{D}_5\text{Br}$. Bottom: ^1H NMR spectrum collected 5 min after the addition of 317a. Signals are broad due to a rapid exchange between 317a and 308a- d_4 . B. Top: ^1H NMR spectrum from -9.6 ppm to -12.6 ppm of 308a- d_4 in $\text{C}_6\text{D}_5\text{Br}$. Hydride signal (-11.65 ppm, 16%) belongs to the CD_3OH addition product. Bottom: ^1H NMR spectrum from -9.6 ppm to -12.6 ppm collected 5 min after the addition of 317a. C. Top: $^{31}\text{P}\{^1\text{H}\}$ NMR spectrum of 308a- d_4 in $\text{C}_6\text{D}_5\text{Br}$. Bottom: $^{31}\text{P}\{^1\text{H}\}$ NMR spectrum collected 5 min after the addition of 317a. D. Top: $^{11}\text{B}\{^1\text{H}\}$ NMR spectrum of 308a- d_4 in $\text{C}_6\text{D}_5\text{Br}$. Bottom: $^{11}\text{B}\{^1\text{H}\}$ NMR spectrum collected 5 min after the addition of 317a. 317a and 308a- d_4 signals were observed distinctly when the acquisition time was set to be 20 ms	81
Figure III-18. Consumption of 74 over time for EtOH-CyOH addition rate comparison	83
Figure III-19. Consumption of 74 over time for phenol derivatives addition rate comparison.....	85

Figure III-20. $^{31}\text{P}\{^1\text{H}\}$ NMR spectra of 74 (0.020 mmol), cyclohexanol (0.020 mmol) mixture (Top: without 317a. Bottom: with 317a (0.0015 mmol)) recorded after 15 h of stirring at room temperature.....	86
Figure III-21. $^{31}\text{P}\{^1\text{H}\}$ NMR spectrum of 74 (0.020 mmol), <i>tert</i> -butyl alcohol (0.20 mmol) and 317a (0.0015 mmol) mixture recorded after a week of stirring at room temperature. The peak at 44.1 ppm was generated (11%)	87
Figure III-22. ^1H NMR spectrum (from -10 ppm to -14 ppm) of 74 (0.020 mmol), <i>tert</i> -butyl alcohol (0.20 mmol) and 317a (0.0015 mmol) mixture recorded after a week of stirring at room temperature. The peak at 12.36 ppm (t, $J_{\text{H-P}} = 16.1$ Hz) was generated (11%).....	88
Figure III-23. Bottom: $^{31}\text{P}\{^1\text{H}\}$ NMR spectrum of 74 (0.020 mmol), <i>tert</i> -butyl alcohol (0.20 mmol) and 317a (0.0015 mmol) mixture recorded after a week of stirring at room temperature. Middle: $^{31}\text{P}\{^1\text{H}\}$ NMR spectrum of the same mixture recorded after further heating at 50 °C for 48 h. Top: $^{31}\text{P}\{^1\text{H}\}$ NMR spectrum recorded after the middle mixture was added 400 μL <i>tert</i> -butyl alcohol and further heating at 50 °C for 24 h	89
Figure IV-1. ORTEP drawings showing selected atom labeling of 401, 402 and 403. Hydrogen atoms (except Ir-H) are omitted for clarity. 401. Ir1–B1, 2.396(3) Å; Ir1–C1, 2.200(3) Å; Ir1–C2, 2.223(3) Å; Ir1–C3, 2.213(3) Å; Ir1–C4, 2.248(3) Å; C1–C2, 1.402(4) Å; C3–C4, 1.405(4) Å; C3–B1, 1.556(4) Å; C5–B1–C6, 120.4(2)°; C6–B1–C3, 117.5(2)°; C3–B1–C5, 115.6(2)°. 402. The structure contains two independent molecules and each is disordered, including the Ir position. One of the independent molecules is drawn. See section 4.4.5 for additional information. 403. Ir1–B1, 2.475(4) Å; Ir1–C3, 2.262(4) Å; C3–C4, 1.523(6) Å; C3–B1, 1.530(6) Å; C1–O1, 1.160(5) Å; C2–O2, 1.136(6) Å; C1–Ir1–C3, 175.7(2)°; P1–Ir1–P2 140.36(4)°; C5–B1–C6, 122.0(3)°; C6–B1–C3, 118.2(3)°; C3–B1–C5, 114.6(3)°.....	97
Figure IV-2. ChemDraw interpretations and POV-Ray rendition of the ORTEP drawing (50% thermal ellipsoids, truncated molecules with boron center and atoms around boron) of 401 and 403	99
Figure IV-3. $^{31}\text{P}\{^1\text{H}\}$ NMR spectra at room temperature of in situ internal hexene addition experiment after heating at 100 °C for certain time in C_6D_6	110
Figure IV-4. A. $^{31}\text{P}\{^1\text{H}\}$ NMR spectra of the reaction of 1-hexene with 74 under argon atmosphere. B. $^{31}\text{P}\{^1\text{H}\}$ NMR spectra of in situ addition of 1-hexene to 74 experiment under CO atmosphere.	111
Figure IV-5. Consumption of 74 over time for 74 (0.050 M) and 1-hexene (0.50 M) addition reaction showing disappearance of 74 on a log scale.....	112

Figure IV-6. Consumption of 74 over time for 74 (0.050 M) and 1-hexene (1.0 M) addition reaction showing disappearance of 74 on a log scale.....	113
Figure IV-7. Consumption of 74 over time for 74 (0.050 M) and 1-hexene (2.0 M) addition reaction showing disappearance of 74 on a log scale.....	113
Figure IV-8. Experimental rate constant is positively related to 1-hexene concentration	114
Figure IV-9. ¹ H NMR spectra recorded for the thermolysis of 402.....	115
Figure IV-10. ¹ H NMR spectra recorded for the thermolysis of 403.....	116
Figure IV-11. A. ³¹ P{ ¹ H} NMR spectra recorded for thermolysis of 403 to generate 74 at 100 °C without CO in tube IV-6. B. ³¹ P{ ¹ H} NMR spectra recorded for thermolysis of 403 to generate 74 at 100 °C with 1 atm CO in tube IV-7.....	117
Figure IV-12. ORTEP drawings showing selected atom labeling of 402.....	118
Figure V-1. The four structural types under study in this work.....	125
Figure V-2. ³¹ P{ ¹ H} NMR spectrum record on a 500 MHz Varian NMR after 1 equiv. of NaEt ₃ BH were added to 69 in toluene, showing four or more complexes formed.....	127
Figure V-3. Top: ³¹ P{ ¹ H} NMR recorded at room temperature on a 500 MHz Varian NMR for a mixture of 70 (0.10 mmol), pyridine (0.10 mmol) and sodium bis(trimethylsilyl)amide (0.10 mmol) in 2 mL toluene after being heated at 45 °C for 12 h. Bottom: ³¹ P{ ¹ H} NMR recorded at room temperature on a 500 MHz Varian NMR for the same mixture after adding additional pyridine (0.20 mmol) and being heated at 45 °C for another 12 h	128
Figure V-4. POV-Ray rendition of the ORTEP drawing (50% thermal ellipsoids) of V-1RhN, V-1RhNq, V-1IrCq, V-2RhC, and V-3RhN showing selected atom labelling. Hydrogen atoms, disorders of ⁱ Pr groups in V-1IrCq and V-2RhC crystals, and solvent molecules (toluene) in V-1RhNq and V-1IrCq crystals are omitted for clarity. Only one of the V-1IrCq in the asymmetric unit is shown in the ORTEP drawing above.....	131
Figure V-5. DFT-calculated Wiberg bond indices shown in blue for the bonds within the four-membered metallacycle. ΔG ₂₉₈ values (in kcal/mol) are given for the isomerization from left to right within each box (negative ΔG value favors the isomer with the M-N bond).	133

Figure V-6. Correlation between the free energy of isomerization and the M–C WBI values for compounds under study	135
Figure V-7. Correlation between $\Delta G_{\text{isomerization}}$ and M–N WBI bond order	136
Figure V-8. VT-NMR experiment of V-1IrCq/V-1IrNq on a 500 MHz Varian NMR..	144
Figure V-9. $^3\text{P}\{^1\text{H}\}$ NMR (202 MHz, C_6D_6) spectrum recorded at room temperature after the reaction mixture were heated at 65 °C for 24 h. The sample contains a mixture of an unidentified complex, V-3RhC, V-3RhN, and V-1RhN at a ratio of 1:3:17:1	148
Figure VI-1. C–H activation of pyridine by (PBP)Ir, (PBP)Rh, and (PAIP)Rh.	165
Figure VI-2. Bottom. ^1H NMR spectrum for reaction mixture of quinoline, V-1RhNq ethylene, 1,4-dioxane and before heating. Top. ^1H NMR spectrum for the same mixture after heating at 100 °C for 84 h.....	172
Figure VI-3. Bottom. ^1H NMR spectrum for reaction mixture of quinoline, norbornene, 1,4-dioxane and V-1RhNq before heating. Middle. ^1H NMR spectrum for reaction mixture of quinoline, norbornene, 1,4-dioxane and V-1RhNq after heating at 100 °C for 48 h. Top. ^1H NMR spectrum for the same mixture after heating at 100 °C for 96 h.....	173
Figure VI-4. Bottom. ^1H NMR spectrum for reaction mixture of pyridine, ethylene, 1,4-dioxane and V-1RhN before heating. Top. ^1H NMR spectrum for the same mixture after heating at 125 °C for 48 h.	175
Figure VI-5. Bottom. ^1H NMR spectrum for reaction mixture of pyridine, styrene, 1,4-dioxane and (PBP)RhPyH before heating. Top. ^1H NMR spectrum for the same mixture after heating at 100 °C for 20 h.....	176
Figure VI-6. Bottom. ^1H NMR spectrum for reaction mixture of quinoline, 2,3,4,5,6-pentafluorostyrene, 1,4-dioxane and V-1RhNq before heating. Top. ^1H NMR spectrum for the same mixture after heating at 100 °C for 20 h.....	177
Figure VI-7. Bottom. ^1H NMR spectrum for reaction mixture of quinoline, 5-bicyclo[2.2.1]hept-2-enyl(triethoxy)silane, 1,4-dioxane and V-1RhNq before heating. Top. ^1H NMR spectrum for the same mixture after heating at 100 °C for 132 h.....	178
Figure VI-8. Bottom. ^1H NMR spectrum for the reaction mixture after heating the reaction at 125 °C for 24 h. Top. ^1H NMR spectrum for the reaction mixture after heating the reaction at 150 °C for 24 h.....	179

Figure VI-9. ¹ H NMR spectrum for the reaction mixture after heating the reaction at 125 °C for 24 h	180
Figure VI-10. Bottom. ¹ H NMR spectrum for the reaction mixture after heating the at 125 °C for 24 h. Top. ¹ H NMR spectrum for pure o-(trimethylsilyl)cinchonine.....	181
Figure VI-11. ¹ H NMR spectrum for the reaction mixture after heating at 125 °C for 24 h	182
Figure VI-12. ¹ H NMR spectrum for the reaction mixture after heating the at 125 °C for 24 h.....	183
Figure VI-13. ¹ H NMR spectrum for the reaction mixture after heating at 125 °C for a week.....	184
Figure VI-14. ¹ H NMR spectrum for the reaction mixture after heating at 125 °C for a week.....	185
Figure VI-15. Bottom. ¹ H NMR spectrum for quinoline, 1-hexene, 1,4-dioxane and V-1RhNq in C ₆ D ₆ . Top. ¹ H NMR spectrum for the reaction mixture after heating at 100 °C for 40 h.....	186
Figure VI-16. Bottom. ¹ H NMR spectrum for quinoline, 2,5-dihydrofuran, 1,4-dioxane and V-1RhNq in C ₆ D ₆ . Top. ¹ H NMR spectrum for the reaction mixture after heating at 100 °C for 20 h.....	187
Figure VI-17. Bottom. ¹ H NMR spectrum for 2,2'-bipyridine, norbornene, 1,4-dioxane and [(PBP)RhH ₂] in C ₆ D ₆ . Top. ¹ H NMR spectrum for the reaction mixture after heating at 100 °C for a week	188
Figure VI-18. Bottom. ¹ H NMR spectrum for 2-tolylpyridine, norbornene, 1,4-dioxane and [(PBP)RhH ₂] in C ₆ D ₆ . Top. ¹ H NMR spectrum for the reaction mixture after heating at 100 °C for 16 h	189
Figure VII-1. Interactions between NaHMDS and (PBP)IrHCl/Br	216

LIST OF SCHEMES

	Page
Scheme I-1. The interconversion between anionic borate complex, Z-type borane complex and X-type boryl ligand	5
Scheme I-2. Synthesis of the first example of metallaboratrane complexes.....	5
Scheme I-3. The generation of borate ligand from (TPB)Fe.	8
Scheme I-4. H ₂ and H–E (E = C, Si, N) bond activation by (DPB)M (M = Ni, Co, Fe) .	11
Scheme I-5. Activation of allyl acetates by (PBP)Pd.....	12
Scheme I-6. Activation of B–Ph bond by (DPB)Pd.....	12
Scheme I-7. Reversible phenyl migration between Rh and boron of (DPB)Rh complexes	13
Scheme I-8. Ir insertion into B–Ph bond of 6 to generate 45.....	14
Scheme I-9. Reactivity of diamino-based (PBP)M with boryl participation	16
Scheme I-10. Reactivity of diamino-based (PBP)M with no boryl participation	17
Scheme I-11. Diarylboryl (PBP)Ir and (PBP)Rh complexes and their reactivity	19
Scheme I-12. Diarylboryl (PBP)Pd complexes and their reactivity.....	20
Scheme I-13. Hydroarylation of inactivated olefins with 2-phenylpyridines	22
Scheme I-14. Rh(I) catalyzed pyridine ortho alkylation	24
Scheme II-1. Syntheses of AgX adducts of 6.....	27
Scheme III-1. Selected H–X splitting examples relevant to hydrogenation catalysis	42
Scheme III-2. C–H activation utilizing Lewis-basic PNP unit in Pd complex 305	43
Scheme III-3. C–H activation utilizing Lewis-acidic (PBP or PAIP) non-innocent pincer ligand and H–X cleavage utilizing Lewis-acidic PBP	44
Scheme III-4. Addition of O–H, and F–H bonds across iridium–boryl unit of 74	45
Scheme III-5. Addition of O–H, N–H, F–H bonds across iridium–boryl unit of 74	47

Scheme III-6. Proposed mechanisms for the X-H splitting	53
Scheme III-7. Reactivity of the Yamashita/Nozaki diaminoboryl (PBP)Rh fragment with certain alcohols and phenols.....	55
Scheme IV-1. Typical outcomes of a reaction between an olefin (ethylene for simplicity) and a transition metal complex.....	93
Scheme IV-2. The new reactivity reported in this work	94
Scheme IV-3. Reactions of 72, 73, and 74 with Ethylene	95
Scheme IV-4. Proposed mechanism.....	101
Scheme IV-5. Reaction of 74 with 1-hexene	102
Scheme V-1. Traditional directed C-H activation of 2-phenylpyridine (top) and boryl- or aluminyl-directed C-H activation of the 2-position of a pyridine ring.....	123
Scheme V-2. Synthesis of (PBP)Rh/Ir pyridyl complexes	126
Scheme VI-1. Transition metal catalyzed hydroarylation of olefins by substrates with pyridyl groups.....	164
Scheme VI-2. Ortho norbornylation of quinoline to generate different isomers	168
Scheme VI-3. Ortho alkylation of pyridine.....	168
Scheme VI-4. Norbornylation of substrates containing pyridyl group	169
Scheme VI-5. Ortho ethylation of 610 by (PBP)Rh to generate 611 and 612	170

LIST OF TABLES

	Page
Table II-1. $^{11}\text{B}\{^1\text{H}\}$ NMR, $^{31}\text{P}\{^1\text{H}\}$ NMR chemical shifts and J Values (in Hz) of Ag Complexes	29
Table III-1. Spectral data for all the products	48
Table III-2. Spectral details for Sample III-1 and Sample III-2 recorded 5 min after addition of $^n\text{BuNH}_2$ to 74.....	70
Table III-3. Solution in J. Young tube III-1 and III-2 with a total volume of 0.50 mL ...	82
Table III-4. Data table for 74 consumption in tube III-1 and tube III-2 over time for EtOH-CyOH comparison.....	82
Table III-5. Solution in J. Young tube III-3 - III-5 with a total volume of 0.50 mL.....	84
Table III-6. Data table for 74 consumption over time for phenol derivatives addition rate comparison.....	84
Table III-7. Solution in J. Young tube III-6 – III-7 with a total volume of 0.44 mL.....	85
Table IV-1. Selected spectral data of 403 and 403'	109
Table IV-2. Constituents in tubes IV-3, IV-4 and IV-5	112
Table IV-3. Results of Tube IV-3, IV-4 and IV-5.....	114
Table V-1. Selected NMR chemical shift data (in ppm, C_6D_6 , solvent) for the experimentally observed complexes of types V-1 to V-3	130
Table V-2. Absolute free energies and enthalpies in the gas phase at 298K and free energies and enthalpies for the M–C/M–N isomerizations (negative values favor the M-N isomer) calculated at the B97D3/LANL2DZ/6-31G(d) level in gas phase	157
Table V-3. Wiberg bond indices calculated at the B97D3/LANL2DZ/6-31G(d) level of theory for Type V-1 to Type V-4 Rh and Ir complexes	158
Table V-4. ETS-NOCV analysis of the interaction between 2-pyridyl anion and the formally positive charged rest of the molecule. The two largest decomposed NOCV contributions ($\Delta\rho_1$ and $\Delta\rho_2$) constructed with the density isosurface contour value of 0.002 are shown. Blue and red surfaces identify regions of	

electron density accumulation and depletion, respectively. It is clear the electrons “flow” from CN anion to metal cation 159

Table VI-1. Ortho selective norbornylation of quinoline catalyzed by different metals with additives..... 166

Table VI-2. Ortho selective norbornylation of quinoline..... 167

Table VII-1. ortho borylation of thiophene and 2-bromo thiophene catalyzed by Ir metal catalysts..... 215

Table VII-2. Summary of metalation attempts: NbCl₅ + BINOL-OTMS-PⁱPr₂. 221

CHAPTER I

INTRODUCTION AND LITERATURE REVIEW

1.1 General Introduction for Pincer Ligands

Transition metal catalysts have broad applications in organic synthesis. Their reactivity could be affected by the supporting ligands, thus synthesizing different types of ligands to adjust the property of metal centers for catalyzing different reactions attracts a lot of attention.¹⁻⁴ The pincer-type ligands, defined as tridentate chelating agents binding to metal center in a meridional configuration, are widely utilized as supporting ligands.⁵⁻⁶ They are usually abbreviated using the donor atoms binding to the metal. In 1976, Shaw reported the first design of a PCP-type pincer ligand with two bulky phosphine side arms and an aryl center donor (Figure I-1, **1A**).⁷ In his case, two tertiary di-*t*-butylphosphines of the diposphine ligand bind to Ni metal center, and the resulting product was stable under 240 °C. In general, pincer-type metal complexes have great thermal-stability and show applications in bond activation, organic transformations, and catalysis.^{5-6, 8-14}

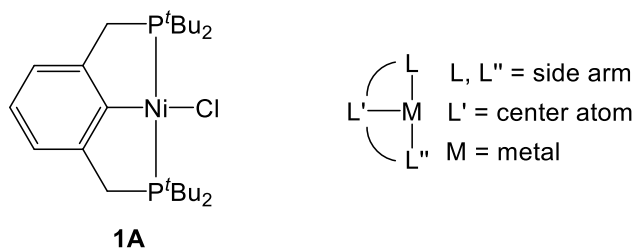


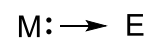
Figure I-1. General design of pincer type metal complexes and the first reported (PCP)NiCl

L-type ligands

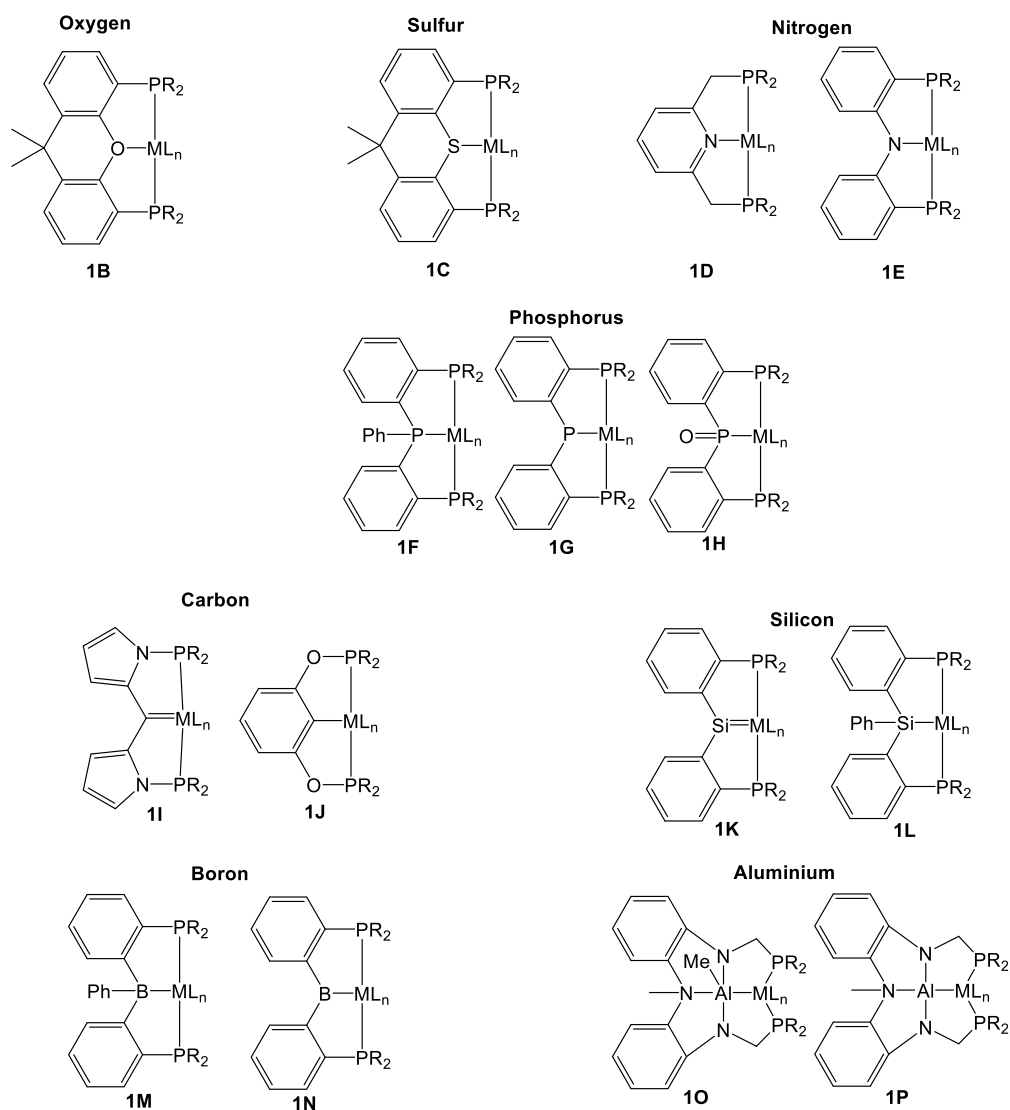
2e donor

X-type ligands

1e donor

Z-type ligands

2e acceptor

Figure I-2. L-type ligands, X-type ligands, and Z-type ligands**Figure I-3. Pincer complexes with different center atoms and phosphine outer donors**

Pincer ligands with different center atoms and sidearms were synthesized.⁶ The three ligands coordinated to metal center can be L-type, X-type or Z-type (Figure I-2). Among them, complexes with phosphine outer donors (L-type) and different center atoms (L-type, X-type or Z-type) have been broadly studied. Some representative examples are showed in Figure I-3. For group 16 elements, oxygen and sulfur center atoms could bind to the metal as L-type ligands (**1B**¹⁵, **1C**¹⁶). For group 15 elements, nitrogen and phosphorus center atoms could bind to the metal as L-type ligands or X-type ligands (**1D** – **1H**^{17, 18, 19, 20, 21}). For group 14 elements, carbon and silicon center atoms could also bind to the metal as L-type ligands or X-type ligands (**1I** – **1L**^{22, 23, 24, 25}). For group 13 elements, boron and aluminum center atoms could bind to the metal center as Z-type ligands or X-type ligands (**1M** – **1P**^{26, 27, 28, 29}). Besides the scaffolds mentioned above, the center atom also includes Zn³⁰, Ga³¹, In³², Ge³³, Sb³⁴, *etc.*

1.2 Versatile Binding Modes of Boron for Borane/tris(phosphine) TPB and Borane/bis(phosphine) DPB Ligands.

1.2.1 General Considerations on Metal Boron Interactions

As a group 13 element, boron could bind to the metal center as an anionic borate ligand through zwitterionic interaction, a 2e acceptor Z-type borane ligand, a 1e donor X-type boryl ligand, a 2e donor borylene ligand or a 3e donor boride ligand (Figure I-4).³⁵⁻³⁶ The first two binding modes have pyramidalized boron centers, while the others feature a boron center with p empty orbital, which could react with Lewis basic substrates. The M–B distances varied significantly for complexes with different metals and boron with different substituents, but the general trend can be concluded that M–B distance of borate

> borane > boryl > borylene and boride. The coordination of Lewis base to the boron elongated the M–B distances in the metal boryl complexes and metal borylene complexes.³⁶⁻³⁷

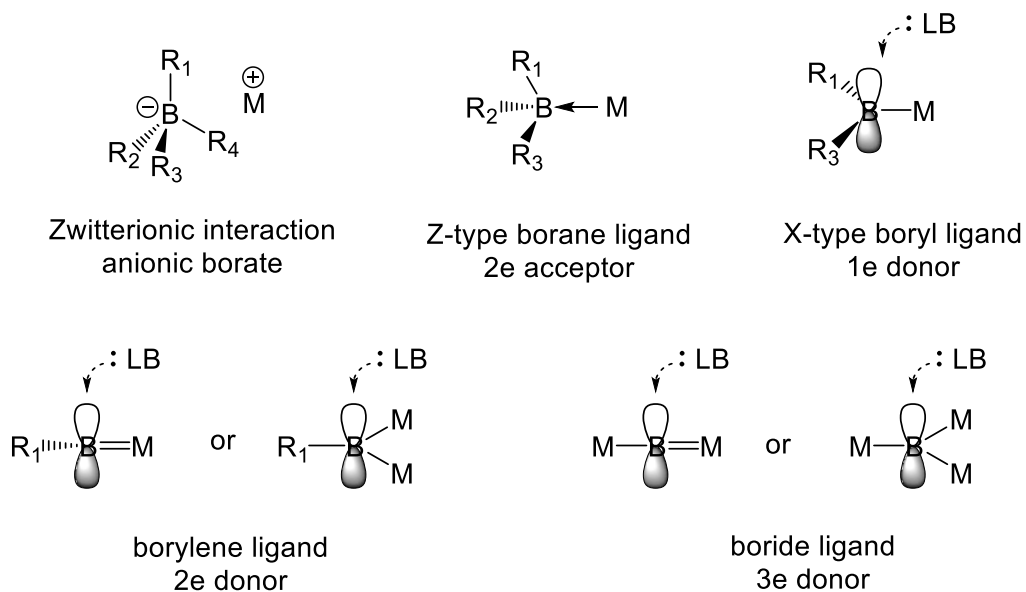
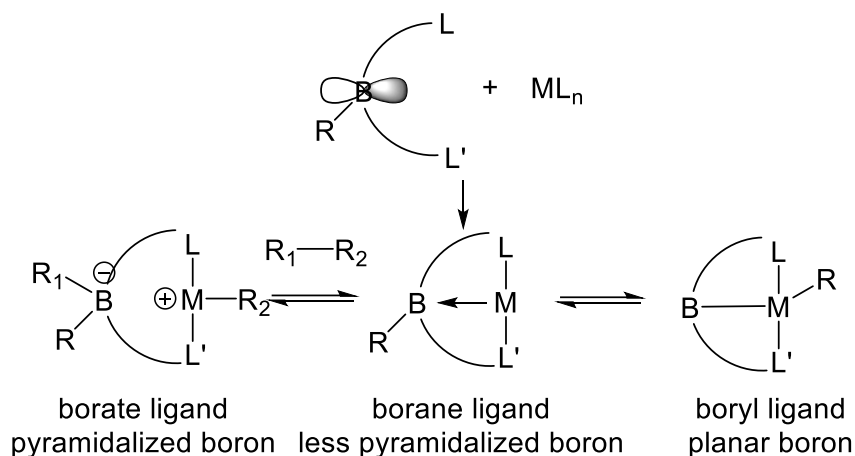


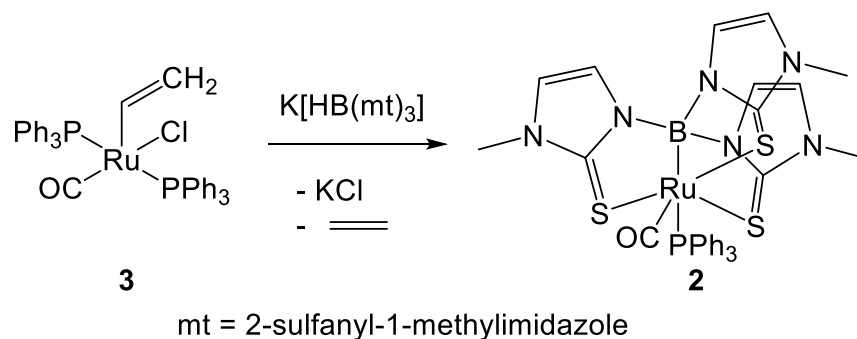
Figure I-4. Interaction between boron and metal center

The reversible interconversion between anionic borate complex, Z-type borane complex and X-type boryl ligand was observed in metal complexes featuring polydentate borane ligand (Scheme I-1). Thus, the study of polydentate borane ligand and their binding modes with the metal center is intriguing.



Scheme I-1. The interconversion between anionic borate complex, Z-type borane complex and X-type boryl ligand

In 1999, Hill reported the first solid-state of a borane complex (**2**).³⁸ At room temperature, the treatment of ruthenium precursor **3** with Na[HB(mt)₃] (mt = 2-sulfanyl-1-methylimidazole) in CH₂Cl₂ resulted in an intramolecular activation of the bridging B–H bond to form **2**, which has a Ru–B distance of 2.161(5) Å and a tetrahedral B that has a chemical shift at 17.1 ppm (Scheme I-1). Since then, different polydentate ligands containing borane centers were synthesized to study the Z-type B–M bonds and their reactivity.³⁶



Scheme I-2. Synthesis of the first example of metallaboratrane complexes

Among them, borane/tris(phosphine) TPB **4**, **5**, and borane/bis(phosphine) DPB **6**, **7**, **8** were widely used to form Z-type B–M bonds for the analysis of B–M bonds with/without an extra phosphine sidearm (Figure I-5). The metallaboratranes synthesized based on TBP and DBP were summarized in section 1.2.2 and section 1.2.3. Tetradentate TPB ligand is quite rigid and the resulting metallaboratranes featuring borane ligand with no metal insertion reported (details in section 1.2.2). However, DPB ligands with a labile B–Ph group introduce more binding modes with the metal center and the interconversion between borate/borane/boryl ligand were also reported for (DPB)M (details in section 1.2.3).

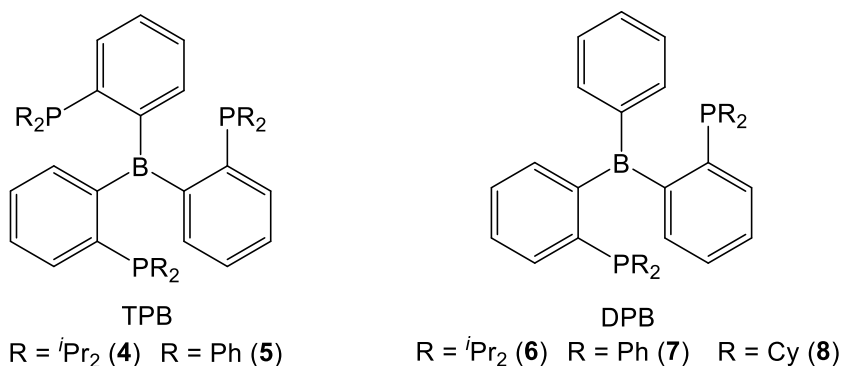


Figure I-5. TPB 4, 5 and DPB 6, 7, 8

1.2.2 Metallaboratranes with Borane/tris(phosphine) Ligand

Since 2007, after Bourissou reported the synthesis of **4**³⁹, different metallaboratranes were synthesized based on this ligand. Group 11⁴⁰⁻⁴², group 10⁴¹, and group 9⁴³⁻⁴⁶ metallaboratranes all feature Z-type M–B bonds (Figure I-6). The M–B coordination for group 8 metallaboratranes include regular Z-type bonds and $\eta^4\text{-B,Ph,P}$ coordination (Figure I-5: **9**, **10**).⁴⁷⁻⁵⁷

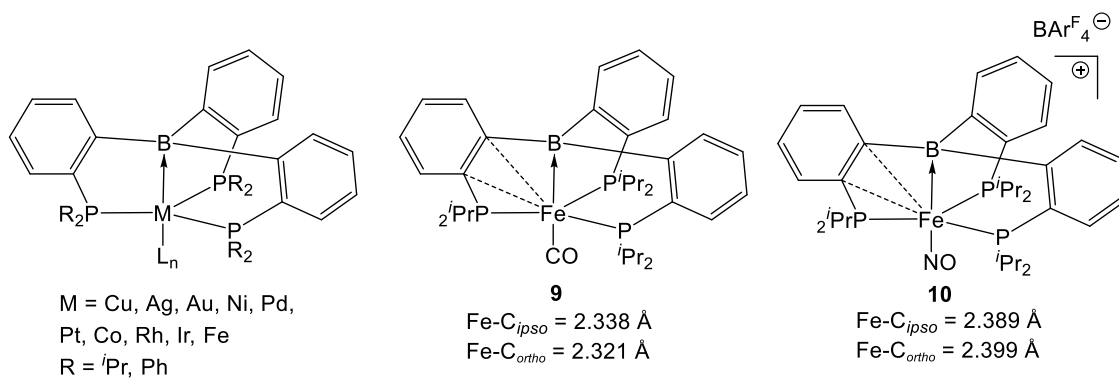


Figure I-6. Metallaboratranes synthesized based on 4 and 5

Z-type M–B coordination strength could be characterized by a combined analysis of boron pyramidalizations, M–B bond distances, and boron chemical shifts. In most cases, a shorter bond distance comes together with more pyramidalized boron and an upfield boron chemical shift, indicating a stronger Z-type M–B bond. It can be rationalized that as the metal boron interaction getting stronger, the boron changes from an sp^2 hybridized boron to an sp^3 hybridized boron. However, four reported cases (**11**, **12**, **13**, **14**) do not follow this trend due to the distortion of the metal center (Figure I-7).^{44-45, 49}

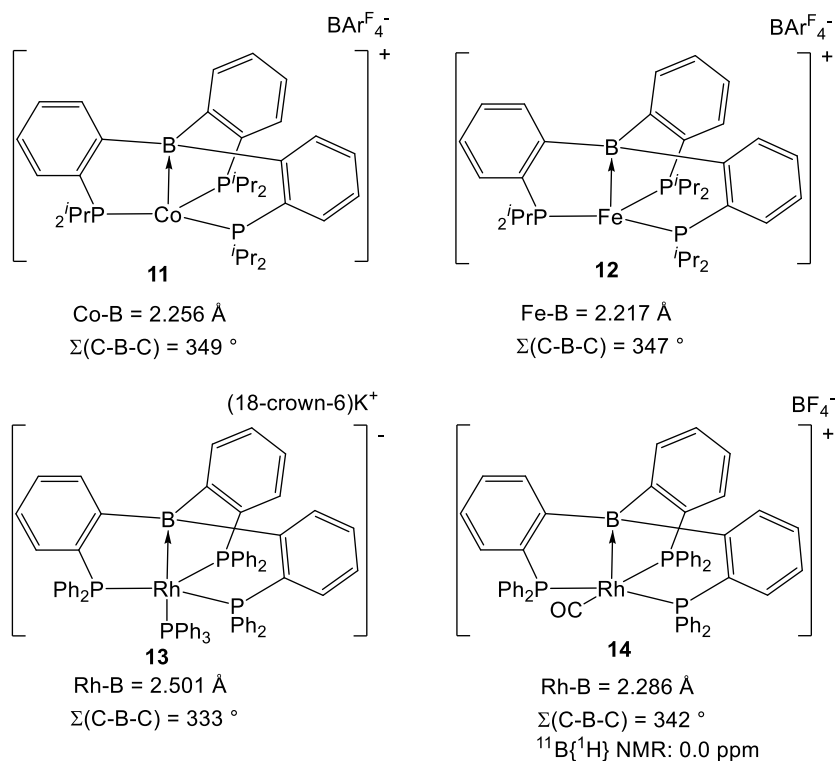
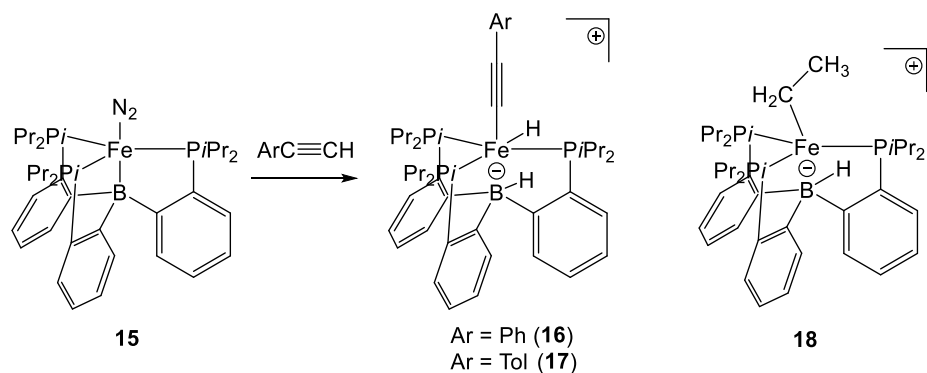


Figure I-7. Reported structures given unusual M–B distance and boron pyramidalization.

The TPB ligand is so ridged that no metal insertion into the supporting ligand to generate boryl ligand was observed in (TPB)M complexes. The generation of borate ligand was reported for some (TPB)Fe complexes (Scheme I-3, **16-18**).



Scheme I-3. The generation of borate ligand from (TPB)Fe.

1.2.3 Metallaboratranes with Borane/bis(phosphine) Ligand

With a labile B–Ph group, metal complexes with DPB ligands feature more binding modes. Metallaboratranes bearing DPB ligand were synthesized with different metals as summarized in Figure I-9. η^n -B,Ph ($n = 2, 3, 6, 7$) bonds are more common when DPB was used as ligand. Ag(DPB) complex has the longest M–B distance (2.742 Å), indicating no Ag–B interaction, and the details will be discussed in section II.⁵⁸ Z-type coordination was observed in Au⁵⁹⁻⁶¹, Pd^{26, 62-65}, Pt⁶⁶, Rh^{62, 67-69}, Ir⁷⁰ and Fe⁷¹ metallaboratranes, characterized by a short M–B bond length, a pyramidalized boron center, and a long M–C_{ipso} distance. The M–B distances in the (DPB)M complexes featuring Z-type M–B bonds are longer than the corresponding (TPB)M complexes. η^2 -B,C coordination was observed in Cu⁷², Ni^{73, 74}, Co⁷⁵, Rh^{67, 69} and Fe⁷⁶ metallaboratranes, characterized by a short M–B bond length, a planar boron center, and a short M–C_{ipso} distance. η^3 -B,C,C coordination was observed in Ni⁷³ and Fe⁷⁵⁻⁷⁶ metallaboratranes, characterized by a short M–B bond length, a planar boron center, and short M–C_{ipso} and M–C_{ortho} distances. η^6 -Ph coordination was observed in Ru metallaboratranes⁷⁷, characterized by a significant M–B distance, a pyramidalized boron center, and equal distances between the metal center and all the phenyl carbons. η^7 -B,Ph coordination was observed in Fe⁷⁶ and Ru⁷⁷ metallaboratranes, characterized by a short M–B bond length, a planar boron center, and equal distances between the metal center and all the phenyl carbons.

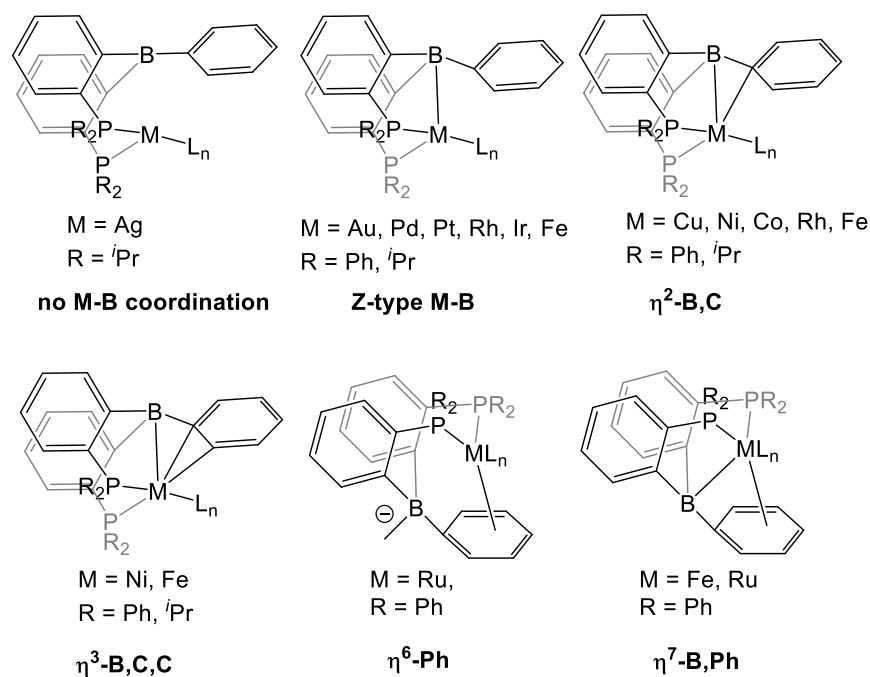
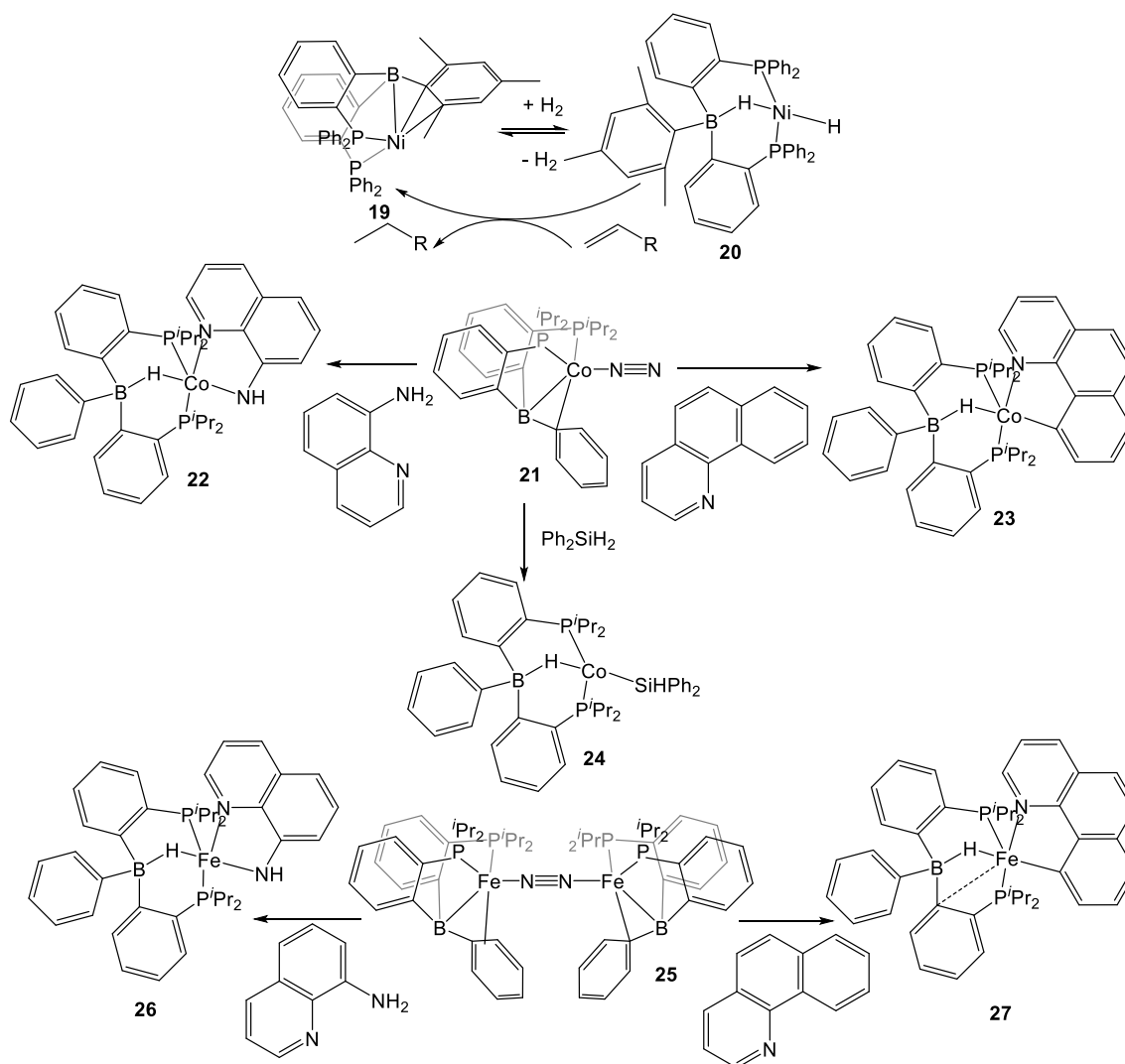


Figure I-8. Metallaboratranes bearing DPB ligand

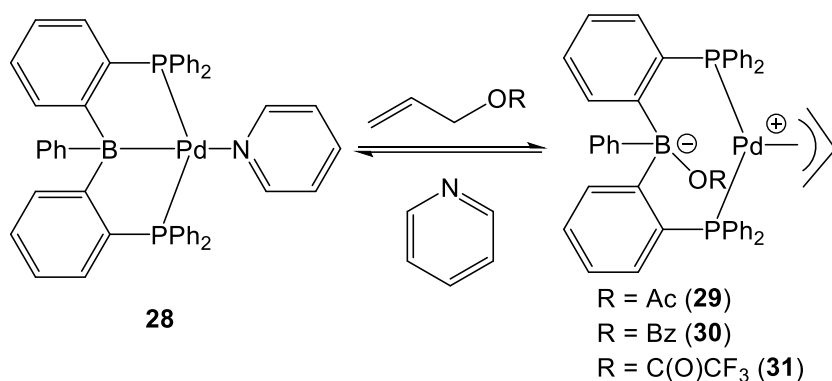
Due to the lability of B–Ph, the metal center can be better accessed for bond activation reactions such as H₂ activation by (DPB)Ni (**19**)⁷³⁻⁷⁴ and H–Si activation by (DPB)Co (**21**) and (DPB)Fe (**25**)⁷⁵ resulted in M–H–B bridging hydride (Scheme I-4, **20**, **24**). The metal center was also available for binding to another Lewis basic site and facilitated the N–H activation of 8-amino quinoline and C–H activation of 7,8-benzoquinoline (Scheme I-4, **22**, **23**, **26**, **27**).⁷⁵



Scheme I-4. H₂ and H-E (E = C, Si, N) bond activation by (DPB)M (M = Ni, Co, Fe)

The transformations between borate/borane/boryl were reported for many (DPB)M, and some are reversible, indicating that DPB is a promising ligand precursor for the synthesis of metal complexes bearing different types of boron ligand.

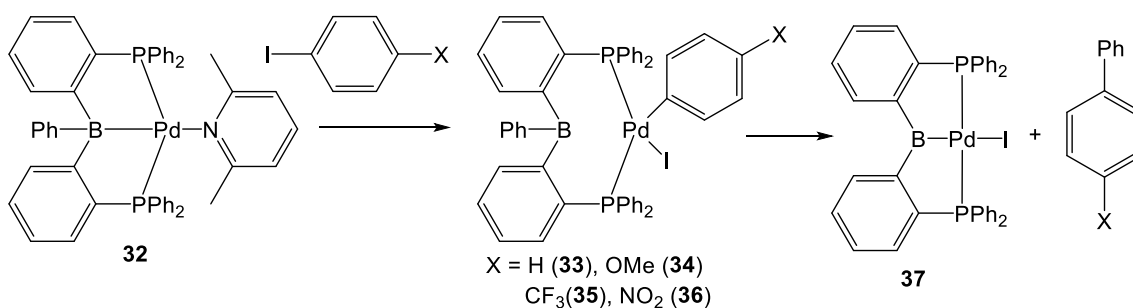
The activation of allyl acetates by (PBP)Pd (**28**) resulted in reversible transformation into allyl complex **29/30/31** featuring borate ligand⁶³ (Scheme I-3).



Scheme I-5. Activation of allyl acetates by (PBP)Pd

The activation of B–Ph bonds was observed in (DPB)Pd⁷⁸, (DPB)Rh^{27, 69} and (DPB)Ir²⁷, resulted in (PBP)M (M = Pd, Rh, Ir) with X-type boryl ligands.

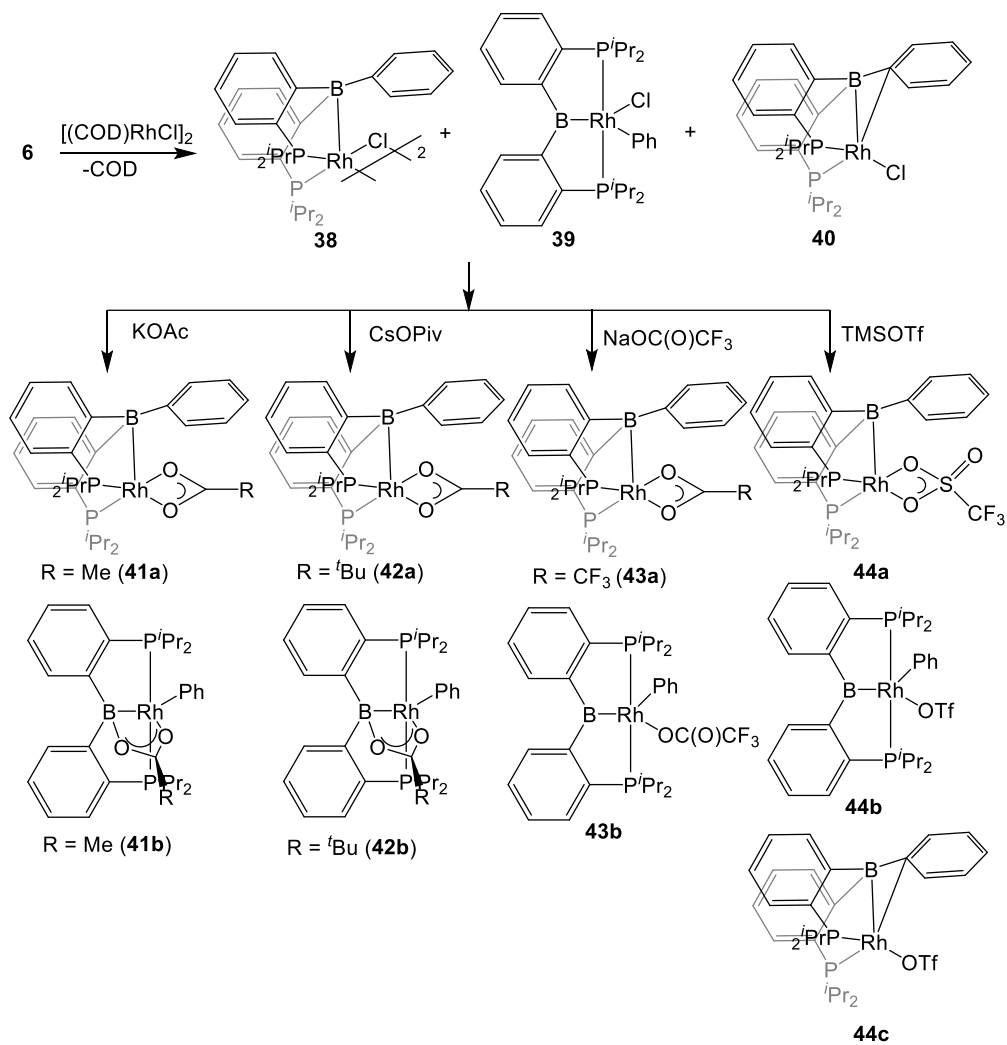
In 2016, Tauchert group reported that, for (DPB)Pd, after activation of Ar–I bond by **32**, **33-36** were generated with no Pd–B interaction. After heating, the C–C cross-coupling products and **37**, a pincer Pd complex with an X-type boryl center donor, were generated (Scheme I-6).⁷⁸



Scheme I-6. Activation of B–Ph bond by (DPB)Pd

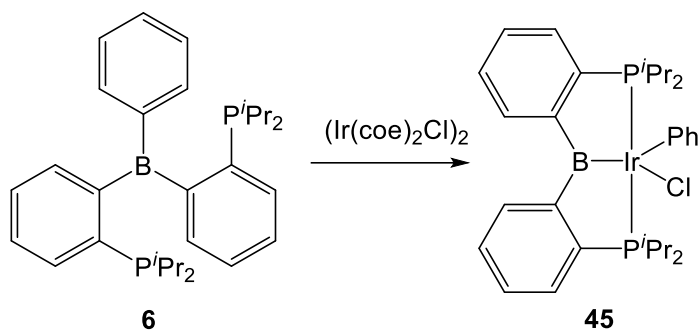
Reversible phenyl migration between the metal center and the supporting ligand was observed on a series of (DPB)Rh complexes with oxygenous ligands reported by Ozerov

group in 2017, indicating reversible conversion between boryl ligand and borane ligand (Scheme I-7).⁶⁹



Scheme I-7. Reversible phenyl migration between Rh and boron of (DPB)Rh complexes

Ir insertion into B–Ph bond of **6** was achieved by treating Ir precursor ($\text{Ir}(\text{coe})_2\text{Cl}$)₂ with **6** at 100 °C, which was reported by Ozerov group. B–Ph insertion happened to form **45** with X-type boryl center donor²⁷ (Scheme I-8).



Scheme I-8. Ir insertion into B–Ph bond of 6 to generate 45

In addition, as some of these conversions are reversible, they provide unique reactivity for metal complexes featuring diaryl-based boryl ligand, which will be discussed in section 1.3 and chapter III-V.

1.3 Pincer Complexes with Boryl Center Donor

As discussed in the previous section, after activation of the B–Ph bond of DPB ligand by the metal center, a pincer complex with X-type boryl center donor was generated.

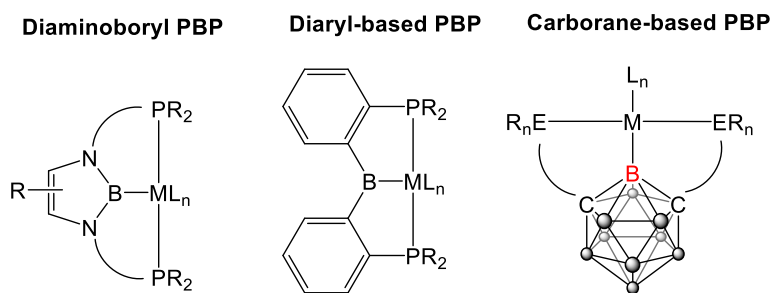


Figure I-9. Pincer metal complexes with a central boryl X-type donor

Besides diaryl-based (PBP)M complexes, the pincer complexes with boryl-type center donors have other scaffolds as summarized in Figure I-10. The diamino-based PBP

complexes have a similar structure as diaryl-based PBP, and the reactivity of this type of (PBP)M complexes were more explored, which will be discussed in the following section to compare with the reactivity of diaryl-based PBP metal complexes. The carborane-based PBP⁷⁹⁻⁸² will not be discussed here because its empty orbital on boron is tied up in the carborane cage. The diaryl-based PBP pincer possessed a boryl donor with a more accessible empty orbital than the diamino-based ligand (stabilized by π -donation from the amino groups).

1.3.1 Diaminoboryl PBP Complexes

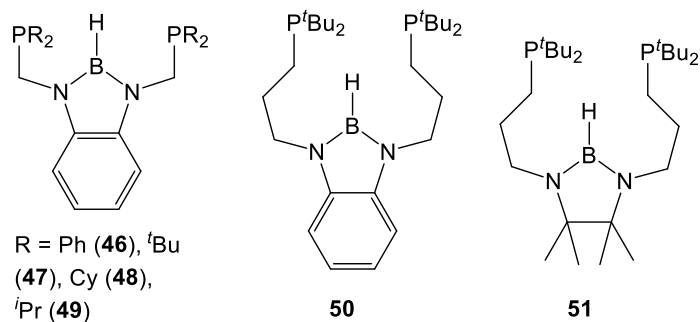


Figure I-10. Diaminoboryl-based Pincer Ligands

The synthesis of diaminoboryl PBP pincer ligand was reported by Yamashita and Nozaki in 2009.⁸³ The formation of boryl pincer complexes by this ligand was accomplished by metal insertion to B–H bond of **46-51** (Figure I-11). A variety of diamino-based (PBP)M (M = Ni⁸⁴⁻⁸⁸, Pd⁸⁹, Pt⁹⁰, Co^{84, 91}, Rh⁹²⁻⁹³, Ir^{82,93-96}, Fe⁹⁴, Ru⁹⁵⁻⁹⁹, Os⁹⁹) complexes were reported. In addition, diamino-based (PBP)Ir complexes **52** and **53** featuring longer sidearms were also reported (Figure I-12).¹⁰⁰⁻¹⁰¹ The X-type M–B bonds are significantly shorter than the Z-type M–B bonds with the same metal. The summary of all the M–B–N and N–B–N angles are 360 °, agrees with an sp² hybridized boron center.

However, based on the reported reactivity, this diamino-based boryl ligand features a boryl center with weak Lewis acidity.

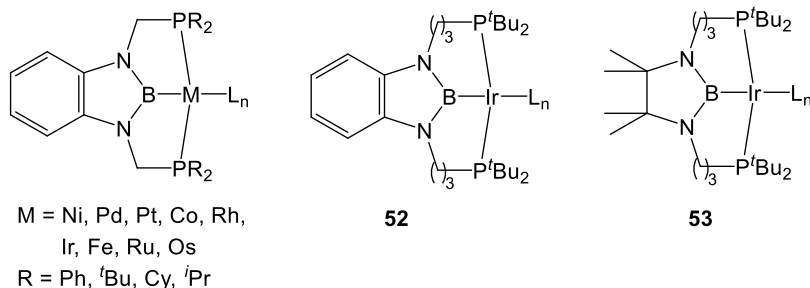
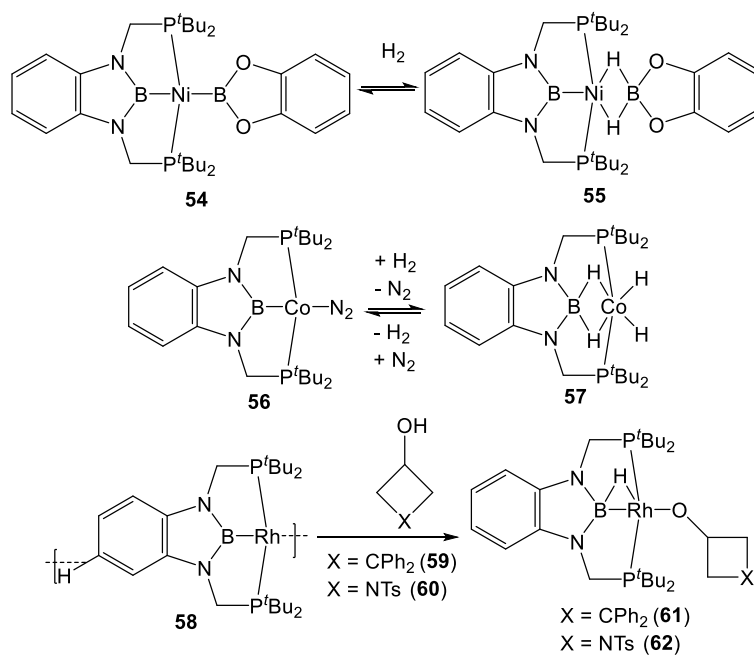


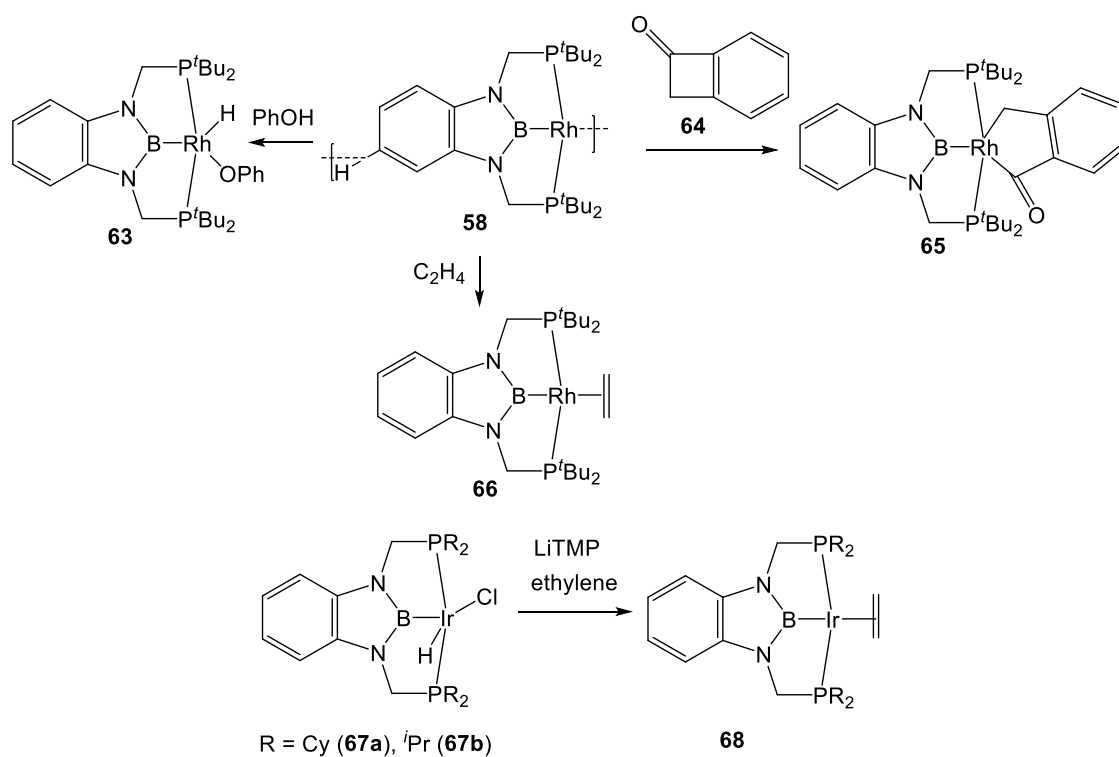
Figure I-11. Diamino-based (PBP)M complexes

Reported reactivity of diamino-based (PBP)M with boryl participation include H_2 activation by diamino-based (PBP)Ni⁸⁸ (**54**) and (PBP)Co⁹¹ (**56**), and the activation of secondary alcohol **59** and **60** with strained C–C bond by **58** to generate **61** or **62**⁹³ (Scheme I-9).



Scheme I-9. Reactivity of diamino-based (PBP)M with boryl participation

Even the activation of PhOH by **58** resulted in the formation of **63**, featuring an intact X-type boryl ligand, indicating a boryl center with poor Lewis acidity (Scheme I-10). Complex **58** also mediated C–C bond cleavage of cyclobutane **64** to form **65**. No reductive elimination to form B–C bond was observed. Ethylene binds to diamino-based (PBP)Rh (**66**) and (PBP)Ir (**67**) as L-type ligands and no activation or boryl participations were reported, which is quite different from the reactivity of diaryl-based (PBP)Ir (See section IV).



Scheme I-10. Reactivity of diamino-based (PBP)M with no boryl participation

1.3.2 Diarylboryl PBP Complexes

The synthesis of some diarylboryl (PBP)M complexes were discussed in section 1.2.2 (Figure I-13). Compared to diamino-based (PBP)M complexes, diaryl-based

(PBP)M complexes possess Lewis acidic boryl groups that actively participate in bond cleavage reactions mediated by the complexes.

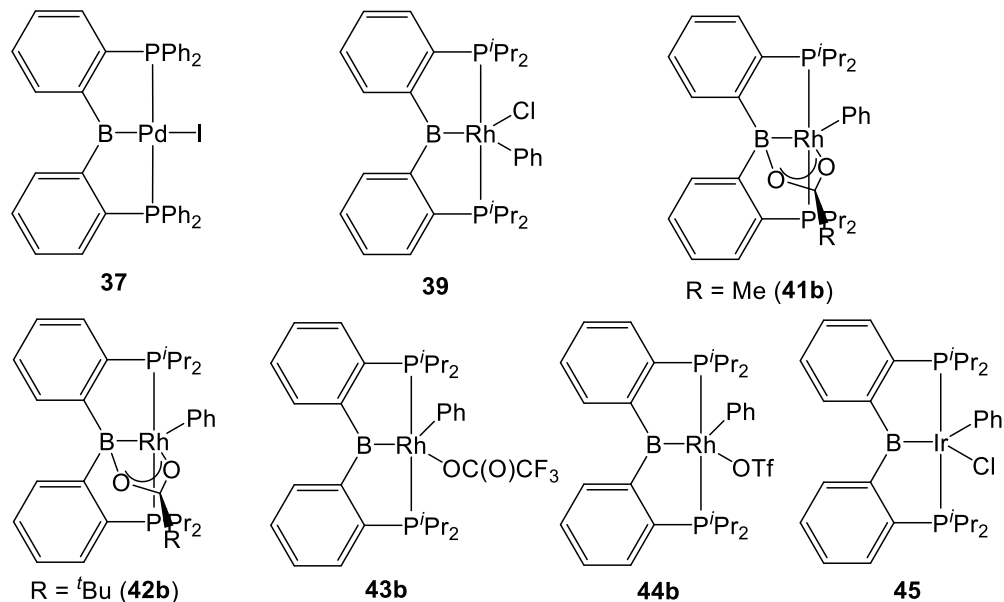
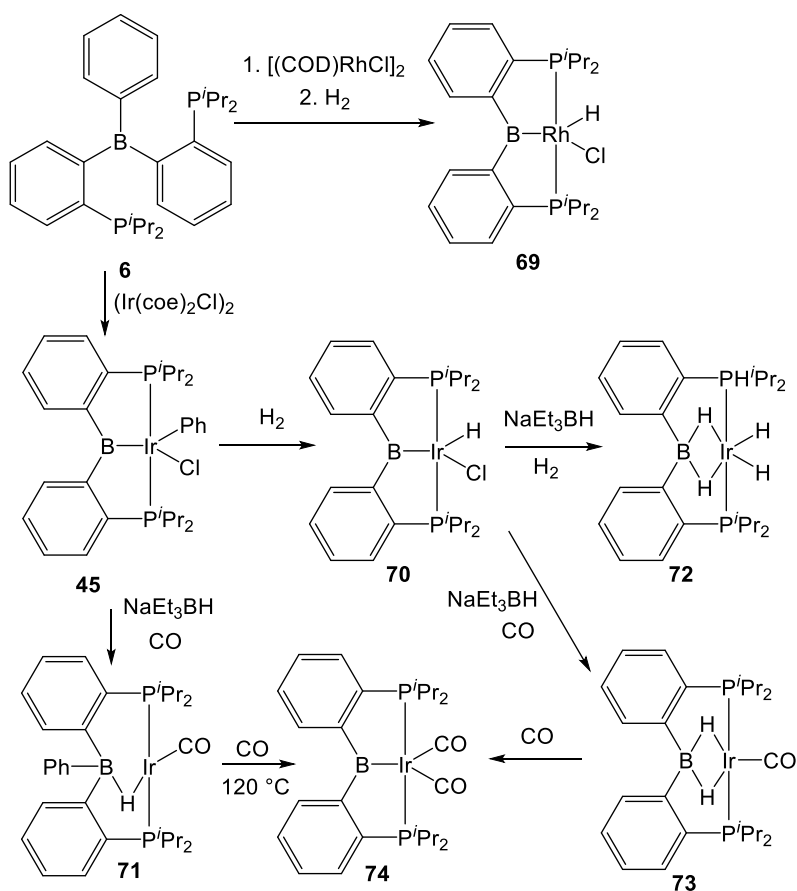


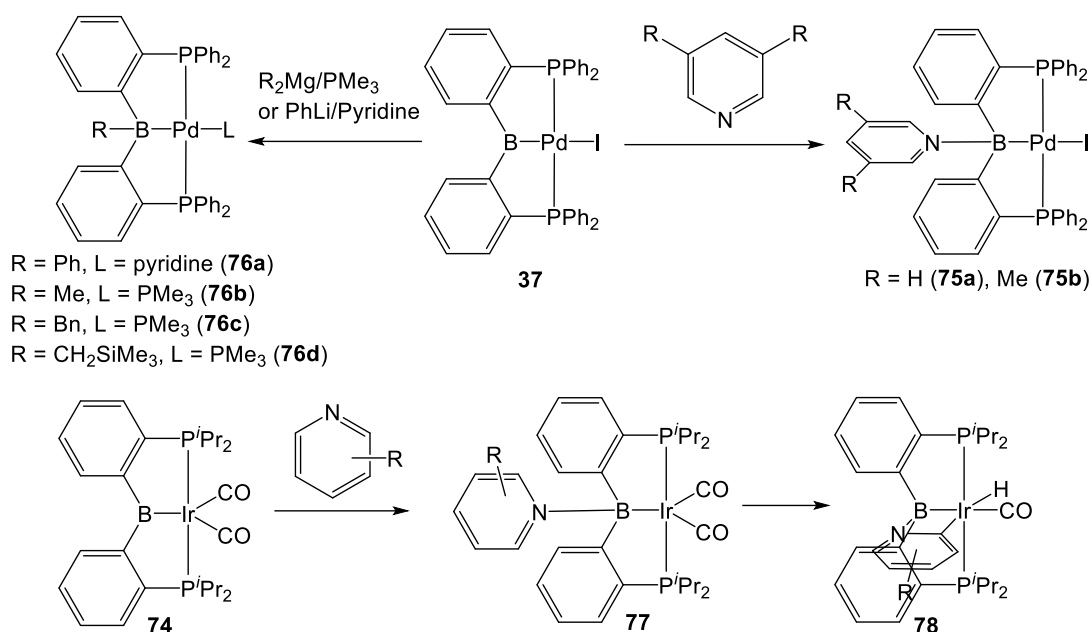
Figure I-12. Boryl pincer complexes generated by B-Ph insertion

The synthesis of diaryl-based (PBP)Rh **69** was accomplished by treating the resulting product of **6** and [(COD)RhCl]₂ with hydrogen gas at 100 °C, which was reported by Ozerov group.²⁷ The synthesis of a variety of diaryl-based (PBP)Ir precursors was also reported by Ozerov group.¹⁰² The reaction of **45** with dihydrogen result in **70**, which was the precursor for **72** and **73**. The chloride of **45** was replaced with hydride by NaEt₃BH. Under CO atmosphere, the phenyl group was transferred to boron and generate **71**. After heating under CO, benzene was eliminated to form **74**. Treatment of **70** with NaEt₃BH under CO atmosphere result in **73**, which, after heating, also generated **74** (Scheme I-11).¹⁰²



Scheme I-11. Diarylboryl (PBP)Ir and (PBP)Rh complexes and their reactivity

The diaryl-based (PBP)Pd and (PBP)Ir complexes feature Lewis acidic X-type boryl ligands. (PBP)Pd (**37**) reacted with pyridines to form **75a** and **75b**. (PBP)Ir (**74**) reacted with pyridines to form **77** reversibly, followed by a selective ortho C–H activation of pyridines to generate **78**. In addition, reductive elimination between boryl and the non-pincer ligand on the metal center was observed for (PBP)Pd complexes. For instance, reacting **37** with anionic carbon groups (Ph, Me, Bn, CH_2Me_3) afforded Pd(0) complexes **76a–76d** with Z-type borane ligand (Scheme I-12).⁷⁸ More reactivity of (PBP)Rh and (PBP)Ir will be discussed in chapter III–chapter VI.



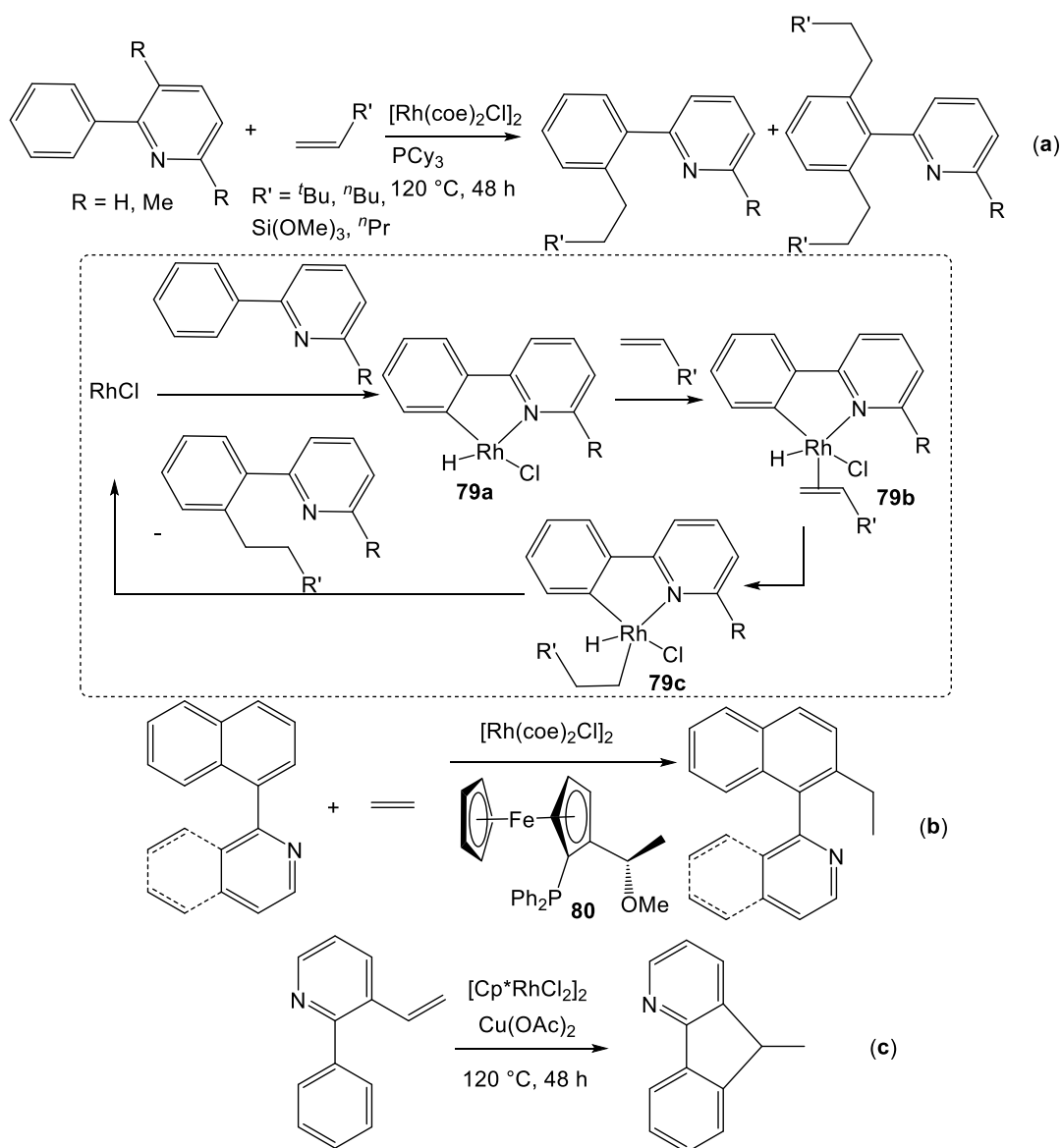
Scheme I-12. Diarylboronyl (PBP)Pd complexes and their reactivity

1.4 Rhodium Catalyzed Alkylation of Pyridines with Inactivated Alkenes

The addition reaction is an atom economic way to generate desired C–C coupling product with no side product. It attracts people’s attention if functionalization of aromatic C–H bond can be achieved by adding a C–H bond to alkenes to generate the alkylated product. This kind of reactivity can be achieved by using a transition metal catalyst.^{103, 104} The hydroarylation catalyzed by rhodium complexes usually initiated by a C–H activation, followed by the aryl insertion into the alkene. Thus, the substrate could be arene with phosphorous or heterocyclic directing groups, aromatic ketones/ketimines, or phenols/anilines.¹⁰⁵⁻¹⁰⁶ Here, hydroarylation of olefins with substrates containing pyridyl groups catalyzed by Rh complexes was summarized.

1.4.1 Pyridyl as An Intact Directing Group

In 1994, Kim and co-workers reported the alkylation of 2-phenylpyridines with olefins by $[\text{Rh}(\text{coe})_2\text{Cl}]_2/\text{PCy}_3$ (Scheme I-13, equation **a**).¹⁰⁷ Olefin added selectively to the aromatic C–H ortho to the pyridyl group and formed the linear product. The proposed mechanism attributes this selectivity to the coordination between the pyridyl group and Rh (Scheme I-13, **79a–79c**). The substituent on the C3 position of pyridine added steric hindrance, resulting in only the mono alkylated product.^{107, 108} When chiral phosphine ligand (**80**) was used instead of PCy_3 , this reactivity introduced axial chirality to rotation restricted biaryl compounds (Scheme I-13, equation **b**).¹⁰⁹ In 2012, Shibata and co-workers reported an intramolecular cyclization of 2-aryl-3-vinylpyridines with Rh(III)-catalyst and $\text{Cu}(\text{OAc})_2$ as a catalytic additive (Scheme I-13, equation **c**).¹¹⁰ Besides phenyl alkylation with olefins, the pyridyl group was also introduced as a directing group for thienyl alkylation¹¹¹ or C3 pyridyl alkylation¹¹². Introducing a pyridyl group for selective C–H alkylation of 1-naphthylamide was also reported.¹¹³

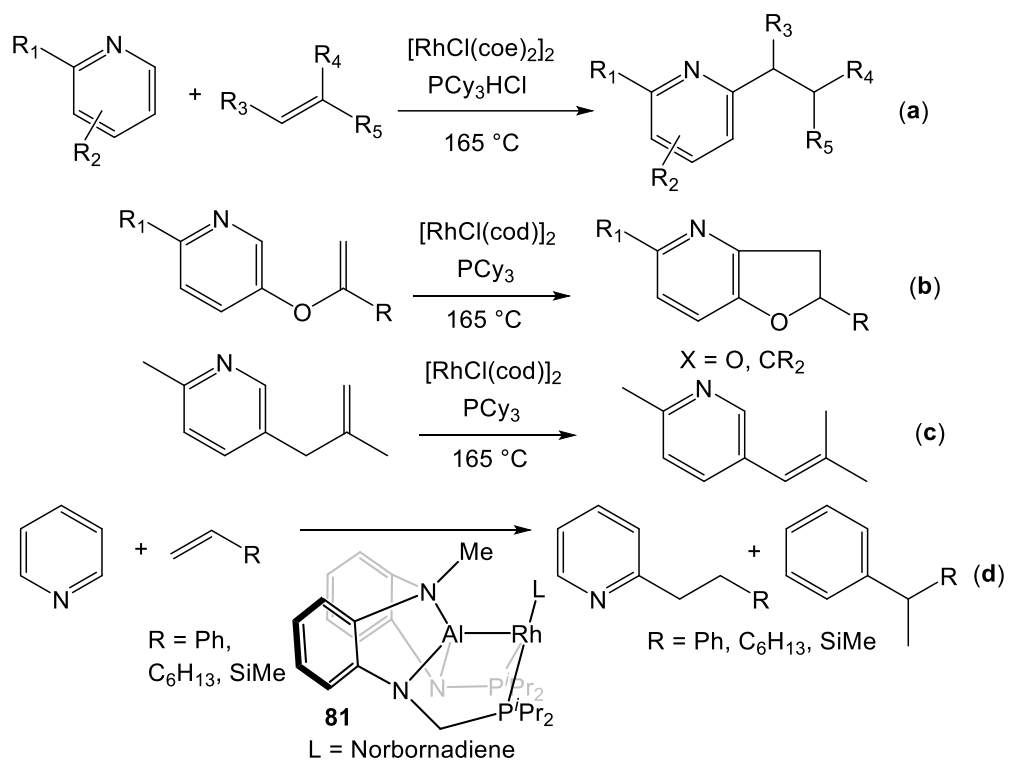


Scheme I-13. Hydroarylation of inactivated olefins with 2-phenylpyridines

1.4.2 C–H Alkylation of the Pyridyl Groups

In 2007, Ellman and co-workers reported the ortho alkylation of pyridines catalyzed by Rh(I) catalyst (Scheme I-14, equation a).¹¹⁴ Based on their research, no reactivity was observed when no additive or Lewis acids such as MgBr_2 were added to the

Rh/PCy₃ system. However, using a Brønsted acid, such as 2,6-lutidine hydrobromide as an additive, provided the desired ortho alkylated pyridines. Thus, the best condition was the combination of RhCl(coe)₂ and PCy₃HCl. The substrate scope was limited to pyridines with ortho substituents and increased steric hindrance led to an increase in both alkylation rate and isolated yield of alkylated product. Consistent with the findings of Carmona and Esteruelas in 2006¹¹⁵⁻¹¹⁶, substituents at the 2- and 5-positions introduce steric interactions that either promote or attenuate, respectively, the propensity of forming the C-bound Rh complex necessary for C–H functionalization relative to the N-bound form. Thus, pyridine and 2,5-disubstituted pyridines were alkylated in less than 5% yield. With different olefin, both linear and branched products were observed. In 2010, they reported that cyclization of tethered pyridines and quinolines were accomplished with Rh/PCy₃ system (Scheme I-14, equation **b**).¹¹⁷ Alkene isomerization was observed in this reaction (Scheme I-14, equation **c**). In 2018, Nakao and co-workers reported pyridine *ortho*-alkylation catalyzed by Rh complex **81** featuring an aluminyl type pincer ligand (Scheme I-14, equation **d**).²⁹



Scheme I-14. Rh(I) catalyzed pyridine ortho alkylation

CHAPTER II

SILVER HALIDE COMPLEXES OF A BORANE/BIS(PHOSPHINE) LIGAND*

2.1 Introduction

Incorporation of Z-type, Lewis-acidic sites into polydentate ligands has become one of the widely used tools to influence reactivity at the metal centers.^{35, 118-119} Ligands containing borane sites connected to flanking phosphine donors via an *ortho*-phenylene linkage have been especially prominent (Figure II-1).^{35, 119} Borane/bis(phosphine) DPB^{59, 67} and borane/tris(phosphine) TPB³⁹ are closely related and have been used to analyze the fundamentals of the M-Z bonding^{40-42, 47, 59} and in applications such as hydrogenation⁷³ and dinitrogen reduction¹²⁰. Our group recently became interested in **6** as a precursor to boryl/bis(phosphine) pincer complexes of Rh and Ir, which are obtained via insertion of the transition metal into the B-Ph bond.^{27, 37, 69} Tauchert et al. disclosed the related work with Pd.^{63-64, 78}

* Reproduced in whole from “Silver Halide Complexes of a Borane/Bis(Phosphine) Ligand” by Cao, Y.; Shih, W.-C.; Bhuvanesh, N.; Ozerov, O. V. Dalton Trans. 2019, 48, 9959-9961. Copyright [2019] by Royal Society of Chemistry. The synthesis and crystal structure of **201** has been developed and solved by our former group members Dr. Wei-Chun Shih. The crystal structure of **204** was solved by crystallographer Dr. Nattamai Bhuvanesh.

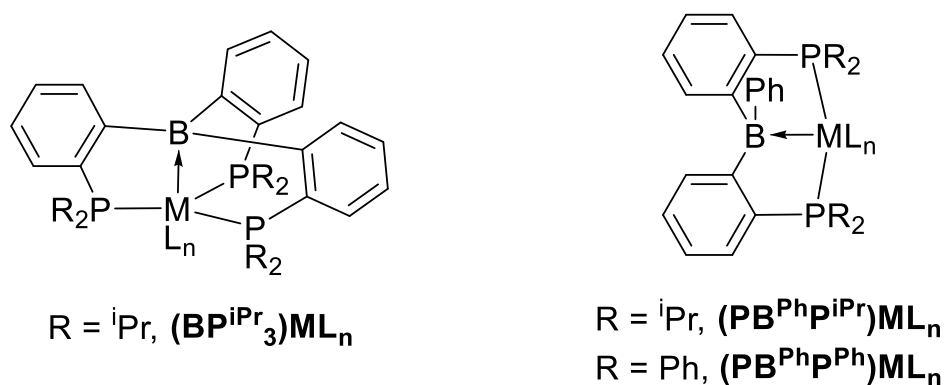


Figure II-1. Generic depiction of complexes of borane/tris(phosphine) and borane/bis(phosphine) ligands emphasizing the Z-type interactions of the metal with the central borane unit

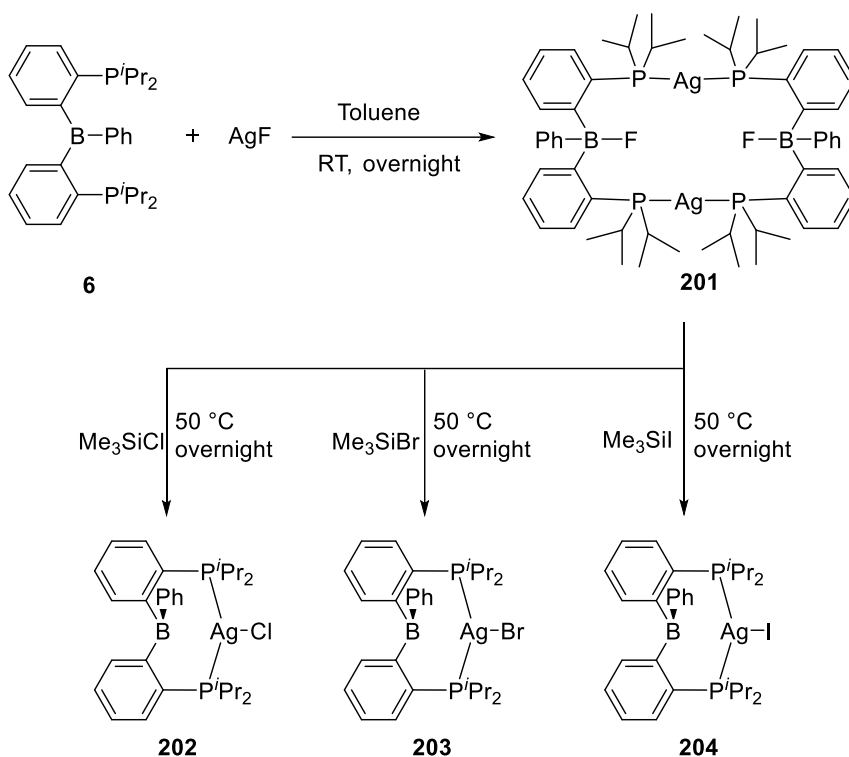
The binding of TPB was studied with Cu, Ag, and Au monochlorides.⁴¹ Bourissou and coworkers examined the CuCl adduct with **6**⁷² and AuCl adducts with both **6** and **7**.⁷² Building on Bourissou's work, Inagaki, Mukai and coworkers utilized cationic (DPB)Au complexes for the catalysis of cyclization reactions.^{60-61, 121} The lack of studies of the complexes of silver with bis(phosphine)/borane ligands moved us to examine the nature of the complexes of **6** with silver monohalides, and specifically whether the borane moiety would show interactions with either the silver center or with the halide.

2.2 Result and Discussion

2.2.1 Synthesis of Silver Complexes with Borane Ligand

Stirring AgF with **5** in a 1:1 ratio in toluene overnight resulted in the formation of **201**, which was isolated in 89% yield upon workup (Scheme II-1). The other AgX complexes were prepared by treatment of pure **201** with 2-20 equiv. of the corresponding Me₃SiX reagent (Scheme II-1). These reactions resulted in the formation of Me₃SiF (¹H NMR: 0.020 ppm) and new complexes **202/203/204**. We were able to isolate a 68%

yield of an analytically pure solid of the iodo complex **204**. The bromide and chloride analogs **203** and **202** were the dominant products as indicated by NMR spectroscopy, but persistently contained ca. 2-3% of an impurity that we were not able to identify or completely remove. We cannot rule out that these impurities are isomers of **202** or **203**, but they do not appear to possess the structure of **204**.



Scheme II-1. Syntheses of AgX adducts of **6**

2.2.2 Spectroscopic Characterization

The NMR spectra of the **202/203/204** complexes were very similar to each other and starkly different from the spectra of **201**, which presented an especially complex pattern in the ^{31}P NMR spectrum. This pattern was analyzed as arising from a pair of inequivalent ^{31}P nuclei attached to each Ag atom. The two ^{31}P nuclei at the same Ag are

coupled to each other, in addition to each being coupled (with its own coupling constants) to one ^{19}F nucleus and one silver nucleus. Since silver is composed of two $S = 1/2$ isotopes (^{107}Ag and ^{109}Ag) in a ca. 52:48 ratio, each type of the ^{31}P nucleus gives rise to a concentric, overlapping pair of ddd resonances (Figure II-2).

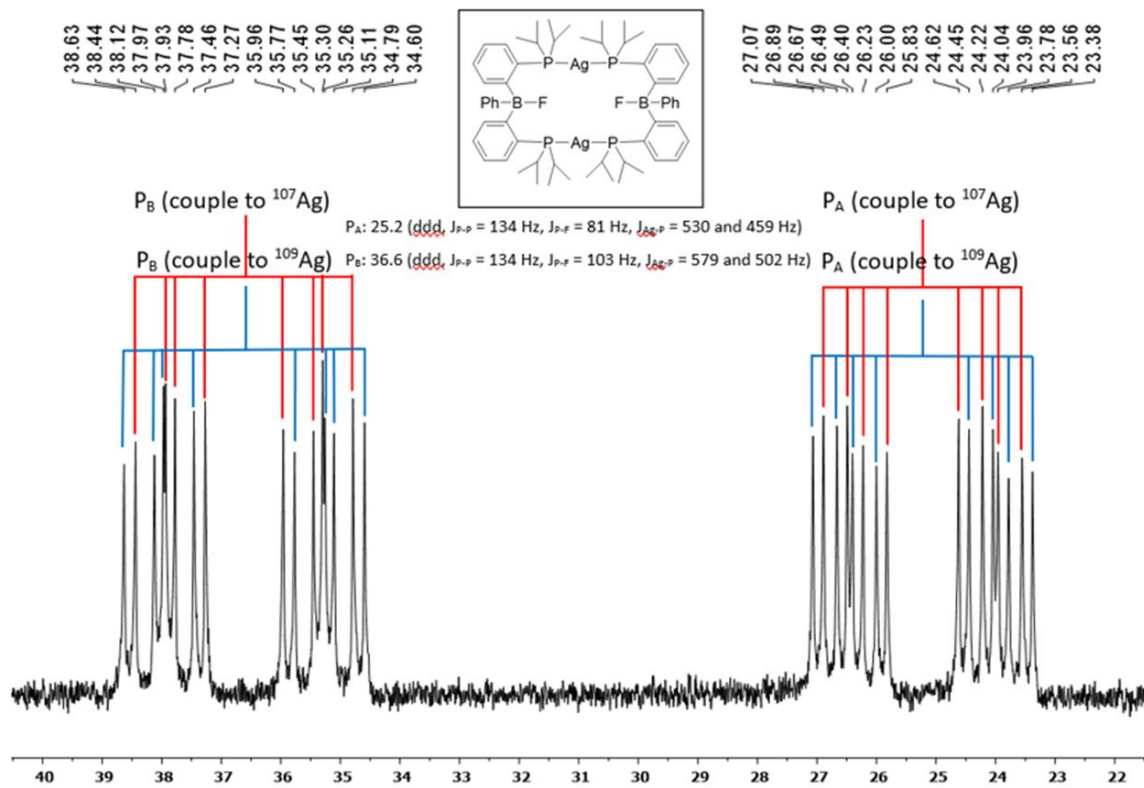


Figure II-2. $^{31}\text{P}\{^1\text{H}\}$ NMR spectrum of **201** in C_6D_6 at RT measured on a 500 MHz Varian NMR

The ^{19}F NMR resonance of **201** is relatively broad, consistent with fluorine being attached to a quadrupolar boron nucleus. In addition, **201** displayed an ^{11}B NMR resonance at 7.7 ppm, indicating an sp^3 -hybridized, four-coordinate boron. On the other hand, **202/203/204** gave rise to a ^{11}B NMR resonance in the 61-64 ppm range, contained

equivalent phosphines and time-averaged C_s symmetry overall in its NMR spectra. The magnitude of the J_{Ag-P} values in **202/203/204** was about 20% smaller than in **201**.

Table II-1. $^{11}B\{^1H\}$ NMR, $^{31}P\{^1H\}$ NMR chemical shifts and J Values (in Hz) of Ag Complexes

	$^{11}B\{^1H\}$ NMR	$^{31}P\{^1H\}$ NMR	J_{Ag-P}^{107}	J_{Ag-P}^{109}
201	7.7	25.2; 36.6	459; 502	530; 579
202	61.5	36.8	372	430
203	61.8	35.8	367	424
204	63.6	32.7	354	410

Taken together, these spectroscopic data suggested that the boron of $PB^{Ph}P^{iPr}$ abstracted the fluoride from AgF, but the heavier halides in the complexes **202/203/204** remained bound to silver.

2.2.3 X-ray Diffraction Studies

The X-ray diffraction studies on **201** (Figure II-3) and **204** (Figure II-4) corroborated this conclusion. **201** was found to be a dimeric molecule where each of the newly formed fluoroborate/bis(phosphine) ligands bridges two silver centers. Although the solid-state structure does not possess a crystallographic 2-fold axis of symmetry, it can be viewed as nearing the C_2 symmetry it displays in solution on the NMR time scale. The two phosphorus atoms in each PBP ligand (and the two phosphorus atoms attached to each silver) are made different by virtue of the conformation the ligand adopts. For example, although the two phosphorus atoms are separated by similar distances from the fluoride in the same ligand, one is positioned much farther from the B-Ph group than the other. The geometry about Ag deviates from linearity (P-Ag-P angles of ca. 151-153°), with the Ag atom being drawn slightly into the center of the dimer, towards the borate moieties. After the Ag-P bonds, the next four closest non-hydrogen contacts are with the

two fluorides (Ag-F distances in the 2.66-2.96 Å range) and the C_{ipso}/C_{ortho} carbons of the B-Ph groupⁱ (Ag-C distances in the ca. 2.7-2.9 Å range). These distances are quite long (cf. Ag-P bond distances of ca. 2.42-2.44 Å), but the geometry clearly points to the presence of an interaction between the cationic Ag centers and the anionic fluoroborate centers in this zwitterionic molecule. Each Ag atom shows close contact with only one Ph group, again underlining the pairwise inequivalence of the P atoms in **201**. It is interesting that NMR spectra of **201** show lack of fluxionality, indicating the persistence of this inequivalence on the NMR timescale.

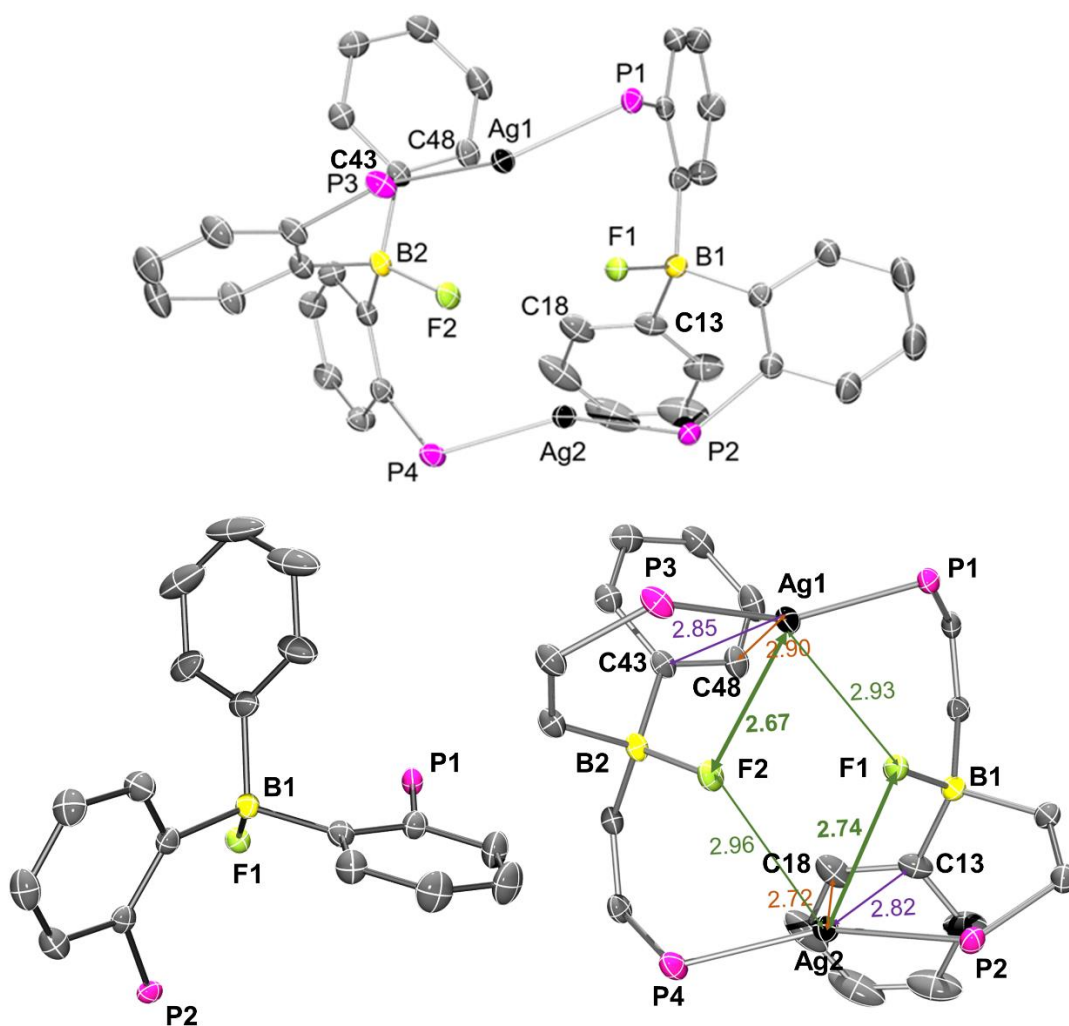


Figure II-3. Top: POV-Ray rendition of the ORTEP drawing (50% thermal ellipsoids) of 201 showing selected atom labelling. Hydrogen atoms and isopropyl groups are omitted for clarity. Selected bond distances (Å) and angles (°) for 201: Ag1-P1, 2.4342(6); Ag1-P3, 2.4425(8); Ag2-P2, 2.4323(8); Ag2-P4, 2.4255(7); Ag681, 2.928(1); Ag682, 2.667(1); Ag2-F1, 2.735(1); Ag2-F2, 2.960(1); Ag1-C48, 2.901(2); Ag1-C43, 2.850(2); Ag2-C18, 2.720(2); Ag2-C13, 2.820(2); F1-B1, 1.464(2); F2-B2, 1.463(2); P1-Ag1-P3, 153.03(2); P2-Ag2-P4, 151.12(2). Bottom: POV-Ray rendition of the ORTEP drawing (50% thermal ellipsoids) of truncated 201 showing selected atom labelling and selected interatomic distances rounded to 0.01 Å

The structure of **204** is best described as approximately trigonal planar about the Ag center, with ostensibly little if any interaction between Ag and B. The angles in the P2AgI plane are within the 112-128° range, adding up to ca. 356.5°. Likewise, the sum of the C-B-C angles about the boron center is ca. 357°. The Ag-B distance of ca. 2.74 Å is ca. 0.2 Å longer than the Ag-B distance in (TPB)AgCl.⁴¹

Interestingly, the very weak interaction between Ag and the borane moiety in **204** is in contrast to the analogous (DPB)AuCl⁵⁹ and (DPB)CuCl⁷² complexes (Figure II-4). For Au, a meaningful Au→B bond was established, which results in a near-square-planar environment about Au with a short Au-B bond distance of 2.309(9) Å. For Cu, the solid-state structure contained four independent molecules with a varying degree of interaction between Cu and the B-C_{Ph} bond, with closest approach of the B and C to Cu in one of them of ca. 2.4 Å. The P₂CuCl fragment in these structures is definitively pyramidalized, with the Cu atom displaced from the P₂Cl plane towards the B-C bond. Qualitatively, it is possible to conclude that the order of the strength of interaction of the borane moiety in **6** with MHal follows the order of Au > Cu > Ag, even if different structural modes are observed. With the TPB ligand, the metallatrane cage enforces the same structural motif for all three coinage metal-monochloride complexes, but the strength of interaction was also determined to be in the Au > Cu > Ag order.⁴¹

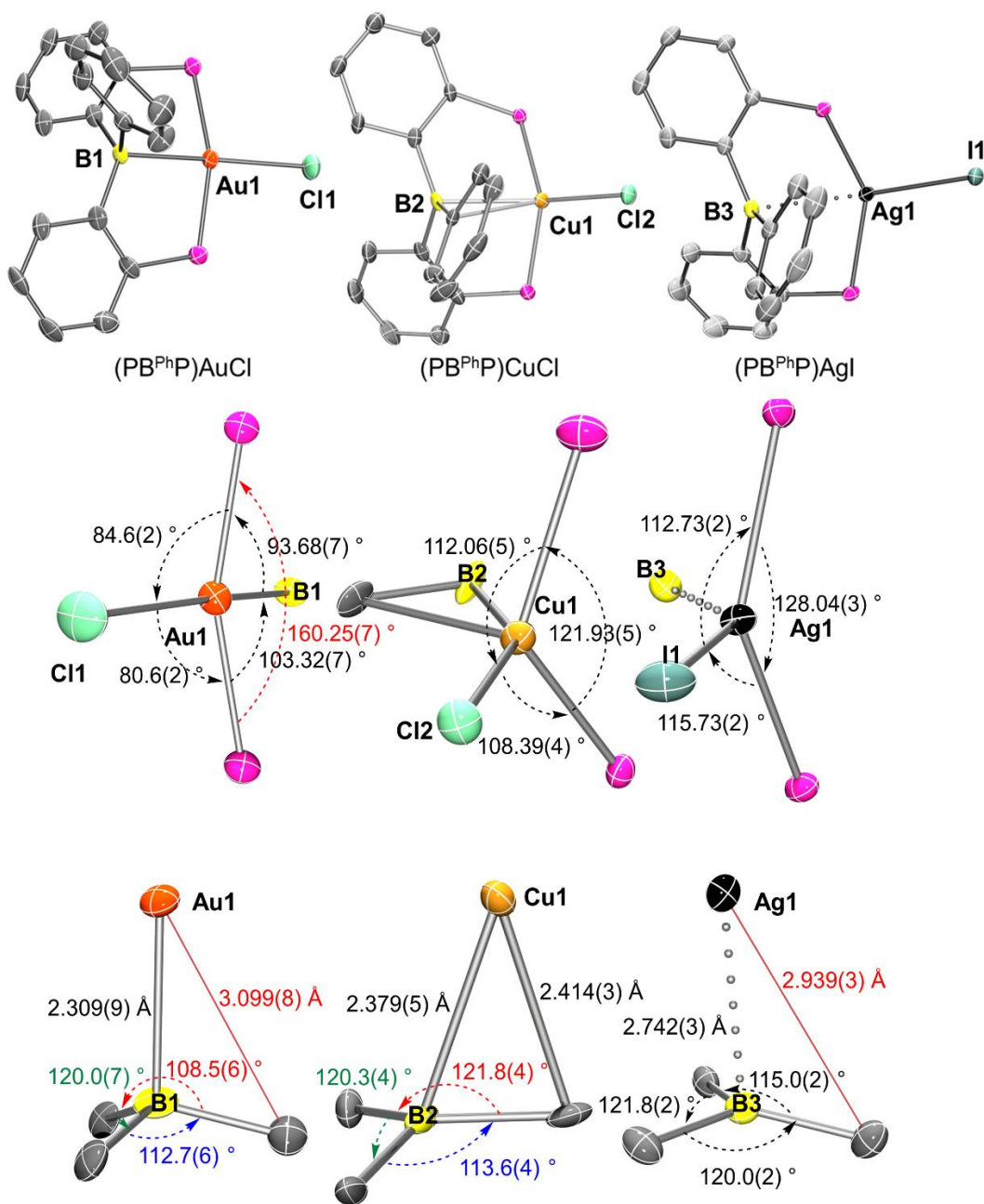


Figure II-4. POV-Ray rendition of the ORTEP drawing (50% thermal ellipsoids) of 204, $(\text{DPB})\text{AuCl}$ and $(\text{DPB})\text{CuCl}$. Top: Front view showing selected atom labelling and M-B Distance. Hydrogen atoms and isopropyl groups are omitted for clarity. Middle: Truncated molecules with metal center and atoms around metal. Bottom: Truncated molecules with boron center and atoms around boron

2.3 Conclusion

In summary, we have determined that the ligand **6** readily binds to silver monohalides. The binding proceeds with abstraction of fluoride, but the heavier halides remain bound to silver. These latter complexes contain a borane moiety in the same molecule as the silver center, but the spectroscopic and structural evidence points to a very weak interaction between B and Ag at best. The weakness of this interaction contrasts with the observations in the analogous AuCl and CuCl complexes reported by Bourissou et al. earlier,^{59, 72} but the Au > Cu > Ag trend for the strength of interaction with a Z-type borane among the coinage metals appears to be general.

2.4 Experimental Section

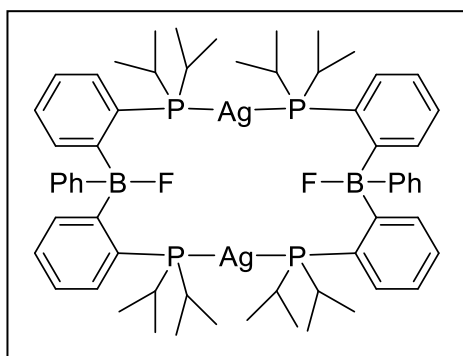
2.4.1 General Considerations

Unless specified otherwise, all manipulations were performed under an Ar atmosphere using standard Schlenk line or glovebox techniques. Toluene, diethyl ether, pentane, and isooctane were dried and deoxygenated (by purging) using a solvent purification system (Innovative Technology Pure Solv MD-5 Solvent Purification System) and stored over molecular sieves in an Ar-filled glove box. C₆D₆ was dried over NaK/Ph₂CO/18-crown-6, distilled or vacuum transferred and stored over molecular sieves in an Ar-filled glovebox. CH₂Cl₂, CDCl₃, cyclohexane, and C₆D₁₂ were dried over CaH₂, distilled or vacuum transferred and stored over molecular sieves in an Ar-filled glove box. All other chemicals were used as received from commercial vendors.

2.4.2 Physical Methods

NMR spectra were recorded on a Varian Inova 400 (^1H NMR, 399.535 MHz; ^{11}B NMR, 128.185 MHz; ^{31}P NMR, 161.734 MHz) and Varian Inova 500 (^1H NMR, 499.703 MHz; ^{13}C NMR, 125.697 MHz; ^{31}P NMR, 202.265 MHz; ^{19}F NMR, 470.106 Hz) spectrometer. Chemical shifts are reported in δ (ppm). For ^1H and ^{13}C NMR spectra, the residual solvent peak was used as an internal reference (^1H NMR: δ 7.16 for C_6D_6 , 7.24 for CDCl_3 ; ^{13}C NMR: δ 128.62 for C_6D_6 , 77.16 for CDCl_3). ^{11}B NMR spectra were referenced externally with BF_3 etherate at δ 0. ^{31}P NMR spectra were referenced externally with 85% phosphoric acid at δ 0. ^{19}F NMR spectra were referenced with pure trifluoroacetic acid to δ -78.5 ppm. Elemental analyses were performed by CALI Labs, Inc. (Highland Park, NJ).

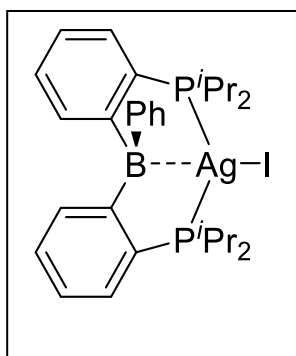
2.4.3 Synthesis and Characterization of Silver Complexes



201. To a solution of **5** (71 mg, 0.15 mmol) in toluene (1 mL) was added silver fluoride (19 mg, 0.15 mmol), and the resulting suspension was stirred at room temperature overnight. The solution was filtered through Celite, and the volatiles were

removed under vacuum. The resulting solid was recrystallized in toluene layer pentane (1:3), yielding a white solid (80 mg, 89%). $^{31}\text{P}\{^1\text{H}\}$ NMR (202 MHz, C_6D_6): δ 25.2 (ddd, $J_{\text{P-P}} = 134$ Hz, $J_{\text{P-F}} = 81$ Hz, $J^{107}_{\text{Ag-P}} = 459$ Hz, $J^{109}_{\text{Ag-P}} = 530$ Hz), 36.6 (ddd, $J_{\text{P-P}} = 134$ Hz, $J_{\text{P-F}} = 103$ Hz, $J^{107}_{\text{Ag-P}} = 502$ Hz, $J^{109}_{\text{Ag-P}} = 579$ Hz). $^{11}\text{B}\{^1\text{H}\}$ NMR (128 MHz, C_6D_6): δ 7.7 (br). ^{19}F NMR (470 MHz, C_6D_6) δ -181.7 (br). ^1H NMR (500 MHz, C_6D_6) δ 8.78 (d,

$J_{\text{H-H}} = 5.2$ Hz, 1H), 7.49 (m, 1H), 7.36 (m, 2H), 7.12 (m, 5H), 7.03 (t, $J_{\text{H-H}} = 7.1$ Hz, 1H), 6.97 (d, $J_{\text{H-H}} = 7.4$ Hz, 1H), 6.83 (t, $J_{\text{H-H}} = 7.3$ Hz, 1H), 6.07 (t, $J_{\text{H-H}} = 7.1$ Hz, 1H), 2.80 (m, 1H, CHMe_2), 2.27 (m, 1H, CHMe_2), 2.14 (m, 1H, CHMe_2), 2.08 (m, 1H, CHMe_2), 1.28 (m, 6H, CHMe_2), 1.17 (dd, $J_{\text{H-H}} = 18.1$ Hz, $J_{\text{H-P}} = 7.6$ Hz, 3H, CHMe_2), 1.01 (m, 6H, CHMe_2), 0.94 (dd, $J_{\text{H-H}} = 16.8$ Hz, $J_{\text{H-P}} = 6.7$ Hz, 3H, CHMe_2), 0.78 (dd, $J_{\text{H-H}} = 8.9$ Hz, $J_{\text{H-P}} = 7.5$ Hz, 3H, CHMe_2), 0.74 (dd, $J_{\text{H-H}} = 15.2$ Hz, $J_{\text{H-P}} = 7.0$ Hz, 3H, CHMe_2). $^{13}\text{C}\{^1\text{H}\}$ NMR (126 MHz, C_6D_6) δ 167.5 (s), 162.9 (s), 158.9 (s), 139.1 (dd, $J_{\text{P-C}} = 12.4$ Hz, $J_{\text{P-C}} = 7.7$ Hz), 137.0 (d, $J_{\text{P-C}} = 14.4$ Hz), 135.4 (s), 133.9 (m), 132.1 (s), 129.9 (d, $J_{\text{P-C}} = 3.5$ Hz), 129.4 (s), 129.0 (s), 128.4 (s), 128.2 (d, $J_{\text{P-C}} = 1.9$ Hz), 127.7 (s), 127.1 (s), 125.5 (s), 124.9 (d, $J_{\text{P-C}} = 4.6$ Hz), 124.4 (d, $J_{\text{P-C}} = 5.8$ Hz), 27.8 (dd, $J_{\text{P-C}} = 12.4$ Hz, $J_{\text{P-C}} = 3.8$ Hz), 25.9 (dd, $J_{\text{P-C}} = 13.1$ Hz, $J_{\text{P-C}} = 5.0$ Hz), 24.6 (dd, $J_{\text{P-C}} = 11.7$ Hz, $J_{\text{P-C}} = 5.5$ Hz), 23.5 (d, $J_{\text{P-C}} = 12.6$ Hz), 23.2 (d, $J_{\text{P-C}} = 13.1$ Hz), 22.1 (d, $J_{\text{P-C}} = 6.7$ Hz), 22.0 (d, $J_{\text{P-C}} = 6.1$ Hz), 21.2 (t, $J_{\text{P-C}} = 10.9$ Hz), 21.0 (t, $J_{\text{P-C}} = 9.4$ Hz), 16.3 (dd, $J_{\text{P-C}} = 7.8, 4.7$ Hz). Elem. Anal. Calcd. for $\text{C}_{60}\text{H}_{82}\text{Ag}_2\text{B}_2\text{F}_2\text{P}_4$: C, 59.93; H, 6.87. Found: C, 60.04; H, 6.89



204. To a solution of **201** (60 mg, 0.050 mmol) in toluene (4 mL) was added iodotrimethylsilane (20 μL , 0.10 mmol), and the resulting mixture was stirred at 55 $^\circ\text{C}$ overnight. Large amounts of solid crashed out gradually during the heating. The volatiles were removed under vacuum, and the resulting solid was recrystallized in THF layer pentane (1:2), yielding a fluorescent green solid (48 mg, 68 %). $^{31}\text{P}\{^1\text{H}\}$ NMR (121 MHz, C_6D_6): δ 32.7 (d, $J^{109}_{\text{Ag-P}} = 410$ Hz), 36.8 (d, $J^{107}_{\text{Ag-P}} = 354$ Hz). $^{11}\text{B}\{^1\text{H}\}$ NMR (128 MHz, C_6D_6): δ 63.5 (br). ^1H NMR (500 MHz, C_6D_6) δ 7.38 (dd,

$J_{\text{H-H}} = 7.0, 2.4$ Hz, 2H), 7.21 (d, $J_{\text{H-H}} = 7.5$ Hz, 2H), 7.16 (m, 3H), 7.09 (m, 4H), 7.02 (td, $J_{\text{H-H}} = 7.5, 0.7$ Hz, 2H), 2.39 (m, 2H, CHMe_2), 2.13 (m, 2H, CHMe_2), 1.31 (m, 12H, CHMe_2), 1.09 (dvt, 6H, CHMe_2), 0.78 (dvt, 6H, CHMe_2). $^{13}\text{C}\{^1\text{H}\}$ NMR (126 MHz, CDCl_3): δ 155.8 (m), 144.4 (s), 135.6 (s), 135.4 (td, $J_{\text{P-C}} = 13.3$ Hz, $J_{\text{C-Ag}} = 3.9$ Hz), 132.2 (s), 131.7 (m), 131.5 (t, $J_{\text{P-C}} = 10.3$ Hz), 129.6 (s), 128.3 (s), 127.9 (s), 26.5 (t, $J_{\text{P-C}} = 8.3$ Hz), 24.8 (m), 20.6 (t, $J_{\text{P-C}} = 4.0$ Hz), 20.2 (t, $J_{\text{P-C}} = 4.4$ Hz), 19.5 (s), 17.9 (s). Elem. Anal. Calcd. for $\text{C}_{30}\text{H}_{41}\text{AgBIP}_2$: C, 50.81; H, 5.83. Found: C, 50.57; H, 5.63.

NMR tube reaction to generate 202. To a solution of **201** (12 mg, 0.010 mmol) in C_6D_6 (400 μL) was added chlorotrimethylsilane (5.0 μL , 0.040 mmol), and the resulting mixture was heated at 55 $^\circ\text{C}$ overnight. The *in situ* ^1H NMR (500 MHz, C_6D_6) spectrum indicated the generation of TMSF (0.020 ppm, singlet). The volatiles were removed under vacuum, and the resulting solid was redissolved in C_6D_6 for spectroscopic analysis, showing 97% **202** in solution according to $^{31}\text{P}\{^1\text{H}\}$ NMR spectrum, and the spectroscopic details are similar to **204**. $^{31}\text{P}\{^1\text{H}\}$ NMR (121 MHz, C_6D_6): δ 36.8 (d, $J^{109}_{\text{Ag-P}} = 430$ Hz), 36.8 (d, $J^{107}_{\text{Ag-P}} = 372$ Hz). ^{11}B NMR (128 MHz, C_6D_6): δ 61.4 (br). ^1H NMR (500 MHz, C_6D_6) δ 7.39 (m, 2H), 7.26 (d, $J_{\text{H-H}} = 7.5$ Hz, 2H), 7.16 (m, 3H), 7.08 (m, 4H), 7.03 (t, $J_{\text{H-H}} = 7.1$ Hz, 2H), 2.30 (m, 2H, CHMe_2), 2.12 (m, 2H, CHMe_2), 1.34 (dvt, 6H, CHMe_2), 1.28 (dvt, 6H, CHMe_2), 1.08 (dvt, 6H, CHMe_2), 0.81 (dvt, 6H, CHMe_2).

NMR tube reaction to generate 203. To a solution of **201** (12 mg, 0.010 mmol) in C_6D_6 (400 μL) was added bromotrimethylsilane (5.0 μL , 0.040 mmol), and the resulting mixture was heated at 55 $^\circ\text{C}$ overnight. The *in situ* ^1H NMR (500 MHz, C_6D_6) spectrum indicated the generation of TMSF (0.020 ppm, singlet). The volatiles were removed under

vacuum, and the resulting solid was redissolved in C₆D₆ for spectroscopic analysis, showing at least 98% **203** in solution (¹H NMR evidence), which has similar spectroscopic details to **204**. ³¹P{¹H} NMR (202 MHz, C₆D₆): δ 35.8 (d, $J^{109}_{\text{Ag-P}} = 424$ Hz), 35.8 (d, $J^{107}_{\text{Ag-P}} = 367$ Hz). ¹¹B NMR (128 MHz, C₆D₆): δ 61.8 (br). ¹H NMR (500 MHz, C₆D₆) δ 7.39 (m, 2H), 7.24 (d, $J_{\text{H-H}} = 7.5$ Hz, 2H), 7.16 (m, 3H), 7.05 (m, 4H), 7.03 (t, $J_{\text{H-H}} = 7.4$ Hz, 2H). 2.33 (m, 2H, CHMe₂), 2.11 (m, 2H, CHMe₂), 1.31 (m, 12H, CHMe₂), 1.08 (dvt, 6H, CHMe₂), 0.80 (dvt, 6H, CHMe₂).

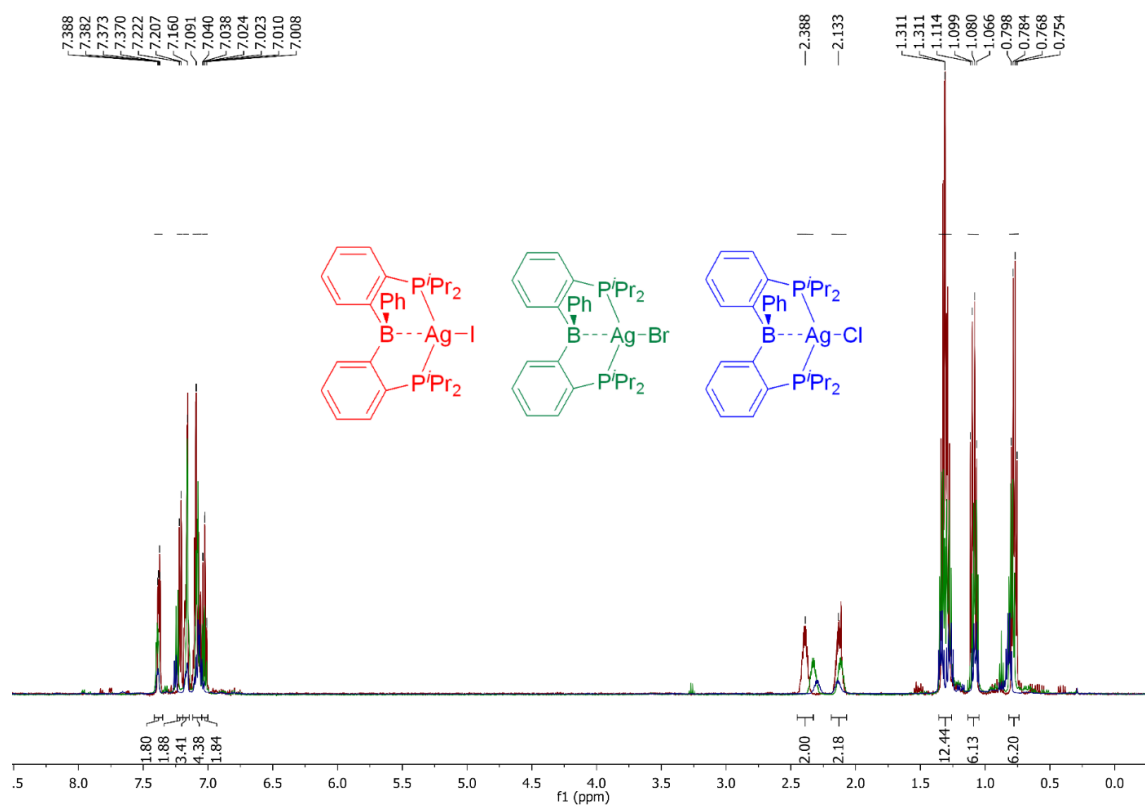


Figure II-5. ¹H NMR stacked spectrum (500 MHz, C₆D₆) of **204/203/202** in C₆D₆. Red, **204**; Green, **203**; Blue, **202**

2.4.4 X-Ray Structural Determination Details.

The X-ray crystal data (cifs) could be obtained by the follow link:
<https://doi.org/10.1039/C9DT02100K>.

X-Ray data collection, solution, and refinement for [(PB^{Ph},FP)Ag]₂ (201, CCDC 1874148). A colorless, multi-faceted block of suitable size (0.52 x 0.29 x 0.28 mm) was selected from a representative sample of crystals of the same habit using an optical microscope and mounted onto a nylon loop. Low temperature (110 K) X-ray data were obtained on a Bruker APEXII CCD based diffractometer (Mo sealed X-ray tube, K_{α} = 0.71073 Å). All diffractometer manipulations, including data collection, integration and scaling were carried out using the Bruker APEXII software.¹²² An absorption correction was applied using SADABS.¹²³ The space group was determined on the basis of systematic absences and intensity statistics and the structure was solved by direct methods and refined by full-matrix least squares on F^2 . The structure was solved in the monoclinic $P2_1/n$ space group using XS¹²⁴ (incorporated in SHELXLE). All non-hydrogen atoms were refined with anisotropic thermal parameters. All hydrogen atoms were placed in idealized positions and refined using riding model. The structure was refined (weighted least squares refinement on F^2) and the final least-squares refinement converged. No additional symmetry was found using ADDSYM incorporated in PLATON program.¹²⁵ The SQUEEZE protocol included in PLATON was used to account for disordered solvent molecules found in the crystal lattice that could not be satisfactorily modeled.¹²⁶

X-Ray data collection, solution, and refinement for (PB^{Ph}P)AgI (204, CCDC 1874150). A Leica MZ 75 microscope was used to identify a suitable colorless block with

well-defined faces with dimensions $0.467 \times 0.372 \times 0.304 \text{ mm}^3$ from a representative sample of crystals of the same habit. The crystal mounted on a nylon loop was then placed in a cold nitrogen stream (Oxford) maintained at 110 K. A BRUKER APEX 2 Duo X-ray (three-circle) diffractometer was employed for crystal screening, unit cell determination, and data collection. The goniometer was controlled using the APEX2 software suite, v2008-6.0.¹²² The sample was optically centered with the aid of a video camera such that no translations were observed as the crystal was rotated through all positions. The detector was set at 6.0 cm from the crystal sample (APEX2, 512x512 pixel). The X-ray radiation employed was generated from a Mo sealed X-ray tube ($K_{\alpha} = 0.71073 \text{ \AA}$ with a potential of 40 kV and a current of 40 mA). 45 data frames were taken at widths of 1.0° . These reflections were used in the auto-indexing procedure to determine the unit cell. A suitable cell was found and refined by nonlinear least squares and Bravais lattice procedures. The unit cell was verified by examination of the $h k l$ overlays on several frames of data. No super-cell or erroneous reflections were observed. After careful examination of the unit cell, an extended data collection procedure (15 sets) was initiated using omega scans. Integrated intensity information for each reflection was obtained by reduction of the data frames with the program APEX2.¹²² The integration method employed a three-dimensional profiling algorithm, and all data were corrected for Lorentz and polarization factors, as well as for crystal decay effects. Finally, the data was merged and scaled to produce a suitable data set. The absorption correction program SADABS¹²³ was employed to correct the data for absorption effects. Systematic reflection conditions and statistical tests of the data suggested the space group $P2_1/n$. A solution was obtained readily using

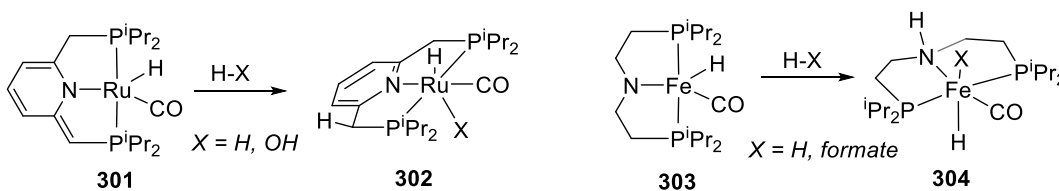
XT/XS in APEX2.^{122, 124, 127-129} Hydrogen atoms were placed in idealized positions and were set riding on the respective parent atoms. All non-hydrogen atoms were refined with anisotropic thermal parameters. Absence of additional symmetry and voids were confirmed using PLATON (ADDSYM). The structure was refined (weighted least squares refinement on F^2) to convergence.^{124, 127-130} Olex2 was employed for the final data presentation.¹³⁰

CHAPTER III

ADDITION OF O-H, N-H AND F-H BONDS ACROSS A BORYL-IRIDIUM UNIT†

3.1 Introduction

Cleavage of chemical bonds by means of metal-ligand cooperation is a burgeoning area of chemistry.¹³¹⁻¹³² The most common general motif involves the splitting of H-H and other H-X bonds utilizing a basic ligand site to accept a proton and a Lewis-acidic site at the transition metal center to accept a hydride or another X⁻ anion. These transformations are critical in many designs for the catalytic hydrogenation and dehydrogenation of polar C-O bond-containing substrates (Scheme III-1).¹³³⁻¹³⁶ The combination of a basic site on the ligand and a Lewis acidic site on the metal can be viewed as a transition metal-based frustrated Lewis pair.¹³⁷⁻¹³⁹

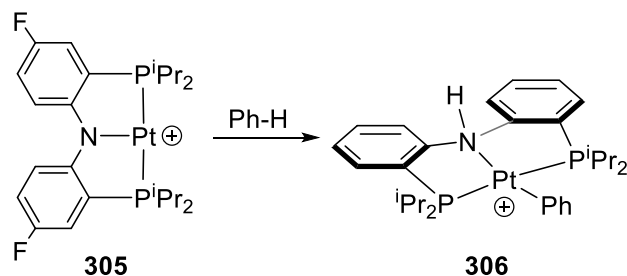


Scheme III-1. Selected H-X splitting examples relevant to hydrogenation catalysis

We recently became interested in the chemistry of metal complexes supported by a boryl/bis(phosphine) PBP pincer ligand and reported on the synthesis of complex **74**.¹⁰²

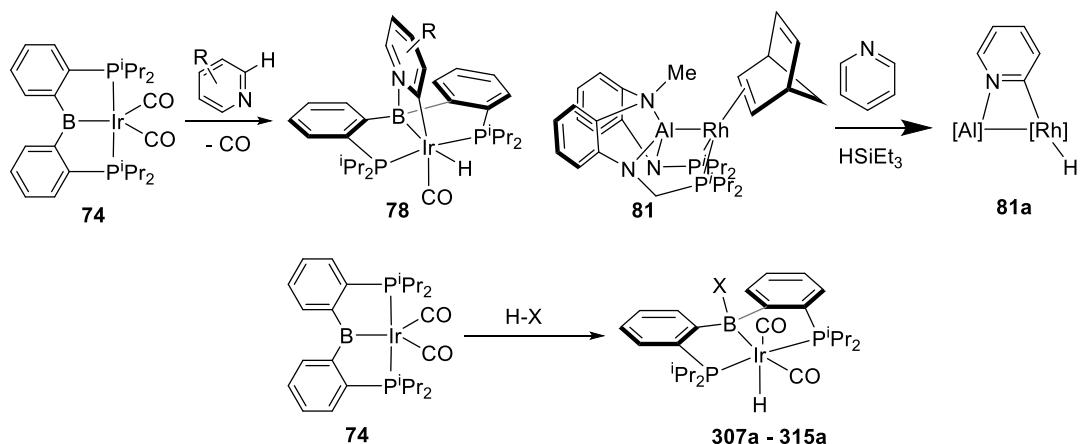
† Reproduced in whole from “Addition of O-H, N-H and F-H Bonds across a Boryl-Iridium Unit” by Cao, Y.; Shih, W.-C.; Ozerov, O. V. *Organometallics*, 2019, 38, 4076-4081. Copyright [2019] by American Chemical Society. The synthesis and crystal structure of **307a** and **316b** has been developed and solved by our former group members Dr. Wei-Chun Shih.

74 contains an electron-rich monovalent Ir center and a Lewis acidic boryl ligand, representing an inverse electronic situation from addition to PNP complexes¹⁴⁰ in Scheme III-2. Supporting ligands that contain an element directly bound to the metal that in addition acts as a non-innocent Lewis acid as opposed to a base are generally much less common.^{29, 118, 141-142} The Lewis acids in the chelating ligands typically interact with the metal or the substrate, but not both.¹⁴³⁻¹⁴⁵ We surmised that **74** should undergo cleavage of H-X bonds, depositing the proton on the basic Ir and the X⁻ anion on the boron center. Herein we present the results of this investigation with polar H-X bonds.



Scheme III-2. C-H activation utilizing Lewis-basic PNP unit in Pd complex 305

We recently reported that **74** mediates selective *ortho*-CH activation of pyridine derivatives (Scheme III-3) whereby the pyridine nitrogen is captured by the Lewis acidic boryl and the electron-rich Ir undergoes oxidative addition (after loss of CO) of an *ortho*-CH bond.³⁷ A closely related transformation was reported by Nakao et al. with a Lewis acidic aluminyl ligand on Rh.²⁹ Although the pyridine chemistry also involves the Lewis acidic non-innocence of the boryl, it is different from the presently reported findings in that the cleavage of the H-X (*ortho*-CH in pyridine) deposits both the H and the X on Ir and in that the heteroatom binding to B is not part of the X-H bond being cleaved.



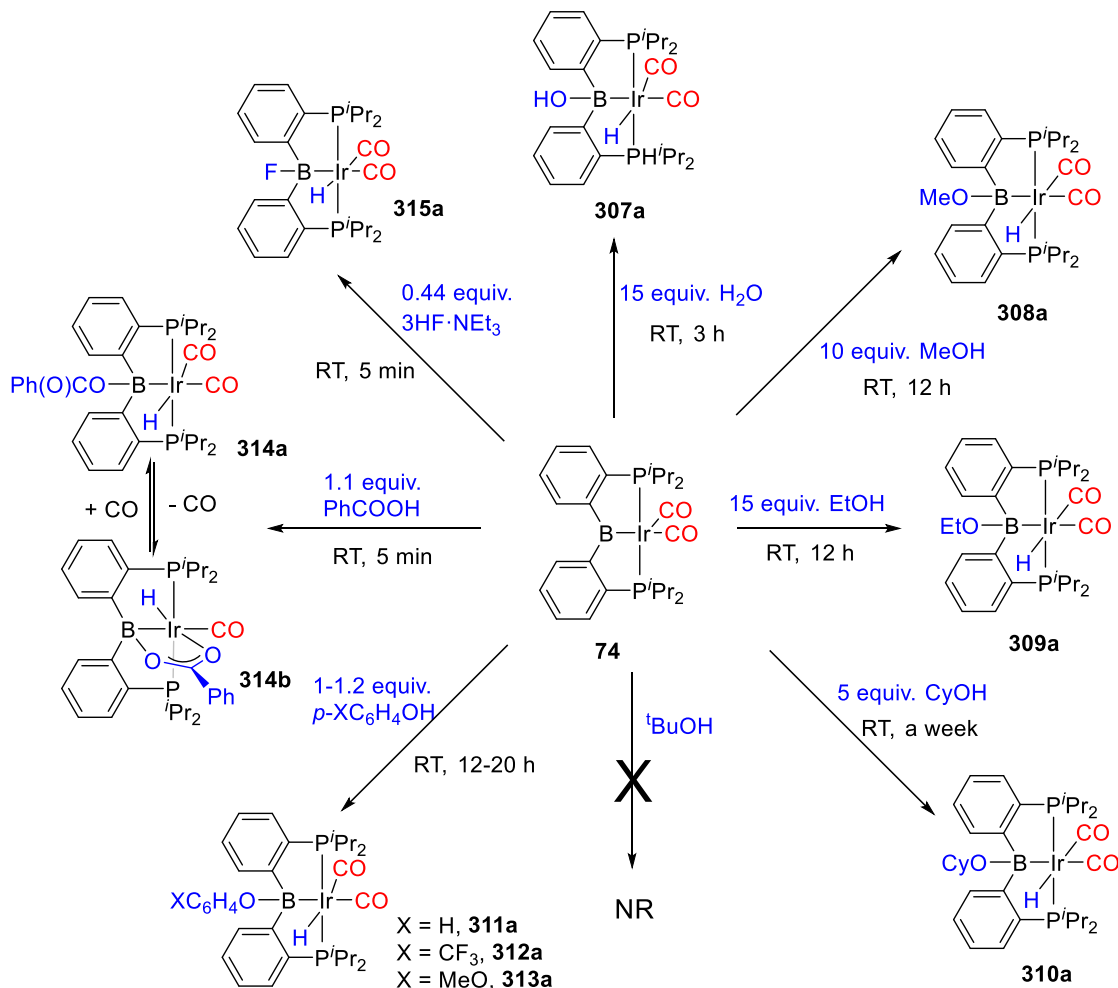
Scheme III-3. C-H activation utilizing Lewis-acidic (PBP or PAIP) non-innocent pincer ligand and H-X cleavage utilizing Lewis-acidic PBP

3.2 Result and Discussion

3.2.1 O-H and F-H Cleavage Reactions

First, we investigated reactions with substrates containing O-H bonds, summarized in Scheme III-4. Reactions of **74** with water, methanol, ethanol, cyclohexanol and $p\text{-XC}_6\text{H}_4\text{OH}$ ($\text{X} = \text{H}, \text{CF}_3, \text{or OMe}$) proceeded to completion at ambient temperature or at $50\text{ }^\circ\text{C}$ (for PhOH), generating pale-yellow compounds **307a-313a**. Compounds **307a**, **309a** and **311a** were isolated and fully characterized, whereas **308a**, **310a**, **312a**, and **313a** were only observed in situ. On the other hand, thermolysis of **74** with $t\text{BuOH}$ for 2 d at $50\text{ }^\circ\text{C}$ did not form an analogous product (94% **74** remained unreacted). Reactions of **74** with 1.1 equiv of benzoic acid or 0.44 equiv. $\text{Et}_3\text{N}\cdot 3\text{HF}$ resulted in immediate color change and were judged to be complete in <5 min at ambient temperature based on NMR evidence. The reaction with PhCOOH produced a 95:5 mixture of **314a** and **314b**. Addition of 1 atm of CO to this mixture permitted formation of pure **314a**, whereas subjecting a similar mixture to dynamic vacuum and isolation by recrystallization yielded

pure **314b** (See section 3.4.3 for details). The reaction with Et₃N•3HF yielded only a single product **315a**. It is interesting to note that under the conditions of the experiments in Scheme III-4, the diarylboryl moiety appears to be resistant to protolysis of the boron-carbon bonds, in contrast to metal boryls with heteroatom substituents.¹⁴⁶⁻¹⁴⁷

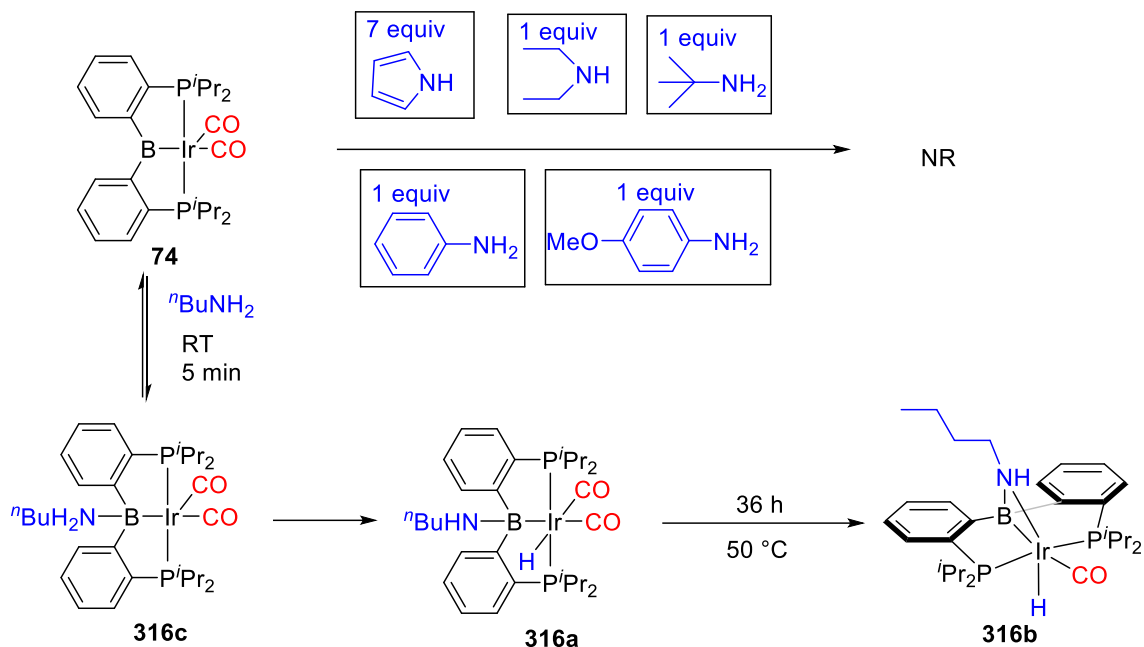


Scheme III-4. Addition of O–H, and F–H bonds across iridium–boryl unit of 74

3.2.2 N–H Cleavage Studies.

Probing the potential N–H addition, it was determined (NMR evidence) that no reaction took place after diethylamine, *t*-butylamine, aniline, *p*-anisidine or pyrrole (1-7

equiv.) were individually added to C₆D₆ solutions of **74** and heated at 50 °C for 12 h (Scheme III-5). In contrast, addition of 2.5 equiv. of *n*-butylamine to the dark-red solution of **74** resulted in an immediate lightening of the color. The ³¹P{¹H} NMR spectra taken within 5 min of mixing show two signals. One was tentatively identified as **316a** (7%) based on the similarity of the NMR spectroscopic features with **307a-315a** (vide infra). The other was interpreted as a time- and weight-averaged signal for **74** and **316c** in rapid equilibrium. IR spectroscopy of this mixture (the signals of **316a** were obscured) indicated the presence of two pairs of overlapping bands, one of which belongs to **74** and the other we assign to **316c**. **316c** possesses CO stretching frequencies quite similar to the DMAP adduct of **74** we characterized previously.³⁷ The fraction of **316c** increased with a higher concentration of ⁿBuNH₂ added as evidenced by the relative increase in intensity of the IR bands of **316c** and the more upfield shift of the average ¹¹B NMR resonance (details in section 3.4.3.3). Following thermolysis of the mixture resulting from the treatment of **74** with ⁿBuNH₂ and workup, **316b** was isolated in a pure form.



Scheme III-5. Addition of O–H, N–H, F–H bonds across iridium–boryl unit of 74

3.2.3 Spectroscopic Characterization

Products **307a-315a** show spectroscopic characteristics consistent with possessing analogous structures resulting from the addition of an X–H bond across the B–Ir unit (Table III-1). Each displays an Ir–H resonance in the narrow -11.2 to -11.5 ppm region of their ^1H NMR spectra, and a ^{31}P NMR resonance in the likewise narrow 50.1-55.4 ppm range. The presence of a signal between 12.6-22.9 ppm in the $^{11}\text{B}\{^1\text{H}\}$ NMR spectra indicates sp^3 hybridization for the boron in **307a-316a**. These compounds also display two CO stretching bands of approximately equal intensity in their IR spectra, consistent with the *cis*-dicarbonyl nature. The hydride is thus disposed *trans* to one of the CO ligands in **307a-316a**. In principle, both *syn*- and *anti*-isomers are conceivable with respect to the orientation of Ir–H vs B–X. Based on the very high degree of similarity of the

spectroscopic data, we assume that all of **307a-316a** are *anti*-isomers based on the structural determination for **309a** (vide infra).

Table III-1. Spectral data for all the products

Compound number	¹ H NMR (Ir-H) (ppm)	¹¹ B NMR (ppm)	³¹ P NMR (ppm)	ν_{CO} (cm ⁻¹)
307a	-11.24	19.7	54.4	2001; 1957
308a	-11.50	23.5	53.9	2006; 1961
309a	-11.50	22.9	53.6	2004; 1958
310a	-11.56	25.0	50.1	2007; 1976
311a	-11.35	15.7	53.9	2021; 1976
312a	-11.35	15.7	53.9	2030; 1985
313a	-11.34	16.6	53.9	2027; 1981
314a	-11.24	12.6	53.6	2028; 1981
314b	-22.44	26.5	60.0	1953
315a	-11.36	18.6	55.4	2019; 1979
316a	-11.31	21.0	54.0	- ^a
316b	-17.68	9.6	56.0; 48.6	1927
316c	NA	See section ^b	See section ^b	1922 ^c ; 1881
317a	-11.11	95.0	55.2	2078; 2032

^a Only 7% **316a** generated in situ, IR bands not detected. ^b At ambient temperature, a weighted average of the equilibrium mixture **74** and **316c** was observed. ^c This band overlaps with one of the bands for **74**.

A single ¹H NMR Ir-H signal at a higher field than for **307a-316a** was detected for each of **314b** (-22.44 ppm) and **316b** (-17.68 ppm). We interpret this as supportive of a hydride *trans* to a donor (O or N) of weaker *trans* influence compared to CO. Resonances at 26.5 ppm for **314b** and 9.6 ppm for **316b** in the ¹¹B{¹H} NMR spectrum substantiate a four-coordinate boron center. The presence of only a single CO stretch in the IR spectra of **314b** or **316b** confirms their monocarbonyl structure. In addition, the C₁ symmetry of the NMR spectra of **316b** is consistent with the presence of a four-coordinate nitrogen as a chiral center.

3.2.4 X-ray Diffraction Studies

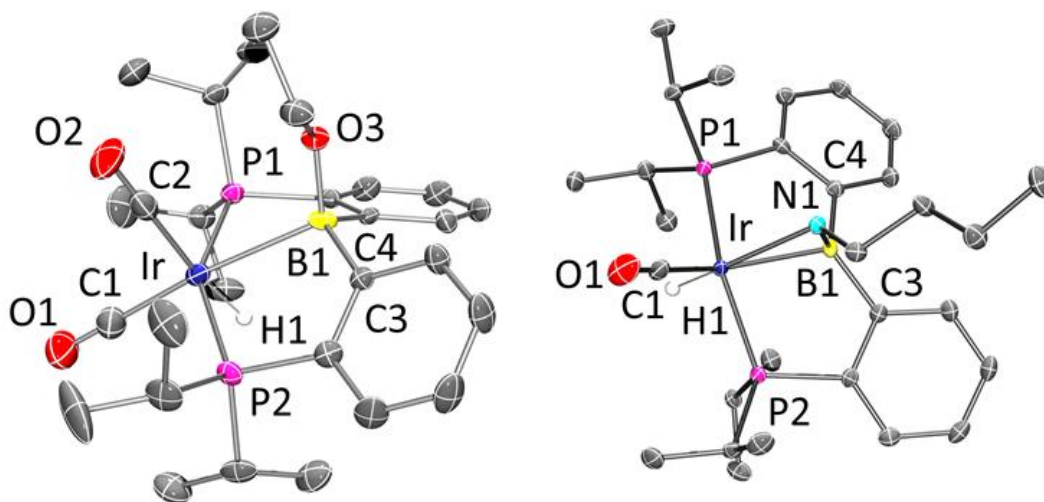


Figure III-1. POV-Ray rendition of the ORTEP drawing (50% thermal ellipsoids) of 309a and 316b showing selected atom labeling. Hydrogen atoms are omitted except Ir-H for clarity. Selected bond distances (Å) and angles (°) for 309a: Ir-C1, 1.978(8); Ir-C2, 1.883(7); Ir-B1, 2.479(8); Ir-P1, 2.330(2); Ir-P2, 2.307(2); Ir-H1, 1.4350(8); B1-O3, 1.466(8); C1-O1, 1.15(1); P1-Ir-P2, 150.04(6); C3-B1-Ir, 108.0(4); C3-B1-C4, 114.9(5); C4-B1-Ir, 104.2(4). Selected bond distances (Å) and angles (°) for 316b: Ir-C1, 1.906(4); Ir-P1, 2.2907(8); Ir-P2, 2.2714(8); Ir-H1, 1.31(3); Ir-B1, 2.272(4); Ir-N1, 2.176(2); C1-O1, 1.146(5); B1-N1, 1.516(4); P1-Ir-P2, 138.47(3); Ir-B1-C3, 115.8(13); Ir-B1-C4, 113.4(2); C3-B1-C4, 122.0(3)

Solid-state structures of **309a** and **316b** were determined by X-ray diffractometry on suitable single crystals (Figure III-1). Both structures can be viewed as distorted octahedral about Ir, with the N donor in **316b** taking the place of the “missing” carbonyl. The structure of **309a** can be analyzed as arising from the Ir→B interaction of the IrXL₄ fragment with a Z-type borane. The Ir-B distance of 2.479(8) Å in **309a** is expectedly longer than the Ir-B_{boryl} distance in **74** (2.137(3) Å)¹⁰² or the typical Ir-Bpin (pin = pinacolate) distances of 2.02-2.07 Å.¹⁴⁸⁻¹⁵⁰ However, it is also considerably longer than is typical for Ir→BR₃ (or Rh→BR₃) interactions recorded in related complexes with the Z-

type borane being a part of a chelating ligand.^{46, 67-70} Nonetheless, other considerations strongly support the presence of an Ir→B interaction in **309a**. The ¹¹B NMR chemical shift of 22.9 ppm is upfield of that for Ph₂BOEt (45.1 ppm)¹⁵¹ as a reference for a free diarylalkoxyborane. The B-O distance in **309a** (1.466(8) Å) is similar to the B-O distance in **3B** (1.4542(16) Å, Figure III-2)¹⁵², an amine adduct of a diarylalkoxyborane and considerably longer than that in ferrocenyl boronate **3A** (1.365(2) Å)¹⁵³ with an sp² hybridized boron. The sum of non-iridium angles about the boron center in **309a** is ca. 332.8°, in line with the values in related Z-type borane complexes.^{46, 70, 143, 151}

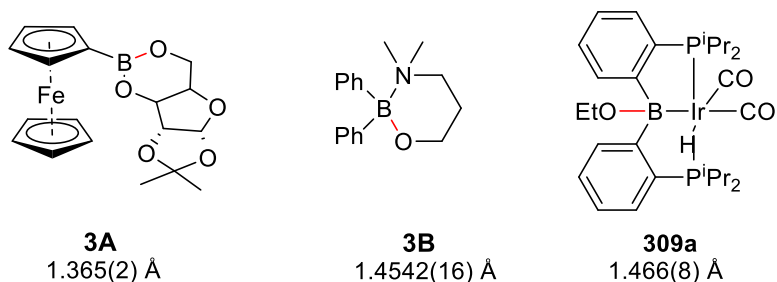


Figure III-2. Comparison of B–O bond distances

For the structure of **316b**, three idealized arrow representations can be conceived (Figure III-4): 1) the amido-Ir fragment donating to a boryl-Ir Lewis acid (**3F**), 2) the aminoborane as a Z-type acceptor at B and an L donor via N (**3G**), and 3) a complex of the B=N π -bond or aminoborane (**3H**), i.e., a “borataimmonium.”¹⁵⁴⁻¹⁵⁶ These are not isomers but rather different “dramatizations” of a description of the same structure.¹⁵⁷ In addition, representation **3G** may be viewed as a dramatization of the necessarily dissymmetric bonding/back-bonding interaction depicted in the representation **3H**. The ¹¹B NMR chemical shift of **316b** (9.6 ppm) indicates a sp³-hybridized boron. The Ir–B

distance (2.272(4) Å) is squarely in the range of Ir→B Z-type complexes. The Ir-N distance in **316b** (2.176(2) Å) is considerably longer than the typical Ir-N_{amido} distances^{148, 158-161} but is in the range for Ir-N_{amine} structures. For example, Ir-N distances in the complexes of the [(^tBu₂PCH₂CH₂)₂NH] ligand are ca. 2.2 Å.¹⁶²⁻¹⁶⁴ The B-N distance in **316b** (1.516(4) Å) is notably shorter than the B-N distances in **3C** (1.613(3) Å)³⁷ or **3D** (1.582(3) Å)¹⁶⁵, even though **316b** contains a sp³, not a sp² nitrogen. While it is longer than the B-N bond in a pyrrolyl-substituted three-coordinate boron in **3E** (1.472(7) Å)¹⁶⁶, the B-N, Ir-N, and the Ir-B distances appear to be more consistent with the representation **3G**. On the other hand, consideration of the pyramidalization at B is less clear cut. The sum of non-Ir angles about B is ca. 348.4°, whereas the sum of non-nitrogen angles about B is similar at 351.2°. Both values suggest low pyramidalization but undoubtedly, in part this is a geometric consequence of the acute B/Ir/N triangle.

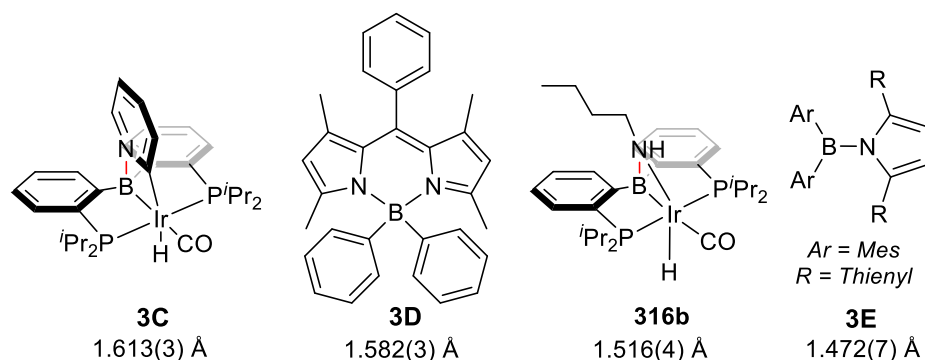


Figure III-3. Comparison of B–N bond distances

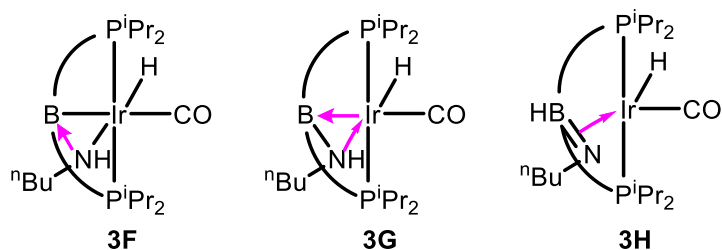


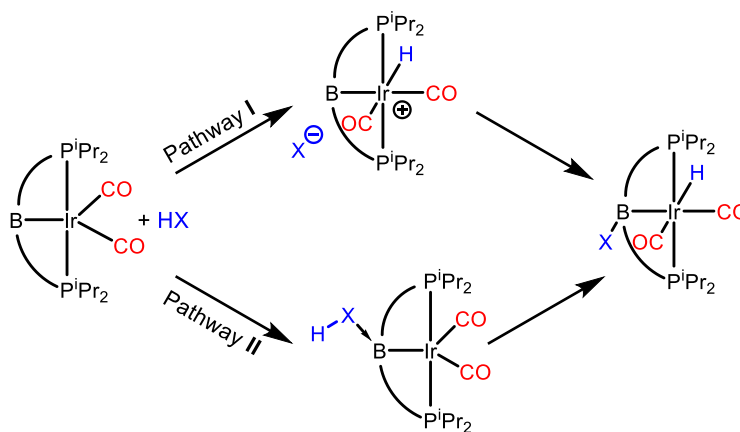
Figure III-4. Plausible representations of the structure of 316b

3.2.5 Mechanistic Considerations

The faster apparent reactions with PhCOOH vs phenol or alcohols, and the lack of reaction with the weakest O-H acid tested (*t*BuOH) suggested the Brønsted acidity of ROH is important for the rate of the reaction. Confirming this notion, in separate comparative experiments, it was observed that 1) the reaction of **74** with EtOH was faster than with cyclohexanol 2) the reaction with *p*-F₃CC₆H₄OH was faster than with PhOH, which was faster than with *p*-MeOC₆H₄OH. We surmised that the reaction with ROH substrates might be initiated via the initial protonation of the Ir center in **74** by ROH (pathway I in Scheme III-6). This seemed plausible based on the studies by Brookhart et al.¹⁶⁷ that showed that protonation of a (POCOP)IrCO (another neutral, monovalent Ir pincer/carbonyl complex) by water or lower alcohols was kinetically relevant. In support of this proposal, we prepared compound **317a** by protonation of **74** with [(Et₂O)₂H][B(C₆F₅)₄]. It displays a ¹H NMR Ir-H resonance at a similar frequency to **307a-316a**, and a pair of CO stretching bands in the IR spectrum. However, in contrast to **307a-316a**, **317a** gives rise to a ¹¹B NMR chemical shift (95 ppm) indicative of a sp² hybridization at B and to IR CO stretching bands at considerably higher energies. The ¹¹B NMR chemical shift was unchanged upon dissolution of **317a** in THF. These data

show that protonation of Ir in **74** is not accompanied by coordination of either the anion or the ethereal solvents to **317a**.

In order to estimate the acidity of **317a** and thus the basicity of **74**¹⁶⁸, **317a** was treated with ca. 2 equiv. of Et₃N or ⁱPr₂NEt in THF. This resulted in partial deprotonation (2% and 5%, respectively) to **74**, suggesting that **74** is more basic than trialkylamines by about an order of magnitude of K_B. Such basicity is very much in line with a proposal of rate-limiting protonation of **74** by ROH in the reactions of O-H cleavage.



Scheme III-6. Proposed mechanisms for the X-H splitting

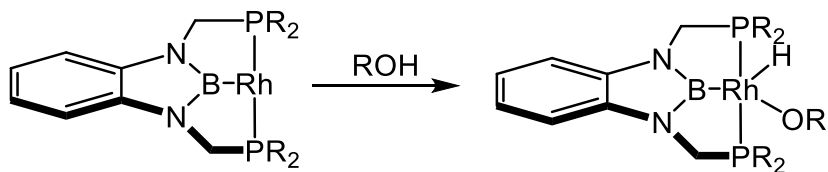
We further surmised that if **317a** is an intermediate in the reactions of **74** with ROH, then it may also serve as a catalyst for these reactions. Indeed, we discovered that reaction of **74** with 5 equiv. of cyclohexanol was accelerated by the addition of 0.075 equiv. of **317a** (67% vs 33% conversion after 15 h at RT). Similarly, when **74** was allowed to react with 10 equiv. of ^tBuOH in the presence 0.075 equiv. of **317a**, after 1 week at RT, 11% conversion to a new product was observed. However, the observed selected NMR resonances did not match those of **307a-316a** closely enough, and the low

content prevent a more complete identification for a confident assignment. Thermolysis of this mixture at 50 °C or higher, and/or using pure tert-butyl alcohol as solvent led to the generation of complex mixtures of unidentified compounds, and thus we were unable to achieve full conversion to, or isolation of the new product.

It must be concluded that pathway I (Scheme III-6) is not a plausible mechanism for the formation of N-H cleavage products tested in this study because the N-H acidity of these substrates is clearly insufficient. We propose that cleavage of the N-H bond in ⁿBuNH₂ instead takes place via initial coordination of the nitrogen lone pair to B (pathway II) and subsequent proton transfer to Ir. The nature of the proton transfer step is not clear at this point – it may proceed intramolecularly, or with assistance from an external base. We cannot rule out a concerted splitting of the N-H bond across B-Ir but given the observation of **316c** and the great disparity in N-H and B-Ir bond lengths, it seems rather unlikely. The lack of reactivity with the N-H substrates other than ⁿBuNH₂ can be ascribed to the lower favorability of their coordination to B – either because of lower basicity (e.g., anilines and pyrrole) or the apparently prohibitive steric encumbrance (^tBuNH₂ or Et₂NH).

317a as an intermediate in O-H cleavage means that the reaction is not concerted and kinetic selectivity for the *syn*-geometry for **307a-316a** should not be expected. Thus, the *anti*-geometry in the solid-state structure of **309a** and presumably all of **307a-316a** is not surprising. In addition, we determined that **317a** undergoes ready exchange with free CD₃OD (leading to the formation of **317a-d₁** with an Ir-D), and with **308-d₄** derived from the addition of CD₃OD to **74** (leading to the observation of **317a-d₁** and CD₃OH). These experiments suggest that the O-H cleavage products under the reaction conditions may

exchange protons (from Ir-H) and/or RO groups (from B-OR), potentially providing a path to the equilibration of the putative *syn*- and *anti*-isomers of **307a-316a**. With regard to the formation of **316c**, it is possible that the proton transfer (Scheme III-6) is not intramolecular, and thus there may also be no reason to expect kinetic selectivity for the *syn*- isomer. It is also possible that *syn*-/*anti*- equilibration pathways are available to **316c**. The *anti*-monocarbonyl final product of N-H cleavage (**316b**) clearly forms via a sequence of multiple events which we have not established in full detail. It is thus not clear whether the *anti*-geometry of **316b** is a consequence of the initial *anti*-selective formation of **316c** or follows from some other considerations.



Scheme III-7. Reactivity of the Yamashita/Nozaki diaminoboryl (PBP)Rh fragment with certain alcohols and phenols

The reactivity of **74** with O-H bonds contrasts with that observed by Yamashita and Nozaki in the reactions of their (PB*P)Rh fragment (Scheme III-7). Yamashita and Nozaki observed or proposed⁹²⁻⁹³ oxidative addition of the O-H bond to the Rh center (i.e., O binding to Rh) in reactions with alcohols and phenols instead of the 1,2-addition described in the present paper, with O binding to boron. The difference presumably arises from the saturated nature of the Ir center in **74** contrasted with the unsaturated Rh center in the (PB*P)Rh fragment. The boron of the boryl ligand is a relatively weak Lewis acid and the Ir center in **74** can only function as a base, but not as a Lewis acid.

3.3 Conclusion

In summary, we have demonstrated that polar X-H (X = F, O, N) bonds can be split across the boryl-iridium unit in the pincer complex **74**. Mechanistic studies suggest that for O-H bonds, the reaction proceeds via initial protonation of **74** by ROH, with subsequent capture of the RO⁻ anion. Among the tested amines, only the small ⁿBuNH₂ gave products of N-H cleavage. This reaction is ostensibly initiated by the binding of the neutral amine to the Lewis acidic boron of the Ir boryl complex.

3.4 Experimental Section

3.4.1 General Considerations

Unless specified otherwise, all manipulations were performed under an Ar atmosphere using standard Schlenk line or glovebox techniques. Toluene, tetrahydrofuran (THF), and pentane were dried and deoxygenated (by purging) using a solvent purification system (Innovative Technology Pure Solv MD-5 Solvent Purification System) and stored over molecular sieves in an Ar-filled glove box. C₆D₆ was dried over NaK/Ph₂CO/18-crown-6, distilled and stored over molecular sieves in an Ar-filled glovebox. C₆D₅Br and fluorobenzene were dried over CaH₂, vacuum transferred and stored over molecular sieves in an Ar-filled glove box. Alcohols and amines were vacuum transferred and stored over molecular sieves in an Ar-filled glove box. **74** and **70** were prepared via literature procedures.^{27, 102} All other chemicals were used as received from commercial vendors.

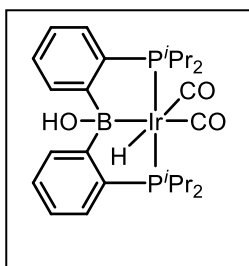
3.4.2 Physical Methods

NMR spectra were recorded on Varian Inova 400 (¹¹B NMR, 128.185 MHz), Bruker 400MHz (¹¹B NMR, 128.185 MHz, ¹H NMR, 399.535 MHz; ³¹P NMR, 161.734

MHz) and Varian Inova 500 (^1H NMR, 499.703 MHz; ^{13}C NMR, 125.697 MHz; ^{31}P NMR, 202.265 MHz, ^{11}B NMR, 160.231 MHz) spectrometer. Chemical shifts are reported in δ (ppm). For ^1H and ^{13}C NMR spectra, the residual solvent peak was used as an internal reference (^1H NMR: δ 7.16 for C_6D_6 , 7.28 for $\text{C}_6\text{D}_5\text{Br}$ *meta* proton; ^{13}C NMR: δ 128.62 for C_6D_6 , 122.4 for $\text{C}_6\text{D}_5\text{Br}$ *ipso* carbon). ^{11}B NMR spectra were referenced externally with BF_3 etherate at δ 0. ^{31}P NMR spectra were referenced externally with 85% phosphoric acid at δ 0. ^{19}F NMR spectra were referenced with pure trifluoro acetic acid to δ -78.5 ppm. Elemental analyses were performed by CALI Labs, Inc. (Highland Park, NJ)

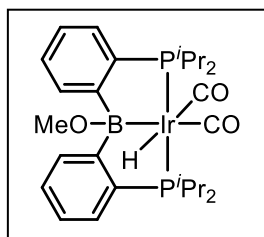
3.4.3 Synthesis and Characterization of Iridium Complexes

3.4.3.1 O–H Cleavage



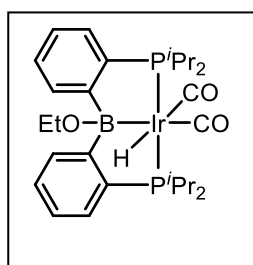
(PB^{OH}P)Ir(H)(CO)₂ (307a). In a 25 mL Schlenk flask, water (27 μL , 1.5 mmol) was added to a THF solution (1.0 mL) of **74** (65 mg, 0.10 mmol). After stirring at room temperature for 3 h, the solution color changed from dark red to pale yellow. The volatiles were removed under vacuum, and yellow solid was obtained. The sample was recrystallized in toluene/pentane mixture (1/10) in a -35 $^\circ\text{C}$ freezer overnight, yielding yellow crystals (62 mg, 93%). ATR-IR: ν_{CO} 2001, 1957 cm^{-1} $\nu_{\text{Ir-H}}$ 2113 cm^{-1} . ^1H NMR (500 MHz, C_6D_6) δ 7.88 (d, $J_{\text{H-H}} = 7.4$ Hz, 2H), 7.24 (m, 2H), 7.10 (m, 2H), 7.05 (m, 2H), 2.69 (m, 2H, CHMe_2), 2.19 (m, 2H, CHMe_2), 1.88 (s, 1H, OH), 1.07 (m, 12H, CHMe_2), 0.98 (dvt, $J_{\text{H-H}} \approx J_{\text{H-P}} = 6.9$ Hz, 6H, CHMe_2), 0.66 (dvt, $J_{\text{H-H}} \approx J_{\text{H-P}} = 7.1$ Hz, 6H, CHMe_2), -11.24 (t, $J_{\text{H-P}} = 15.6$ Hz, 1H, Ir-H). $^{31}\text{P}\{^1\text{H}\}$ NMR (202 MHz, C_6D_6): δ 54.4. $^{11}\text{B}\{^1\text{H}\}$ NMR (128 MHz, C_6D_6): δ 19.7. $^{13}\text{C}\{^1\text{H}\}$ NMR (126 MHz, C_6D_6) δ 182.3 (s, CO), 171.6 (s, CO), 169.7 (br

s, C-B), 143.0 (vt, $J_{P-C} = 28.7$ Hz), 132.3 (vt, $J_{P-C} = 10.9$ Hz), 130.1 (s), 128.7 (m), 126.0 (vt, $J_{P-C} = 3.9$ Hz), 30.6 (vt, $J_{P-C} = 14.0$ Hz, $CHMe_2$), 27.9 (vt, $J_{P-C} = 17.7$ Hz, $CHMe_2$), 20.7 (s, $CHMe_2$), 20.6 (s, $CHMe_2$), 20.1 (s, $CHMe_2$), 19.0 (s, $CHMe_2$).



(PB^{OMe}P)Ir(H)(CO)₂ (308a). In a J. Young tube, methanol (16 μ L, 0.40 mmol) was added to a THF solution (2.0 mL) of **74** (26 mg, 0.040 mmol). After stirring at room temperature for 12 h, the solution color changed from dark red to pale yellow. The volatiles

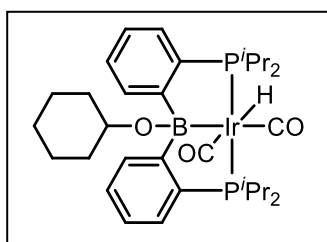
were removed under vacuum, and yellow solid was obtained. The sample was dissolved in C_6D_6 for spectral characterization. ATR-IR: ν_{CO} 2006, 1961 cm^{-1} . 1H NMR (400 MHz, C_6D_6): δ 7.84 (d, $J_{H-H} = 7.5$ Hz, 2H), 7.24 (t, $J_{H-H} = 7.3$ Hz, 2H), 7.13 (m, 2H), 7.05 (m, 2H), 3.47 (s, 3H, OCH_3), 2.67 (m, 2H, $CHMe_2$), 2.23 (m, 2H, $CHMe_2$), 1.14 (m, 12H, $CHMe_2$), 1.00 (dvt, $J_{H-H} \approx J_{H-P} = 7.1$ Hz, 6H, $CHMe_2$), 0.66 (dvt, $J_{H-H} \approx J_{H-P} = 7.1$ Hz, 6H, $CHMe_2$), -11.50 (t, $J_{H-P} = 15.1$ Hz, 1H, Ir-H). $^{31}P\{^1H\}$ NMR (202 MHz, C_6D_6): δ 53.9. $^{11}B\{^1H\}$ NMR (160 MHz, C_6D_6): δ 23.5. $^{13}C\{^1H\}$ NMR (101 MHz, C_6D_6): δ 181.0 (s, CO), 170.9 (s, CO), 143.9 (vt, $J_{P-C} = 28.9$ Hz), 132.4 (vt, $J_{P-C} = 10.9$ Hz), 129.7 (s), 125.6 (vt, $J_{P-C} = 3.9$ Hz), 55.3 (s, OCH_3), 30.9 (vt, $J_{P-C} = 14.0$ Hz, $CHMe_2$), 28.0 (vt, $J_{P-C} = 17.6$ Hz), 20.8 (s, $CHMe_2$), 20.6 (s, $CHMe_2$), 20.0 (s, $CHMe_2$), 19.4 (s, $CHMe_2$).



(PB^{OEt}P)Ir(H)(CO)₂ (309a). In a 25 mL Teflon screw-capped round-bottomed flask, ethanol (70 mg, 1.6 mmol) was added to a toluene solution (2.0 mL) of **74** (65 mg, 0.10 mmol). After stirring at room temperature overnight, the solution color changed from dark

red to pale yellow. The volatiles were removed under vacuum, and yellow solid was

obtained. The sample was recrystallized in toluene/pentane mixture (1/3) in a -35 °C freezer overnight, yielding orange crystals (60 mg, 87%). ATR-IR: ν_{CO} 2004, 1958 cm^{-1} . ^1H NMR (500 MHz, C_6D_6): δ 7.86 (d, $J_{\text{H-H}} = 7.5$ Hz, 2H), 7.24 (t, $J_{\text{H-H}} = 7.1$ Hz, 2H), 7.13 (m, 2H), 7.05 (m, 2H), 3.62 (q, $J_{\text{H-H}} = 6.9$ Hz, 2H, OCH_2CH_3), 2.75 (m, 2H, CHMe_2), 2.24 (m, 2H, CHMe_2), 1.29 (t, $J_{\text{H-H}} = 6.9$ Hz, 3H, OCH_2CH_3), 1.17 (m, 12H, CHMe_2), 1.00 (dvt, $J_{\text{H-H}} \approx J_{\text{H-P}} = 7.1$ Hz, 6H, CHMe_2), 0.66 (dvt, $J_{\text{H-H}} \approx J_{\text{H-P}} = 7.1$ Hz, 6H, CHMe_2), -11.50 (t, $J_{\text{H-P}} = 15.2$ Hz, 1H, Ir-H). $^{31}\text{P}\{^1\text{H}\}$ NMR (202 MHz, C_6D_6): δ 53.6. $^{11}\text{B}\{^1\text{H}\}$ NMR (128 MHz, C_6D_6): δ 22.9. $^{13}\text{C}\{^1\text{H}\}$ NMR (101 MHz, C_6D_6): δ 180.8 (s, CO), 170.5 (s, CO), 167.0 (br), 143.4 (vt, $J_{\text{P-C}} = 29.2$ Hz), 131.9 (vt, $J_{\text{P-C}} = 10.8$ Hz), 129.0 (s), 128.6 (s), 125.0 (vt, $J_{\text{P-C}} = 3.9$ Hz), 61.7 (s, OCH_2CH_3), 30.3 (vt, $J_{\text{P-C}} = 14.0$ Hz, CHMe_2), 27.5 (vt, $J_{\text{P-C}} = 17.5$ Hz), 20.2 (s, CHMe_2), 20.0 (s, CHMe_2), 19.5 (s, CHMe_2), 18.8 (s, CHMe_2), 18.4 (s, OCH_2CH_3). Elem. Anal. Calcd for $\text{C}_{28}\text{H}_{42}\text{BIrO}_3\text{P}_2$: C, 48.63; H, 6.12. Found: C, 49.15; H, 6.12.



In situ observation of cyclohexanol addition product

(310a). In a J. Young tube was added **74** (0.020 mmol, 0.20 mL, 0.10 M in C_6D_6), cyclohexanol (0.10 mmol, 0.20 mL, 0.50 M in C_6D_6), and 1,4 dioxane (0.020 mmol, 0.10 mL, 0.20 M in

C_6D_6). The reaction mixture was stirred at room temperature for 5 days to completion, which was monitored by $^{31}\text{P}\{^1\text{H}\}$ NMR spectroscopy. **310a.** ATR-IR: ν_{CO} 2007, 1976 cm^{-1} . $^{31}\text{P}\{^1\text{H}\}$ NMR (162 MHz, C_6D_6): δ 50.1. $^{11}\text{B}\{^1\text{H}\}$ NMR (160 MHz, C_6D_6): δ 25.0. ^1H NMR (400 MHz, C_6D_6): δ 8.04 (d, $J_{\text{H-H}} = 7.5$ Hz, 2H), 7.23 (t, $J_{\text{H-H}} = 7.3$ Hz, 2H), 7.13 (m, 2H), 7.02 (t, $J_{\text{H-H}} = 7.4$ Hz, 2H), , 3.67 (m, 1H, B-O-CH), 2.63 (m, 2H, CHMe_2), 2.27

(m, 2H, CHMe_2), 0.99 (dvt, $J_{\text{H-H}} = 8.6$ Hz, $J_{\text{H-P}} = 7.0$ Hz, 6H, CHMe_2), 0.69 (dvt, $J_{\text{H-H}} = 8.8$ Hz, $J_{\text{H-P}} = 7.0$ Hz, 6H, CHMe_2), -11.56 (t, $J_{\text{H-P}} = 15.2$ Hz, 1H), Peaks overlap with free cyclohexanol.

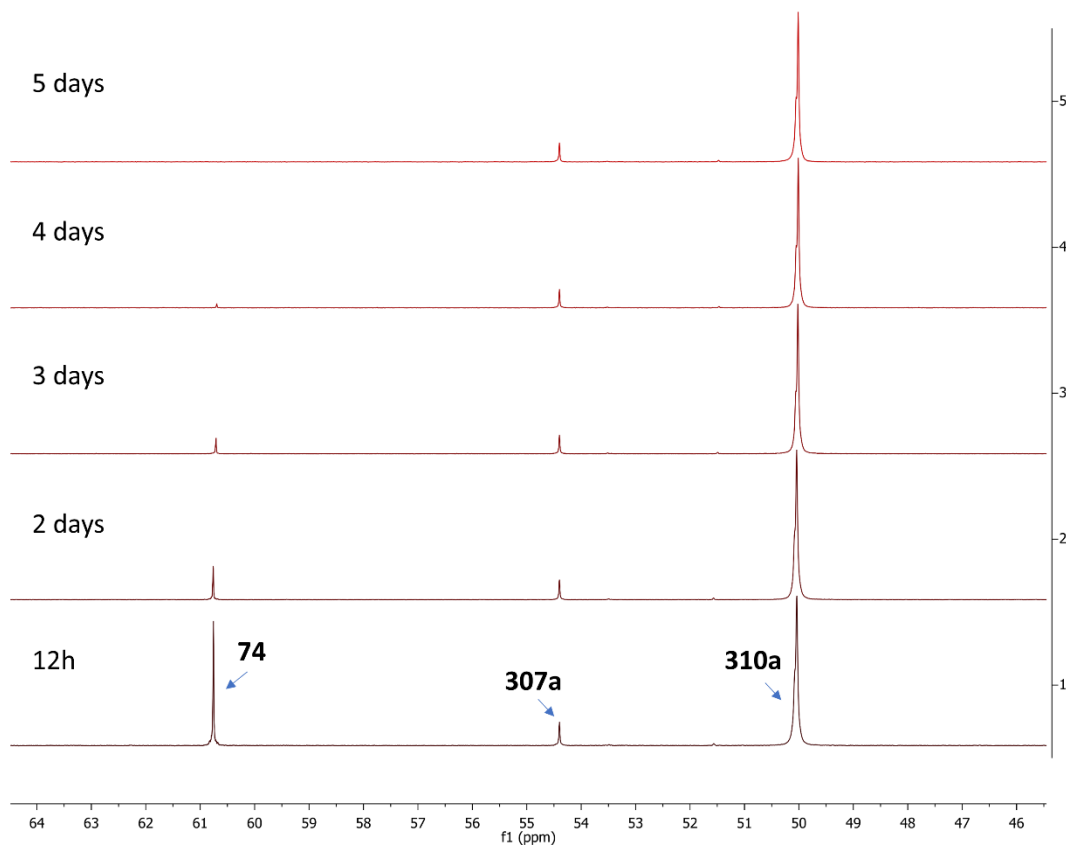


Figure III-5. $^{31}\text{P}\{^1\text{H}\}$ NMR spectra recorded for **74** (0.040 M), cyclohexanol (0.20 M), and 1,4 dioxane (0.040 M) mixture after a certain period of time at room temperature

Attempted reaction of **74 with *tert*-butyl alcohol.** In a J. Young tube, to a solution of **74** (51 mg, 0.080 mmol) in 0.40 mL C_6D_6 was added *tert*-butyl alcohol (8.0 μL , 0.083 mmol). After 12 h at room temperature, no color change was observed, and no change was observed by $^{31}\text{P}\{^1\text{H}\}$ NMR spectroscopy. The mixture was heated at 50 $^\circ\text{C}$ for 48 h. No color change was observed, and 94% of the starting material was intact (room

temperature $^{31}\text{P}\{^1\text{H}\}$ NMR evidence). The same mixture was further heated at 100 °C for 12 h, multiple compounds were generated, and none of them show similarity of NMR spectroscopic features to **307a–315a**.

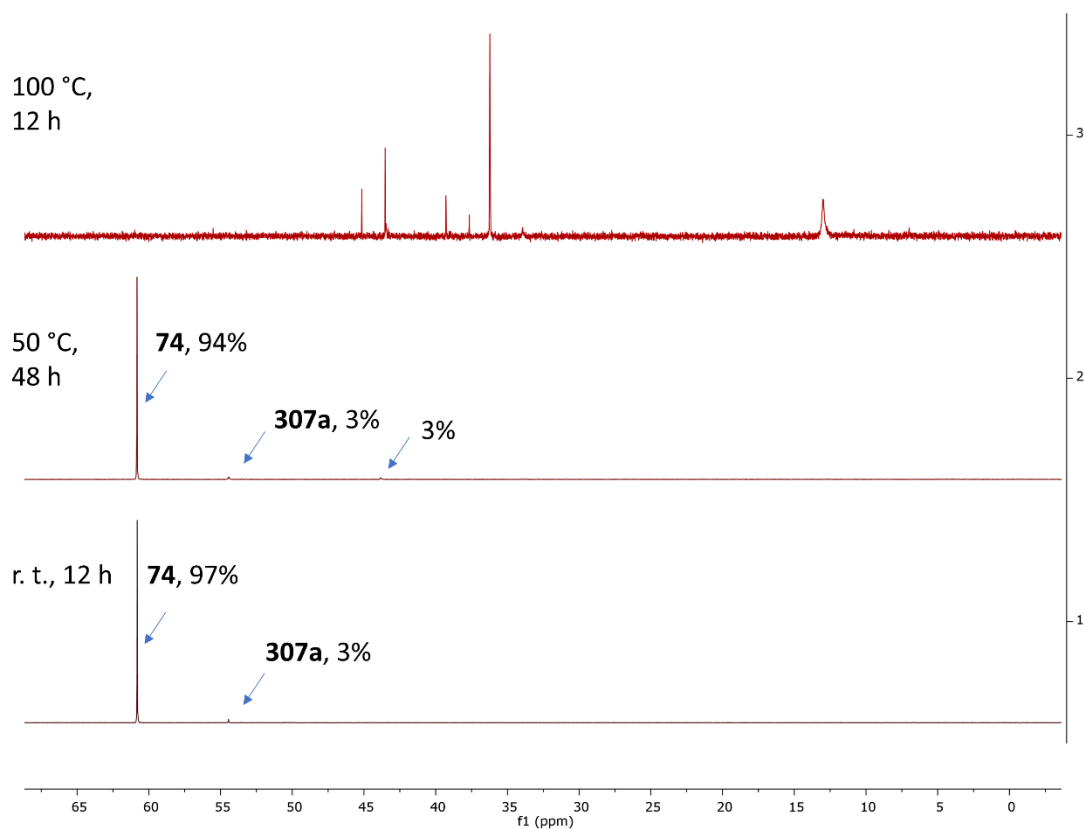
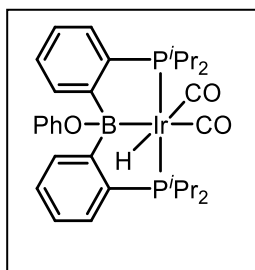


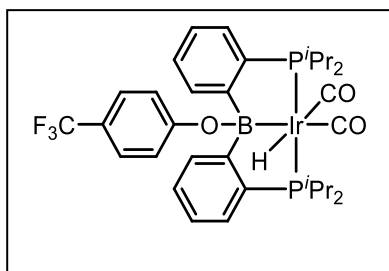
Figure III-6. *In situ* $^{31}\text{P}\{^1\text{H}\}$ NMR spectra of **74** and *tert*-butyl alcohol mixture



(PB^{OPhP})Ir(H)(CO)₂ (311a). In a 25 mL Teflon screw-capped round-bottomed flask, to a solution of **74** (50 mg, 0.077 mmol) in 1.0 mL toluene was added phenol solution (90 μL , 1.0 M in C_6D_6 , 0.090 mmol). After stirring at 50 °C for 12 h, the solution color

changed from dark red to yellow. The volatiles were removed under vacuum, and the resulting solid was recrystallized in toluene/pentane (1/3) in -35 °C overnight to yield

yellow solid (46 mg, 81%). ATR-IR: ν_{CO} 2021, 1976 cm^{-1} , $\nu_{\text{Ir-H}}$ 2143 cm^{-1} . ^1H NMR (500 MHz, C_6D_6) δ 7.74 (d, $J_{\text{H-H}} = 7.5\text{Hz}$, 2H), 7.14 (m, 4H), 7.04 (m, 4H), 6.74 (m, 1H), 6.60 (m, 2H), 2.75 (m, 2H, CHMe_2), 2.20 (m, 2H, CHMe_2), 1.16 (m, 12H, CHMe_2), 0.95 (dvt, $J_{\text{H-H}} \approx J_{\text{H-P}} = 6.9\text{ Hz}$, 6H, CHMe_2), 0.64 (dvt, $J_{\text{H-H}} \approx J_{\text{H-P}} = 6.9\text{ Hz}$, 6H, CHMe_2), -11.35 (t, $J_{\text{H-P}} = 15.2\text{ Hz}$, 1H, Ir-H). $^{31}\text{P}\{^1\text{H}\}$ NMR (202 MHz, C_6D_6): δ 53.9. $^{11}\text{B}\{^1\text{H}\}$ NMR (128 MHz, C_6D_6): δ 15.7. $^{13}\text{C}\{^1\text{H}\}$ NMR (126 MHz, C_6D_6) δ 177.3 (s, CO), 170.0 (s, CO), 161.8 (s), 142.7 (t, $J_{\text{P-C}} = 29.7\text{ Hz}$), 133.1 (t, $J_{\text{P-C}} = 10.9\text{ Hz}$), 129.9 (s), 129.3 (s), 125.6 (t, $J_{\text{P-C}} = 4.0\text{ Hz}$), 121.8 (s), 118.7 (s), 30.4 (vt, $J_{\text{P-C}} = 13.8\text{ Hz}$, CHMe_2), 28.1 (vt, $J_{\text{P-C}} = 17.4\text{ Hz}$, CHMe_2), 20.8 (s, CHMe_2), 20.5 (s, CHMe_2), 19.9 (s, CHMe_2), 19.3 (s, CHMe_2).



In situ observation of 4-(trifluoromethyl)phenol addition product (312a). In a J. Young tube, to a solution

of **74** (0.020 mmol, 0.20 mL, 0.10 M in C_6D_6) was added 4-(trifluoromethyl)phenol solution (0.020 mmol, 40 μL ,

0.50 M in C_6D_6), dioxane (0.020 mmol, 0.10 mL, 0.20 M in C_6D_6) and 0.16 mL C_6D_6 .

After stirring at room temperature for 12 h, the solution color changed from dark red to

light orange. ATR-IR: ν_{CO} 2030, 1985 cm^{-1} . ^1H NMR (400 MHz, C_6D_6) δ 7.68 (d, $J_{\text{H-H}} =$

7.5Hz, 2H), 7.26 (d, $J_{\text{H-H}} = 8.6\text{Hz}$, 2H), 7.11 (m, 4H), 7.02 (m, 2H), 6.46 (d, $J_{\text{H-H}} = 8.5\text{Hz}$,

2H), 2.62 (m, 2H, CHMe_2), 2.17 (m, 2H, CHMe_2), 1.10 (m, 12H, CHMe_2), 0.91 (dvt, $J_{\text{H-}}$

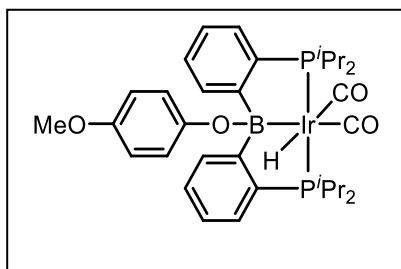
$\text{H} \approx J_{\text{H-P}} = 7.9\text{ Hz}$, 6H, CHMe_2), 0.60 (dvt, $J_{\text{H-H}} \approx J_{\text{H-P}} = 8.0\text{ Hz}$, 6H, CHMe_2), -11.36 (t, $J_{\text{H-}}$

$\text{P} = 15.2\text{ Hz}$, 1H, Ir-H). $^{31}\text{P}\{^1\text{H}\}$ NMR (202 MHz, C_6D_6): δ 53.9. $^{11}\text{B}\{^1\text{H}\}$ NMR (160 MHz,

C_6D_6): δ 15.7. $^{13}\text{C}\{^1\text{H}\}$ NMR (101 MHz, C_6D_6) δ 177.1 (s, CO), 174.0 (s, CO), 164.4 (s),

159.3 (s), 142.6 (t, $J_{\text{P-C}} = 29.6\text{ Hz}$), 132.9 (t, $J_{\text{P-C}} = 10.9\text{ Hz}$), 130.1 (s), 129.2 (m), 127.8

(q, $J_{C-F} = 3.8$ Hz, CF_3), 125.9 (t, $J_{P-C} = 4.1$ Hz), 121.1 (s), 116.1 (s), 30.4 (vt, $J_{P-C} = 13.7$ Hz, $CHMe_2$), 28.2 (vt, $J_{P-C} = 17.4$ Hz, $CHMe_2$), 20.6 (s, $CHMe_2$), 20.3 (s, $CHMe_2$), 19.8 (s, $CHMe_2$), 19.3 (s, $CHMe_2$). $^{19}F\{^1H\}$ NMR (470 MHz, C_6D_6) δ 95.5 (s). ($^{13}C\{^1H\}$ NMR and $^{19}F\{^1H\}$ NMR was recorded by reacting 0.040 mmol **74** with 0.070 mmol 4-(trifluoromethyl)phenol in C_6D_6 at room temperature for 6 h)



In situ observation of 4-methoxyphenol addition

product (313a). In a J. Young tube, to a solution of **74** (0.020 mmol, 0.20 mL, 0.10 M in C_6D_6) was added 4-methoxyphenol solution (0.020 mmol, 40 μ L, 0.50 M in

C_6D_6), dioxane (0.020 mmol, 0.10 mL, 0.20 M in C_6D_6) and 0.16 mL C_6D_6 . After stirring at room temperature for 19 h, the solution color changed from dark red to orange. ATR-IR: ν_{CO} 2027, 1981 cm^{-1} . 1H NMR (400 MHz, C_6D_6) δ 7.74 (d, $J_{H-H} = 7.7$ Hz, 2H), 7.14 (m, 4H), 7.03 (d, $J_{H-H} = 7.3$ Hz, 2H), 6.67 (d, $J_{H-H} = 9.0$ Hz, 2H), 6.46 (d, $J_{H-H} = 9.0$ Hz, 2H), 3.30 (s, 3H, OMe), 2.77 (m, 2H, $CHMe_2$), 2.22 (m, 2H, $CHMe_2$), 1.17 (m, 12H, $CHMe_2$), 0.96 (dvt, $J_{H-H} \approx J_{H-P} = 7.8$ Hz, 6H, $CHMe_2$), 0.65 (dvt, $J_{H-H} \approx J_{H-P} = 8.0$ Hz, 6H, $CHMe_2$), -11.34 (t, $J_{H-P} = 15.1$ Hz, 1H, Ir-H). $^{31}P\{^1H\}$ NMR (202 MHz, C_6D_6): δ 53.9. $^{11}B\{^1H\}$ NMR (160 MHz, C_6D_6): δ 16.7. $^{13}C\{^1H\}$ NMR (101 MHz, C_6D_6) δ 177.4 (s, CO), 170.1 (m), 155.8 (s), 153.2 (s), 142.8 (t, $J_{P-C} = 29.9$ Hz), 133.2 (t, $J_{P-C} = 11.1$ Hz), 129.8 (s), 125.6 (t, $J_{P-C} = 4.1$ Hz), 122.2 (s), 114.8 (s), 55.7 (s, OMe), 30.4 (vt, $J_{P-C} = 13.9$ Hz, $CHMe_2$), 28.0 (vt, $J_{P-C} = 17.5$ Hz, $CHMe_2$), 20.8 (s, $CHMe_2$), 20.5 (s, $CHMe_2$), 19.9 (s, $CHMe_2$), 19.2 (s, $CHMe_2$). ($^{13}C\{^1H\}$ NMR was recorded by reacting 0.040 mmol **74** with 0.10 mmol 4-methoxyphenol in C_6D_6 at room temperature for 6 h)

In situ observation of 314a/314b. In a J. Young tube, to a solution of **74** (13 mg, 0.020 mmol) in 0.40 mL C₆D₆ was added a benzoic acid solution (20 μL, 1.0 M in C₆D₆, 0.020 mmol). The color of the mixture changed from dark red to clear immediately. The room temperature solution after 5 min of mixing was composed of 95:5 **314a:314b** (³¹P{¹H} NMR evidence). After heating at 50 °C for 12 h, ³¹P{¹H} NMR spectrum was taken at room temperature, and the ratio shifted to 72:28 **314a:314b**. After heating at 110 °C for 12 h, ³¹P{¹H} NMR spectrum was taken at room temperature, and the ratio shifted to 23:77 **314a:314b**. By cooling the mixture to room temperature for 4 h, the ratio shifted back to 77:23 **314a:314b** by ³¹P{¹H} NMR.

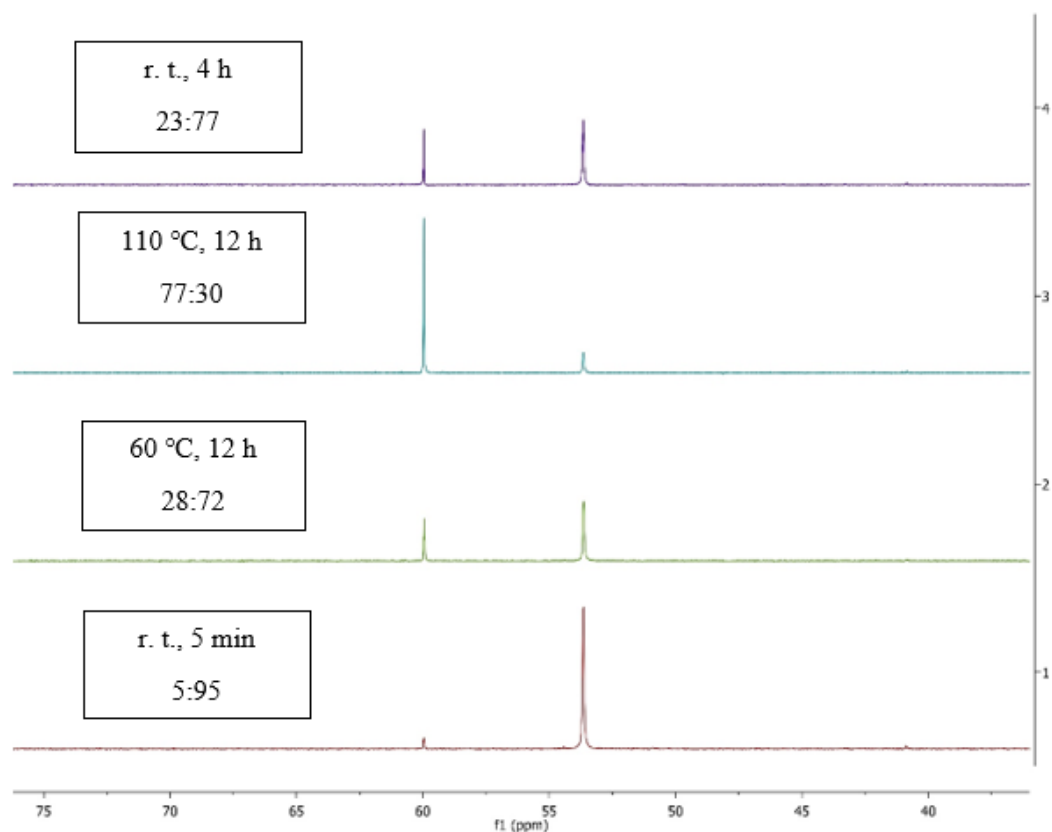
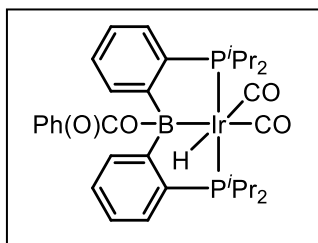
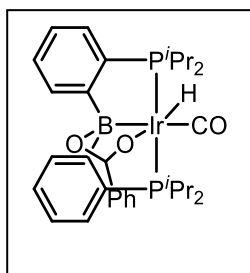


Figure III-7. ³¹P{¹H} NMR spectra of 314a and 314b mixture after certain periods of time



(PB^{OC(O)Ph}P)Ir(H)(CO)₂ (314a). In a J. Young tube, to a solution of **74** (50 mg, 0.077 mmol) in 0.50 mL C₆D₆ was added benzoic acid (11 mg, 0.090 mmol). The color of the solution changed from dark red to clear immediately. Based on

³¹P{¹H} NMR spectroscopic evidence at room temperature after 5 min of mixing, a mixture of 95:5 **314a**:**314b** formed and no starting material remained. Addition of 1 atm CO after freeze-pump-thaw resulted in the observation of only **314a** via analysis of spectra. ATR-IR: ν_{CO} 2028, 1981 cm⁻¹, ν_{C=O} 1674 cm⁻¹, ν_{Ir-H} 2118 cm⁻¹. ¹H NMR (500 MHz, C₆D₆) δ 7.88 (d, J_{H-H} = 7.4 Hz, 2H), 7.24 (m, 2H), 7.10 (m, 2H), 7.05 (m, 2H), 2.69 (m, 2H, CHMe₂), 2.19 (m, 2H, CHMe₂), 1.88 (s, 1H, OH), 1.07 (m, 12H, CHMe₂), 0.98 (dvt, J_{H-H} ≈ J_{H-P} = 6.9 Hz, 6H, CHMe₂), 0.66 (dvt, J_{H-H} ≈ J_{H-P} = 7.1 Hz, 6H, CHMe₂), -11.24 (t, J_{H-P} = 15.6 Hz, 1H, Ir-H). ³¹P{¹H} NMR (202 MHz, C₆D₆): δ 53.6. ¹¹B{¹H} NMR (128 MHz, C₆D₆): δ 12.6. ¹³C{¹H} NMR (126 MHz, C₆D₆) δ 177.1 (s, CO), 169.8 (s, CO), 166.6 (s), 141.7 (t, J_{P-C} = 30.6 Hz), 136.8 (s), 132.8 (t, J_{P-C} = 11.0 Hz), 131.6 (s), 130.6 (s), 130.3 (s), 125.6 (t, J_{P-C} = 4.2 Hz), 30.8 (t, J_{P-C} = 14.0 Hz, CHMe₂), 27.7 (t, J_{P-C} = 17.7 Hz, CHMe₂), 20.7 (s, CHMe₂), 19.9 (s, CHMe₂), 19.5 (s, CHMe₂).

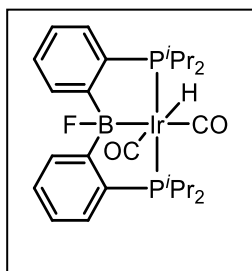


(PB^{OC(Ph)O}P)Ir(H)(CO) (314b). In a 100 mL Teflon screw-capped round-bottomed flask, a solution of benzoic acid addition product (50 mg, 0.065 mmol) in 5 mL toluene was heated at 110 °C for 6 h. The color of the solution changed from clear to pale yellow.

Dynamic vacuum was applied to the mixture to remove CO in 10 minutes, and the resulting solid was recrystallized in toluene/pentane (1/10) in -35 °C, to yield pale yellow

solid (35 mg, 73%). ATR-IR: ν_{CO} 1953 cm^{-1} , $\nu_{\text{Ir-H}}$ 2244 cm^{-1} . $^{31}\text{P}\{^1\text{H}\}$ NMR (202 MHz, C_6D_6): δ 60.0. $^{11}\text{B}\{^1\text{H}\}$ NMR (128 MHz, C_6D_6): δ 26.5. ^1H NMR (500 MHz, C_6D_6) δ 8.54 (d, $J_{\text{H-H}} = 7.5$ Hz, 2H), 7.96 (m, 2H), 7.42 (m, 2H), 7.24 (m, 2H), 7.12 (m, 2H), 6.95 (m, 1H), 6.88 (m, 2H), 2.20 (m, 4H, CHMe_2), 1.25 (dvt, $J_{\text{H-H}} \approx J_{\text{H-P}} = 7.0$ Hz, 6H, CHMe_2), 1.15 (dvt, $J_{\text{H-H}} \approx J_{\text{H-P}} = 6.9$ Hz, 6H, CHMe_2), 0.95 (dvt, $J_{\text{H-H}} \approx J_{\text{H-P}} = 7.3$ Hz, 6H, CHMe_2), 0.72 (dvt, $J_{\text{H-H}} \approx J_{\text{H-P}} = 7.0$ Hz, 6H, CHMe_2), -22.44 (t, $J_{\text{H-P}} = 15.5$ Hz, 1H, Ir-H). $^{13}\text{C}\{^1\text{H}\}$ NMR (126 MHz, C_6D_6): δ 184.9 (CO), 179.0 (OCO), 167.4 (br), 145.8 (t, $J_{\text{C-P}} = 27.9$ Hz), 133.6 (t, $J_{\text{C-P}} = 10.9$ Hz), 132.8 (s), 131.2 (s), 131.0 (s), 130.4 (s), 129.9 (s), 129.8 (t, $J_{\text{C-P}} = 2.4$ Hz), 126.4 (t, $J_{\text{C-P}} = 3.8$ Hz), 30.5 (t, $J_{\text{C-P}} = 12.5$ Hz, CHMe_2), 28.3 (t, $J_{\text{C-P}} = 17.4$ Hz, CHMe_2), 21.0 (s, CHMe_2), 20.3 (s, CHMe_2), 19.4 (s, CHMe_2). Elem. Anal. Calcd for $\text{C}_{32}\text{H}_{43}\text{B}\text{IrO}_3\text{P}_2$: C, 51.89; H, 5.85. Found: C, 51.37, H, 6.06.

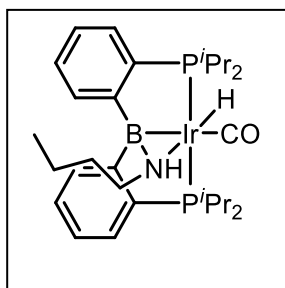
3.4.3.2 F–H Cleavage



(PB^FP)Ir(H)(CO)₂ (315a). In a J. Young tube, to a solution of **74** (65 mg, 0.10 mmol) in 0.50 mL C_6D_6 was added triethylamine trihydrofluoride ($3\text{HF}\cdot\text{NEt}_3$, 7.0 μL , 0.044 mmol). The color of the solution changed from dark red to clear immediately. Based on $^{31}\text{P}\{^1\text{H}\}$ NMR *in situ*, **315a** formed and no starting material remained. The volatiles were removed under vacuum, and the resulting solid was recrystallized from toluene/pentane (1/3) in -35 $^\circ\text{C}$ to yield white solid (47 mg, 71%). ATR-IR: ν_{CO} 2019, 1979 cm^{-1} , $\nu_{\text{Ir-H}}$ 2130 cm^{-1} . $^{31}\text{P}\{^1\text{H}\}$ NMR (202 MHz, C_6D_6): δ 55.4. $^{11}\text{B}\{^1\text{H}\}$ NMR (128 MHz, C_6D_6): δ 18.6. ^{19}F NMR (470 MHz, C_6D_6): δ -120.4. ^1H NMR (500 MHz, C_6D_6) δ 8.01 (d, $J_{\text{H-H}} = 7.3$ Hz, 2H), 7.26 (t, $J_{\text{H-H}} = 7.1$ Hz, 2H), 7.11 (m, 2H), 7.06 (t, $J_{\text{H-H}} = 7.1$ Hz, 2H), 2.52 (m,

2H, *CHMe*₂), 2.18 (m, 2H, *CHMe*₂), 1.09 (dvt, $J_{\text{H-H}} \approx J_{\text{H-P}} = 7.4$ Hz, 6H, *CHMe*₂), 1.03 (dvt, $J_{\text{H-H}} \approx J_{\text{H-P}} = 7.7$ Hz, 6H, *CHMe*₂), 0.95 (dvt, $J_{\text{H-H}} \approx J_{\text{H-P}} = 7.1$ Hz, 6H, *CHMe*₂), 0.65 (dvt, $J_{\text{H-H}} \approx J_{\text{H-P}} = 7.2$ Hz, 6H, *CHMe*₂), -11.36 (t, $J_{\text{H-P}} = 15.4$ Hz, 1H, Ir-*H*). ¹³C{¹H} NMR (126 MHz, C₆D₆): δ 177.6 (s, CO), 170.8 (s, CO), 169.5 (br), 142.4 (t, $J_{\text{C-P}} = 30.1$ Hz), 132.5 (t, $J_{\text{C-P}} = 11.1$ Hz), 130.3 (s), 126.0 (t, $J_{\text{C-P}} = 3.6$ Hz), 30.6 (t, $J_{\text{C-P}} = 13.9$ Hz, *CHMe*₂), 27.9 (t, $J_{\text{C-P}} = 17.7$ Hz, *CHMe*₂), 20.5 (s, *CHMe*₂), 20.5 (s, *CHMe*₂), 20.0 (s, *CHMe*₂), 19.3 (s, *CHMe*₂).

3.4.3.3 N–H Cleavage



(PB^{NHnBu}P)Ir(H)(CO) (316b). In a 100 mL Teflon screw-capped round-bottomed flask, to a solution of **74** (65 mg, 0.10 mmol) in 2.0 mL toluene was added ⁿBuNH₂ (25 μ L, 0.25 mmol). After stirring at 50 °C for 36 h, the solution color changed from dark red

to pale yellow. The volatiles were removed under vacuum. The resulting solid was recrystallized in pentane in -35 °C overnight to yield yellow solid (58 mg, 84%). ATR-IR: ν_{CO} 1927 cm^{-1} , $\nu_{\text{Ir-H}}$ 2131 cm^{-1} . ³¹P{¹H} NMR (202 MHz, C₆D₆): δ 56.0(d, $J_{\text{P-P}} = 234.2$ Hz), 48.6(d, $J_{\text{P-P}} = 234.2$ Hz). ¹¹B{¹H} NMR (128 MHz, C₆D₆): δ 9.6. ¹H NMR (500 MHz, C₆D₆) δ 8.50 (d, $J_{\text{H-H}} = 7.6$ Hz, 1H), 8.32 (d, $J_{\text{H-H}} = 7.5$ Hz, 1H), 7.31 (m, 1H), 7.40 (m, 1H), 7.22 (m, 2H), 7.13 (m, 1H), 7.10 (m, 1H), 2.30 (m, 1H, *CHMe*₂), 2.17 (m, 1H, *CHMe*₂), 1.98 (m, 3H), 1.83 (m, 1H, *CHMe*₂), 1.43 (m, 1H, *CHMe*₂), 1.27 (m, 6H, *CHMe*₂), 1.09 (m, 2H, *CH*₂Me), 0.93 (m, 17H), 0.72 (dd, $J_{\text{H-H}} = 6.9$ Hz, $J_{\text{H-P}} = 15.1$ Hz, 3H, *CHMe*₂), 0.59 (t, $J_{\text{H-H}} = 7.4$ Hz, 3H, *CH*₂Me), -17.68 (t, $J_{\text{H-P}} = 9.6, 21.6$ Hz, 1H, Ir-*H*). ¹³C{¹H} NMR (126 MHz, C₆D₆) δ 185.8 (s, CO), 143.8 (s), 143.4 (s), 141.7 (s), 141.3

(s), 134.8 (d, $J_{P-C} = 22.8$ Hz), 132.8 (d, $J_{P-C} = 22.1$ Hz), 131.3 (s), 130.2 (d, $J_{P-C} = 19.1$ Hz), 129.5 (s), 128.9 (s), 126.9 (d, $J_{P-C} = 5.6$ Hz) 126.3 (d, $J_{P-C} = 5.3$ Hz), 55.9 (s, CH_2), 36.4 (d, $J_{P-C} = 35.9$ Hz, $CHMe_2$), 36.3 (s, CH_2), 31.0 (d, $J_{P-C} = 32.8$ Hz, $CHMe_2$), 30.3 (dd, $J_{P-C} = 20.1$ Hz, $J_{P-C} = 4.5$ Hz, $CHMe_2$), 24.4 (dd, $J_{P-C} = 22.8$ Hz, $J_{P-C} = 7.1$ Hz, $CHMe_2$), 20.6 (s, CH_2), 20.4 (m), 19.7 (s), 19.1 (m), 18.9 (s), 14.5 (s). Elem. Anal. Calcd for $C_{29}H_{46}BIrNOP_2$: C, 50.51; H, 6.72; N, 2.03. Found: C, 50.64; H, 6.44; N, 1.87.

Sample III-1: In situ observation of 74/316a/316c 5 min after adding 0.10 mmol n BuNH₂ to 0.040 mmol 74. In a J. Young tube, to a dark red solution of **74** (26 mg, 0.040 mmol) in 400 μ L C_6D_6 was added n -butylamine solution (100 μ L, 1.0 M in C_6D_6 , 0.10 mmol) to make 500 μ L solution with 0.080 M **74**, 0.20 M n BuNH₂ in C_6D_6 . The color of the solution changed to light red immediately, and after 5 min of mixing, two signals were observed by $^{31}P\{^1H\}$ NMR spectrum. One was tentatively identified as **316a** (7%) based on the similarity of the NMR spectroscopic features with **307a-315a**. The other was interpreted as a time- and weight-averaged signal for **74** and **316c** in rapid equilibrium. $^{11}B\{^1H\}$ NMR, 1H NMR and ATR-IR spectra were also collected for characterization. The ratio between **74** and **316c** is about 1 : 1 according to ATR-IR spectrum.

Sample III-2: In situ observation of 74/316c 5 min after adding 0.05 mmol n BuNH₂ to 0.020 mmol 74. In a J. Young tube, to a solution of **74** (13 mg, 0.020 mmol) in 400 μ L C_6D_6 was added n BuNH₂ (50 μ L, 1.0M in C_6D_6 , 0.05 mmol) to make 450 μ L of a solution that was 0.044 M in **74**, and 0.11 M in n BuNH₂. The color of the solution changed to light red immediately and after 5 min of mixing, only one signal was observed

by $^{31}\text{P}\{^1\text{H}\}$ NMR spectrum, indicating that the sample contains a mixture of **74**/**316c**. $^{11}\text{B}\{^1\text{H}\}$ NMR, ^1H NMR and ATR-IR spectra were also recorded. The ratio between **74** and **316c** is about 3 : 1 according to ATR-IR spectrum. The mixture was heated at 50 °C in an oil bath for 16 h, followed by the dynamic vacuum at 50 °C to remove all the volatiles. The resulting solid was redissolved in C_6D_6 , showing 95% conversion to **316b** ($^{31}\text{P}\{^1\text{H}\}$ NMR evidence).

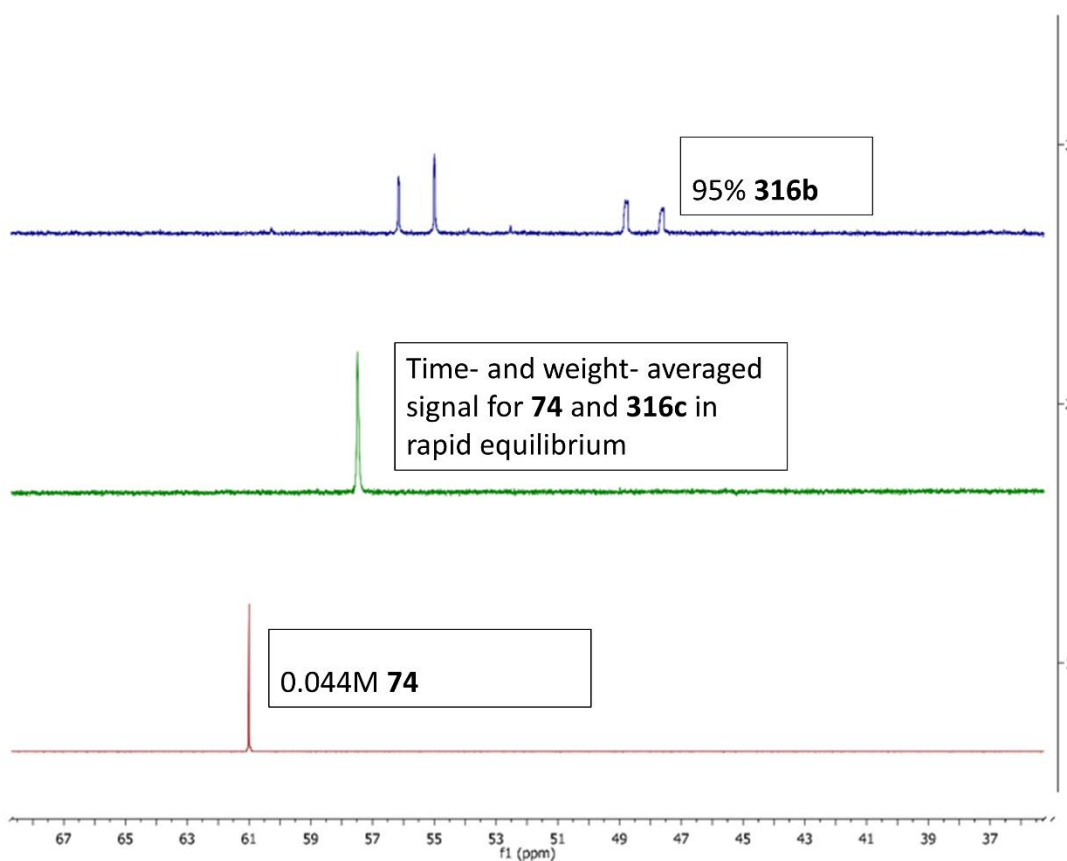


Figure III-8. Bottom: $^{31}\text{P}\{^1\text{H}\}$ NMR spectrum of pure **74** (0.044M, 202 M Hz, C_6D_6). **Middle:** $^{31}\text{P}\{^1\text{H}\}$ NMR (202 M Hz, C_6D_6) spectrum of Sample III-2 recorded 5 min after addition of $^n\text{BuNH}_2$ to **74**. Sample contains a mixture of **74**/**316c**. **Top:** $^{31}\text{P}\{^1\text{H}\}$ NMR (202 M Hz, C_6D_6) spectrum of Sample III-2 recorded after 16 h heating at 50 °C and dynamic vacuum to remove volatiles. Sample contains 95% **316b**

Table III-2. Spectral details for Sample III-1 and Sample III-2 recorded 5 min after addition of ⁿBuNH₂ to **74**

	Sample III-1	Sample III-2
³¹ P{ ¹ H} NMR (202 MHz, C ₆ D ₆):	54.0 (s) (7%),^a 54.3 (s)	57.5 (s)
¹¹ B{ ¹ H} NMR (128 MHz, C ₆ D ₆):	26.4 (s), 46.2 (s)	67.3 (s)
¹ H NMR (500 MHz, C ₆ D ₆):	7.77 (d, J _{H-H} = 7.5 Hz, 2H), 7.33 (m, 2H), 7.21 (t, J _{H-H} = 7.0 Hz, 2H), 7.08 (t, J _{H-H} = 7.2 Hz, 2H), 2.24 (m, 4H, CHMe ₂), 1.11 (dvt, J _{H-H} ≈ J _{H-P} = 6.9 Hz, 12H, CHMe ₂), 0.93(dvt, J _{H-H} ≈ J _{H-P} = 7.0 Hz, 12H, CHMe ₂). - 11.31 (t, J_{H-P} = 15.7 Hz, 1H, Ir-H).	7.94 (d, J _{H-H} = 7.5 Hz, 2H), 7.35 (m, 2H), 7.20 (td, J _{H-H} = 7.4, 1.0 Hz, 2H), 7.10 (td, J _{H-H} = 7.4, 1.0 Hz, 2H), 2.28 (m, 4H, CHMe ₂), 1.10 (dvt, J _{H-H} ≈ J _{H-P} = 7.0 Hz, 12H, CHMe ₂), 0.91(dvt, J _{H-H} ≈ J _{H-P} = 7.0 Hz, 12H, CHMe ₂)
ATR-IR:	1957, 1922 ^b , 1880 cm ⁻¹	1964, 1922 ^c , 1881 cm ⁻¹

a. Bolded signals belongs to **316a**; b. Two pairs of bands were observed (1957, 1922 cm⁻¹ belongs to **74**, and 1922, 1880 cm⁻¹ belongs to **316c**. The ratio is about 1 : 1). c. Two sets of bands were observed (1964, 1922 cm⁻¹ belongs to **74**, and 1922, 1881 cm⁻¹ belongs to **316c**. The ratio is about 3 : 1).

Attempted reaction of 74 with diethylamine. In a J. Young tube, to a solution of **74** (13 mg, 0.020 mmol) in 0.40 mL C₆D₆ was added diethylamine solution (20 μL, 1.0 M in C₆D₆, 0.020 mmol). After stirring at room temperature for 12 h, no color change was observed, and no new complex generated (³¹P{¹H} NMR evidence). The same mixture was heated at 50 °C for 12 h, no change was observed by the *in situ* ³¹P{¹H} NMR spectrum at room temperature.

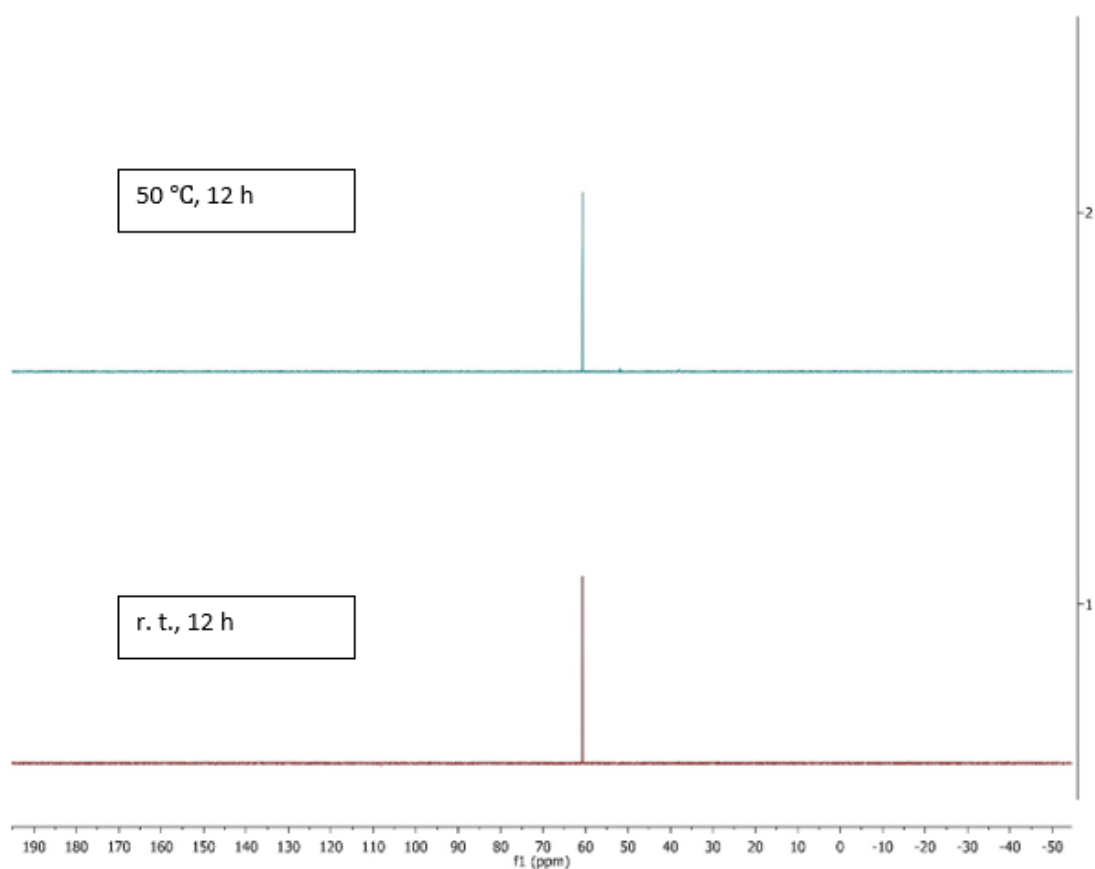


Figure III-9. ³¹P{¹H} NMR spectra of **74** and diethylamine mixture after certain periods of time

Attempted reaction of 74 with *tert*-butylamine. In a J. Young tube, to a solution of **74** (13 mg, 0.020 mmol) in 0.40 mL C₆D₆ was added *tert*-butylamine solution (20 μL, 1.0 M in C₆D₆, 0.020 mmol). The impurity at 66 ppm was **73** in the starting material.¹⁰² After stirring at room temperature for 12 h, no color change was observed, and no new complex generated (³¹P{¹H} NMR evidence). The same mixture was heated at 50 °C for 12 h, no change was observed by the *in situ* ³¹P{¹H} NMR spectrum at room temperature. Heating the mixture further at 100 °C for 12 h, the ³¹P{¹H} NMR spectrum at room temperature showing that the starting material still remained intact.

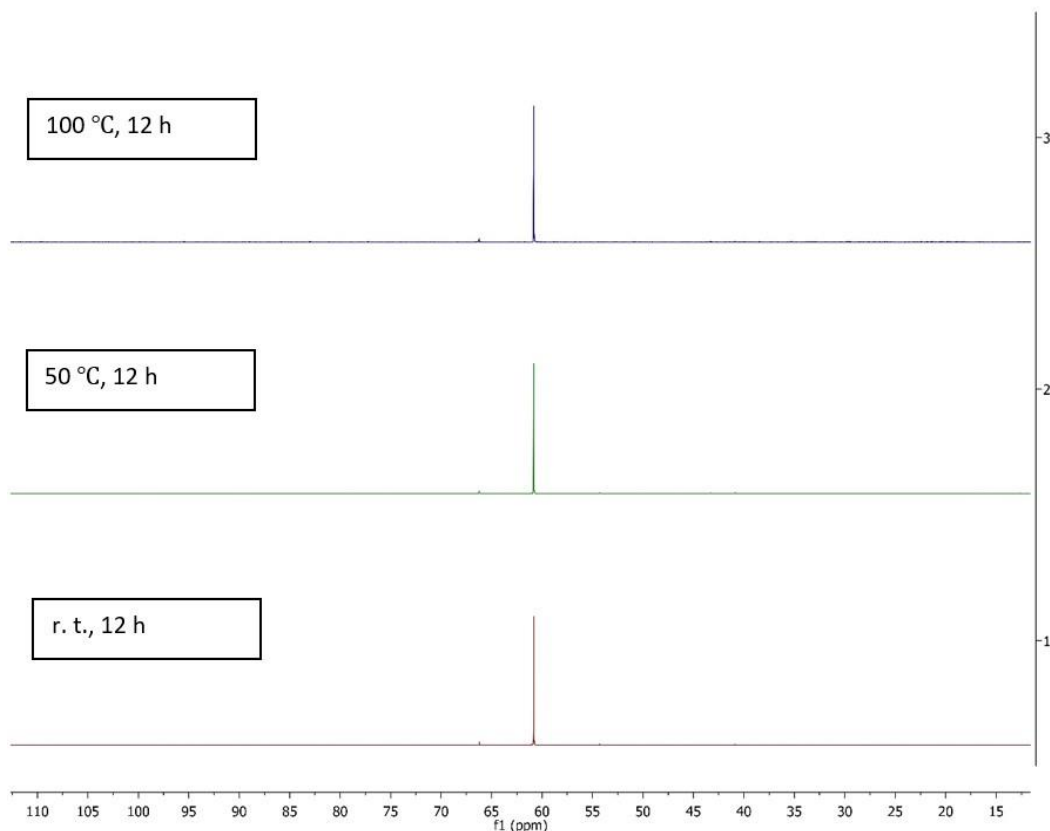


Figure III-10. ³¹P{¹H} NMR spectrum of **74** and *tert*-butylamine mixture after certain periods of time

Attempted reaction of 74 with aniline. In a J. Young tube, to a solution of **74** (13 mg, 0.020 mmol) in 0.40 mL C_6D_6 was added aniline solution (20 μ L, 1.0 M in C_6D_6 , 0.020 mmol). After stirring at room temperature for 12 h, no color change was observed, and no new complex generated ($^{31}P\{^1H\}$ NMR evidence). The same mixture was heated at 50 °C for 12 h, no change was observed by the *in situ* $^{31}P\{^1H\}$ NMR spectrum at room temperature.

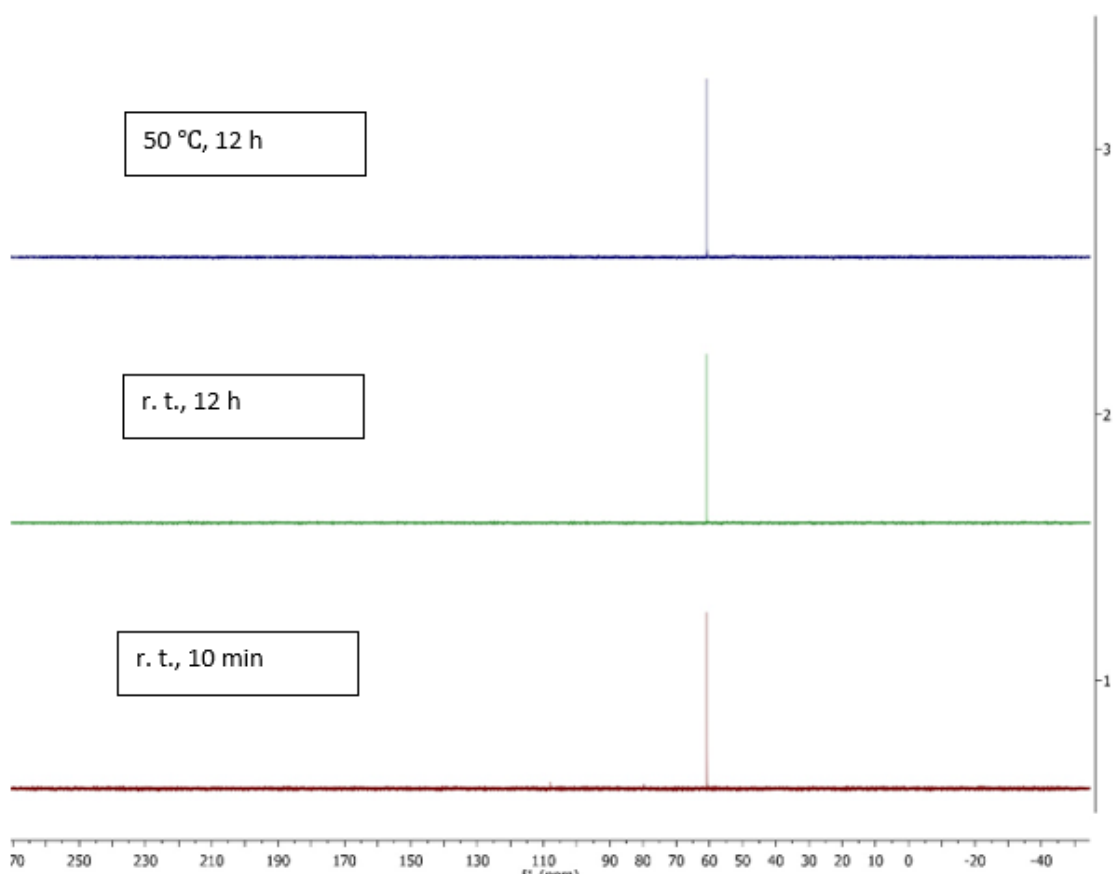


Figure III-11. $^{31}P\{^1H\}$ NMR spectrum of **74** and aniline mixture after certain periods of time

Attempted reaction of 74 with *p*-anisidine. In a J. Young tube, to a solution of **74** (13 mg, 0.020 mmol) in 0.40 mL C₆D₆ was added *p*-anisidine solution (20 μL, 1.0 M in C₆D₆, 0.020 mmol). The impurity at 66 ppm was **73** in the starting material.¹⁰² After stirring at room temperature for 48 h, no color change was observed, and no new complex generated (³¹P{¹H} NMR evidence). The same mixture was heated at 50 °C for 12 h, no change was observed by the *in situ* ³¹P{¹H} NMR spectrum at room temperature.

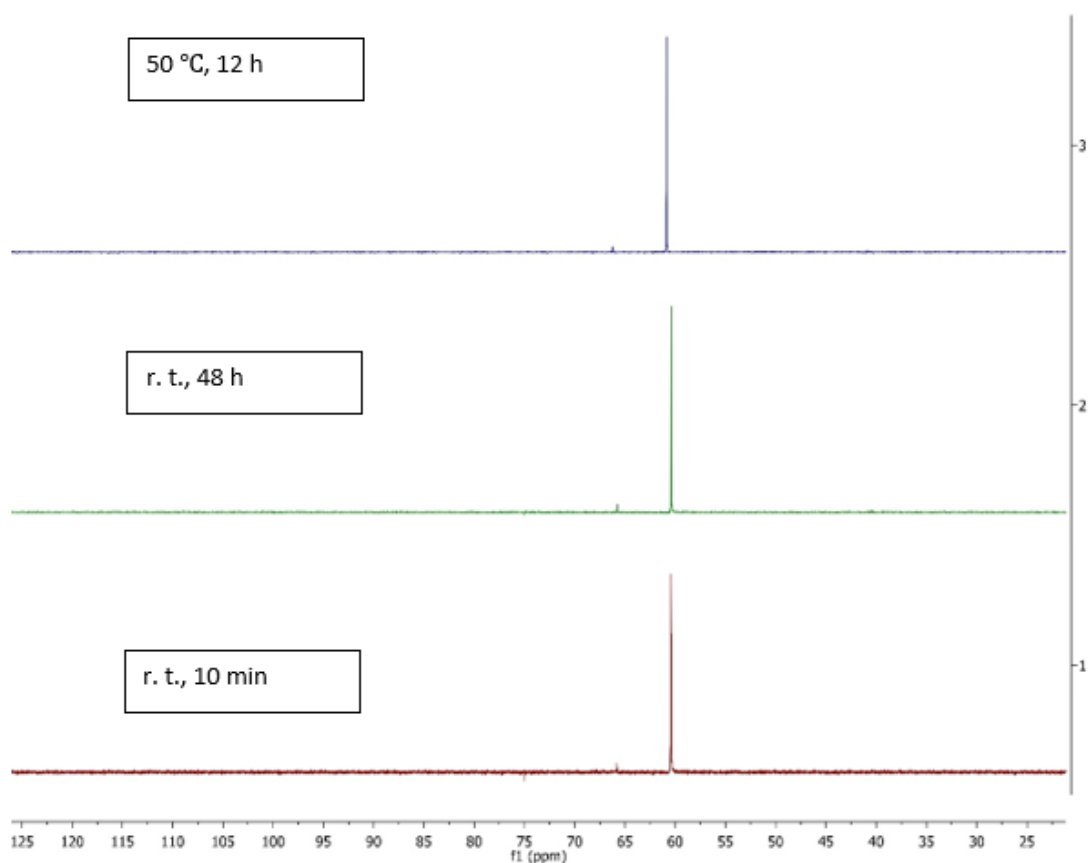


Figure III-12. ³¹P{¹H} NMR spectrum of **74** and *p*-anisidine mixture after certain periods of time

Attempted reaction of 74 with pyrrole. In a J. Young tube, to a solution of **74** (13 mg, 0.020 mmol) in 0.40 mL C₆D₆ was added pyrrole (10 μL, 0.14 mmol). After stirring at room temperature for 12 h, no color change was observed, and no new complex generated (³¹P{¹H} NMR evidence). The same mixture was heated at 50 °C for 12 h, no change was observed by the *in situ* ³¹P{¹H} NMR spectrum at room temperature.

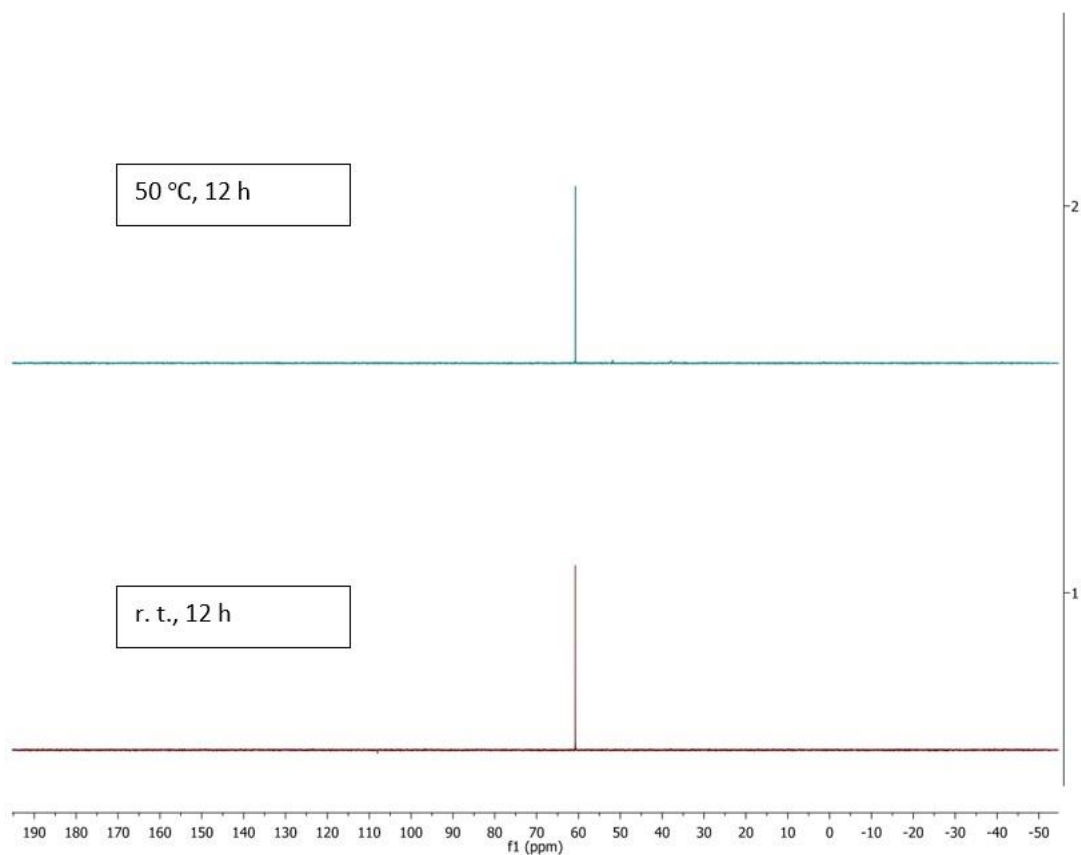
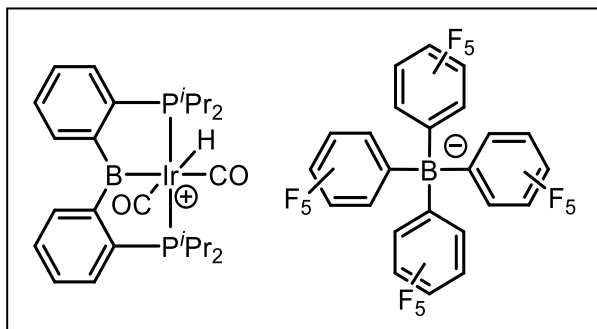


Figure III-13. ³¹P{¹H} NMR spectrum of **74** and pyrrole mixture after certain periods of time

3.4.3.4 Mechanistic investigations



$[(\text{PBP})\text{Ir}(\text{H})(\text{CO})_2][\text{BAr}^{\text{F20}}]$ (317a).

Method I: To a solution of **74** (13 mg, 0.020 mmol) in fluorobenzene was added $\text{H}(\text{Et}_2\text{O})_2(\text{BAr}^{\text{F20}})$ (17 mg, 0.020 mmol). A clear solution was generated

after stirring the mixture at room temperature for 30 min. Method II: In a 50 mL Teflon screw-capped round-bottomed flask, to a solution of **70** (0.20 g, 0.32 mmol) in fluorobenzene was added KBAr^{F20} (0.23 g, 0.32 mmol) and 1 atm of CO. A clear solution was generated after stirring at room temperature for 30 min. The resulting mixture was passed through Celite and the volatiles were removed under vacuum. The resulting solid was dissolved in $\text{C}_6\text{D}_5\text{Br}$ for NMR spectroscopic characterization. ATR-IR: ν_{CO} : 2078, 2032 cm^{-1} . $^{31}\text{P}\{^1\text{H}\}$ NMR (202 MHz, $\text{C}_6\text{D}_5\text{Br}$): δ 55.2. $^{11}\text{B}\{^1\text{H}\}$ NMR (128 MHz, $\text{C}_6\text{D}_5\text{Br}$): δ 95.0, -15.8. ^1H NMR (400 MHz, $\text{C}_6\text{D}_5\text{Br}$) δ 7.83 (d, $J_{\text{H-H}} = 4.2$ Hz, 2H), 7.26 (m, 6H), 2.35 (m, 2H, CHMe_2), 2.05 (m, 2H, CHMe_2), 0.90 (dvt, $J_{\text{H-H}} = 10.4$ Hz, $J_{\text{H-P}} = 6.8$ Hz, 6H, CHMe_2), 0.79 (dvt, $J_{\text{H-H}} = 10.0$ Hz, $J_{\text{H-P}} = 7.2$ Hz, 6H, CHMe_2), 0.71 (dvt, $J_{\text{H-H}} = 10.8$ Hz, $J_{\text{H-P}} = 7.2$ Hz, 6H, CHMe_2), 0.60 (dvt, $J_{\text{H-H}} = 10.0$ Hz, $J_{\text{H-P}} = 7.2$ Hz, 6H, CHMe_2), -11.11 (t, $J_{\text{H-P}} = 14.3$ Hz, 1H, Ir-H). $^{13}\text{C}\{^1\text{H}\}$ NMR (126 MHz, $\text{C}_6\text{D}_5\text{Br}$): δ 170.1 (s, CO), 167.9 (s, CO), 156.4 (br), 149.7 (br), 148.1 (m), 139.5 (br), 137.7 (br), 135.7 (br), 133.6 (t, $J_{\text{C-P}} = 8.8$ Hz), 132.7 (t, $J_{\text{C-P}} = 4.2$ Hz), 131.9 (s), 130.3 (t, $J_{\text{C-P}} = 2.6$ Hz), 28.5 (t, $J_{\text{C-P}} = 16.9$ Hz, CHMe_2), 27.0 (t, $J_{\text{C-P}} = 14.8$ Hz, CHMe_2), 18.7 (s, CHMe_2), 18.6 (s, CHMe_2), 18.6 (s, CHMe_2), 17.9 (s, CHMe_2).

Deprotonation of **317a**.

In a J. Young tube, **317a** (0.020 mmol, 27 mg) was dissolved in THF. $^{11}\text{B}\{^1\text{H}\}$ NMR spectrum was recorded, indicating no coordination between **317a** and THF.

In a J. Young tube, to a solution of **317a** (0.020 mmol, 27 mg) in THF was added NEt_3 (5.0 μL , 0.036 mmol) and the mixture was stirred at room temperature for 12 h. 2% of **317a** was consumed to generate **74**.

In a J. Young tube, to a solution of **317a** (0.020 mmol, 27 mg) in THF was added $i\text{Pr}_2\text{NEt}$ (7.0 μL , 0.040 mmol) and the mixture was stirred at room temperature for 12 h. 5% of **317a** was consumed to generate **74**.

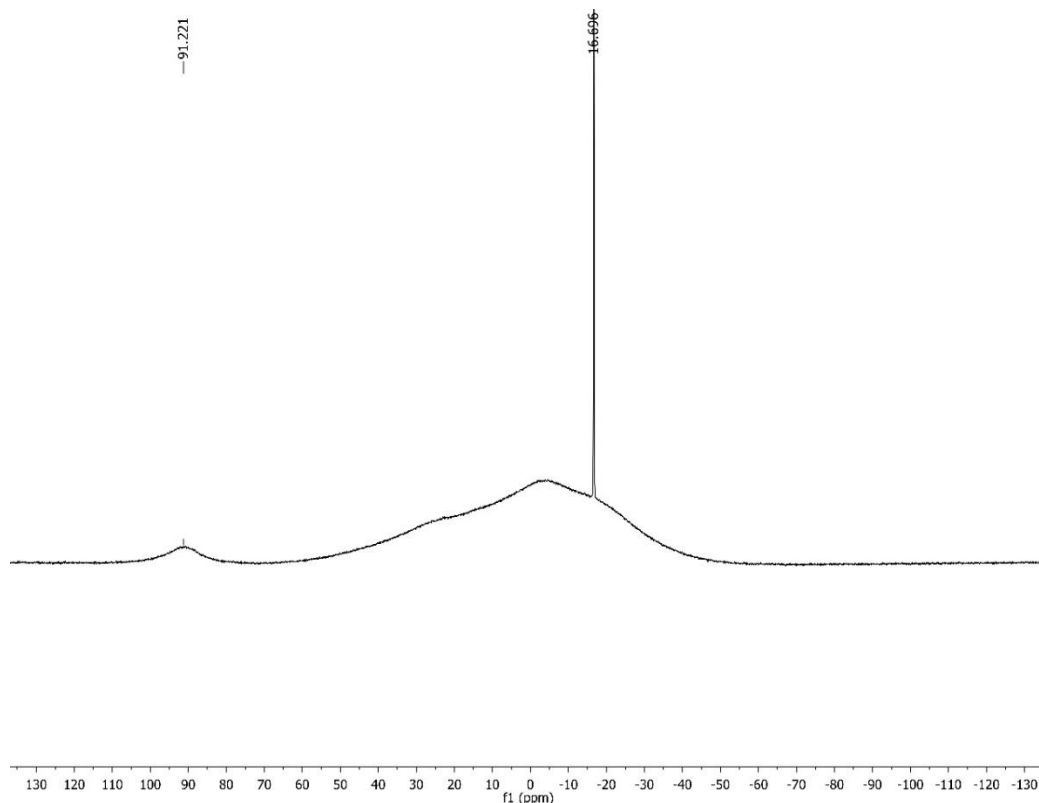


Figure III-14. $^{11}\text{B}\{^1\text{H}\}$ NMR spectrum of **317a** in THF measured on a 500 MHz Varian NMR

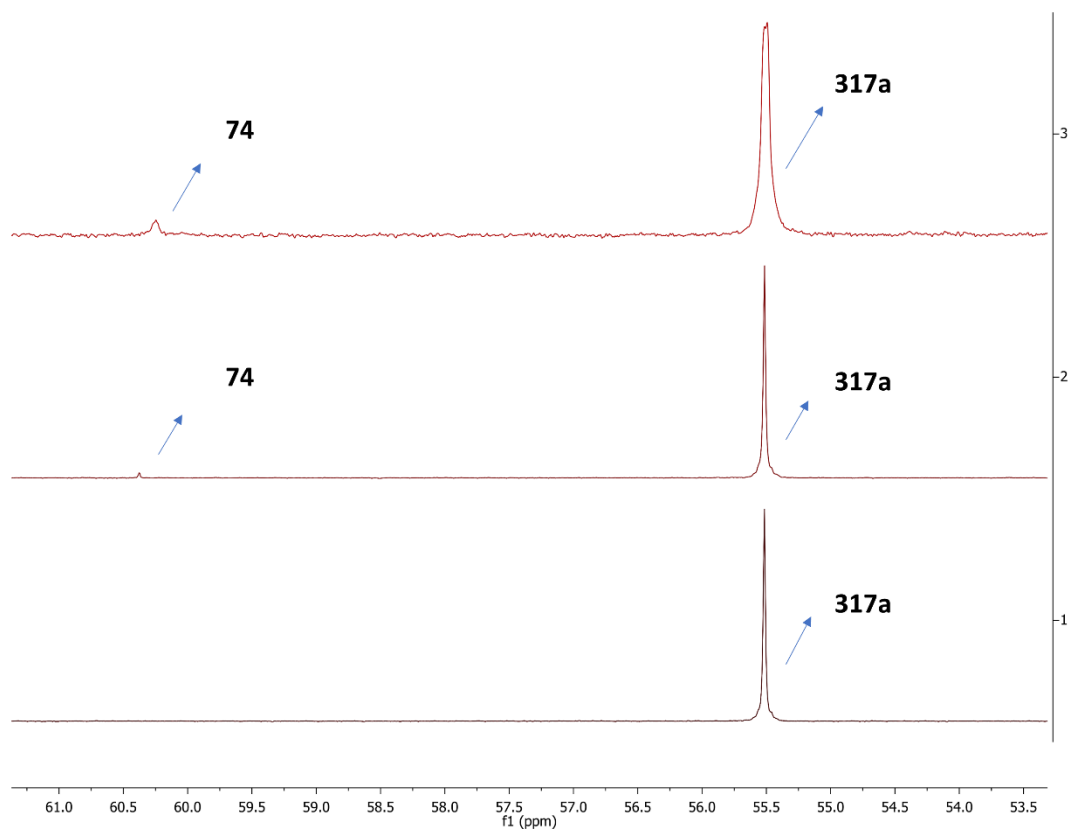


Figure III-15. Bottom: $^{31}\text{P}\{^1\text{H}\}$ NMR spectrum of 317a in THF; Middle: $^{31}\text{P}\{^1\text{H}\}$ NMR spectrum of 317a mixed with NEt_3 after 12 h of stirring. The sample contains 2% of 74 and 98% of 317a; Top: $^{31}\text{P}\{^1\text{H}\}$ NMR spectrum of 317a mixed with $i\text{Pr}_2\text{NEt}_3$ after 12 h of stirring. The sample contains 5% of 74 and 95% of 317a

H, D exchange between CD₃OD and 317a. In a Schlenk flask, to 500 μ L CD₃OD and 100 μ L C₆D₆ was dissolved **317a** (27 mg, 0.020 mmol). The mixture was transferred to a J. Young tube to record ¹H NMR spectra after 1 h and 12 h. Hydride signal integration decreased after stirring at r. t. for 12 h, indicating H, D exchange between CD₃OD and **317a**.

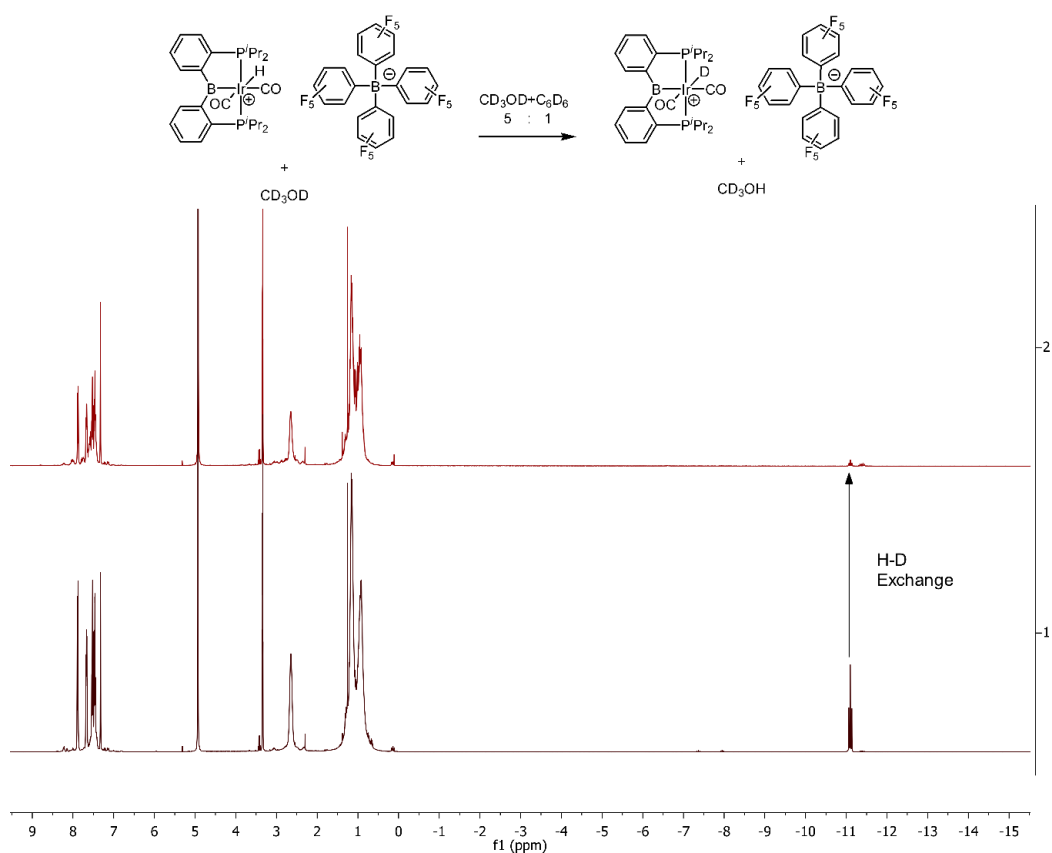
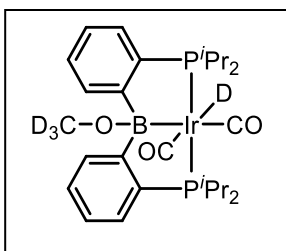


Figure III-16. Bottom: ¹H NMR spectrum of **317a** in CD₃OD/C₆D₆ (5 : 1) after stirring at r. t. for 1 h; **Top:** ¹H NMR spectrum of **317a** in CD₃OD/C₆D₆ (5 : 1) after stirring at r. t. for 12 h



In situ observation of CD₃OD addition product (**308a-d₄**) and exchange between **317a** and **308a-d₄**.

(**PB^{OCD₃}P**)IrD(CO)₂ (**308a-d₄**). In a J. Young tube was added **74** (13 mg, 0.020 mmol), 0.20 mL C₆H₆ and 0.10 mL of CD₃OD. The

mixture was stirred at room temperature for 12 h, and all volatiles were removed. The resulting solid was dissolved in C₆D₅Br. To the solution was added **317a** (0.020 mmol, 26 mg). Exchange was observed between **317a** and **308a-d₄** (NMR spectroscopic evidence).

308a-d₄. ³¹P{¹H} NMR (202 MHz, C₆D₅Br): δ 53.8. ¹¹B{¹H} NMR (160 MHz, C₆D₅Br): δ 22.3, ¹H NMR (500 MHz, C₆D₅Br) δ 7.96 (d, J_{H-H} = 7.4 Hz, 2H), 7.20 (m, 4H), 7.07 (t, J_{H-H} = 7.1 Hz, 2H), 2.66 (m, 2H, CHMe₂), 2.33 (m, 2H, CHMe₂), 1.11 (m, 12H, CHMe₂), 1.02 (dvt, J_{H-H} = 8.2 Hz, J_{H-P} = 7.1 Hz, 6H, CHMe₂), 0.62 (dvt, J_{H-H} = 8.3 Hz, J_{H-P} = 6.8 Hz, 6H, CHMe₂).

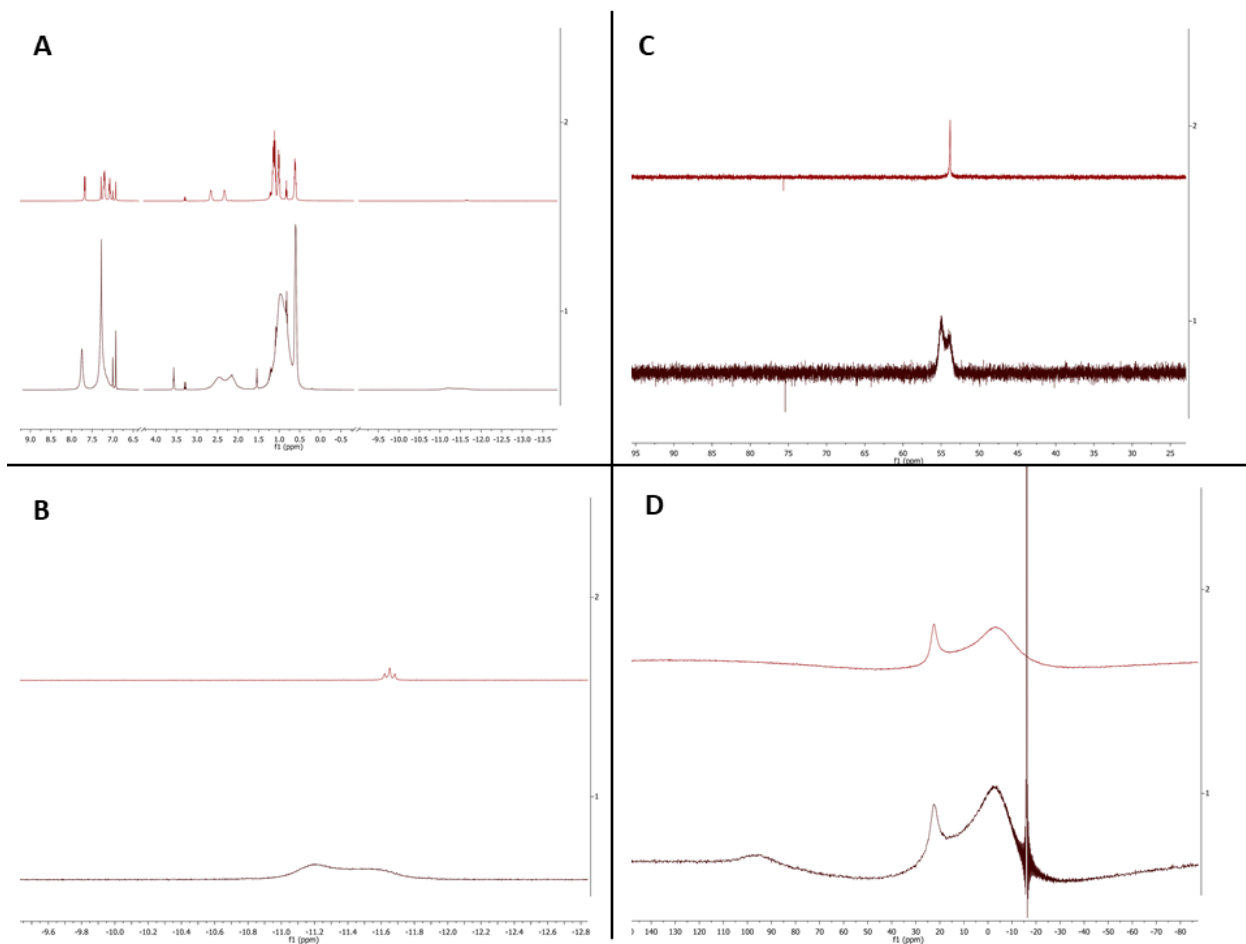


Figure III-17. A. Top: ^1H NMR spectrum of $308a-d_4$ in $\text{C}_6\text{D}_5\text{Br}$. Bottom: ^1H NMR spectrum collected 5 min after the addition of $317a$. Signals are broad due to a rapid exchange between $317a$ and $308a-d_4$. B. Top: ^1H NMR spectrum from -9.6 ppm to -12.6 ppm of $308a-d_4$ in $\text{C}_6\text{D}_5\text{Br}$. Hydride signal (-11.65 ppm, 16%) belongs to the CD_3OH addition product. Bottom: ^1H NMR spectrum from -9.6 ppm to -12.6 ppm collected 5 min after the addition of $317a$. C. Top: $^{31}\text{P}\{^1\text{H}\}$ NMR spectrum of $308a-d_4$ in $\text{C}_6\text{D}_5\text{Br}$. Bottom: $^{31}\text{P}\{^1\text{H}\}$ NMR spectrum collected 5 min after the addition of $317a$. D. Top: $^{11}\text{B}\{^1\text{H}\}$ NMR spectrum of $308a-d_4$ in $\text{C}_6\text{D}_5\text{Br}$. Bottom: $^{11}\text{B}\{^1\text{H}\}$ NMR spectrum collected 5 min after the addition of $317a$. $317a$ and $308a-d_4$ signals were observed distinctly when the acquisition time was set to be 20 ms

O–H cleavage reaction rate comparison between cyclohexanol and ethanol at room temperature. Two solutions were prepared in J. Young tubes as described in Table III-3. Both J. Young tubes were stirred at room temperature and monitored by NMR spectroscopy at intervals specified in Table III-4. Concentration of **74** ([Ir]) was calculated by ¹H NMR spectroscopy with 0.020 mmol 1,4-dioxane as internal standard with a total volume of 0.50 mL. [Ir]/[Ir]₀ was calculated by concentration of **74** divided by initial concentration of **74** in each tube:

Table III-3. Solution in J. Young tube III-1 and III-2 with a total volume of 0.50 mL

	Tube III-1	Tube III-2
74 (0.10 M in C ₆ D ₆)	0.020 mmol, 0.20 mL	0.020 mmol, 0.20 mL
1,4-Dioxane (0.20 M in C ₆ D ₆)	0.020 mmol, 0.10 mL	0.020 mmol, 0.10 mL
C ₆ D ₆	0.16 mL	0.16 mL
Substrate (0.50 M in C ₆ D ₆)	0.020 mmol, 40 μL ethanol	0.020 mmol, 40 μL cyclohexanol

Table III-4. Data table for **74 consumption in tube III-1 and tube III-2 over time for EtOH-CyOH comparison**

Tube III-1: cyclohexanol			Tube III-2: ethanol		
Time/min	[Ir]/M	[Ir]/[Ir] ₀	Time/min	[Ir]/M	[Ir]/[Ir] ₀
0	0.042	1.0	0	0.043	1.0
853	0.025	0.59	131	0.032	0.75
1732	0.019	0.45	366	0.022	0.52
2230	0.016	0.38	877	0.012	0.29
3403	0.011	0.27	2406	0.0048	0.11
4220	0.0095	0.23	3250	0.0032	0.075
6788	0.0051	0.12	4243	0.0022	0.051

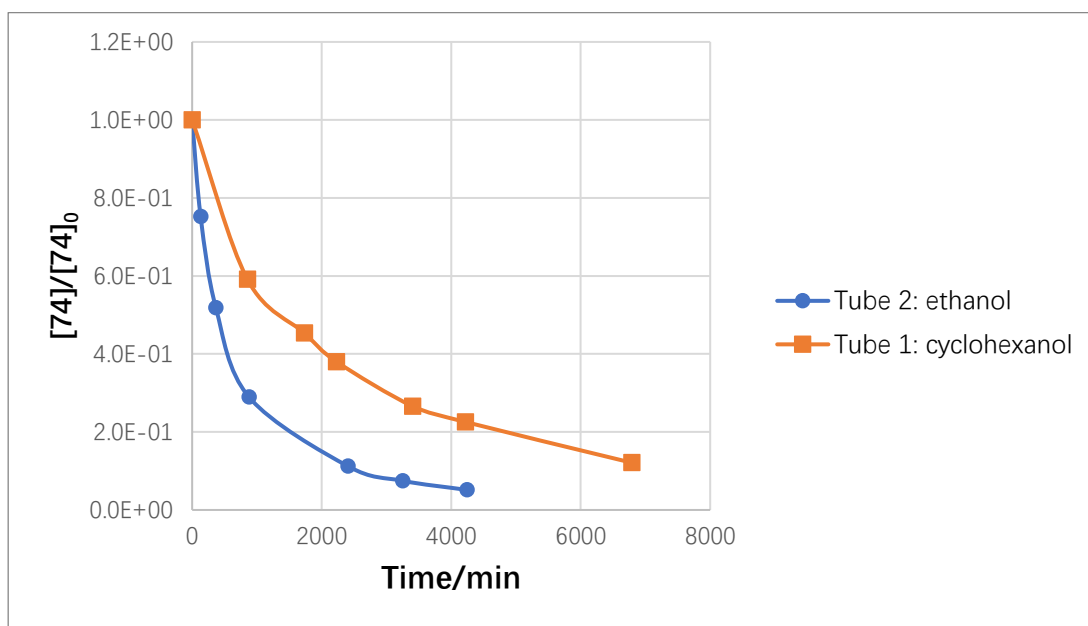


Figure III-18. Consumption of 74 over time for EtOH-CyOH addition rate comparison

O–H cleavage reaction rate comparison between phenol, 4-(trifluoromethyl)phenol and 4-methoxyphenol. Three solutions were prepared in J. Young tubes as described in Table III-5. All three J. Young tubes were stirred at room temperature and monitored by NMR spectroscopy at intervals specified in Table III-6. Concentration of **74** ([Ir]) was calculated by ¹H NMR spectroscopy with 0.020 mmol 1,4-dioxane as internal standard with a total volume of 0.50 mL. [Ir]/[Ir]₀ was calculated by concentration of **74** divided by initial concentration of **74** in each tube:

Table III-5. Solution in J. Young tube III-3 - III-5 with a total volume of 0.50 mL

	Tube III-3	Tube III-4	Tube III-5
74 (0.10 M in C ₆ D ₆)	0.020 mmol, 0.20 mL	0.020 mmol, 0.20 mL	0.020 mmol, 0.20 mL
1,4-Dioxane (0.20 M in C ₆ D ₆)	0.020 mmol, 0.10 mL	0.020 mmol, 0.10 mL	0.020 mmol, 0.10 mL
C ₆ D ₆	0.16 mL	0.16 mL	0.16 mL
Substrate (0.50 M in C ₆ D ₆)	0.020 mmol, 40 μL phenol	0.020 mmol, 40 μL 4-(trifluoromethyl)phenol	0.020 mmol, 40 μL 4-methoxyphenol

Table III-6. Data table for 74 consumption over time for phenol derivatives addition rate comparison

Tube III-3: phenol			Tube III-4: 4-(trifluoromethyl)phenol			Tube III-5: 4-methoxyphenol		
Time /min	[Ir]/M	[Ir]/[Ir] ₀	Time /min	[Ir]/M	[Ir]/[Ir] ₀	Time /min	[Ir]/M	[Ir]/[Ir] ₀
0	0.043	1.0	0	0.040	1.0	0	0.043	1.0
14	0.032	0.74	14	0.0040	0.10	48	0.038	0.90
28	0.026	0.61	27	0.0028	0.070	115	0.035	0.83
59	0.019	0.44	40	0.0024	0.060	148	0.034	0.79
84	0.015	0.34	52	0.0020	0.050	176	0.032	0.76
127	0.011	0.25	64	0.0016	0.040	212	0.031	0.74
170	0.0078	0.18	83	0.0014	0.035	348	0.028	0.65
206	0.0062	0.14	101	0.0012	0.030	512	0.025	0.59
243	0.0050	0.12	138	0.0010	0.025	1144	0.018	0.43
288	0.0038	0.088	164	0.00080	0.020			
360	0.0028	0.065	252	0.00060	0.015			
871	0.00060	0.014	722	0.00020	0.0050			

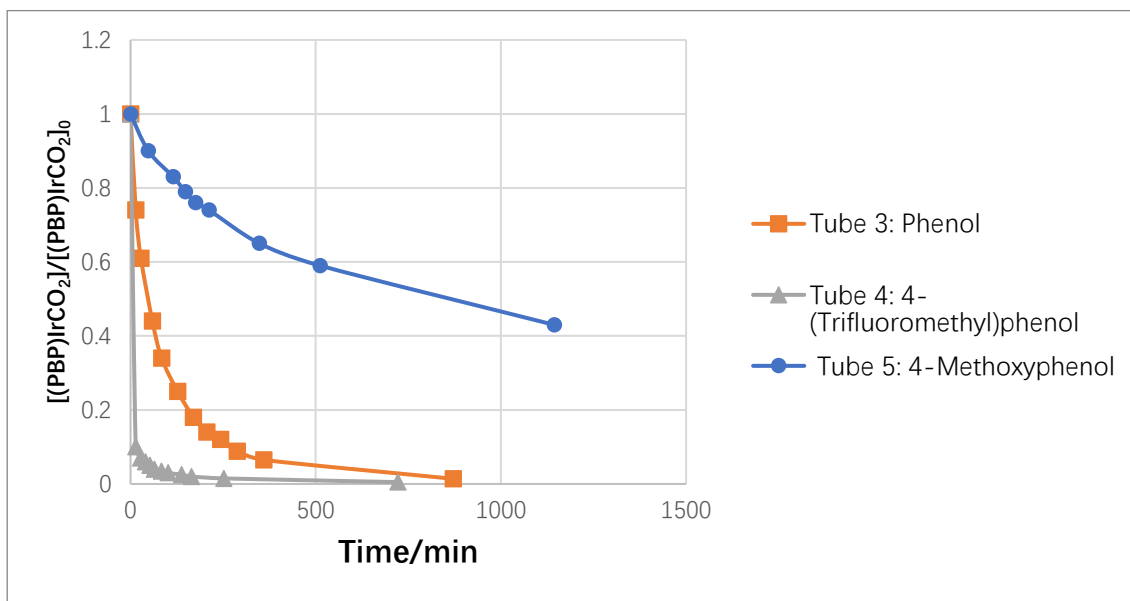


Figure III-19. Consumption of 74 over time for phenol derivatives addition rate comparison

O–H cleavage acceleration with catalytic amount of 317a. Two solutions were prepared in J. Young tubes as described in Table III-7. Both tubes were stirred at room temperature for 15 h. $^{31}\text{P}\{^1\text{H}\}$ NMR spectra was recorded for tube III-6 – III-7 to compare the reaction rate. Tube III-7 with **317a** reacted faster compared to tube III-6 without **317a** to form **310a**.

Table III-7. Solution in J. Young tube III-6 – III-7 with a total volume of 0.44 mL

	Tube III-6	Tube III-7
74 (0.10 M in C_6D_6)	0.020 mmol, 0.20 mL	0.020 mmol, 0.20 mL
1,4-Dioxane (0.20 M in C_6D_6)	0.020 mmol, 0.10 mL	0.020 mmol, 0.10 mL
Fluorobenzene	0.10 mL	0.10 mL
Cyclohexanol (0.50 M in C_6D_6)	0.020 mmol, 40 μL	0.020 mmol, 40 μL
317a	0 mg	2.0 mg, 0.0015 mmol

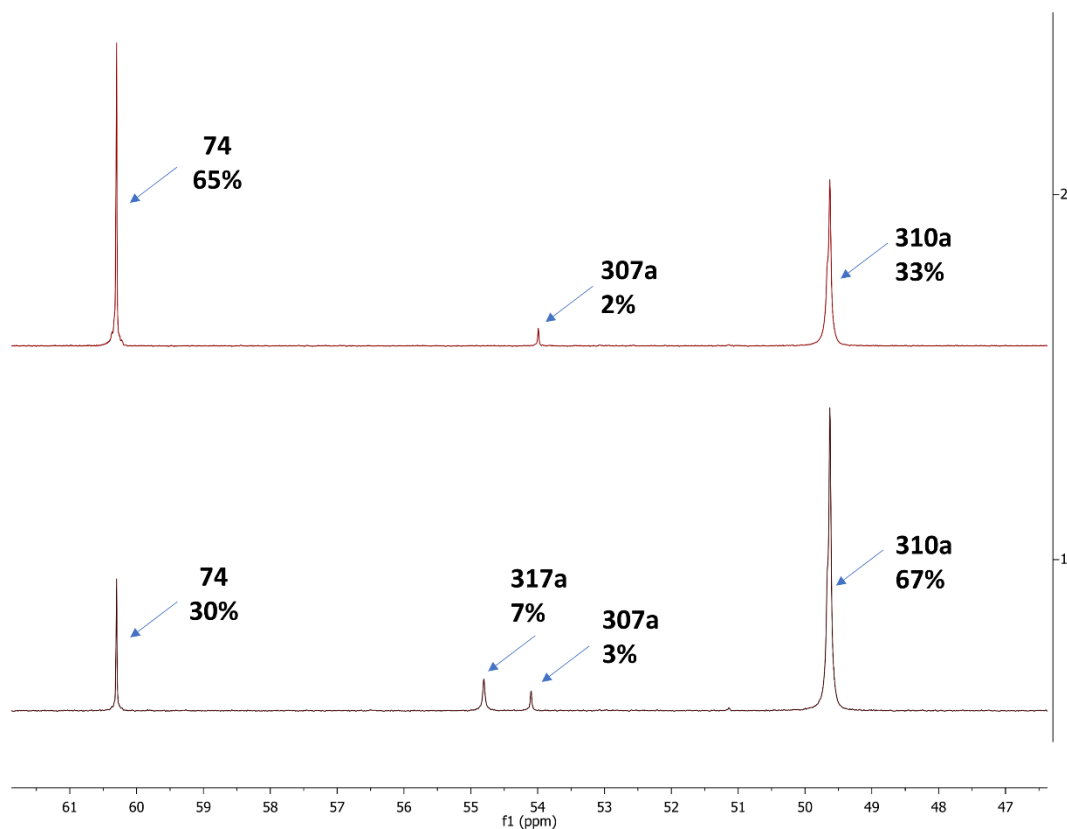


Figure III-20. $^{31}\text{P}\{^1\text{H}\}$ NMR spectra of **74** (0.020 mmol), cyclohexanol (0.020 mmol) mixture (Top: without **317a**. Bottom: with **317a** (0.0015 mmol)) recorded after 15 h of stirring at room temperature

Attempted acceleration of 74 reacting with *tert*-butyl alcohol. In a J. Young tube, to **74** (0.020 mmol, 0.20 mL, 0.10 M in C_6D_6) was added **317a** (0.0015 mmol, 2.0 mg), *tert*-butyl alcohol (0.20 mmol, 20 μL) and 0.20 mL $\text{C}_6\text{H}_5\text{F}$. The mixture was stirred at room temperature for a week. Based on *in situ* $^{31}\text{P}\{^1\text{H}\}$ NMR spectrum, one new peak at 44.1 ppm (11%) was observed. Based on *in situ* ^1H NMR spectrum, one hydride at -12.36 (t, $J_{\text{H-P}} = 16.1$ Hz, 11%) was observed. With the same reaction mixture, further heating at 50 $^\circ\text{C}$ led to the generation of an unidentified compound. Adding additional

tert-butyl alcohol (400 μL) as solvent and heat at 50 $^{\circ}\text{C}$ for 24 h lead to the generation of mixtures with several different unidentified compounds.

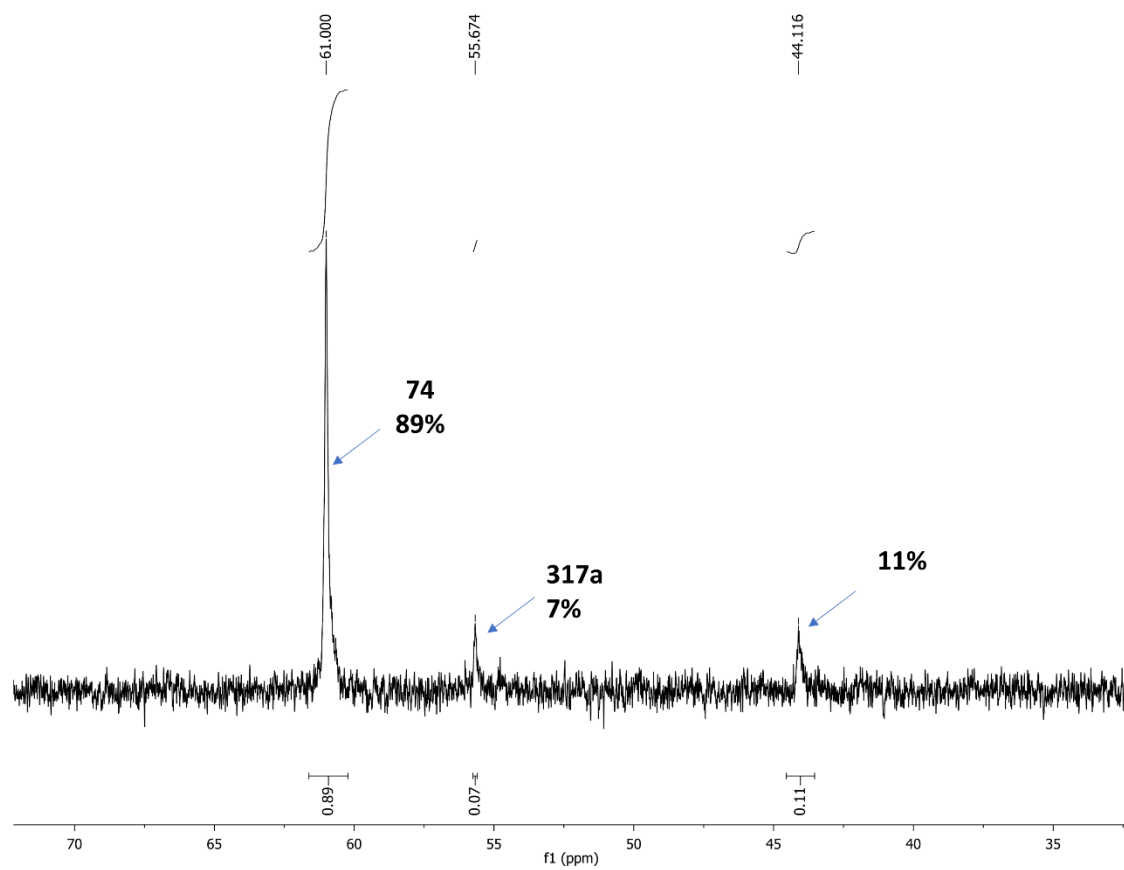


Figure III-21. $^{31}\text{P}\{^1\text{H}\}$ NMR spectrum of 74 (0.020 mmol), *tert*-butyl alcohol (0.20 mmol) and 317a (0.0015 mmol) mixture recorded after a week of stirring at room temperature. The peak at 44.1 ppm was generated (11%)

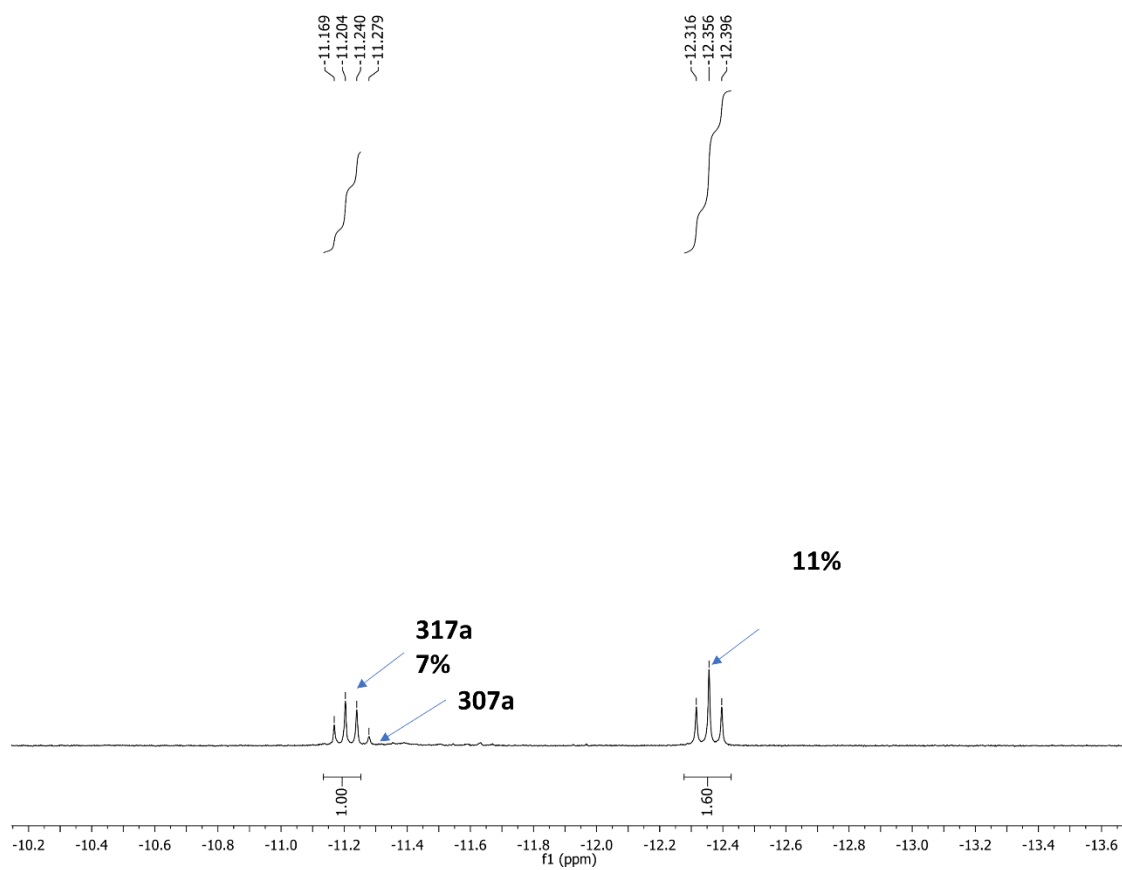


Figure III-22. ¹H NMR spectrum (from -10 ppm to -14 ppm) of 74 (0.020 mmol), *tert*-butyl alcohol (0.20 mmol) and 317a (0.0015 mmol) mixture recorded after a week of stirring at room temperature. The peak at 12.36 ppm (t, $J_{H-P} = 16.1$ Hz) was generated (11%)

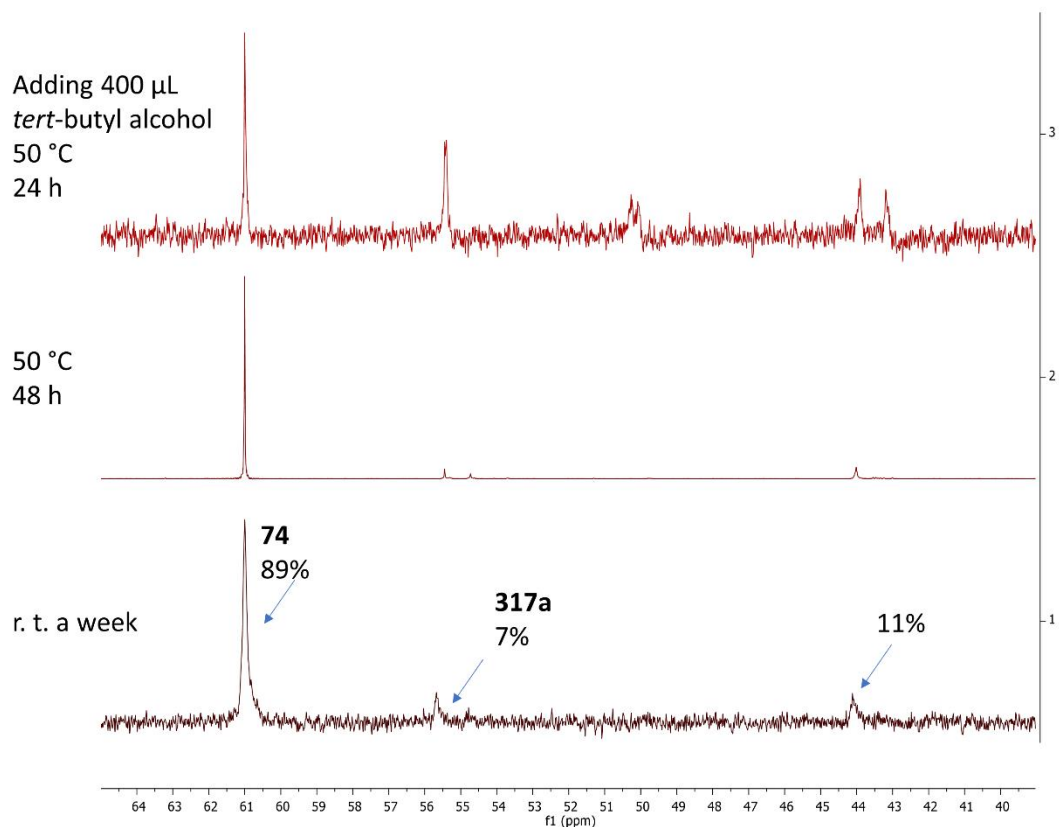


Figure III-23. Bottom: $^{31}\text{P}\{^1\text{H}\}$ NMR spectrum of **74** (0.020 mmol), *tert*-butyl alcohol (0.20 mmol) and **317a** (0.0015 mmol) mixture recorded after a week of stirring at room temperature. **Middle:** $^{31}\text{P}\{^1\text{H}\}$ NMR spectrum of the same mixture recorded after further heating at 50 °C for 48 h. **Top:** $^{31}\text{P}\{^1\text{H}\}$ NMR spectrum recorded after the middle mixture was added 400 μL *tert*-butyl alcohol and further heating at 50 °C for 24 h

3.4.4 X-Ray Structural Determination Details

The X-ray crystal data (cifs) could be obtained by the follow link:

<https://pubs.acs.org/doi/10.1021/acs.organomet.8b00785>

X-Ray data collection, solution, and refinement for $(\text{PB}^{\text{OEt}}\text{P})\text{Ir}(\text{H})(\text{CO})_2$ (309a**, CCDC 1858841).** A pale yellow, multi-faceted block of suitable size (0.12 x 0.12 x 0.03 mm) was selected from a representative sample of crystals of the same habit using

an optical microscope and mounted onto a nylon loop. Low temperature (150 K) X-ray data were obtained on a Bruker APEXII CCD based diffractometer (Mo sealed X-ray tube, $K_{\alpha} = 0.71073 \text{ \AA}$). All diffractometer manipulations, including data collection, integration and scaling were carried out using the Bruker APEXII software.¹²² An absorption correction was applied using SADABS.¹²³ The space group was determined on the basis of systematic absences and intensity statistics and the structure was solved by direct methods and refined by full-matrix least squares on F^2 . The structure was solved in the orthorhombic P $2_12_12_1$ space group using XS¹²⁴ (incorporated in SHELXLE). All non-hydrogen atoms were refined with anisotropic thermal parameters. All hydrogen atoms were placed in idealized positions and refined using riding model with the exception of the hydrogen bound to iridium which was located from the difference map. The structure was refined (weighted least squares refinement on F^2) and the final least-squares refinement converged. No additional symmetry was found using ADDSYM incorporated in PLATON program.¹⁶⁹

X-Ray data collection, solution, and refinement for (PBⁿ-BuP)Ir(CO)(H) (316b, CCDC 1858841). A light yellow, multi-faceted block of suitable size (0.90 x 0.66 x 0.49 mm) was selected from a representative sample of crystals of the same habit using an optical microscope and mounted onto a nylon loop. Low temperature (110 K) X-ray data were obtained on a Bruker APEXII CCD based diffractometer (Mo sealed X-ray tube, $K_{\alpha} = 0.71073 \text{ \AA}$). All diffractometer manipulations, including data collection, integration and scaling were carried out using the Bruker APEXII software.¹²² An absorption correction was applied using SADABS.¹²³ The space group was determined on the basis of

systematic absences and intensity statistics and the structure was solved by direct methods and refined by full-matrix least squares on F^2 . The structure was solved in the monoclinic P 2₁/c space group using XS¹²⁴ (incorporated in SHELXLE). All non-hydrogen atoms were refined with anisotropic thermal parameters. All hydrogen atoms were placed in idealized positions and refined using riding model with the exception of the hydrogen bound to iridium which was located from the difference map. The structure was refined (weighted least squares refinement on F^2) and the final least-squares refinement converged. No additional symmetry was found using ADDSYM incorporated in PLATON program.¹⁶⁹

CHAPTER IV

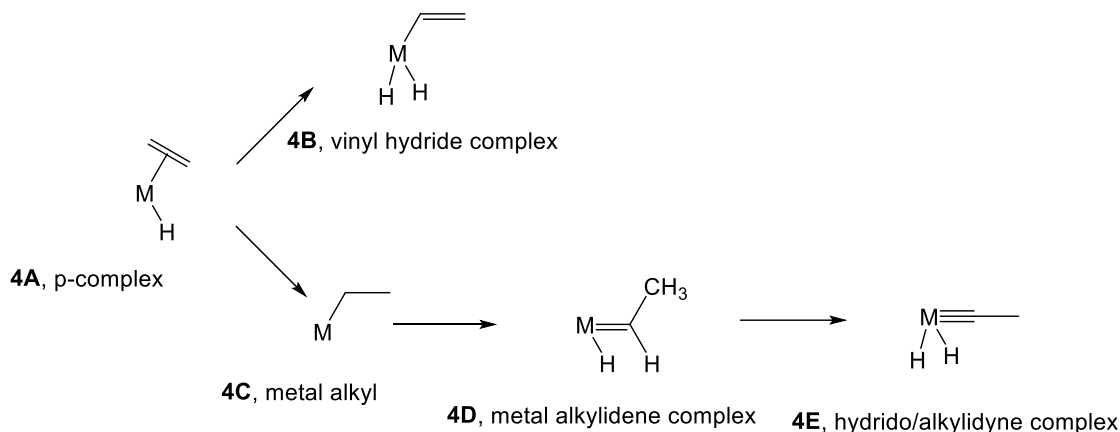
REVERSIBLE ADDITION OF ETHYLENE TO A Pincer-BASED BORYL-IRIDIUM UNIT WITH THE FORMATION OF A BRIDGING ETHYLIDENE[‡]

4.1 Introduction

The nature of the elementary reactions of binding ethylene and other alkenes to transition metal centers is of importance to many common and impactful catalytic processes that utilize alkenes as feedstocks.¹⁷⁰⁻¹⁷⁶ The initial interaction between a suitably unsaturated transition metal complex and an alkene (Scheme IV-1) typically results in a π -complex (**4A**)¹⁷⁷, which may then undergo C-H oxidative addition to yield a vinyl hydride isomer (**4B**)¹⁷⁸⁻¹⁷⁹, or isomerization via an initial insertion product **4C** to a metal alkylidene complex (**4D**)¹⁸⁰⁻¹⁸², or even a hydrido/alkylidyne isomer (**4E**).¹⁸³⁻¹⁸⁴ The latter two isomerizations typically require the presence of hydride ligands in the metal fragment and proceed by a combination of insertion of the olefin into M-H and subsequent single or double α -H elimination. Moreover, since isomerization of a free hydrocarbon olefin into a free alkylidene is unfavourable by >70 kcal/mol,¹⁸⁵ only the metal centers with an enormous preference for binding an alkylidene vs olefin are thermodynamically capable of it.¹⁸⁰⁻¹⁸² This thermodynamic capacity is more or less restricted to highly electron-rich

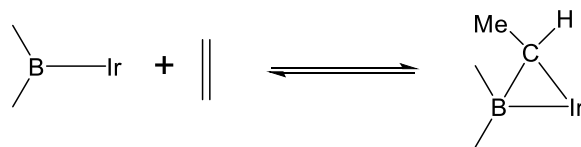
[‡] Reproduced in whole from “Reversible Addition of Ethylene to a Pincer-Based Boryl-Iridium Unit with the Formation of a Bridging Ethylidene” by Cao, Y.; Shih, W.-C.; Bhuvanesh, N.; Ozerov, O. V. *Chem. Sci.* 2020, 11, 10998-11002. Copyright [2020] by Royal Society of Chemistry. The synthesis and crystal structure of **401**, **403** has been developed and solved by our former group members Dr. Wei-Chun Shih. The crystal structure of **402** was solved by crystallographer Dr. Nattamai Bhuvanesh.

early- to mid-periodic table metals in low oxidation states and with propensity to form multiple metal-ligand bonds.



Scheme IV-1. Typical outcomes of a reaction between an olefin (ethylene for simplicity) and a transition metal complex

In the present work, we report unexpected findings that emerged in the course of our exploration of the reactivity of Ir complexes of a diarylboryl-containing PBP pincer ligand.^{27, 37, 78, 80, 83-84, 96, 100, 102, 186-187} In particular, we discovered that ethylene can reversibly add to the boryl-iridium unit as a bridging ethylidene. Complexes of monodentate boryl ligands are well established and important intermediates in such organometallic catalytic processes as hydroboration¹⁸⁸ and C-H borylation.¹⁸⁹ Some variants of aromatic C-H borylation rely on the presence of sacrificial olefin reagents.^{150, 189} To the best of our knowledge, formation of alkylidenes bridging a boron and a transition metal in C-H borylation of arenes or olefins,¹⁸⁹ or in olefin hydroboration,¹⁸⁸ has not been documented or considered.

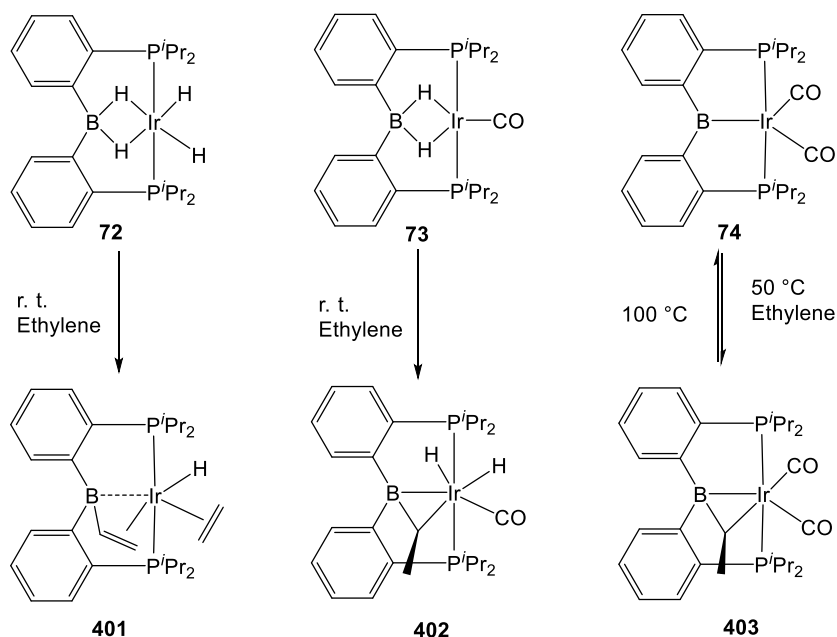


Scheme IV-2. The new reactivity reported in this work

4.2 Result and Discussion

4.2.1 Reaction of Ethylene with (PBP)Ir Complexes

For the reactions with ethylene, we chose the recently disclosed complexes **72**, **73**, and **74**.¹⁰² Solutions of **72**, **73**, and **74** in toluene or benzene were blanketed with an atmosphere of ethylene and allowed to react with stirring overnight (Scheme IV-3). Reactions with **72** and **73** proceeded at ambient temperature, while reaction with **74** required thermolysis at 50 °C for 36 h. Upon removal of volatiles and recrystallization, the new complexes **401**, **402**, and **403** were obtained in pure form. NMR spectroscopic analysis of **401** indicated that it possesses an intact PBP ligand with apparent C_s symmetry, a sp^3 -hybridized boron center (^{11}B NMR: δ 20.3 ppm), a single hydride, an Ir-bound ethylene, and a vinyl group. These data point to the structure depicted in Scheme 2, which was confirmed by an X-ray diffraction study (vide infra). **401** is the product of addition of two equivalents of ethylene to the (PBP)Ir fragment. This is atypical for reactions of (pincer)IrH₂ or (pincer)IrH₄ with an olefin, which normally yield either a (pincer)Ir(η^2 -olefin) complex or a (pincer)Ir(H)(alkenyl) isomer in cases of high steric congestion,¹⁷⁸ both being products of the reaction of the pincer complex with only one alkene.



Scheme IV-3. Reactions of **72**, **73**, and **74** with Ethylene

Complexes **402** and **403** both also contained all the expected ^1H NMR resonances for the PBP ligand and their ^{11}B NMR chemical shifts (17.8 and 20.4 ppm, respectively) also indicated sp^3 hybridization at boron. However, there were no resonances in either **402** or **403** that could be ascribed to a π -bound ethylene or a vinyl group. Instead, **402** and **403** each possessed a pair of ^1H NMR resonances in a 1:3 integral ratio consistent with a CHCH_3 fragment (**402**: δ 3.37 (m, 1H) and 1.75 (d, $J_{\text{H-H}} = 7.0$ Hz, 3H) ppm; **403**: δ 2.72 (m, 1H) and 1.39 (dd, $J_{\text{H-H}} = 7.0$, $J_{\text{P-H}} = 0.7$ Hz, 3H) ppm). **402** displayed resonances for two inequivalent hydrides (-11.10 and -12.88 ppm), whereas **403** displayed none. These data were consistent with the presence of an ethylidene (CHCH_3) unit bridging B and Ir. Furthermore, the observed C_1 symmetry in the NMR spectra of **402** and **403** was consistent with the presence of a carbon center with four different substituents (the methine carbon of the bridging alkylidene). IR spectroscopic observations suggested the presence of a

single CO ligand in **402** ($\nu_{\text{CO}} = 1977 \text{ cm}^{-1}$) and two CO ligands in **403** ($\nu_{\text{CO}} = 1987$ and 1942 cm^{-1}).

Interestingly, addition of ethylene to **74** is partially reversible. Thermolysis of a solution of **403** at $90 \text{ }^{\circ}\text{C}$ led to the appearance of signals for **74** and free ethylene. Traces of free ethylene were also observed upon thermolysis of **402** at $80 \text{ }^{\circ}\text{C}$ for 10 min.

4.2.2 Structural Characterization

Solid-state structures of **401**, **402**, and **403** were determined by single-crystal X-ray diffractometry (Figure IV-1). The structure of **402** contained two independent molecules in the asymmetric unit. Both molecules displayed disorder, which was successfully modelled through varying the positions of the atoms in the Ir-CHMe unit, as well as CO for one of the molecules. The disorder likely involves other atoms in the molecules, but it was not possible to improve the model via consideration of the other atom positions. Because of this, while the connectivity of the non-hydrogen atoms was unambiguously established, the metrics associated with the immediate coordination sphere of Ir cannot be reliably interpreted.

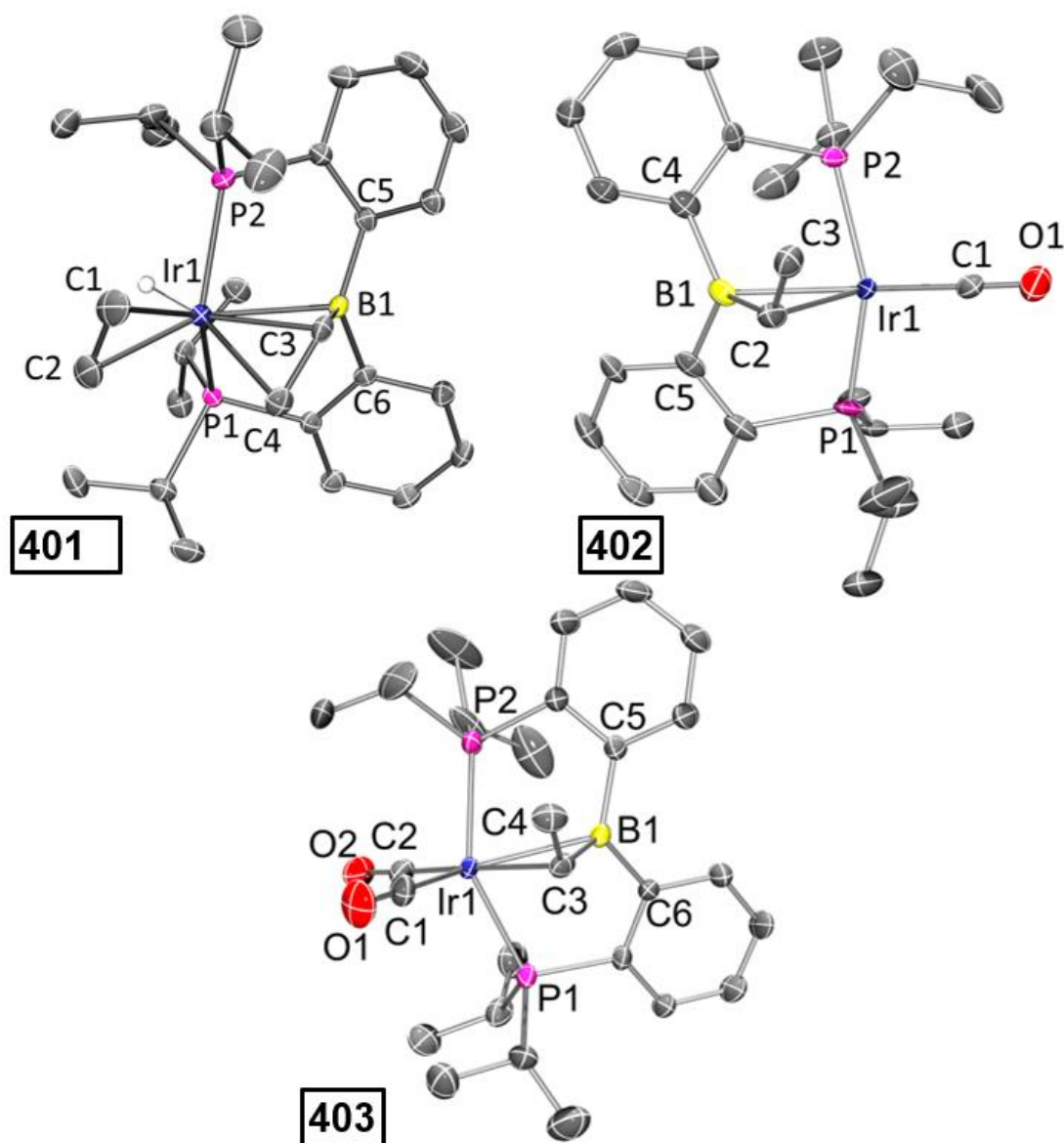


Figure IV-1. ORTEP drawings showing selected atom labeling of 401, 402 and 403. Hydrogen atoms (except Ir-H) are omitted for clarity. 401. Ir1–B1, 2.396(3) Å; Ir1–C1, 2.200(3) Å; Ir1–C2, 2.223(3) Å; Ir1–C3, 2.213(3) Å; Ir1–C4, 2.248(3) Å; C1–C2, 1.402(4) Å; C3–C4, 1.405(4) Å; C3–B1, 1.556(4) Å; C5–B1–C6, 120.4(2)°; C6–B1–C3, 117.5(2)°; C3–B1–C5, 115.6(2)°. 402. The structure contains two independent molecules and each is disordered, including the Ir position. One of the independent molecules is drawn. See section 4.4.5 for additional information. 403. Ir1–B1, 2.475(4) Å; Ir1–C3, 2.262(4) Å; C3–C4, 1.523(6) Å; C3–B1, 1.530(6) Å; C1–O1, 1.160(5) Å; C2–O2, 1.136(6) Å; C1–Ir1–C3, 175.7(2)°; P1–Ir1–P2 140.36(4)°; C5–B1–C6, 122.0(3)°; C6–B1–C3, 118.2(3)°; C3–B1–C5, 114.6(3)°

In the structure of **401**, the coordination sphere of Ir contains a hydride, two phosphines, two olefin donors, and a relatively distant interaction with a boron center (2.396(3) Å). If the latter were ignored, the molecule could be viewed as a monovalent, five-coordinate IrXL₄ center with a geometry intermediate between square pyramidal and trigonal planar ($\tau = 0.43$).¹⁹⁰ This geometry probably results from a combination of innate electronic preferences and the constraint imposed by the chelating ligand. The Ir-B distance in **401** is ca. 0.1 Å longer than those recorded for Ir and Rh complexes of BP₃ and PB(Ph)P where the central borane site functioned as a Z-type ligand^{46, 67-70}, and it is ca. 0.25 Å longer than the Ir-B(boryl) bond distance in **74**.¹⁰² The sum of C-B-C angles about boron (ca. 354°) indicates only modest pyramidalization. The proximity of B to Ir is also dictated by the vinyl-Ir interaction. Furthermore, the BCHCH₂ unit could alternatively be viewed as a η^3 -borataallyl^{155, 191} fragment bound to Ir (Figure IV-2). The related η^3 -binding of a B-Ph group in boranes coordinating to transition metals has also been reported.^{72-73, 75-76, 192} The B1-C3 distance of 1.556(4) Å is shorter than the B-C_{aryl} distances in **401** or **403** (ca. 1.59-1.61 Å).

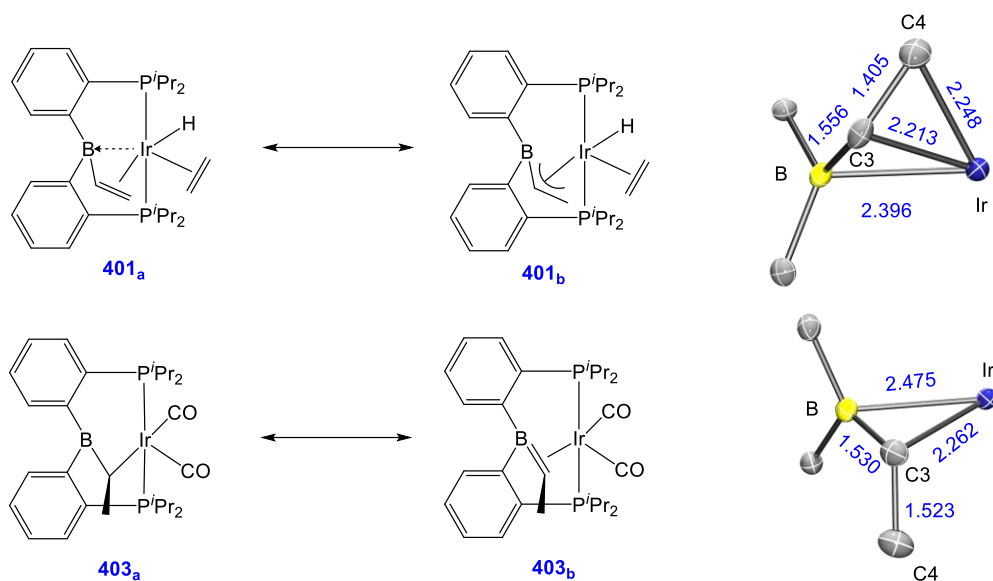


Figure IV-2. ChemDraw interpretations and POV-Ray rendition of the ORTEP drawing (50% thermal ellipsoids, truncated molecules with boron center and atoms around boron) of **401 and **403****

The structure of **403** contains an even more distant interaction between Ir and B (2.475(4) Å) and the boron center is also only slightly pyramidalized (sum of C-B-C angles ca. 355°). If the Ir-B interaction were discounted, the molecule could be viewed as an IrXL₄ five-coordinate ($\tau = 0.60$),¹⁹⁰ where X is the boryl-substituted alkyl ligand connected to Ir via C3. However, the Ir-C3 distance of 2.261(4) Å is considerably longer than the sum of Ir and C covalent radii (2.17 Å).¹⁹³ In fact, it is even slightly longer than the Ir-C distances (2.20-2.25 Å) to the π -bound olefins in **401**. In addition, the B1-C3 distance (1.530(6) Å) is shorter than is expected for a single B-C bond (cf. the B-C_{aryl} distances in **401** and **403**). These metrics point to an alternative view of this structure as an η^2 -borataalkene¹⁵⁴ complex of monovalent Ir (Figure IV-2). It is important to

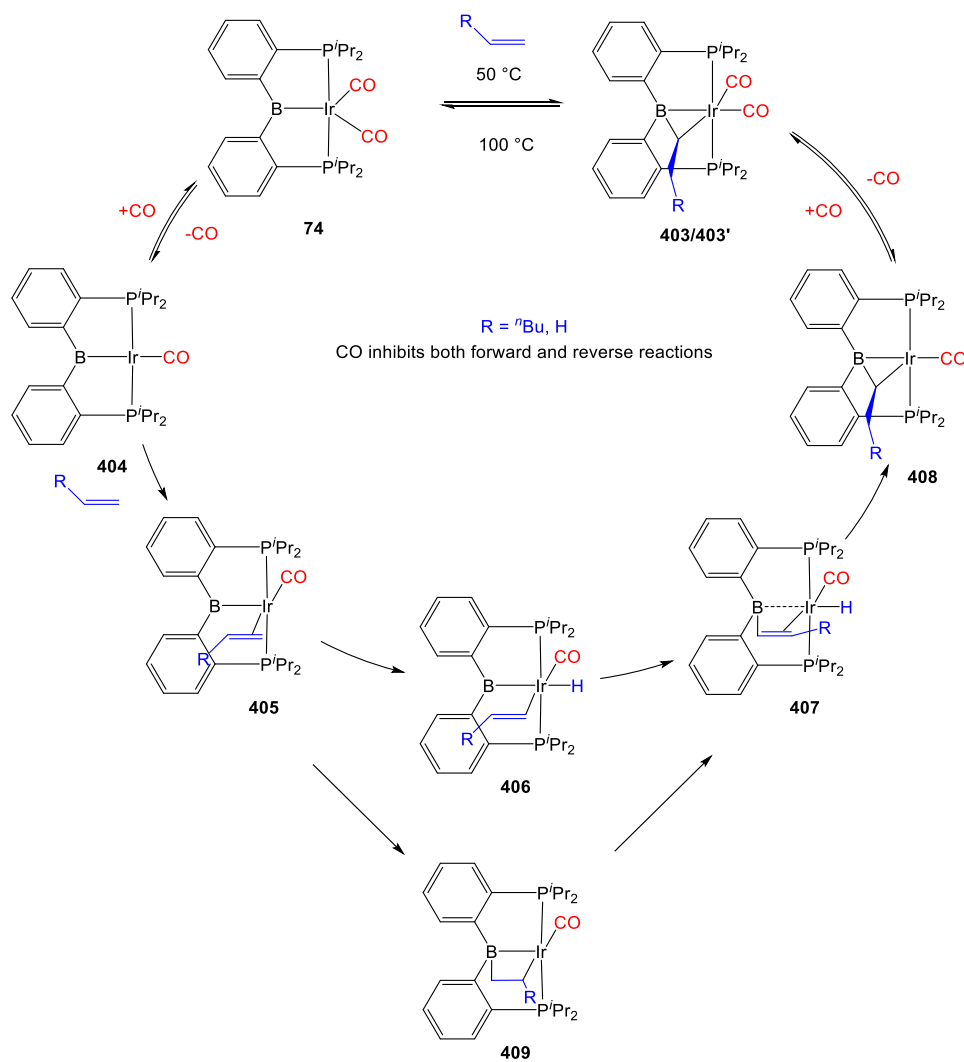
emphasize that the alternative descriptions of the observed structures for **401** (vinylborane vs borataallyl complex) and **403** (boryl-substituted alkyl or borataalkene complex) are not possible isomers but rather idealized or extreme descriptions of the same molecule.

4.2.3 Mechanistic Analysis

We recently reported that **74** can selectively activate the *ortho*-C-H bonds in pyridine derivatives. **74** is an 18-electron complex at Ir and thus cannot undergo direct oxidative addition. Thus, the mechanism of C-H activation of pyridines was proposed whereby one of the CO ligands in **74** has to dissociate to allow for the C-H oxidative addition to take place at the monocarbonyl intermediate. It was observed that the C-H activation of pyridines was retarded by the presence of free CO.

We surmised that the activation of ethylene by **74** may proceed by a related mechanism¹⁹⁴ (Scheme IV-4). We propose that dissociation of CO creates unsaturation and permits coordination of the olefin to give intermediate **405** and then oxidative addition of the vinylic C-H bond to give **406**. The resultant vinyl group may then migrate from Ir to B to give **407**, and then insertion into the Ir-H produces **408** and after recapturing CO, **403**, with the observed bridging ethylidene structure. We previously observed facile migration of phenyl between B and Ir (or Rh) in complexes of this PBP ligand.²⁷ The proposed migration of a vinyl is reasonable by analogy. Alternatively, one could envision that **405** is converted to **407** via a 2,1-olefin insertion into the Ir-B bond and the subsequent β -hydrogen elimination from the resultant boroalkyl **409**. Although insertions of olefins into M-B bonds are well precedented,¹⁹⁵⁻¹⁹⁹ it is not clear that the chelate constraint here

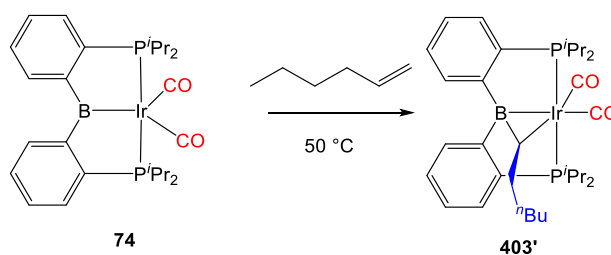
would enable 1,2-insertion or that it should proceed with the regioselectivity needed for the eventual production of **403'**.



Scheme IV-4. Proposed mechanism

We tested our mechanistic proposal by examining whether the rate of ethylene addition to **74** was affected by the presence of free CO. Owing to the practical challenges in varying the pressures or concentrations of two gaseous reagents (C_2H_4 and CO) in NMR tube experiments, we elected to carry out test reactions with 1-hexene instead. First, we

established that 1-hexene indeed formed the analogous product. (Scheme IV-5) Treatment **74** with 80 equivalents of 1-hexene, after thermolysis at 50 °C for 16 h, resulted in the formation of a product **403'**, whose NMR spectroscopic features closely matched those of **403**, except for the presence of a pentyl group in place of a methyl in the bridging alkylidene (See Table IV-1). Interestingly, the reaction of **74** with *trans*-2-hexene also gave **403'** as the major product after 5 d at 100 °C (see section 4.4.4). We then examined the progress of reactions of **74** with 1-hexene under the atmosphere of Ar vs CO but otherwise identical conditions (C₆D₆ solution 50 °C, 90 h) and concentrations. NMR analysis revealed 73% conversion to **403'** under Ar, and no detectable conversion under CO. Higher concentrations of 1-hexene correlated with faster conversion of **74** to **403'**. Thus, the reaction displays positive dependence on [1-hexene] and apparent inverse dependence on [CO], indicating that reversible dissociative displacement of CO with 1-hexene constitutes the rate-determining sequence.



Scheme IV-5. Reaction of **74** with 1-hexene

The mechanism proposed in Scheme IV-4 suggested, by the principle of microscopic reversibility, that loss of ethylene from **403** should also be retarded by the presence of free CO. Indeed, thermolysis (100 °C, 2 h) of two identically constituted C₆D₆ solutions of **403** resulted in diminished conversion to **74** (17% vs 35%) in the

reaction carried out under 1 atm of CO as opposed to 1 atm of Ar. Overall, the CO inhibition experiments support the proposed mechanism (Scheme IV-4) for the reactions of **74**. It is also reasonable to think that the reaction of **73** with ethylene proceeds by a similar mechanism, initiated by the dissociation of CO or H₂ from **73**. The product of the reaction of **74** with ethylene can be viewed as analogous to the intermediate **407** in Scheme IV-4 (with η^2 -ethylene in place of CO).

4.3 Conclusion

In summary, we have described a series of unusual outcomes in the reactions of ethylene with simple pincer complexes of Ir. These reactions demonstrate that the boryl of the PBP ligand is not merely an electronically special ligand or even a potential Lewis acid to Lewis basic sites. The presence of the boryl donor in the pincer can also significantly alter the preferred reactions products when contrasted with pincer complexes with different central heteroatoms.

4.4 Experimental Section

4.4.1 General Considerations

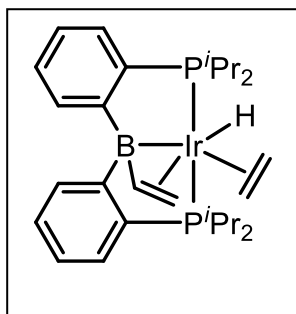
Unless specified otherwise, all manipulations were performed under an Ar atmosphere using standard Schlenk line or glovebox techniques. Toluene, diethyl ether, pentane, and isooctane were dried and deoxygenated (by purging) using a solvent purification system (Innovative Technology Pure Solv MD-5 Solvent Purification System) and stored over molecular sieves in an Ar-filled glove box. C₆D₆ was dried over NaK/Ph₂CO/18-crown-6, distilled or vacuum transferred and stored over molecular sieves in an Ar-filled glovebox. CH₂Cl₂, CDCl₃, cyclohexane, and C₆D₁₂ were dried over CaH₂,

distilled or vacuum transferred and stored over molecular sieves in an Ar-filled glove box. **72**, **73** and **74** were prepared via literature procedures.¹⁰² All other chemicals were used as received from commercial vendors.

4.4.2 Physical Methods

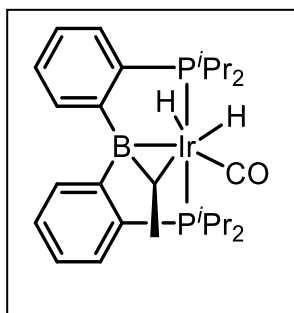
NMR spectra were recorded on a Varian Inova 300, Mercury 300 (¹H NMR, 299.952 MHz; ¹³C NMR, 75.421 MHz; ³¹P NMR, 121.422 MHz), Varian Inova 400 (¹H NMR, 399.535 MHz; ¹¹B NMR, 128.185 MHz; ³¹P NMR, 161.734 MHz) and Varian Inova 500 (¹H NMR, 499.703 MHz; ¹³C NMR, 125.697 MHz; ³¹P NMR, 202.265 MHz) spectrometer. Chemical shifts are reported in δ (ppm). For ¹H and ¹³C NMR spectra, the residual solvent peak was used as an internal reference (¹H NMR: δ 7.16 for C₆D₆, 7.24 for CDCl₃; ¹³C NMR: δ 128.62 for C₆D₆, 77.16 for CDCl₃). ¹¹B NMR spectra were referenced externally with BF₃ etherate at δ 0. ³¹P NMR spectra were referenced externally with 85% phosphoric acid at δ 0. Elemental analyses were performed by CALI Labs, Inc. (Highland Park, NJ)

4.4.3 Synthesis and Characterization of Iridium Complexes



(PB^{Vinyl}P)Ir(H)(C₂H₄) (401). In a 25 mL Teflon screw-capped round-bottomed flask, **72** (0.10 g, 0.10 mmol) was dissolved in toluene (2 mL). The solution was degassed twice via freeze-pump-thaw, and the flask was refilled with ethylene (1 atm). The reaction was stirred at room temperature overnight. The volatiles were removed under vacuum, and the resulting solid was recrystallized in toluene/pentane 1:3, yielding a pale orange solid (82 mg, 72%).

^1H NMR (500 MHz, C_6D_6): δ 8.30 (d, $J_{\text{H-H}} = 7.5$ Hz, 1H), 8.09 (d, $J_{\text{H-H}} = 7.5$ Hz, 1H), 7.32 (td, $J_{\text{H-H}} = 7.4$ Hz, 1.0 Hz, 1H), 7.24 (m, 2H), 7.14 (m, 1H), 7.03 (m, 1H), 6.97 (m, 1H), 4.45 (m, 1H, B-CH=CH₂), 2.96-1.89 (br, 6H, CH₂=CH₂ B-CH=CH₂), 2.70 (br, 1H, CHMe₂), 2.40 (br, 1H, CHMe₂), 2.28 (br, 1H, CHMe₂), 1.98 (br, 1H, CHMe₂), 1.28 (dvt, $J_{\text{H-H}} = 7.1$ Hz, 3H, CHMe₂), 1.13 (m, 9H, CHMe₂), 0.83 (dvt, $J_{\text{H-H}} = 6.4$ Hz, 3H, CHMe₂), 0.73 (dvt, $J_{\text{H-H}} = 6.9$ Hz, 3H, CHMe₂), 0.55 (dvt, $J_{\text{H-H}} = 7.7$ Hz, 3H, CHMe₂), 0.35 (dvt, $J_{\text{H-H}} = 7.3$ Hz, 3H, CHMe₂), -13.70 (br, 1H, Ir-H). $^{31}\text{P}\{^1\text{H}\}$ NMR (202 MHz, C_6D_6): δ 32.3 (br). $^{11}\text{B}\{^1\text{H}\}$ NMR (128 MHz, C_6D_6): δ 20.3 (br). $^{13}\text{C}\{^1\text{H}\}$ NMR (101 MHz, C_6D_6): δ 165.2 (br, C_q), 157.5 (br, C_q), 142.3 (br, C_q), 137.2 (br, C_q), 133.6 (t, $J_{\text{C-P}} = 10.0$ Hz, CH), 131.4 (t, $J_{\text{C-P}} = 10.8$ Hz, CH), 130.9 (s, CH), 129.9 (s, CH), 129.8 (s, CH), 129.3 (s, CH), 128.9 (s, CH), 125.6 (t, $J_{\text{C-P}} = 3.0$ Hz, CH), 125.5 (br, CH), 74.6 (br, Ir-CH=CH₂), 56.3 (br, CH₂=CH₂), 35.5 (m, CHMe₂), 32.0 (t, $J_{\text{C-P}} = 14.1$ Hz, CHMe₂), 27.5 (t, $J_{\text{C-P}} = 17.0$ Hz, CHMe₂), 27.1 (t, $J_{\text{C-P}} = 14.6$ Hz, CHMe₂), 22.1 (s, CH₃), 20.7 (s, CH₃), 20.4 (s, CH₃), 19.4 (s, CH₃), 19.0 (s, CH₃), 18.7 (s, CH₃), 18.6 (s, CH₃), 18.5 (s, CH₃). Elem. Anal. Calcd for C₂₈H₄₄B₁IrP₂: C, 52.09; H, 6.87. Found: C, 52.09; H, 6.58.

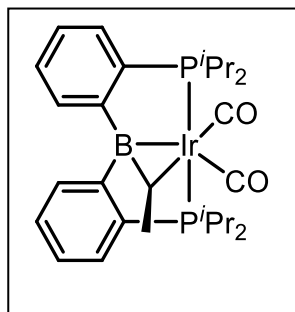


(PB^{CHCH₃}P)Ir(H)₂(CO) (402). In a 25 mL Teflon screw-capped round-bottomed flask, **73** (40 mg, 0.10 mmol) was dissolved in toluene (2 mL). The solution was degassed twice via freeze-pump-thaw, and the flask was refilled with ethylene (1 atm). The reaction was stirred at room temperature overnight. The volatiles

were removed under vacuum, and the resulting solid was recrystallized in pure pentane, yielding a colorless solid (25 mg, 60%).

^1H NMR (499 MHz, C_6D_6) δ 8.43 (dd, $J_{\text{H-H}} = 7.5, 2.3$ Hz, 1H), 8.34 (d, $J_{\text{H-H}} = 7.6$ Hz, 1H), 7.38 (t, $J_{\text{H-H}} = 7.3$ Hz, 1H), 7.25 (t, $J_{\text{H-H}} = 7.4$ Hz, 1H), 7.09 (m, 3H), 6.99 (t, $J_{\text{H-H}} = 7.2$ Hz, 1H), 3.37 (m, 1H, B-CH-CH₃), 2.17 (m, 2H, CHMe₂), 1.81 (m, 2H, CHMe₂), 1.75 (d, $J_{\text{H-H}} = 7.0$ Hz, 3H, B-CH-CH₃), 1.23 (dd, $J_{\text{H-P}} = 15.1$ Hz, $J_{\text{H-H}} = 6.9$ Hz, 3H, CHMe₂), 1.14 (dd, $J_{\text{H-P}} = 15.3$ Hz, $J_{\text{H-H}} = 7.0$ Hz, 3H, CHMe₂), 1.11 (dd, $J_{\text{H-P}} = 14.6$ Hz, $J_{\text{H-H}} = 7.0$ Hz, 3H, CHMe₂), 1.01 (dd, $J_{\text{H-P}} = 15.6$ Hz, $J_{\text{H-H}} = 7.2$ Hz, 3H, CHMe₂), 0.97 (dd, $J_{\text{H-P}} = 16.0$ Hz, $J_{\text{H-H}} = 6.8$ Hz, 3H, CHMe₂), 0.93 (dd, $J_{\text{H-P}} = 15.7$ Hz, $J_{\text{H-H}} = 6.8$ Hz, 3H, CHMe₂), 0.65 (dd, $J_{\text{H-P}} = 14.5$ Hz, $J_{\text{H-H}} = 6.9$ Hz, 3H, CHMe₂), 0.57 (dd, $J_{\text{H-P}} = 15.3$ Hz, $J_{\text{H-H}} = 6.8$ Hz, 3H, CHMe₂), -11.10 (ddd, $J_{\text{H-P}} = 19.6, 13.3$ Hz, $J_{\text{H-H}} = 2.5$ Hz, 1H, Ir-H), -12.88 (t, $J_{\text{H-P}} = 14.5$ Hz, 1H, Ir-H). $^{31}\text{P}\{^1\text{H}\}$ NMR (202 MHz, C_6D_6): δ 42.6 (d, $J_{\text{P-P}} = 257.4$ Hz), 39.3 (d, $J_{\text{P-P}} = 257.9$ Hz). $^{11}\text{B}\{^1\text{H}\}$ NMR (128 MHz, C_6D_6): δ 17.8 (s). $^{13}\text{C}\{^1\text{H}\}$ NMR (126 MHz, C_6D_6) δ 185.5 (dd, $J_{\text{C-P}} = 14.8, 8.8$ Hz, CO), 165.07 (br), 160.17 (br), 141.4 (dd, $J_{\text{C-P}} = 50.3, 3.9$ Hz), 138.4 (dd, $J_{\text{C-P}} = 52.4, 2.9$ Hz), 134.2 (d, $J_{\text{C-P}} = 16.8$ Hz), 131.4 (d, $J_{\text{C-P}} = 15.6$ Hz), 131.3 (br), 130.3 (d, $J_{\text{C-P}} = 2.1$ Hz), 130.2 (br), 129.5 (d, $J_{\text{C-P}} = 2.2$ Hz), 125.3 (d, $J_{\text{C-P}} = 7.2$ Hz), 124.5 (d, $J_{\text{C-P}} = 7.5$ Hz), 56.3 (s, B-CH-CH₃), 32.4 (dd, $J_{\text{C-P}} = 37.1, 2.6$ Hz, CHMe₂), 30.0 (dd, $J_{\text{C-P}} = 22.4, 3.9$ Hz, CHMe₂), 29.6 (dd, $J_{\text{C-P}} = 34.5, 3.6$ Hz, CHMe₂), 27.6 (dd, $J_{\text{C-P}} = 22.6, 4.5$ Hz, CHMe₂), 22.3 (s, CH₃), 21.5 (s, CH₃), 21.0 (s, CH₃), 20.9 (d, $J_{\text{C-P}} = 2.4$ Hz, CHMe₂), 20.7 (d, $J_{\text{C-P}} = 3.2$ Hz, CHMe₂), 20.5 (s, CH₃), 20.4 (s, CH₃), 19.7 (s, CH₃), 19.6 (d, $J_{\text{C-P}} = 3.6$ Hz,

CHMe₂). ATR-IR: $\nu_{\text{CO}} = 1977 \text{ cm}^{-1}$. Elem. Anal. Calcd. for C₂₇H₄₂BIrOP₂: C, 50.08; H, 6.54. Found: C, 50.05; H, 6.46.



(PB^{CHCH₃}P)Ir(CO)₂ (403). In a J. Young tube, **74** (21 mg, 0.030 mmol) was dissolved in C₆D₆ (0.50 mL). The solution was degassed twice via freeze-pump-thaw, and the flask was refilled with ethylene (1 atm). After heating at 50 °C for 36 hours, the volatiles were removed under vacuum, the resulting solid was

recrystallized in pentane, yielding pale yellow solid (18 mg, 79%).

¹H NMR (500 MHz, C₆D₆): δ 8.40 (m, 1H), 8.12 (d, $J_{\text{H-H}} = 7.6 \text{ Hz}$, 1H), 7.40 (m, 1H), 7.28 (m, 1H), 7.18 (m, 1H), 7.05 (m, 2H), 6.92 (t, $J_{\text{H-H}} = 7.4 \text{ Hz}$, 1H), 2.72 (m, 1H, IrCH(B)Me), 2.31 (m, 1H), 2.21 (m, 3H), 1.39 (dd, $J_{\text{H-H}} = 7.0$, $J_{\text{P-H}} = 0.7 \text{ Hz}$, 3H, IrCH(B)Me), 1.15 (m, 6H, CHMe₂), 1.08 (dd, $J_{\text{H-H}} = 16.1$, $J_{\text{P-H}} = 6.8 \text{ Hz}$, 3H, CHMe₂), 0.87 (m, 12H, CHMe₂), 0.75 (dd, $J_{\text{H-H}} = 16.4$, $J_{\text{P-H}} = 7.0 \text{ Hz}$, 3H, CHMe₂). ³¹P{¹H} NMR (202 MHz, C₆D₆): δ 32.6 (d, $J_{\text{P-P}} = 184 \text{ Hz}$), 27.6 (d, $J_{\text{P-P}} = 184 \text{ Hz}$). ¹¹B{¹H} NMR (128 MHz, C₆D₆): δ 20.4. ¹³C{¹H} NMR (101 MHz, C₆D₆) δ 182.0 (dd, $J_{\text{P-C}} = 13.2$, $J_{\text{P-C}} = 10.9 \text{ Hz}$, CO), 181.4 (dd, $J_{\text{P-C}} = 12.1$, $J_{\text{P-C}} = 9.5 \text{ Hz}$, CO), 165.0 (br, B-C), 159.7 (br, B-C), 133.5 (d, $J_{\text{P-C}} = 48.7 \text{ Hz}$), 132.8 (d, $J_{\text{P-C}} = 22.7 \text{ Hz}$), 131.3 (d, $J_{\text{P-C}} = 48.5 \text{ Hz}$), 130.6 (m, 3C), 129.8 (s), 129.2 (s), 125.2 (d, $J_{\text{P-C}} = 7.5 \text{ Hz}$), 125.1 (d, $J_{\text{P-C}} = 7.7 \text{ Hz}$), 45.4 (br, IrCH(B)Me), 30.4 (d, $J_{\text{P-C}} = 32.5 \text{ Hz}$, CHMe₂), 29.0 (d, $J_{\text{P-C}} = 30.4 \text{ Hz}$, CHMe₂), 27.3 (d, $J_{\text{P-C}} = 23.7 \text{ Hz}$, CHMe₂), 24.1 (dd, $J_{\text{P-C}} = 25.7$, 5.2 Hz, CHMe₂), 22.4 (d, $J_{\text{P-C}} = 4.7 \text{ Hz}$, IrCH(B)Me), 19.9 (s, MeCHMe), 19.5 (s, MeCHMe), 19.2 (s, MeCHMe), 18.5 (s, MeCHMe), 18.3 (s, MeCHMe), 17.5 (s, MeCHMe, 2C), 16.8 (d, $J_{\text{P-C}} = 5.0 \text{ Hz}$, MeCHMe). ATR-IR: $\nu_{\text{CO}} = 1987$

cm⁻¹, 1942 cm⁻¹. Elem. Anal. Calcd. for C₂₈H₄₀BIrO₂P₂: C, 49.93; H, 5.99. Found: C, 50.28; H, 5.97.

In situ observation of (PB^{CH(CH₂)₄CH₃P})Ir(CO)₂ (403'). To a J. Young tube was added **74** (13 mg, 0.020 mmol) and 1-hexene (0.40 mL, 1.6 mmol). The tube was placed into a 50 °C oil bath for 16 h. Following the thermolysis, all volatiles were removed under vacuum and the solid was re-dissolved in C₆D₆, ¹H NMR, ³¹P{¹H} NMR and ¹¹B{¹H} NMR spectra were recorded, showing complete consumption of **74** to generate **403'**. ¹H NMR (500 MHz, C₆D₆): δ 8.42 (d, J_{H-H} = 7.6 Hz, 1H), 8.20 (d, J_{H-H} = 7.6 Hz, 1H), 7.38 (tdd, J_{H-H} = 7.5, 2.4, 1.0 Hz, 1H), 7.28 (m, 1H), 7.17 (m, 1H), 7.04 (m, 2H), 6.93 (t, J_{H-H} = 7.4 Hz, 1H), 2.67 (m, 1H, B-C-Ir), 2.29 (m, 4H, (CH₂)₄Me and CHMe₂), 1.92 (m, 1H, CHMe₂), 1.22 (dd, J_{H-H} = 15.2, 7.1 Hz, 3H, CHMe₂), 1.18 (dd, J_{H-H} = 15.9, 6.8 Hz, 3H, CHMe₂), 1.10 (dd, J_{H-H} = 16.1, 6.8 Hz, 3H, CHMe₂), 1.02 (m, 4H, (CH₂)₄Me), 0.95 (dd, J_{H-H} = 16.8, 6.8 Hz, 3H, CHMe₂), 0.87 (m, 6H, CHMe₂), 0.81 (dd, J_{H-H} = 16.4, 7.0 Hz, 3H, CHMe₂), 0.76 (dd, J_{H-H} = 16.4, 7.0 Hz, 3H, CHMe₂), 0.70 (t, J_{H-H} = 7.0 Hz, 3H, CH₂Me). ³¹P{¹H} NMR (202 MHz, C₆D₆): δ 31.7 (d, J_{P-P} = 187 Hz), 27.7 (d, J_{P-P} = 187 Hz). ¹¹B{¹H} NMR (128 MHz, C₆D₆): δ 20.5. ¹³C{¹H} NMR (126 MHz, C₆D₆): δ 182.5 (dd, J_{C-P} = 14.1, 10.2 Hz, CO), 181.5 (dd, J_{C-P} = 12.1, 8.5 Hz, CO), 166.0 (br, B-C_{sp2}), 159.8 (br, B-C_{sp2}), 134.2 (d, J_{C-P} = 48.9 Hz, P-C_{sp2}), 131.7 (d, J_{C-P} = 48.6 Hz, P-C_{sp2}), 131.7 (d, J_{C-P} = 22.5 Hz, C_{sp2}H), 131.7 (d, J_{C-P} = 48.6 Hz, P-C_{sp2}), 131.1 (d, J_{C-P} = 2.2 Hz, C_{sp2}H), 131.0 (d, J_{C-P} = 20.6 Hz, C_{sp2}H), 130.5 (d, J_{C-P} = 2.2 Hz, C_{sp2}H), 130.4 (d, J_{C-P} = 3.0 Hz, C_{sp2}H), 129.5 (d, J_{C-P} = 2.4 Hz, C_{sp2}H), 125.8 (d, J_{C-P} = 7.8 Hz, C_{sp2}H), 125.7 (d, J_{C-P} = 7.8 Hz, C_{sp2}H), 52.6 (br, IrCH(B)Me), 39.0 (d, J_{C-P} = 5.0 Hz, (CH₂)₄Me), 35.7 (s,

(CH₂)₄Me), 32.9 (s, (CH₂)₄Me), 30.8 (d, J_{C-P} = 32.8 Hz, CHMe₂), 29.7 (d, J_{C-P} = 30.5 Hz, CHMe₂), 27.8 (dd, J_{C-P} = 23.8, 4.3 Hz, CHMe₂), 24.6 (dd, J_{C-P} = 25.8, 5.7 Hz, CHMe₂), 23.4 (s, (CH₂)₄Me), 20.6 (s, CHMe₂), 20.0 (d, J_{C-P} = 2.3 Hz, CHMe₂), 19.8 (d, J_{C-P} = 3.3 Hz, CHMe₂), 19.0 (d, J_{C-P} = 4.3 Hz, CHMe₂), 18.9 (d, J_{C-P} = 2.9 Hz, CHMe₂), 18.2 (d, J_{C-P} = 3.8 Hz, CHMe₂), 18.0 (d, J_{C-P} = 3.7 Hz, CHMe₂), 17.4 (d, J_{C-P} = 5.6 Hz, CHMe₂), 14.9 (s, CH₂Me). ATR-IR: ν_{CO} = 1989 cm⁻¹, 1945 cm⁻¹

Table IV-1. Selected spectral data of 403 and 403'

	¹¹ B{ ¹ H} NMR	³¹ P{ ¹ H} NMR	¹³ C{ ¹ H} NMR and for B ^{CHRP}	ν _{CO}
(PB ^{CHCH₃} P)Ir(CO) ₂ (403)	20.4 ppm	32.6 (d, J _{P-P} = 184 Hz) 27.6 (d, J _{P-P} = 184 Hz)	45.4 ppm	1987 cm ⁻¹ 1942 cm ⁻¹
(PB ^{CH(CH₂)₄CH₃} P)Ir(CO) ₂ (403')	20.5 ppm	31.7 (d, J _{P-P} = 187 Hz) 27.7 (d, J _{P-P} = 187 Hz)	52.6 ppm	1989 cm ⁻¹ 1945 cm ⁻¹

In situ NMR study of the reaction of 74 with *trans*-3-hexene. To a J. Young tube was added **74** (13 mg, 0.020 mmol), *trans*-2-hexene (10 μL, 0.080 mmol) and 0.40 mL C₆D₆. The tube was placed into a 100 °C oil bath; it was retrieved four times to collect NMR spectra at room temperature (Figure VI-3). The major new product after 127 h was compound **403'**. At intermediate times, another product displaying an AB pattern in the ³¹P{¹H} NMR spectrum was observed (46.7 ppm (d, J_{P-P} = 163.2 Hz), 44.9 ppm (d, J_{P-P} = 225.2 Hz)). It was not unambiguously identified, but it is likely to be an isomer of **403'** possessing a non-terminal bridging hexylidene.

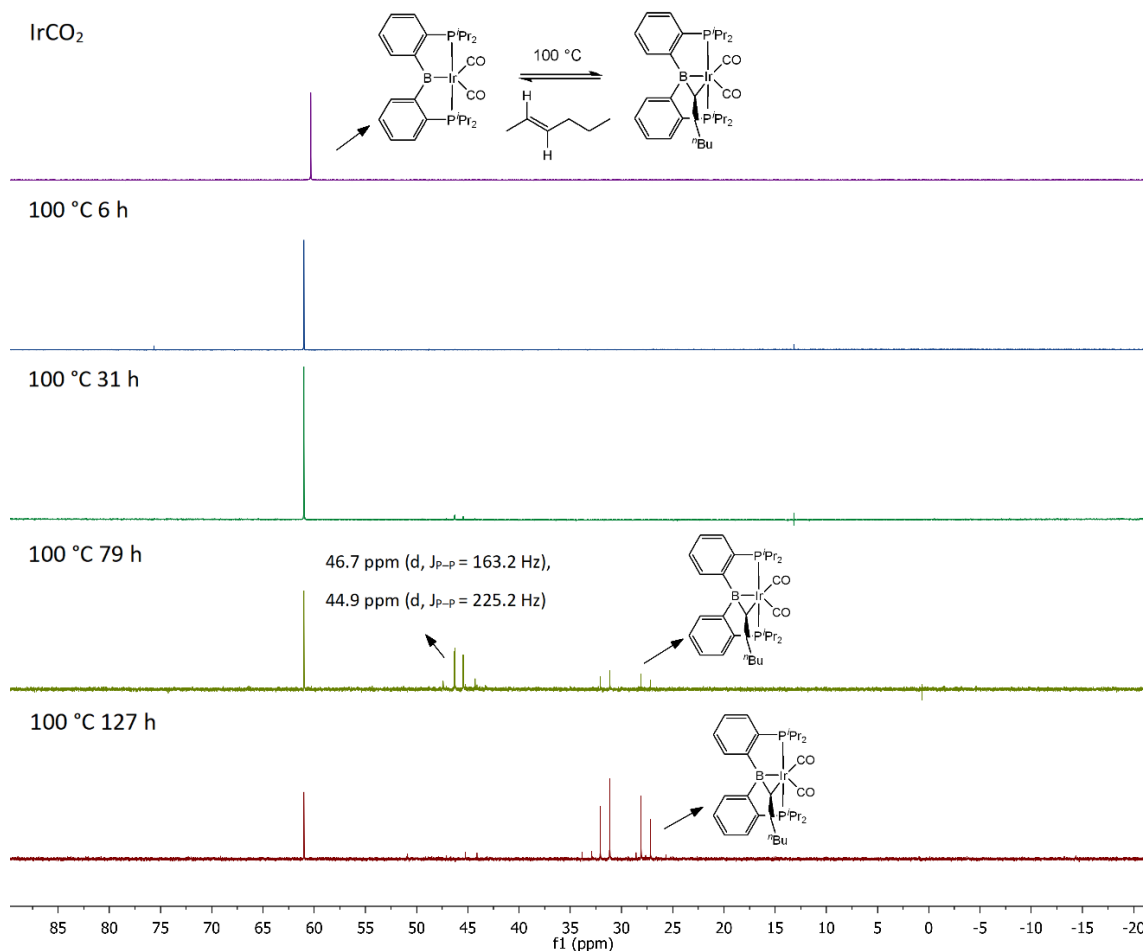


Figure IV-3. $^{31}\text{P}\{^1\text{H}\}$ NMR spectra at room temperature of in situ internal hexene addition experiment after heating at 100 °C for certain time in C_6D_6

4.4.4 In Situ NMR Study of Ethylene Addition

Addition of 1-Hexene with and without CO. Two J. Young NMR tubes (**IV-1** and **IV-2**) were loaded with identical solutions under argon: **74** (0.20 mL 0.10 M in C_6D_6 , 0.020 mmol), 1-hexene (50 μL 2.0M in C_6D_6 , 0.10 mmol), $^t\text{Bu}_2\text{PhP}=\text{O}$ (0.10 mL, 0.20 M in C_6D_6 , 0.020 mmol), and 1,4 dioxane (50 μL 0.20 M in C_6D_6 , 0.010 mmol). $^t\text{Bu}_2\text{PhP}=\text{O}$ was added as $^{31}\text{P}\{^1\text{H}\}$ NMR internal standard and 1,4 dioxane was added as ^1H NMR internal standard, although ^1H NMR spectra were not useful in analysing the mixture due

to extensive overlap. Tube **IV-2** was degassed twice using the freeze-pump-thaw method, followed by introduction of 1 atm of CO. NMR spectra of solutions in both tube **IV-1** and tube **IV-2** were recorded, and then both tubes were placed into the same 50 °C oil bath at the same time. After 90 h, 73% **403'** was generated in tube **IV-1** while 0% generation of the desired product was observed in tube **IV-2** ($^{31}\text{P}\{^1\text{H}\}$ NMR evidence). Traces of water adduct (at 54.6 ppm) was observed in tube **IV-2** due to the reaction of **74** with adventitious water in CO to form **307a**.¹⁹⁴

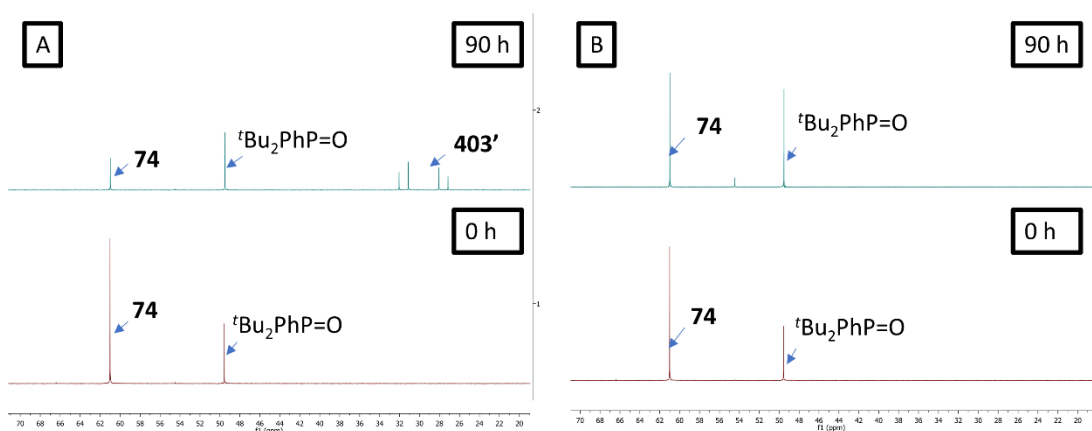


Figure IV-4. A. $^{31}\text{P}\{^1\text{H}\}$ NMR spectra of the reaction of 1-hexene with **74** under argon atmosphere. **B.** $^{31}\text{P}\{^1\text{H}\}$ NMR spectra of in situ addition of 1-hexene to **74** experiment under CO atmosphere.

Reaction rate comparison for **74** reacted with increased amounts of 1-hexene.

To three J. Young tubes was added solutions according to Table IV-2. All tubes were placed into the same 50 °C oil bath at the same time, and all $^{31}\text{P}\{^1\text{H}\}$ NMR spectra were recorded at room temperature after periodically taking the tubes out of the oil bath simultaneously. Concentration of **74** was calculated by using 0.020 mmol $t\text{Bu}_2\text{PhP}=\text{O}$ as

internal standard for $^{31}\text{P}\{^1\text{H}\}$ NMR spectra. The reaction rate displays positive dependence on [1-hexene] and [74].

Table IV-2. Constituents in tubes IV-3, IV-4 and IV-5

	74 0.10 M in C_6D_6	1-Hexene	$t\text{Bu}_2\text{PhP}=\text{O}$ 0.20 M in C_6D_6	C_6D_6	Total Volume
Tube IV-3	0.20 mL, 0.020 mmol, 0.050 M	25 μL , 0.20 mmol, 0.50 M	0.10 mL, 0.020 mmol, 0.050 M	75 μL	0.40 mL
Tube IV-4	0.20 mL, 0.020 mmol, 0.050 M	50 μL , 0.40 mmol, 1.0 M	0.10 mL, 0.020 mmol, 0.050 M	50 μL	0.40 mL
Tube IV-5	0.20 mL, 0.020 mmol, 0.050 M	0.10 mL, 0.80 mmol, 2.0 M	0.10 mL, 0.020 mmol, 0.050 M	0 μL	0.40 mL

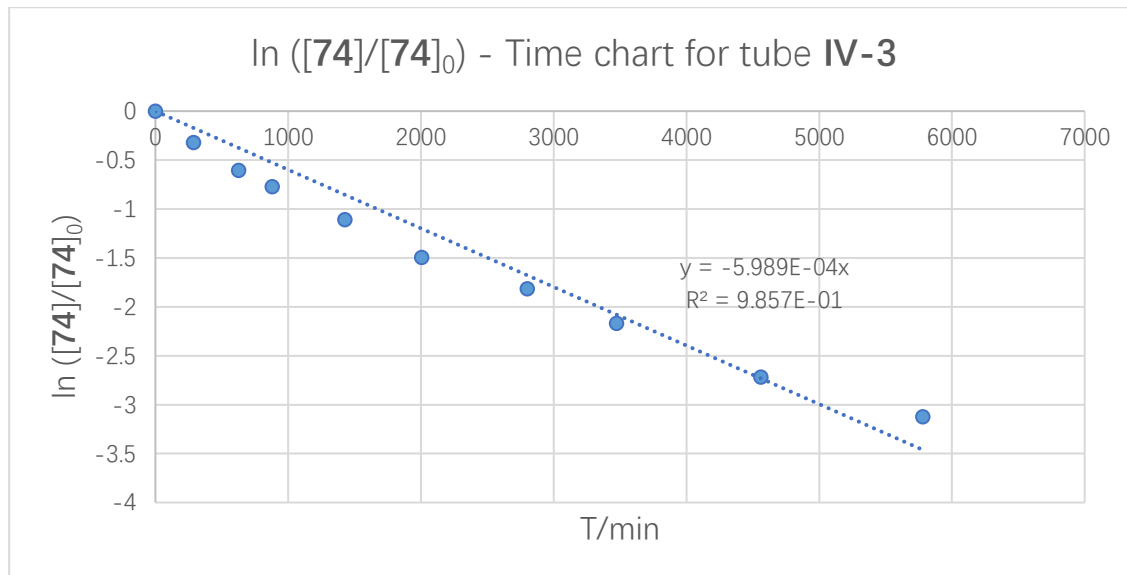


Figure IV-5. Consumption of 74 over time for 74 (0.050 M) and 1-hexene (0.50 M) addition reaction showing disappearance of 74 on a log scale

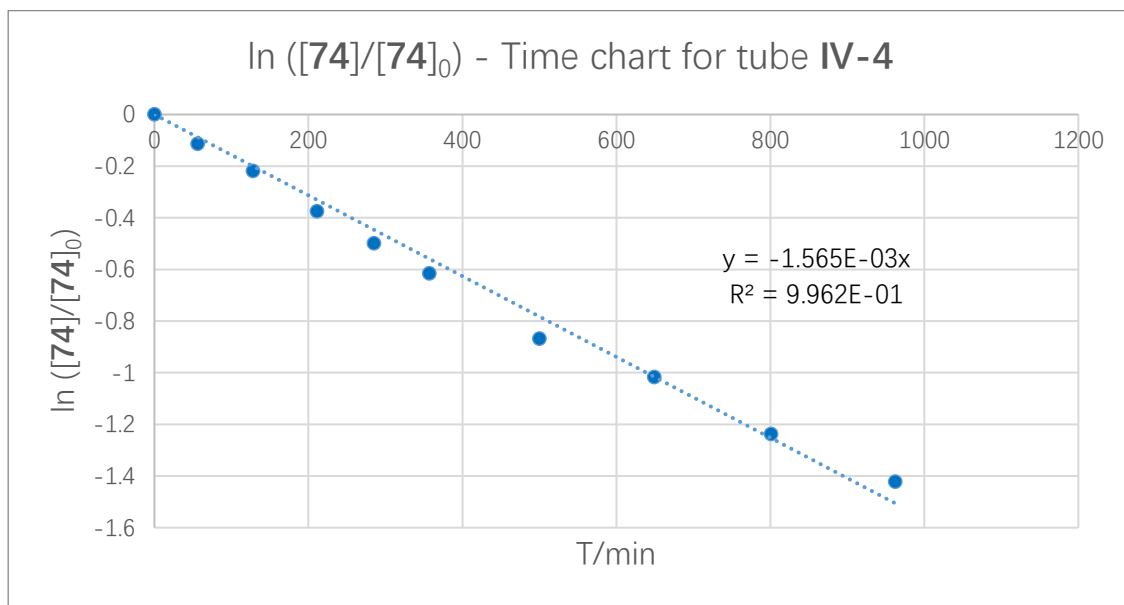


Figure IV-6. Consumption of 74 over time for 74 (0.050 M) and 1-hexene (1.0 M) addition reaction showing disappearance of 74 on a log scale

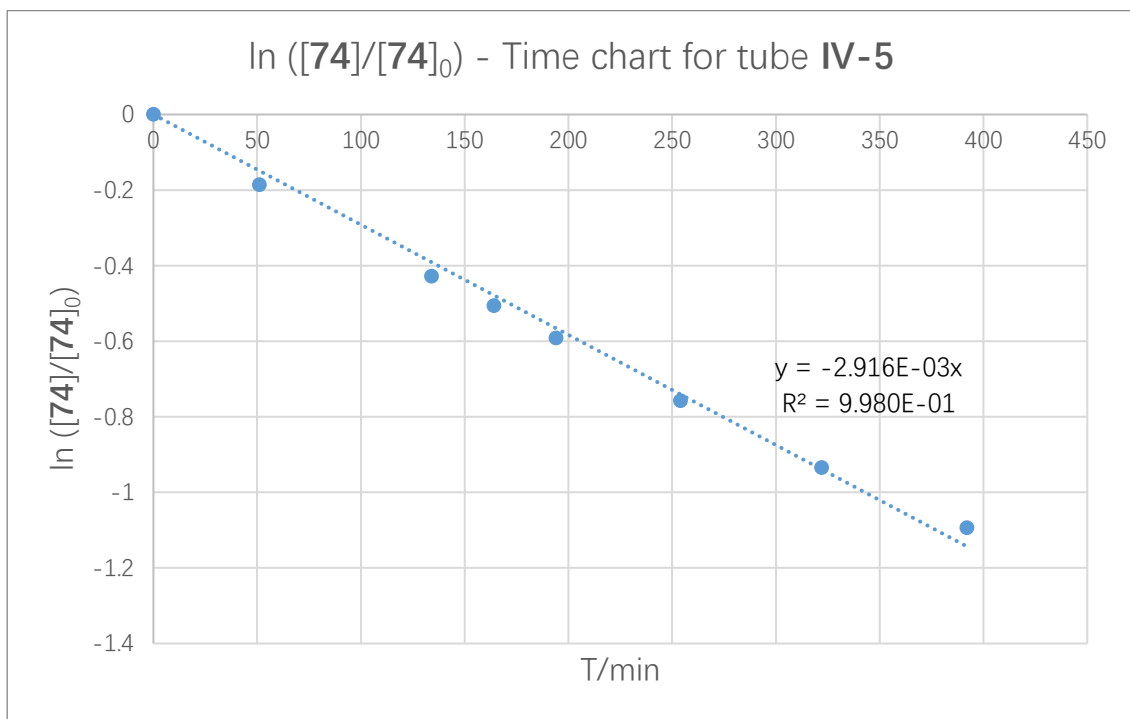


Figure IV-7. Consumption of 74 over time for 74 (0.050 M) and 1-hexene (2.0 M) addition reaction showing disappearance of 74 on a log scale

Table IV-3. Results of Tube IV-3, IV-4 and IV-5

Tube number	1-hexene concentration/M	$k_{\text{obs}} * 10^4/\text{min}^{-1}\text{M}^{-1}$
Tube IV-3	0.50	6.0
Tube IV-4	1.0	16
Tube IV-5	2.0	29

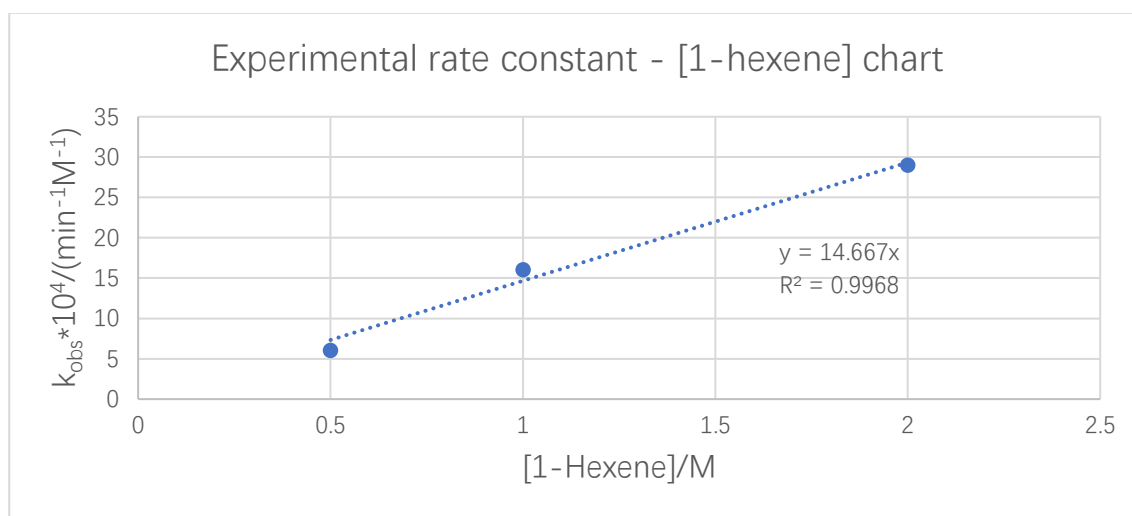


Figure IV-8. Experimental rate constant is positively related to 1-hexene concentration

Ethylene observation in the thermolysis of 402. 402 (0.020 mmol, 14 mg) was dissolved in 0.40 mL C₆D₆, and heated inside the Varian Inova 500 instrument. The spectra were recorded after 10 min when the temperature was stabilized at 80 °C. Free ethylene and hydrides of **73** was observed in the spectra recorded at 80 °C (ca. 1%).

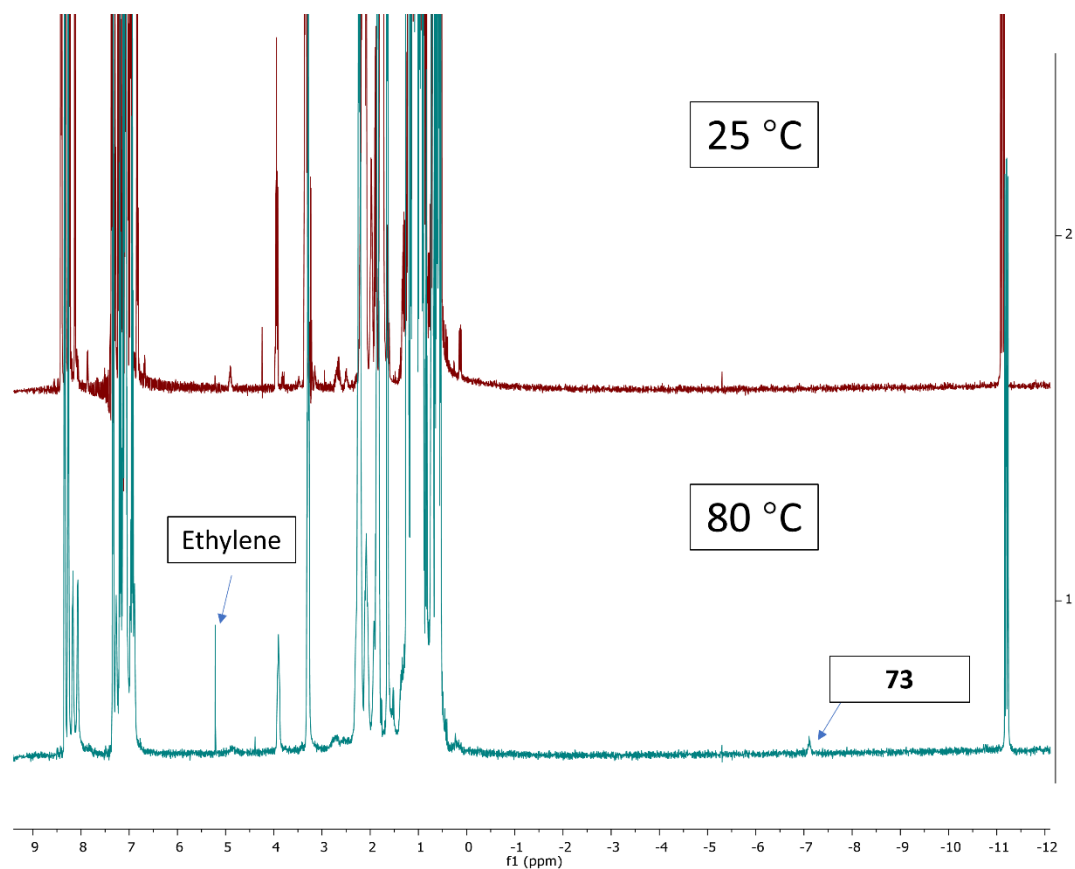


Figure IV-9. ¹H NMR spectra recorded for the thermolysis of 402

Ethylene observation in the thermolysis of 403. 403 (0.020 mmol, 14 mg) was dissolved in 0.40 mL C₆D₆/toluene-d₈, and heated with Varian Inova 400 instrument. The spectra were recorded after the temperature was stabilized at 75 °C, 90 °C and 100 °C for 10 min. Free ethylene was observed in the spectra recorded at 90 °C and 100 °C, but not at 75 °C.

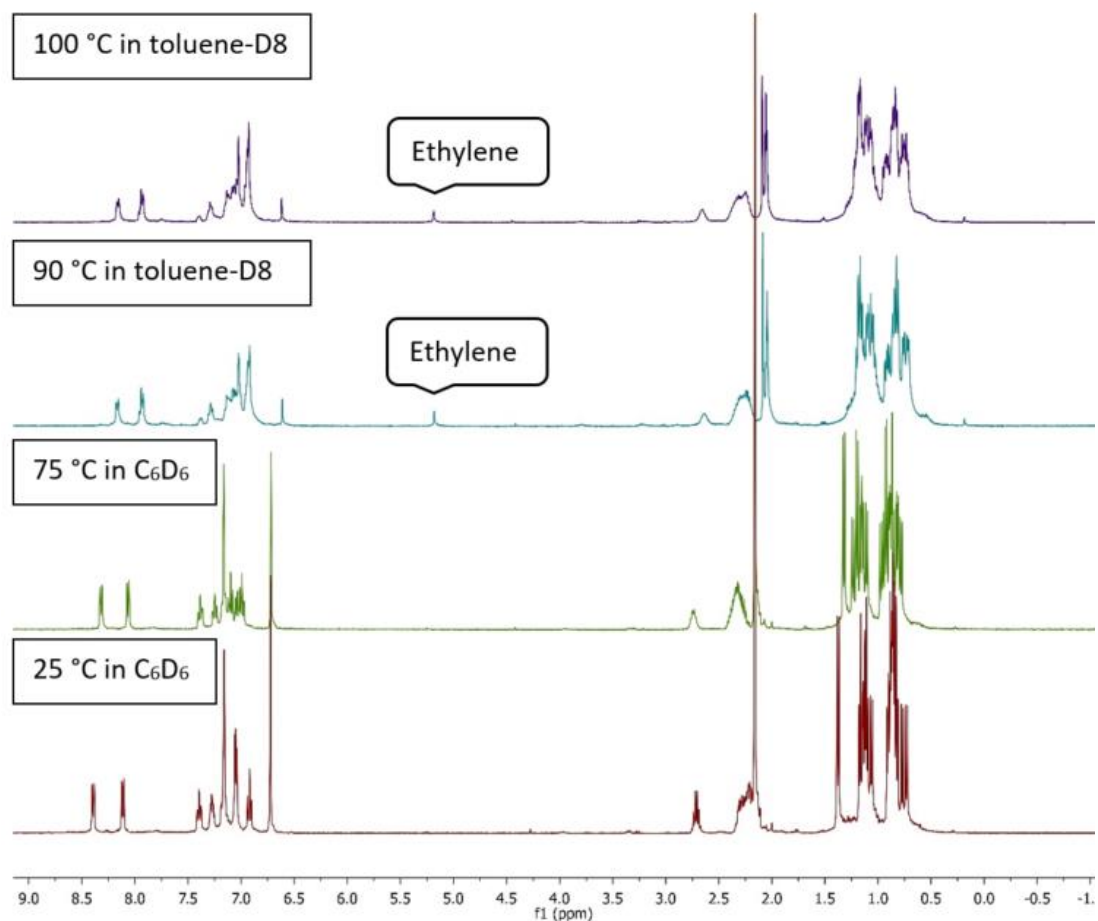


Figure IV-10. ¹H NMR spectra recorded for the thermolysis of 403

74 generation at 100 °C with and without CO. Two J. Young NMR tubes (**IV-6** and **IV-7**) were loaded with identical solutions under argon: **403** (12 mg, 0.020 mmol), $t\text{Bu}_2\text{PhP}=\text{O}$ (0.10 mL, 0.20 M in C_6D_6 , 0.020 mmol) and C_6D_6 0.30 mL. Tube **IV-7** was degassed twice using the freeze-pump-thaw method, followed by introduction of 1 atm of CO. $t\text{Bu}_2\text{PhP}=\text{O}$ was used as an internal standard for the $^{31}\text{P}\{^1\text{H}\}$ NMR spectra. NMR spectra of solutions in both tube **IV-6** and tube **IV-7** were recorded, and then both tubes were placed into the same 100 °C oil bath at the same time. After 123 min, 35% **74** was generated in tube **IV-6** while 17% generation of **74** was observed in tube **IV-7**.

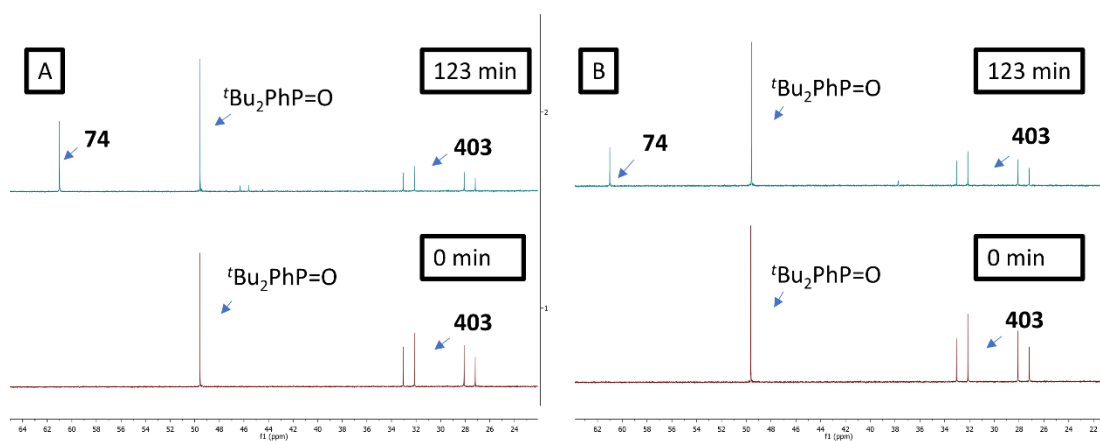


Figure IV-11. A. $^{31}\text{P}\{^1\text{H}\}$ NMR spectra recorded for thermolysis of **403** to generate **74** at 100 °C without CO in tube **IV-6**. **B.** $^{31}\text{P}\{^1\text{H}\}$ NMR spectra recorded for thermolysis of **403** to generate **74** at 100 °C with 1 atm CO in tube **IV-7**

4.4.5 X-Ray Structural Determination Details.

A The X-ray crystal data (cifs) could be obtained by the follow link:

<https://doi.org/10.1039/D0SC04748A>

X-Ray data collection, solution, and refinement for (PB^{Vinyl}P)Ir(H)(C₂H₄) (401, CCDC 1858843). A yellow, multi-faceted block of suitable size (0.32 x 0.25 x 0.05

mm) was selected from a representative sample of crystals of the same habit using an optical microscope and mounted onto a nylon loop. Low temperature (150 K) X-ray data were obtained on a Bruker APEXII CCD based diffractometer (Mo sealed X-ray tube, $K_{\alpha} = 0.71073 \text{ \AA}$). All diffractometer manipulations, including data collection, integration and scaling were carried out using the Bruker APEXII software.¹²² An absorption correction was applied using SADABS.¹²³ The space group was determined on the basis of systematic absences and intensity statistics and the structure was solved by direct methods and refined by full-matrix least squares on F^2 . The structure was solved in the orthorhombic P bca space group using XS¹²⁷ (incorporated in SHELXLE). All non-hydrogen atoms were refined with anisotropic thermal parameters. All hydrogen atoms were placed in idealized positions and refined using riding model with the exception of the hydrogen bound to iridium which was located from the difference map. The structure was refined (weighted least squares refinement on F^2) and the final least-squares refinement converged. No additional symmetry was found using ADDSYM incorporated in PLATON program.¹²⁵

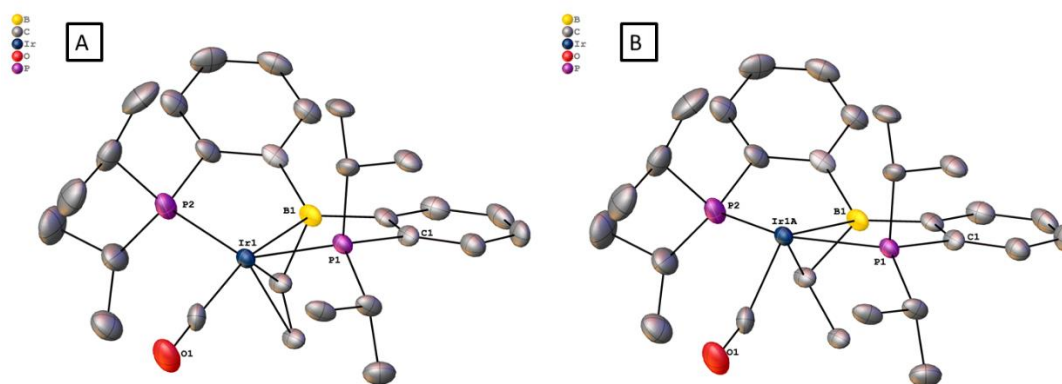


Figure IV-12. ORTEP drawings showing selected atom labeling of 402

X-ray data collection, solution, and refinement for (PB^{CHCH₃}P)Ir(H)₂(CO) (402, CCDC 1858844). A Leica MZ 7₅ microscope was used to identify a suitable colorless block with very well-defined faces with dimensions (max, intermediate, and min) 0.395 x 0.299 x 0.098 mm³ from a representative sample of crystals of the same habit. The crystal mounted on a nylon loop was then placed in a cold nitrogen stream (Oxford) maintained at 110 K. A BRUKER APEX 2 Duo X-ray (three-circle) diffractometer was employed for crystal screening, unit cell determination, and data collection. The goniometer was controlled using the APEX3 software suite, v2017.3-0.²⁰⁰ The sample was optically centered with the aid of a video camera such that no translations were observed as the crystal was rotated through all positions. The detector was set at 6.0 cm from the crystal sample (APEX2, 512x512 pixel). The X-ray radiation employed was generated from a Mo sealed X-ray tube ($K_{\alpha} = 0.70173\text{\AA}$ with a potential of 40 kV and a current of 40 mA). 45 data frames were taken at widths of 1.0°. These reflections were used in the auto-indexing procedure to determine the unit cell. A suitable cell was found and refined by nonlinear least squares and Bravais lattice procedures. The unit cell was verified by examination of the *h k l* overlays on several frames of data. No super-cell or erroneous reflections were observed. After careful examination of the unit cell, an extended data collection procedure (5 sets) was initiated using omega scans. Integrated intensity information for each reflection was obtained by reduction of the data frames with the program APEX3.¹²⁵ The integration method employed a three-dimensional profiling algorithm and all data were corrected for Lorentz and polarization factors, as well as for crystal decay effects. Finally, the data was merged and scaled to produce a suitable data

set. The absorption correction program SADABS¹²³ was employed to correct the data for absorption effects. Systematic reflection conditions and statistical tests of the data suggested the space group *Pca2*₁. A solution was obtained readily (with two slightly different molecules in the asymmetric unit) using XT/XS in APEX2.^{123-125, 128-129, 200} Hydrogen atoms were placed in idealized positions and were set riding on the respective parent atoms. All non-hydrogen atoms were refined with anisotropic thermal parameters. Elongated ellipsoids and the residual electron densities in both the molecules indicated disorder. In the molecule with Ir1 (and Ir1a) shown above the configuration shown in Figure IV-12-A was found to be the major component (93 %). Whereas in the molecule with Ir2 (and Ir2a) the configuration shown in Figure IV-12-B was found to be the major component (70 %). The structure was refined (weighted least squares refinement on F^2) to convergence.^{123-125, 128-130, 200} Olex2 was employed for the final data presentation and structure plots.¹³⁰

X-Ray data collection, solution, and refinement for (PB^{CHCH3}P)Ir(CO)₂ (403, CCDC 1858845). A pale yellow, multi-faceted block of suitable size (0.23 x 0.12 x 0.05 mm) was selected from a representative sample of crystals of the same habit using an optical microscope and mounted onto a nylon loop. Low temperature (150 K) X-ray data were obtained on a Bruker APEXII CCD based diffractometer (Mo sealed X-ray tube, K_{α} = 0.71073 Å). All diffractometer manipulations, including data collection, integration and scaling were carried out using the Bruker APEXII software.¹²² An absorption correction was applied using SADABS.¹²³ The space group was determined on the basis of systematic absences and intensity statistics and the structure was solved by direct methods

and refined by full-matrix least squares on F^2 . The structure was solved in the monoclinic P 2₁/c space group using XS¹²⁷ (incorporated in SHELXLE). All non-hydrogen atoms were refined with anisotropic thermal parameters. All hydrogen atoms were placed in idealized positions and refined using riding model. The structure was refined (weighted least squares refinement on F^2) and the final least-squares refinement converged. No additional symmetry was found using ADDSYM incorporated in PLATON program.¹²⁵⁻

126

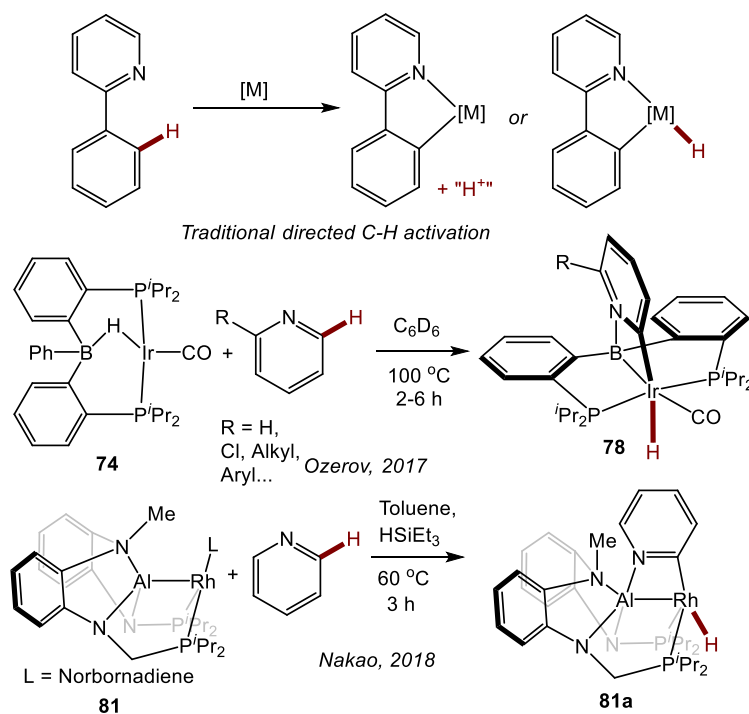
CHAPTER V
COOPERATIVE C-H ACTIVATION OF PYRIDINE BY PBP COMPLEXES OF RH
AND IR CAN LEAD TO BRIDGING 2-PYRIDYLS WITH DIFFERENT
CONNECTIVITY TO THE B-M UNIT

5.1 Introduction

Selective C-H activation and functionalization of pyridines and other azines presents special challenges, in part because these heterocycles can function as good ligands towards many transition metals.²⁰¹⁻²⁰² Selectivity for the 3- (or *meta*-) position is more common with transition metals,^{114, 203-204} but studies of selective 2-position functionalization are also known.^{203, 205-211} In many specific cases, the scope may be limited, and a particular substitution pattern on the azine is often required for selectivity.

In 2017, we reported a new approach to the directed activation of C-H bonds in pyridine derivatives using an Ir system supported by a boryl/bis(phosphine) PBP pincer ligand.^{6, 13, 37, 78, 80, 83-84, 96, 100, 186, 211} The binding of the pyridine (or quinoline) nitrogen to the Lewis acidic boryl site directs Ir to the 2-position in the heterocycle. This approach is distinct from the more classical directed C-H activation, where the directing group donor binds to the same atom (transition metal) which effects C-H cleavage (Scheme V-1).²¹²⁻²¹⁶ Pyridine derivatives have played a prominent role in the development of classical directed C-H activation, but they typically direct the metal not to the C-H bonds of the pyridine ring itself, but to the more remote C-H bonds in a substituent, such as in the 2-phenyl group. We reasoned that the (PBP)Ir system preferred the C-H activation of the

pyridine ring because of the favourability of the Ir/C/N/B trapezoidal four-membered ring formation.³⁷ A similar selectivity was observed by Nakao et al. in the C-H activation of pyridines with a Rh complex²⁹ supported by a closely related aluminyl/bis(phosphine) PAIP pincer (Scheme V-1).^{31, 217}



Scheme V-1. Traditional directed C-H activation of 2-phenylpyridine (top) and boryl- or aluminyl-directed C-H activation of the 2-position of a pyridine ring

Given Nakao's precedent with Rh, we wished to explore the reactivity with pyridine using the (PBP)Rh system,^{27, 69} as well as the variations of the Rh and Ir systems with and without the carbonyl ligand. While exploring the analogous reactivity with (PBP)Rh, we came across an unexpected finding. As with Ir, C-H activation of pyridine resulted in the formation of a 2-pyridyl that is bridging the B-Rh bond. However, the connectivity was reversed, with C of the pyridyl attached to B and the N atom of the

pyridyl attached to Rh. This prompted us to explore this M-C/M-N isomerism in more systematic detail, as it does not appear to have been considered in the literature. This report describes our analysis of the isomeric preference of the 2-pyridyl (or 2-quinolyl) fragment bridging the B-Ir or B-Rh bond in a series of compounds supported by the PBP pincer.

5.2 Result and Discussion

5.2.1 Compounds under Consideration and Nomenclature

We selected four structural types for analysis (Figure V-1). For each type, we considered M-C/M-N isomerism for the Rh and for the Ir version, resulting in sixteen 2-pyridyl compounds that were whose structures were optimized computationally. The compound labels (Figure V-1) are derived from the general type (numeral) and the bond present between the metal (Rh or Ir) and C or N. Some of these compounds were isolated or observed experimentally in this (Scheme V-2) or the previous report.³⁷ In addition, we synthesized a few 2-quinolyl analogs of the 2-pyridyl compounds (Scheme V-2); they are denoted by adding a “q” to the compound label. The Type **V-3** and Type **V-4** compounds are isomeric. We did not attempt the syntheses of the Type **V-4** compounds because DFT calculations indicated that they are considerably higher in energy than the corresponding Type **V-3** isomers (vide infra).

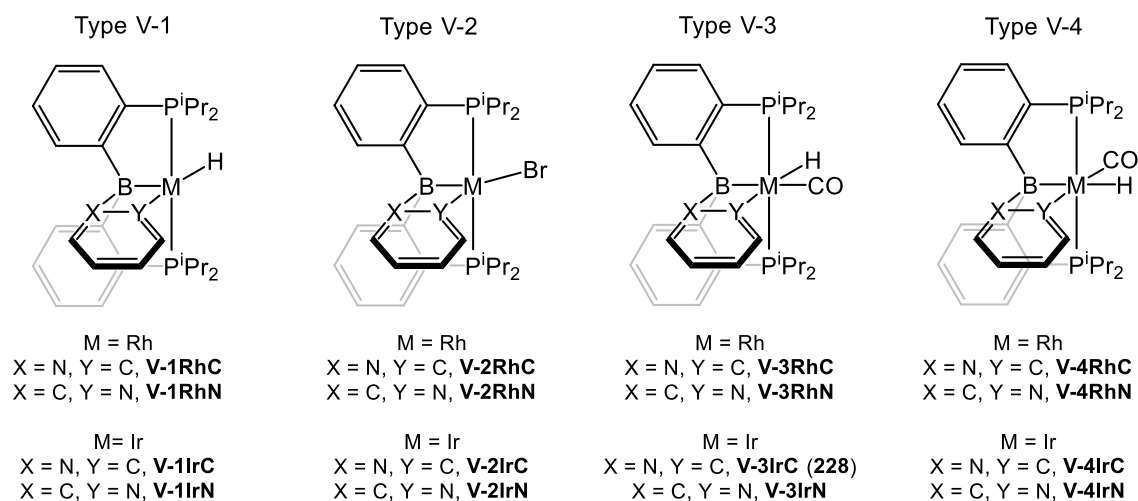
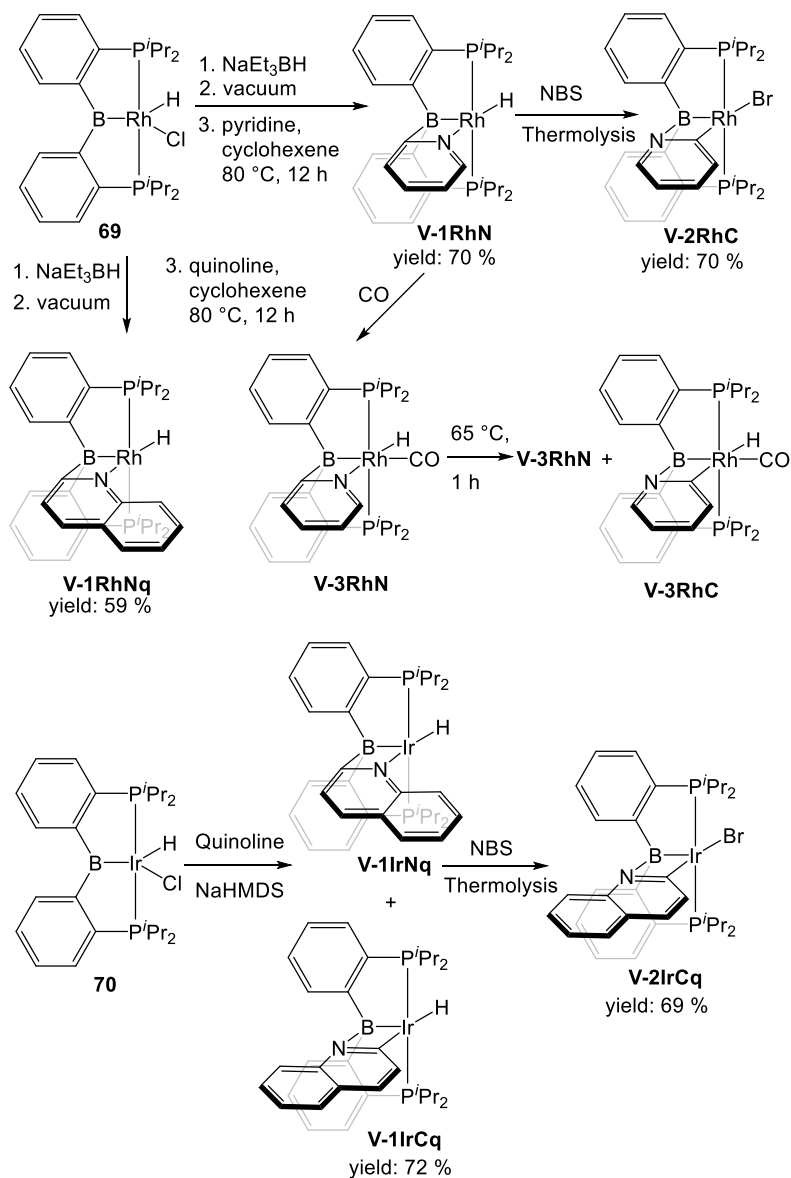


Figure V-1. The four structural types under study in this work

5.2.2 Synthesis of Rh and Ir Complexes

In order to access a Rh species capable of C-H activation, the previously reported **69** was treated with NaBET₃H followed by the removal of volatiles. Although the stoichiometry suggests the formation of “(PBP)RhH₂”, we have not established the nature of the resultant species; from the in-situ NMR observations, it appears that a mixture of a few complexes forms (Figure V-2). Nonetheless, thermolysis of this mixture in the presence of cyclohexene and either pyridine or quinoline led to the formation of complexes **V-1RhN** and **V-1RhNq**, with an isolated yield of 70% and 59% respectively. The corresponding Type **V-1** Ir compound **V-1IrCq** was prepared by the treatment of **70** with NaN(SiMe₃)₂ in the presence of quinoline. Compound **V-1IrCq** exists in equilibrium with the minor isomer **V-1IrNq** (1.00:0.055 ratio at 25 °C and 1.00:0.095 at 65 °C). Attempts to prepare **V-1IrC** in a pure form were not successful. Unlike **V-1RhN**, **V-1IrC** appears to bind an extra equivalent of pyridine, which resulted in a mixture of

products when one equiv. of pyridine was used. Utilization of 3 equiv. of pyridine permitted observation of the pyridine adduct of **V-1IrC** as the dominant product by NMR spectroscopy, but we did not pursue its isolation in a pure solid form (compound **501**, Figure V-3).



Scheme V-2. Synthesis of (PBP)Rh/Ir pyridyl complexes

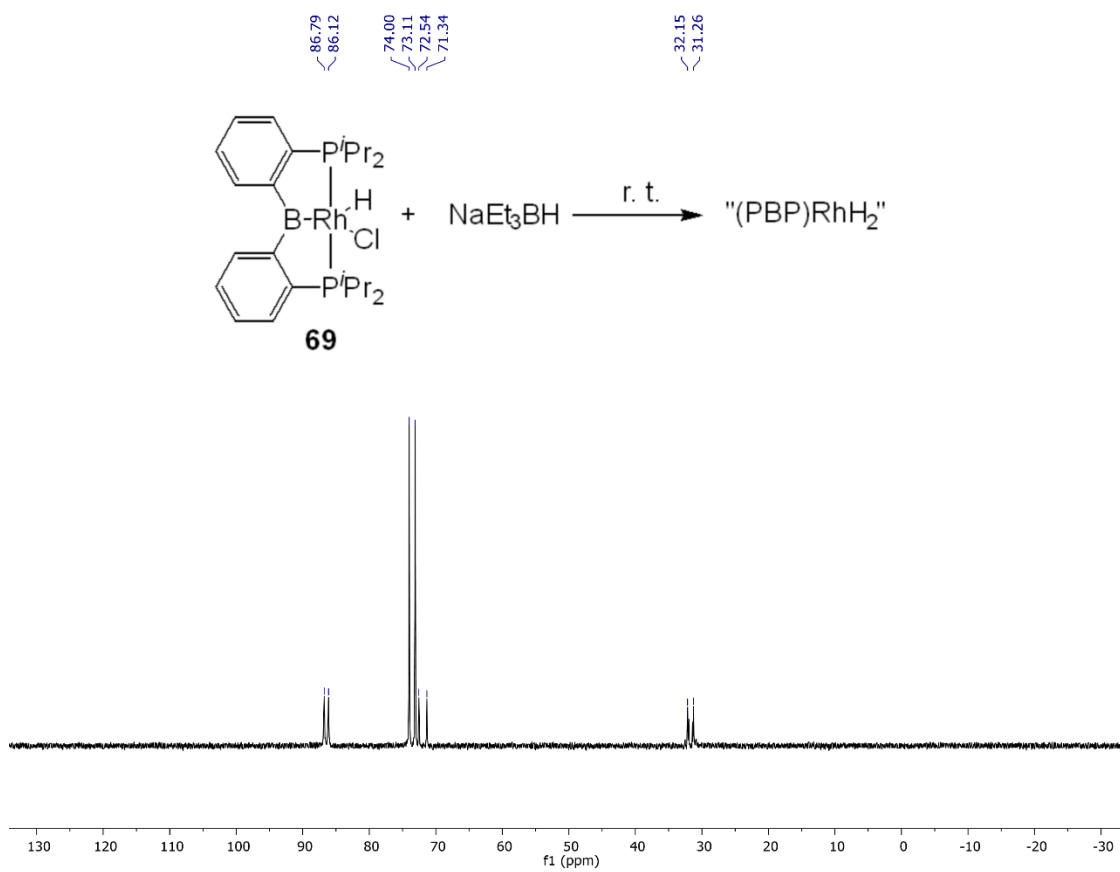


Figure V-2. $^{31}\text{P}\{^1\text{H}\}$ NMR spectrum record on a 500 MHz Varian NMR after 1 equiv. of NaEt_3BH were added to **69 in toluene, showing four or more complexes formed**

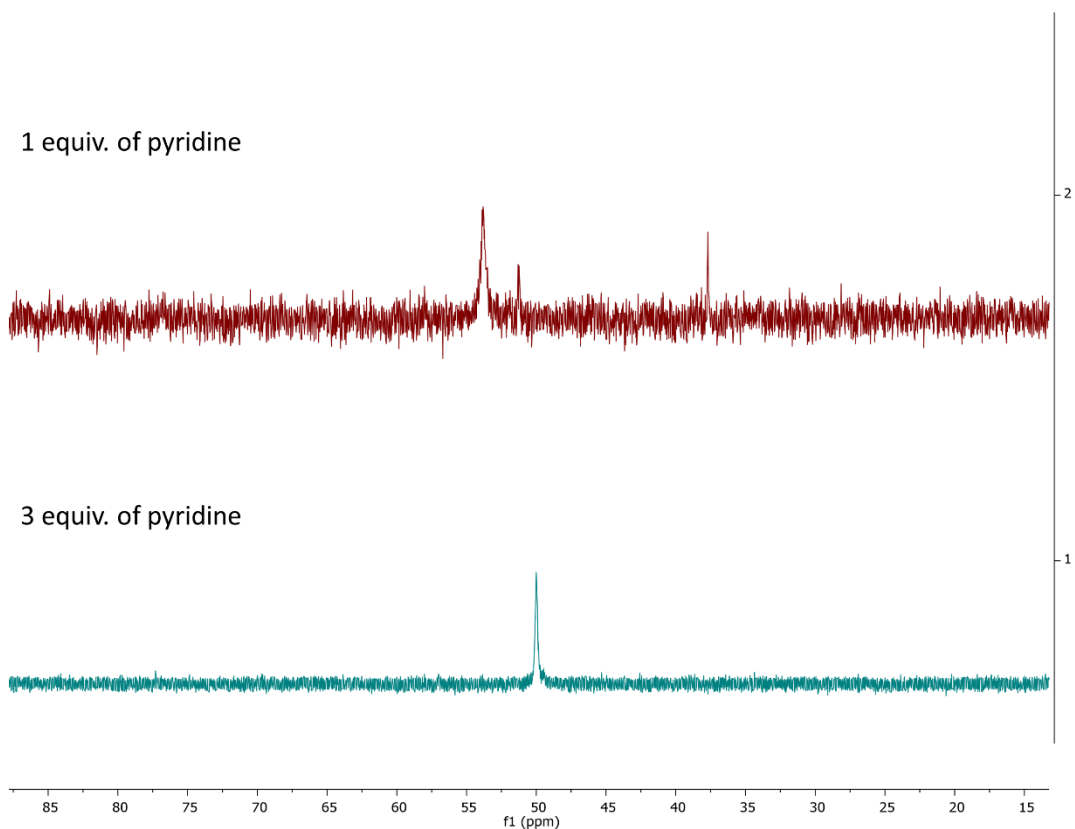


Figure V-3. Top: $^{31}\text{P}\{^1\text{H}\}$ NMR recorded at room temperature on a 500 MHz Varian NMR for a mixture of **70** (0.10 mmol), pyridine (0.10 mmol) and sodium bis(trimethylsilyl)amide (0.10 mmol) in 2 mL toluene after being heated at 45 °C for 12 h. **Bottom:** $^{31}\text{P}\{^1\text{H}\}$ NMR recorded at room temperature on a 500 MHz Varian NMR for the same mixture after adding additional pyridine (0.20 mmol) and being heated at 45 °C for another 12 h

The conversion of the hydride complexes **V-1RhN** and **V-1IrCq** to the bromide derivatives **V-2RhC** and **V-2IrCq** was effected by thermolysis with NBS. Good isolated yields (70% and 69% respectively) were obtained after workup. No evidence of the presence of **V-2RhN** or **V-2IrNq** was noted.

The carbonyl adduct **V-3RhN** was prepared by exposure of **V-1RhN** to carbon monoxide and characterized in situ in solution after 10 min. After removing carbon

monoxide under vacuum, thermolysis of the solution of **V-3RhN** in C₆D₆ for 1 h at 65 °C resulted in the formation of a mixture of **V-3RhN** and **V-3RhC** in a 1.0:0.08 ratio. Extended thermolysis for 24 h at 65 °C led to the formation of multiple complexes along with **V-3RhN** and **V-3RhC**, but in that mixture **V-3RhN** was still present in a much higher concentration than **V-3RhC**. The synthesis of the analogous Ir complex **V-3IrC** was previously reported. The synthesis involved extended thermolysis at 100 °C and no evidence of the presence of **V-3IrN** was noted.

5.2.3 Spectroscopic Characterization

The compounds explored in this study are rich in NMR active nuclei (¹H, ¹³C, ³¹P, ¹¹B, and ¹⁰³Rh). All of the compounds possess C_s-symmetry on the NMR time scale. The M-C/M-N isomers can be distinguished based on the relative ¹H NMR chemical shift of the Rh/Ir-H signal. Since N of pyridyl is less *trans*-influencing than C of 2-pyridyl, a hydride *trans* to N appears at a more upfield frequency vs a hydride *trans* to C. For the Rh compounds **V-1RhN**, **V-1RhNq**, and **V-3RhN** with a hydride *trans* to N, its ¹H NMR chemical shift falls into a narrow range of -15.7 to -17.3 ppm, but for **V-3RhC**, the hydride resonates considerably upfield at δ -11.04 ppm. The contrast is even greater for the Ir pair **V-1IrCq** (δ -0.20 ppm) and **V-1IrNq** (δ -17.10 ppm).

The shape of the ¹³C{¹H} NMR resonance corresponding to the boron- or metal-bound carbon of the 2-pyridyl or 2-quinolyl unit is also telling. In compounds **V-1RhN**, **V-1RhNq**, and **V-3RhN**, this carbon is bound to boron and the corresponding ¹³C NMR resonances in these compounds possess some broadness. In compounds **V-2RhC** and **V-**

1IrCq, this carbon is bound to the metal and displays coupling to the two equivalent ^{31}P nuclei, as well as to ^{103}Rh in **V-2RhC**.

Table V-1. Selected NMR chemical shift data (in ppm, C_6D_6 , solvent) for the experimentally observed complexes of types V-1 to V-3

Complexes	Rh/Ir-H	$^{11}\text{B}\{^1\text{H}\}$	Ir/Rh-C	B-C
V-1RhN	-17.25	3.5	/	188.2
V-1RhNq	-16.81	4.5	/	189.5
V-1IrCq	-0.20	-8.5	201.3	/
V-1IrNq	-17.10	/ ^d	/	/ ^d
V-2RhC	/	1.7	178.0	/
V-2IrCq^e	/	-6.8	176.9	/
V-3RhN	-15.69	2	/	193.5
V-3RhC	-11.04	/ ^d	/ ^d	/
V-3IrC	-14.15		164.9	

^a ^1H NMR chemical shift of the metal-bound hydride. ^b ^{13}C NMR chemical shift of the metal-bound carbon. ^c ^{13}C NMR chemical shift of the boron-bound carbon in the bridging pyridyl or quinolyl. ^d Resonance was not observed due to low concentration. ^e Spectra of **V-2IrCq** were recorded in CDCl_3 .

5.2.4 XRD Structural Characterization

Single crystal X-ray diffractometry permitted the determination of the solid-state structures of **V-1RhN**, **V-1RhNq**, **V-1IrCq**, **V-2RhC**, and **V-3RhN**. The solid-state structure of **V-3IrC** was reported in 2017.

The Ir-B (2.209 (2) and 2.195 (2) Å) and the Ir-C distances (2.034(3) and 2.029(3) Å) in the two crystallographically independent molecules of **V-1IrCq** are slightly shorter than the Ir-B distance of 2.285(2) Å and the Ir-C distance of 2.079(2) Å in the previously reported **V-3IrC**. The B-N and N-C distances in these molecules are very similar. Comparing the Rh-B distances in **V-1RhN** (2.229(2) Å) and **V-3RhN** (2.319(1) Å) also shows that the presence of CO is correlated with the elongation of the M-B bond

(*trans* to CO) by almost 0.1 Å. However, the Rh–N distances (2.163(1) Å in **V-1RhN** and 2.158(1) Å in **V-3RhN**) seem to be unaffected by the presence of the CO ligand.

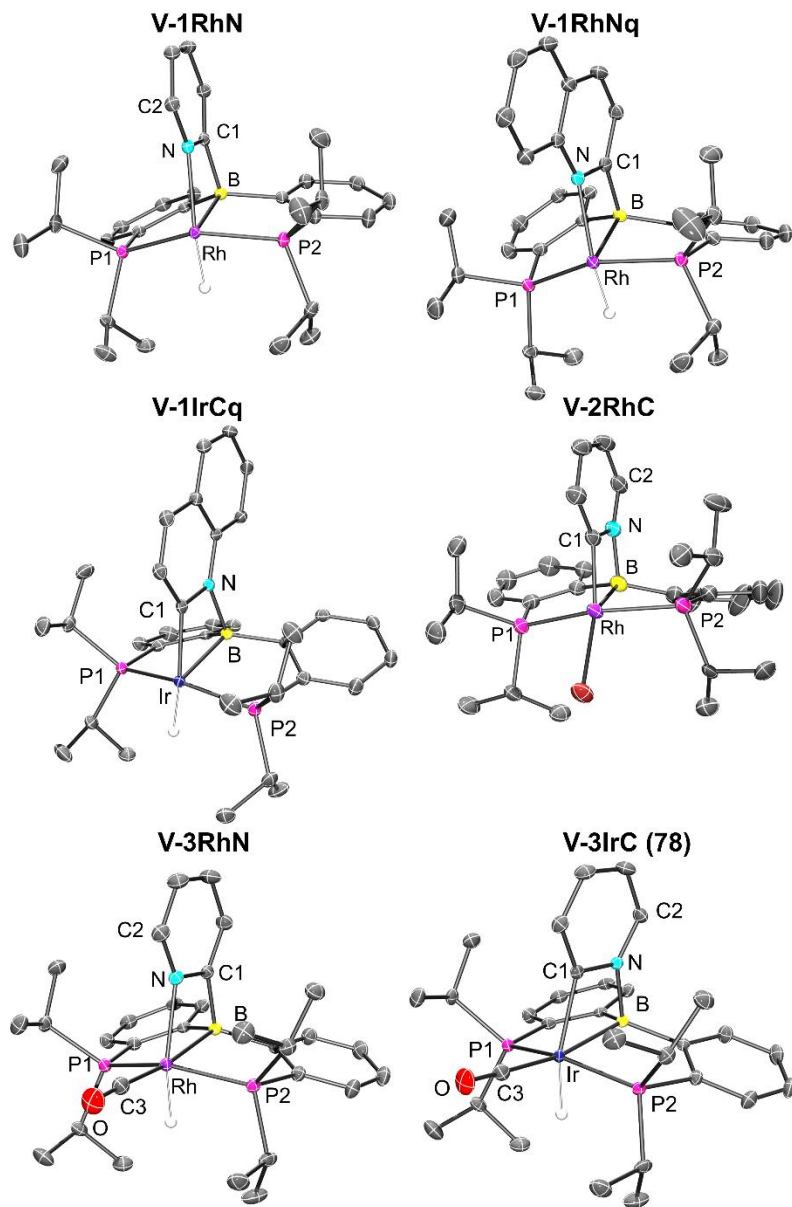


Figure V-4. POV-Ray rendition of the ORTEP drawing (50% thermal ellipsoids) of **V-1RhN**, **V-1RhNq**, **V-1IrCq**, **V-2RhC**, and **V-3RhN** showing selected atom labelling. Hydrogen atoms, disorders of *i*Pr groups in **V-1IrCq** and **V-2RhC** crystals, and solvent molecules (toluene) in **V-1RhNq** and **V-1IrCq** crystals are omitted for clarity. Only one of the **V-1IrCq** in the asymmetric unit is shown in the ORTEP drawing above.

The values for the sum of angles that exclude the pyridyl/quinolyl nitrogen about the boron atom in **V-1RhN**, **V-1RhNq** and **V-3RhN** are in the ca. 339.4°-343.8° range. The range of the corresponding values (excluding the pyridyl/quinolyl carbon) in **V-1IrCq**, **V-2RhC** and **V-3IrC** is ca. 335.6°-341.9°. Likewise, the P-M-P angles in the six structures in Figure V-4 all fall within the ca. 151-161° range. Thus, while there are significant differences in the metrics of the M-C/N-B cycle among the six structures, the conformation of the (PBP)M fragment is close to constant.

The hydride ligand in **V-1RhN**, **V-1RhNq**, **V-1IrCq**, **V-3RhN**, and **V-3IrC** is close to being *trans* to either C or N of the pyridyl (161-174° angle range). In the structure of **V-2RhC**, the C-Rh-Br angle deviates from linearity to a greater extent (149.57(11) °) and **V-2RhC** can be viewed as adopting a Y-shaped geometry as opposed to square-pyramidal for the five-coordinate hydride complexes **V-1RhN**, **V-1RhNq**, **V-1IrCq**.²¹⁸

5.2.5 DFT Studies

The structures of the 16 molecules shown in Figure V-1 were optimized using the B97D3/LANL2DZ/6-31G(d) method (see details in section 5.4.5). Figure V-5 summarizes the results of the calculations, showing the Wiberg bond indices (WBI) within the four-membered rings, as well as the calculated free energies of the isomerization from the M-C to the M-N isomer. The metric details of the DFT-optimized geometries matched those from the XRD structures reasonably well.

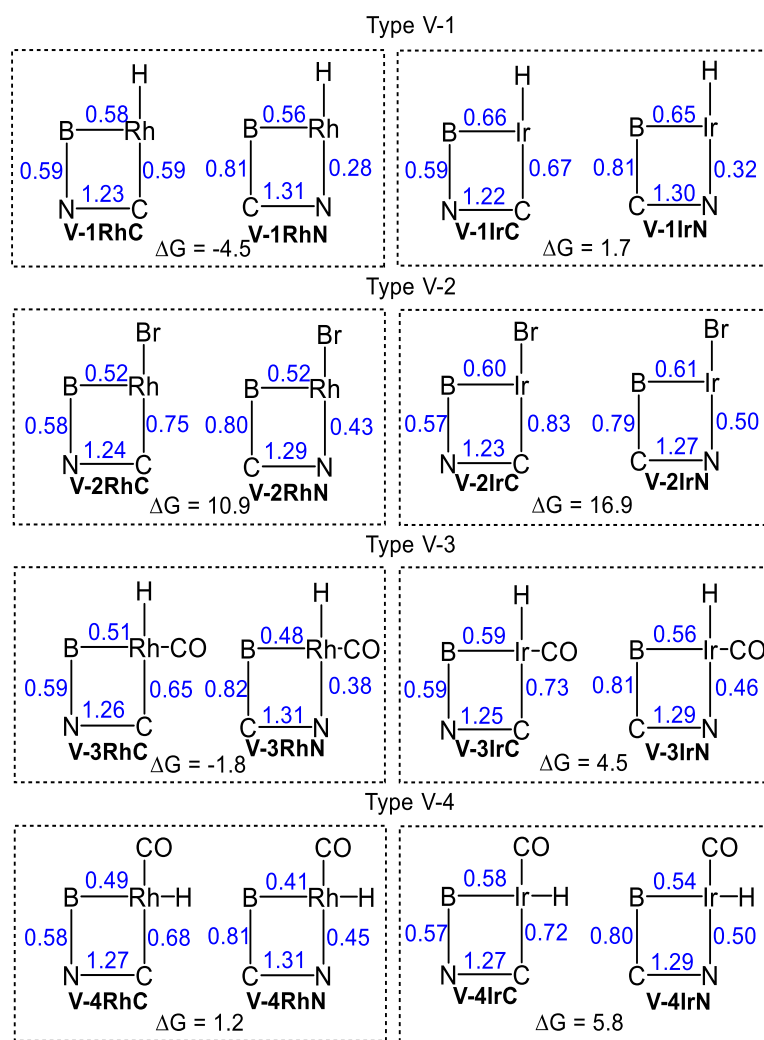


Figure V-5. DFT-calculated Wiberg bond indices shown in blue for the bonds within the four-membered metallacycle. ΔG_{298} values (in kcal/mol) are given for the isomerization from left to right within each box (negative ΔG value favors the isomer with the M-N bond).

Calculations indicate that the isomers with the carbon bound to the transition metal are more favorable for all Ir complexes and for the Rh complexes of Types V-2 and V-4. For the other Rh complexes, the isomer with the nitrogen bound to Rh is preferred. Across all four types, the relative free energy preference of Ir for the metal-carbon bonded isomer is very consistently 5-7 kcal/mol higher than that of Rh.

Overall, the calculated thermodynamic parameters are consistent with the experimental observations we have for the Rh and Ir compounds of Types V-1 to V-3. Moreover, the calculated free energy preferences for **V-1IrC** (over **V-1IrN**) and for **V-3RhN** (over **V-3RhC**) are <2 kcal/mol, suggesting that both isomers in these two pairs should be present at observable concentrations. This is precisely what we observed for **V-1IrCq/V-1IrNq** and for **V-3RhN/V-3RhC** (*vide supra*), with the isomer predicted to be more favorable by DFT present in a higher proportion.

Type V-3 (CO *trans* to B) compounds are isomeric to Type V-4 (H *trans* to B), and DFT calculations predict that any of the four Type V-3 compounds (**V-3IrC**, **V-3IrN**, **V-3RhC**, **V-3RhN**) is lower in free energy than their corresponding Type V-4 analog (**V-4IrC**, **V-4IrN**, **V-4RhC**, **V-4RhN**, respectively) by 13-19 kcal/mol. This is consistent with the lack of observation of **V-4RhC** or **V-4RhN** in the thermolysis of the **V-3RhC/V-3RhN** mixture.

The calculated Wiberg bond indices (WBI) allow a way to analyze the changes in the nature of the bonds in the four-membered cycle for the pairs of isomers. The WBI for the M-B bond in any Ir compound is 0.08-0.13 higher than for the exact Rh analog. Higher WBI values in Ir (vs Rh) compounds are also notable for the M-C and M-N bonds (by 0.04-0.08). This is in general expected for a 5d metal (Ir) compared to its 4d congener (Rh).

Within each M-C/M-N isomeric pair with the same metal, the M-B bond WBI values differ only by 0.04 or less, except for the **V-4RhC/V-4RhN** pair (0.08 difference). The WBI vary even less for the C-B bonds (0.79-0.82 range) and for the N-B bonds (0.57-

0.59) throughout the whole array of compounds. It can be concluded that the changes in the M-B, C-B, and N-B bonding contribute little to the thermodynamic preferences for the M-C vs M-N isomers.

The WBI values for the CN bond vary within a range of 1.22-1.31 for all 16 compounds. Within every M-C/M-N isomeric pair, this value is higher for the N-M bound isomer, by 0.02-0.08, suggesting that coordination to Ir or Rh strengthens the C-N bond slightly, but to a similar degree across all four types of compounds.

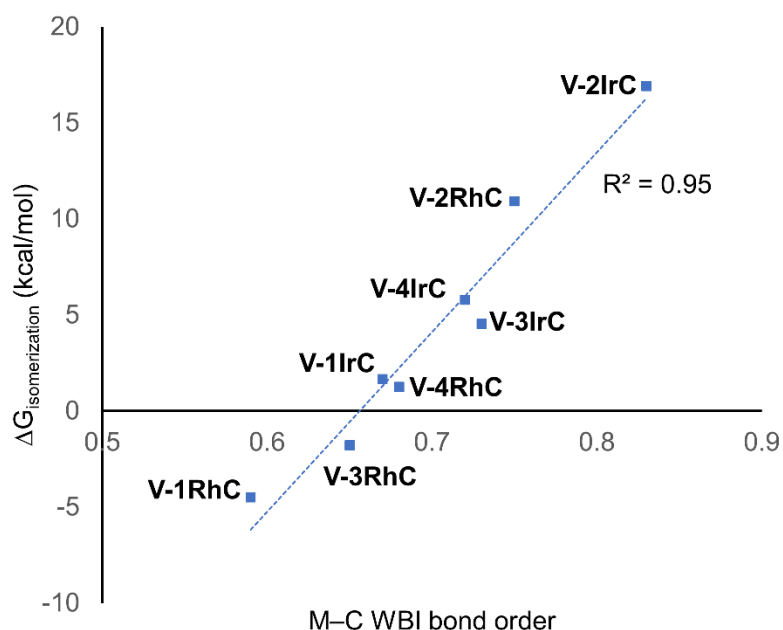


Figure V-6. Correlation between the free energy of isomerization and the M-C WBI values for compounds under study

Considering the M-C bonds, there appears to be a surprisingly linear correlation (Figure V-6) between the WBI values and the thermodynamic isomeric preference, that covers both the Rh and the Ir examples. Higher M-C WBI corresponds to higher preference for the M-C isomer, with ergoneutrality of the isomerization predicted at ca.

0.65 M-C WBI. The WBI values of the M-N bonds trend in the same direction. However, the correlation is more diffuse and not as steep, likely reflecting the intrinsically weaker nature of the M-N bond and its lesser dependence on the environment about the metal center (Figure V-7).

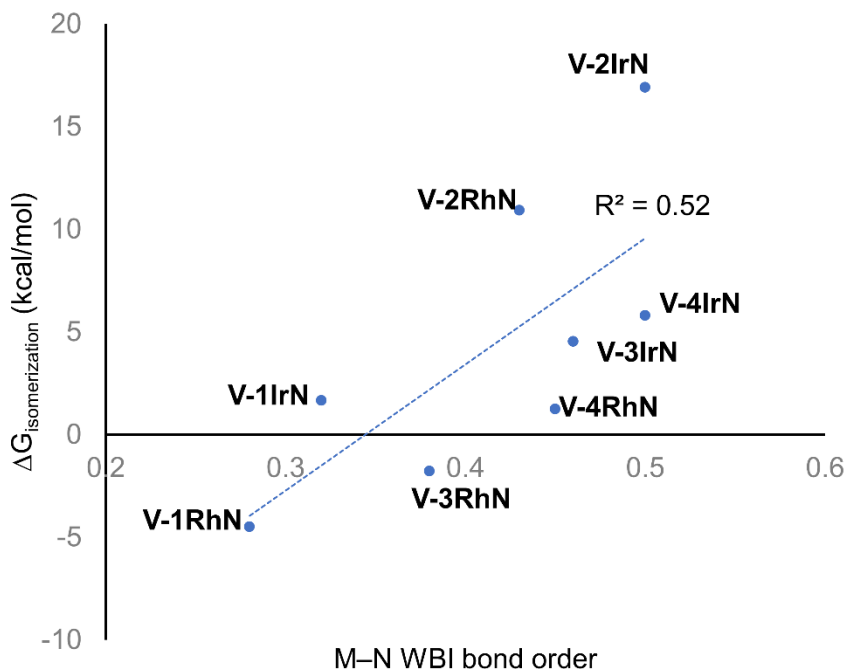


Figure V-7. Correlation between $\Delta G_{\text{isomerization}}$ and M-N WBI bond order

These observations lead us to conclude that the main factor controlling the thermodynamics of the M-C/M-N isomerization is the quality of the M-C bond, or in other words, the capacity of the metal site for making the strongest M-C bond. This capacity is always greater for Ir than for Rh, but it is also strongly influenced by the nature of the ligand *trans* to C. A hydride *trans* to C (Types V-1 and V-3) is a maximal *trans*-influence conflict, leading to the weakest M-C bonds. A bromide *trans* to C (type V-2) is much less *trans*-influencing than a hydride, leading to the strongest M-C bonds. A

carbonyl ligand *trans* to C (Type V-4) represents an intermediate situation. Type V-3 can be viewed as Type V-1 with additional CO ligand coordinated; apparently, CO coordination increases the M-C bond strength and therefore the preference for the M-C bound isomer. Notably, the WBI for the Rh-C bond in **V-2RhC** is higher than the WBI values for all the Ir complexes except **V-2IrC**, meaning that the weak *trans*-influence of Br (vs H or CO) can strengthen the M-C bond *trans* to it to a degree that can overcome the 4d/5d metal handicap.

We have also analyzed the bonding using the extended-transition-state natural orbitals for chemical valence (ETS-NOCV) partitioning of the interaction of the closed shell 2-pyridyl anionic fragment with the formally cationic (PBP)Ir framework (see details in section 5.4.5). The findings dovetailed the WBI analysis: greater energy of interaction was calculated for 1) Ir vs Rh, 2) M-C vs M-N isomers, and 3) for Type V-2 vs the other Types.

5.3 Conclusion

In summary, we have examined the unusual isomerization of a bridging 2-pyridyl unit in an array of Rh and Ir complexes supported by a PBP pincer ligand. The main factor governing the thermodynamic preference appears to be the strength of the M-C bond in the M-C bonded isomer. It was observed that the thermodynamic preference for the M-N vs M-C bond depends both on the nature of the metal center and on the nature of the ligand *trans* to the M-N/M-C bond. The M-C isomer is favored for the 5d metal Ir vs Rh and by the presence of a more weakly *trans*-influencing ligand *trans* to the M-N/M-C bond. For some of the complexes, both isomers were observed experimentally, in

close agreement with theoretical analysis. The interconversion between isomers of similar thermodynamic stability appears to be easily accessible on the experimental timescale. These findings suggest that the possibility of M-C/M-N isomerization of 2-pyridyl and other closely related fragments should be taken into account when investigating C-H bond activation in azines using a combination of a late transition metal and an embedded main group Lewis acid.

5.4 Experimental Section

5.4.1 General Considerations

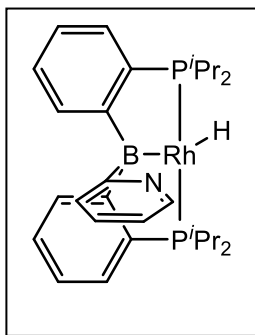
Unless specified otherwise, all manipulations were performed under an Ar atmosphere using standard Schlenk line or glovebox techniques. Toluene and pentane were dried and deoxygenated (by purging) using a solvent purification system (Innovative Technology Pure Solv MD-5 Solvent Purification System) and stored over molecular sieves in an Ar-filled glove box. C₆D₆ and CDCl₃ was dried over NaK/Ph₂CO/18-crown-6, distilled and stored over molecular sieves in an Ar-filled glovebox. Pyridine derivatives and cyclohexene were dried over CaH₂, vacuum transferred and stored over molecular sieves in an Ar-filled glove box. (PBP)RhHCl (**69**) and (PBP)IrHCl (**70**) were prepared via literature procedures.²⁷ All other chemicals were used as received from commercial vendors.

5.4.2 Physical Methods

NMR spectra were recorded on Mercury 300 (¹H NMR, 299.952 MHz; ³¹P NMR, 121.422 MHz), Bruker 400MHz (¹¹B NMR, 128.185 MHz, ¹H NMR, 399.535 MHz; ³¹P NMR, 161.734 MHz) and Varian Inova 500 (¹H NMR, 499.703 MHz; ¹³C NMR, 125.697

MHz; ^{31}P NMR, 202.265 MHz) spectrometer. Chemical shifts are reported in δ (ppm). For ^1H and ^{13}C NMR spectra, the residual solvent peak was used as an internal reference (^1H NMR: δ 7.16 for C_6D_6 , δ 7.26 for CDCl_3 , ^{13}C NMR: δ 128.06 for C_6D_6 , δ 77.2 for CDCl_3). ^{11}B NMR spectra were referenced externally with BF_3 etherate at δ 0. ^{31}P NMR spectra were referenced externally with 85% phosphoric acid at δ 0. FT-IR spectra were recorded on an Agilent Cary 630 ATR-IR spectrometer in a glovebox. Elemental analyses were performed by CALI Labs, Inc. (Highland Park, NJ)

5.4.3 Synthesis and Characterization of Rhodium and Iridium Complexes

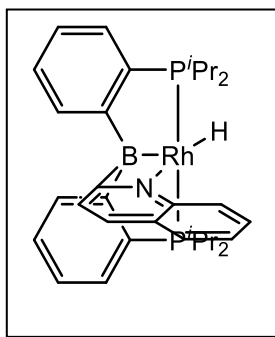


(PB^{Py}P)Rh(H) (V-1RhN). In a 50 mL PTFE screw-capped reaction tube, NaEt_3BH (0.40 mL, 0.40 mmol, 1.0 M in toluene) was added to a toluene solution (5 mL) of **69** (0.22 g, 0.40 mmol). The solution changed color from orange to dark red immediately. After stirring at room temperature for 5 min, a $^{31}\text{P}\{^1\text{H}\}$ NMR spectrum was

recorded, showing two or more complexes formed (Figure V-2). Volatiles were removed under vacuum to remove BEt_3 that was generated. The resulting red solid was directly dissolved in toluene (10 mL), to which were added pyridine (35 μL , 0.44 mmol) and cyclohexene (44 μL , 0.44 mmol). The reaction mixture was stirred at 80 $^\circ\text{C}$ for 12 h, and gradually changed from dark-red to brown color. The solution was filtered through Celite, and volatiles were removed under vacuum. The resulting brown solid was recrystallized in toluene/pentane (1:3), yielding a pale-yellow solid (163 mg, 70%).

^1H NMR (300 MHz, C_6D_6): δ 8.46 (d, $J_{\text{H-H}} = 7.5$ Hz, 2H, $\text{PB}^{\text{Py}}\text{P-Phenyl}$), 8.34 (d, $J_{\text{H-H}} = 4.8$ Hz, 1H, $\text{PB}^{\text{Py}}\text{P-Pyridyl}$), 7.31 (t, $J_{\text{H-H}} = 7.2$ Hz, 2H, $\text{PB}^{\text{Py}}\text{P-Phenyl}$), 7.18 (m, 4H,

PB^{Py}P-Phenyl), 6.68 (m, 2H, PB^{Py}P-Pyridyl), 6.45(m, 1H, PB^{Py}P-Pyridyl), 2.29 (m, 2H, CHMe₂), 1.92 (m, 2H, CHMe₂), 1.32 (dvt, J_{H-H} = J_{H-P} = 7.6 Hz, 6H, CHMe₂), 1.12 (dvt, J_{H-H} = J_{H-P} = 7.0 Hz, 6H, CHMe₂), 1.04 (dvt, J_{H-H} = J_{H-P} = 7.4 Hz, 6H, CHMe₂), 0.57 (dvt, J_{H-H} = J_{H-P} = 7.1 Hz, 6H, CHMe₂), -17.25 (dt, J_{H-P} = 18.5 Hz, J_{H-Rh} = 22.9 Hz, 1H, Rh-H). ³¹P{¹H} NMR (121 MHz, C₆D₆): δ 60.6 (d, J_{P-Rh} = 141.4 Hz). ¹¹B{¹H} NMR (128 MHz, C₆D₆): δ 3.5. ¹³C{¹H} NMR (126 MHz, C₆D₆) δ 188.2 (br, Rh-B-C-N), 165.4 (br, B-Phenyl), 149.6 (s, Pyridyl), 137.9 (td, J_{P-C} = 19.8 Hz, J_{Rh-C} = 3.5 Hz, P-Phenyl), 132.8 (s, Pyridyl), 129.9 (t, J_{P-C} = 9.9 Hz, Phenyl), 129.2 (s, Phenyl), 125.1 (t, J_{P-C} = 3.1 Hz, Phenyl), 122.2 (s, Pyridyl), 121.0 (s, Pyridyl), 30.0 (t, J_{P-C} = 8.3 Hz, CHMe₂), 27.7 (t, J_{P-C} = 14.5 Hz, CHMe₂), 21.3 (t, J_{P-C} = 4.8 Hz, CHMe₂), 20.4 (t, J_{P-C} = 2.1 Hz, CHMe₂), 20.1 (s, CHMe₂), 20.0 (t, J_{P-C} = 3.6 Hz, CHMe₂). Anal. Calc. for C₂₉H₄₁BNP₂Rh: C, 60.13; H, 7.13; N, 2.42. Found: C, 60.25; H, 6.97; N, 2.34.

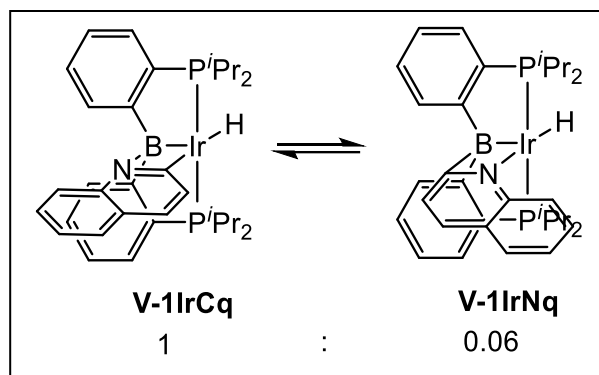


(PB^{Qu}P)Rh(H) (V-1RhNq). In a 50 mL PTFE screw-capped reaction tube, NaEt₃BH (0.52 mL, 0.52 mmol, 1.0 M in toluene) was added to a toluene solution (5 mL) of **69** (0.27 g, 0.50 mmol). The solution changed color from orange to dark-red immediately. After stirring at room temperature for 5 min, volatiles were

removed under vacuum to remove BEt₃ that was generated. The resulting red solid was dissolved in toluene (10 mL), to which were added quinoline (62 μL, 0.52 mmol) and cyclohexene (53 μL, 0.52 mmol). The reaction mixture was stirred at 80 °C for 12 h, and gradually changed from dark-red to brown color. The solution was filtered through Celite,

and volatiles were removed under vacuum. The resulting brown solid was recrystallized in toluene/pentane 1:3, yielding a pale-yellow solid (0.19 g, 59%).

^1H NMR (400 MHz, C_6D_6): δ 8.52 (d, $J_{\text{H-H}} = 7.5$ Hz, 2H, $\text{PB}^{\text{Py}}\text{P-Phenyl}$), 8.08 (d, $J_{\text{H-H}} = 8.3$ Hz, 1H, $\text{PB}^{\text{Qu}}\text{P-Quinolylyl}$), 7.39 (t, $J_{\text{H-H}} = 7.4$ Hz, 1H, $\text{PB}^{\text{Qu}}\text{P-Quinolylyl}$), 7.33 (t, $J_{\text{H-H}} = 7.0$ Hz, 2H, $\text{PB}^{\text{Py}}\text{P-Phenyl}$), 7.15 (m, 6H, $\text{PB}^{\text{Py}}\text{P-Phenyl}$ & Quinolylyl), 7.03 (t, $J_{\text{H-H}} = 7.4$ Hz, 1H, $\text{PB}^{\text{Qu}}\text{P-Quinolylyl}$), 6.94 (d, $J_{\text{H-H}} = 8.2$ Hz, 1H, $\text{PB}^{\text{Qu}}\text{P-Quinolylyl}$), 2.24 (m, 2H, CHMe_2), 1.84 (m, 2H, CHMe_2), 1.37 (dvt, $J_{\text{H-H}} = J_{\text{H-P}} = 7.5$ Hz, 6H, CHMe_2), 1.06 (m, 12H, CHMe_2), 0.19 (dvt, $J_{\text{H-H}} = J_{\text{H-P}} = 6.9$ Hz, 6H, CHMe_2), -16.81 (dt, $J_{\text{H-P}} = 18.5$ Hz, $J_{\text{H-Rh}} = 23.2$ Hz, 1H, Rh-H). $^{31}\text{P}\{^1\text{H}\}$ NMR (121 MHz, C_6D_6): δ 60.3 (d, $J_{\text{P-Rh}} = 141.1$ Hz). $^{11}\text{B}\{^1\text{H}\}$ NMR (128 MHz, C_6D_6): δ 4.5. $^{13}\text{C}\{^1\text{H}\}$ NMR (126 MHz, C_6D_6): δ 189.5 (br, Rh-B-C-N), 164.8 (br, B-Phenyl), 148.5 (s, *Quinolylyl*), 138.3 (td, $J_{\text{P-C}} = 19.5$ Hz, $J_{\text{Rh-C}} = 3.7$ Hz, P-Phenyl), 132.2 (s, *Quinolylyl*), 129.8 (t, $J_{\text{P-C}} = 9.7$ Hz, *Phenyl*), 129.4 (s, *Phenyl*), 128.7 (s, *Quinolylyl*), 128.6 (s, *Quinolylyl*), 128.5 (s, *Quinolylyl*), 125.3 (t, $J_{\text{P-C}} = 3.3$ Hz, *Phenyl*), 124.9 (s, *Quinolylyl*), 121.3 (s, *Quinolylyl*), 29.8 (t, $J_{\text{P-C}} = 8.4$ Hz, CHMe_2), 28.6 (t, $J_{\text{P-C}} = 14.6$ Hz, CHMe_2), 21.6 (t, $J_{\text{P-C}} = 4.6$ Hz, CHMe_2), 20.3 (t, $J_{\text{P-C}} = 4.2$ Hz, CHMe_2), 20.1 (s, CHMe_2), 19.8 (s, CHMe_2). Anal. Calc. for $\text{C}_{33}\text{H}_{43}\text{BNP}_2\text{Rh}$: C, 62.98; H, 6.89; N, 2.23. Found: C, 62.35; H, 6.59; N, 2.25.



Synthesis of (PBP)Ir(Qu)H/(PB^{Qu}P)IrH (V-1IrCq/V-1IrNq). 70 (0.30 g, 0.48 mmol) and quinoline (63 μ L, 0.53 mmol) was dissolved in 2 mL toluene, to which was added sodium bis(trimethylsilyl)amide (88 mg, 0.48 mmol). The reaction mixture was stirred at r. t. for 1 h, and passed through Celite. Volatiles were removed under vacuum, and the resulting solid was recrystallized in toluene/pentane 1:10, yielding an orange solid (0.25 g, 72%). The resulting product exists as an equilibrium in solution, and the ratio was calculated to be **V-1IrCq/V-1IrNq** = 1/0.06 by integration of the most downfield PBP-*Phenyl* signal in ^1H NMR spectrum. NMR spectroscopic data for **V-1IrCq**: ^1H NMR (500 MHz, C_6D_6) δ 8.80 (d, $J_{\text{H-H}} = 7.6$ Hz, 2H, PBP-*Phenyl*), 8.19 (d, $J_{\text{H-H}} = 8.4$ Hz, 1H, *Quinolyl*), 8.00 (d, $J_{\text{H-H}} = 8.5$ Hz, 1H, *Quinolyl*), 7.24 (t, $J_{\text{H-H}} = 7.3$ Hz, 2H, PBP-*Phenyl*), 7.20 (m, 2H, PBP-*Phenyl*), 7.10 (m, 5H, PBP-*Phenyl* & *Quinolyl*), 6.78 (t, $J_{\text{H-H}} = 7.4$ Hz, 1H, *Quinolyl*), 2.47 (m, 2H, CHMe_2), 2.17 (m, 2H, CHMe_2), 1.36 (dvt, $J_{\text{H-H}} = J_{\text{H-P}} = 7.5$ Hz, 6H, CHMe_2), 1.14 (dvt, $J_{\text{H-H}} = J_{\text{H-P}} = 7.2$ Hz, 6H, CHMe_2), 1.03 (dvt, $J_{\text{H-H}} = J_{\text{H-P}} = 7.1$ Hz, 6H, CHMe_2), 0.61 (dvt, $J_{\text{H-H}} = J_{\text{H-P}} = 7.0$ Hz, 6H, CHMe_2), -0.20 (t, $J_{\text{H-P}} = 23.2$ Hz, 1H, Ir-H). ^{31}P NMR (202 MHz, C_6D_6 , with selected range of ^1H decoupled) δ 59.0 (s). $^{11}\text{B}\{^1\text{H}\}$ NMR (128 MHz, C_6D_6) δ -8.5. $^{13}\text{C}\{^1\text{H}\}$ NMR (126 MHz, C_6D_6) δ 201.3 (t, $J_{\text{P-C}} = 6.2$ Hz, Ir-C), 159.0 (br, B-*Phenyl*), 141.6 (s, *Quinolyl*), 141.0 (t, $J_{\text{P-C}} = 23.9$ Hz, P-

Phenyl), 135.6 (s, *Quinoly*), 130.2 (s, *Phenyl*), 130.1 (s, *Quinoly*), 129.8 (t, $J_{P-C} = 8.2$ Hz, *Phenyl*), 129.5 (s, *Quinoly*), 129.0 (s, *Quinoly*), 126.0 (t, $J_{P-C} = 3.6$ Hz, *Phenyl*), 127.7 (s, *Phenyl*), 124.1 (s, *Quinoly*), 122.9 (s, *Quinoly*), 117.7 (s, *Quinoly*), 30.5 (t, $J_{P-C} = 11.7$ Hz, $CHMe_2$), 29.0 (t, $J_{P-C} = 18.1$ Hz, $CHMe_2$), 20.6 (s, $CHMe_2$), 20.5 (t, $J_{P-C} = 3.5$ Hz, $CHMe_2$), 20.3 (m, $CHMe_2$), 19.60 (s, $CHMe_2$). Selected NMR spectroscopic data for **V-1IrNq**. 1H NMR (500 MHz, C_6D_6) δ 8.64 (d, $J_{H-H} = 7.6$ Hz, 2H, *PBP-Phenyl*), 8.14 (d, $J_{H-H} = 7.8$ Hz, 1H, *Quinoly*), 6.84 (d, $J_{H-H} = 8.4$ Hz, 2H, *PBP-Phenyl*), 2.00 (m, 2H, $CHMe_2$), 0.19 (dvt, $J_{H-H} = J_{H-P} = 7.1$ Hz, 6H, $CHMe_2$), -17.10 (t, $J_{P-H} = 19.5$ Hz, Ir-H). ^{31}P NMR (202 MHz, C_6D_6 , with selected range of 1H decoupled) δ 59.0 (d, $J_{P-H} = 19.3$ Hz, Ir-H). Anal. Calc. for $C_{33}H_{43}BIrNP_2$: C, 55.15; H, 6.03; N, 1.95. Found: C, 55.21; H, 6.23; N, 2.01.

VT-NMR experiment of V-1IrCq/V-1IrNq in C_6D_6 . In a J. Young tube, **V-1IrCq/V-1IrNq** was dissolved in 0.4 mL C_6D_6 . 1H NMR were recorded at different temperature using a 500 MHz Varian NMR. **V-1IrCq/V-1IrNq** exists as an equilibrium in solution, and the ratio was calculated by integration of the most downfield *PBP-Phenyl* signal in 1H NMR spectrum. (**Figure V-8**)

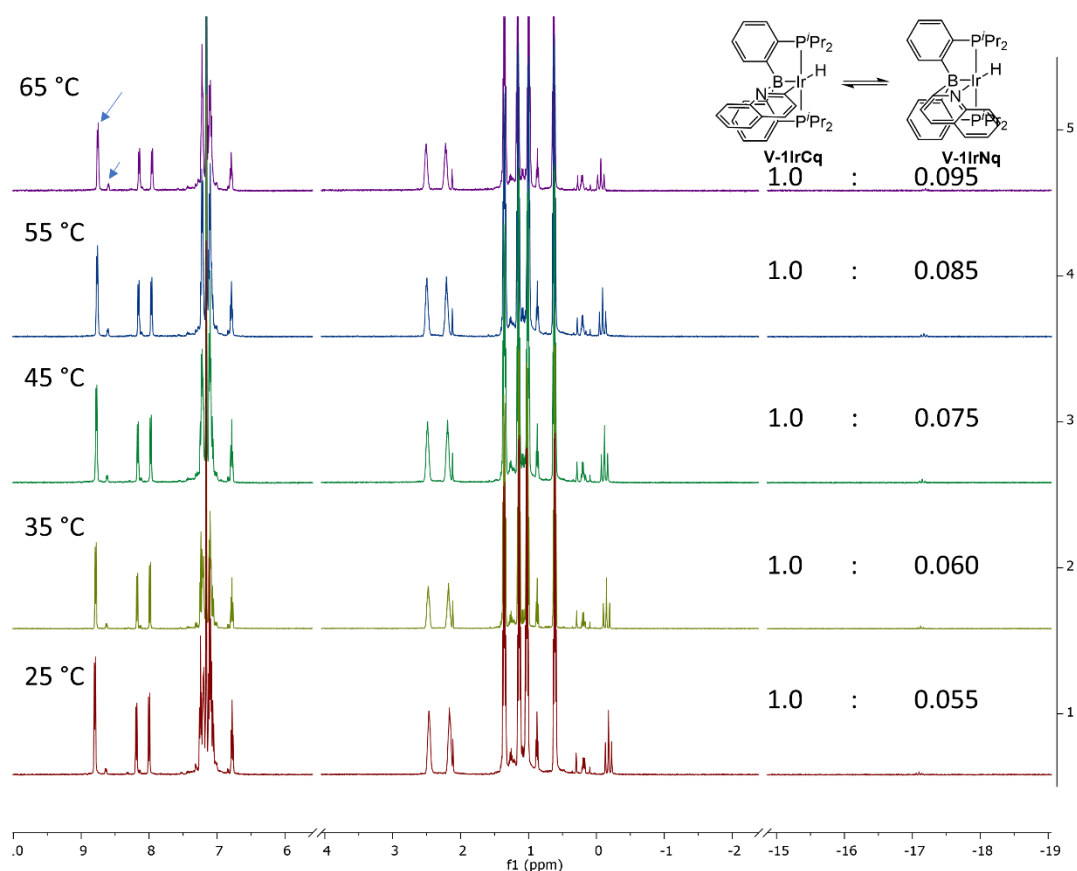
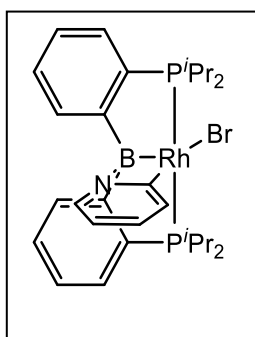
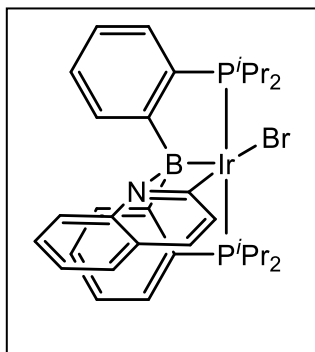


Figure V-8. VT-NMR experiment of V-1IrCq/V-1IrNq on a 500 MHz Varian NMR. (PBP)RhPyBr (V-2RhC)



(PBP)Rh(Py)Br. (V-2RhC). In a J. Young tube, N-bromosuccinimide (0.17 mmol, 30 mg) was added to a solution of **V-1RhN** (100 mg, 0.17 mmol) in 0.40 mL C₆D₆. This reaction mixture was stirred at room temperature for 24 h and heated at 100 °C for 12 h until all **V-1RhN** were consumed. (monitored by ³¹P{¹H} NMR). The resulting mixture was filtered over a pad of silica gel and washed through with dichloromethane. All volatiles were removed under vacuum and the resulting solid was recrystallized from toluene/pentane (1:3), yield an orange solid (80 mg, 70%)

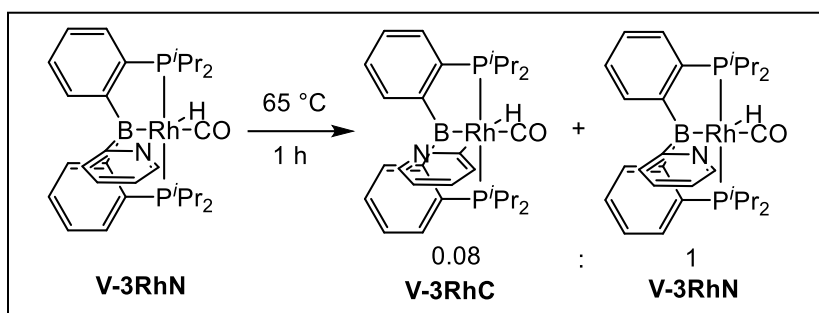
^1H NMR (500 MHz, C_6D_6) δ 8.44 (d, $J_{\text{H-H}} = 7.5$ Hz, 2H, PBP-Phenyl), 7.61 (d, $J_{\text{H-H}} = 8.2$ Hz, 1H, Pyridyl), 7.32 (t, $J_{\text{H-H}} = 6.8$ Hz, 2H, PBP-Phenyl), 7.13 (m, 4H, PBP-Phenyl), 6.62 (d, $J_{\text{H-H}} = 5.6$ Hz, 1H, Pyridyl), 6.09 (t, $J_{\text{H-H}} = 7.7$ Hz, 1H, Pyridyl), 5.59 (t, $J_{\text{H-H}} = 6.5$ Hz, 1H, Pyridyl), 3.56 (m, 2H, CHMe_2), 2.14 (m, 2H, CHMe_2), 1.56 (dvt, $J_{\text{H-H}} = J_{\text{H-P}} = 7.3$ Hz, 6H, CHMe_2), 1.15 (dvt, $J_{\text{H-H}} = J_{\text{H-P}} = 7.5$ Hz, 6H, CHMe_2), 1.08 (dvt, $J_{\text{H-H}} = J_{\text{H-P}} = 6.5$ Hz, 6H, CHMe_2), 0.49 (dvt, $J_{\text{H-H}} = J_{\text{H-P}} = 7.5$ Hz, 6H, CHMe_2). $^{31}\text{P}\{^1\text{H}\}$ NMR (202 MHz, C_6D_6): δ 42.8 (d, $J_{\text{P-Rh}} = 129.2$ Hz). $^{11}\text{B}\{^1\text{H}\}$ NMR (128 MHz, C_6D_6): δ 1.7. $^{13}\text{C}\{^1\text{H}\}$ NMR (126 MHz, C_6D_6) δ 178.0 (dt, $J_{\text{C-Rh}} = 34.8$ Hz, $J_{\text{C-P}} = 10.2$ Hz, C-Rh), 160.1 (br, B-Phenyl), 138.5 (s, Pyridyl), 137.3 (td, $J_{\text{P-C}} = 19.0$ Hz, $J_{\text{Rh-C}} = 3.4$ Hz, P-Phenyl), 134.0 (s, Pyridyl), 131.8 (s, Pyridyl), 131.7 (s, Phenyl), 131.2 (t, $J_{\text{P-C}} = 9.1$ Hz, Phenyl), 129.5 (s, Phenyl), 127.4 (t, $J_{\text{P-C}} = 3.2$ Hz, Phenyl), 116.0 (s, Pyridyl), 27.6 (t, $J_{\text{P-C}} = 12.3$ Hz, CHMe_2), 25.6 (t, $J_{\text{P-C}} = 10.3$ Hz, CHMe_2), 20.6 (s, CHMe_2), 19.9 (t, $J_{\text{P-C}} = 2.3$ Hz, CHMe_2), 19.3 (t, $J_{\text{P-C}} = 3.1$ Hz, CHMe_2), 18.4 (s, CHMe_2). Anal. Calc. for $\text{C}_{29}\text{H}_{40}\text{BBrNP}_2\text{Rh}$: C, 52.92; H, 6.13; N, 2.13. Found: C, 52.40; H, 5.81; N, 1.85.



(PBP)Ir(Qu)Br. (V-2IrCq). To **V-1IrCq/V-1IrNq** (0.14 mmol, 100 mg) in 2 mL toluene was added N-bromosuccinimide (0.14 mmol, 25 mg). The reaction mixture was heated at 50 °C for 12 h. The resulting mixture was filtered over a pad of silica gel and washed through with

dichloromethane. All volatiles were removed under vacuum and the resulting solid was recrystallized from THF/pentane (1:5), yield an orange solid (77 mg, 69%). ^1H NMR (500 MHz, C_6D_6) δ 8.86 (d, $J_{\text{H-H}} = 7.7$ Hz, 2H, PBP-Phenyl), 7.67 (d, $J_{\text{H-H}} = 8.8$ Hz, 1H,

Quinoly), 7.64 (d, $J_{\text{H-H}} = 8.3$ Hz, 1H, *Quinoly*), 7.30 (m, 2H, *PBP-Phenyl*), 7.07 (m, 4H, *PBP-Phenyl*), 6.89 (m, 2H, *Quinoly*), 6.65 (t, $J_{\text{H-H}} = 7.5$ Hz, 1H, *Quinoly*), 6.52 (d, $J_{\text{H-H}} = 8.8$ Hz, 1H, *Quinoly*), 3.79 (m, 2H, CHMe_2), 2.50 (m, 2H, CHMe_2), 1.51 (dvt, $J_{\text{H-H}} = J_{\text{H-P}} = 7.3$ Hz, 6H, CHMe_2), 1.10 (m, 12H, CHMe_2), 0.44 (dvt, $J_{\text{H-H}} = J_{\text{H-P}} = 7.5$ Hz, 6H, CHMe_2). $^{31}\text{P}\{^1\text{H}\}$ NMR (202 MHz, CDCl_3) δ 40.0 (s). $^{11}\text{B}\{^1\text{H}\}$ NMR (128 MHz, CDCl_3) δ -6.8. $^{13}\text{C}\{^1\text{H}\}$ NMR (126 MHz, CDCl_3) δ 176.9 (s, Ir-C), 157.7 (br, *B-Phenyl*), 152.0 (t, $J_{\text{C-P}} = 6.2$ Hz, *Quinoly*), 141.0 (s, *Quinoly*), 136.1 (t, $J_{\text{C-P}} = 24.4$ Hz, *P-Phenyl*), 131.1 (t, $J_{\text{C-P}} = 1.8$ Hz, *Phenyl*), 131.1 (s, *Quinoly*), 130.3 (t, $J_{\text{C-P}} = 8.3$ Hz, *Phenyl*), 129.8 (s, *Quinoly*), 128.7 (s, *Quinoly*), 128.4 (s, *Phenyl*), 126.3 (t, $J_{\text{C-P}} = 3.8$ Hz, *Phenyl*), 123.7 (s, *Quinoly*), 123.6 (s, *Quinoly*), 117.0 (s, *Quinoly*), 25.6 (t, $J_{\text{C-P}} = 15.9$ Hz, CHMe_2), 25.0 (t, $J_{\text{C-P}} = 12.6$ Hz, CHMe_2), 19.4 (s, CHMe_2), 18.9 (t, $J_{\text{C-P}} = 1.6$ Hz, CHMe_2), 18.6 (t, $J_{\text{C-P}} = 2.8$ Hz, CHMe_2), 17.9 (s, CHMe_2). Anal. Calc. for $\text{C}_{29}\text{H}_{40}\text{BBrNP}_2\text{Ir}$: C, 49.70; H, 5.31; N, 1.36. Found: C, 48.95; H, 5.06; N, 1.68.



In situ generation of $(\text{PB}^{\text{Py}}\text{P})\text{RhH}(\text{CO})$ and observation of the mixture of $(\text{PB}^{\text{Py}}\text{P})\text{RhH}(\text{CO})/(\text{PBP})\text{RhPyH}(\text{CO})$ after heating (V-3RhN/V-3RhC). In a J. Young tube, 1 atm of CO was added to a solution of **V-1RhN** (40 mg, 0.086 mmol) in 0.40 mL C_6D_6 after 3 rounds of freeze-pump-thaw. After stirring at room temperature for 10 min,

NMR spectra were recorded, showing the generation of **V-3RhN**. All volatiles were removed and 0.40 mL C₆D₆ was added. ATR-IR spectrum were recorded. The solution was heated at 65 °C for 1 h. ¹H NMR and ³¹P{¹H} NMR spectra were recorded at room temperature after heating, showing a mixture of **V-3RhC/V-3RhN** (0.08:1). (calculated by integration of methyl signals in ¹H NMR spectrum). The mixture was further heated at 65 °C for 24 h. It resulted in a mixture of four different compounds: an unidentified complex, **V-3RhC**, **V-3RhN**, and **V-1RhN** (1:3:17:1). (³¹P{¹H} NMR evidence, **Figure V-9**).

Spectroscopic data for **V-3RhN** under CO atmosphere: ¹H NMR (500 MHz, C₆D₆) δ 8.41 (d, J_{H-H} = 7.6 Hz, 2H, PB^{Py}P-*Phenyl*), 7.90 (d, J_{H-H} = 5.0 Hz, 1H, PB^{Py}P-*Pyridyl*), 7.36 (t, J_{H-H} = 7.0 Hz, 2H, PB^{Py}P-*Phenyl*), 7.15 (m, 4H, PB^{Py}P-*Phenyl*), 6.67 (t, J_{H-H} = 7.6 Hz, 1H, PB^{Py}P-*Pyridyl*), 6.58 (d, J_{H-H} = 7.7 Hz, 1H, PB^{Py}P-*Pyridyl*), 6.28 (dd, J_{H-H} = 7.2, 5.2 Hz, 1H, PB^{Py}P-*Pyridyl*), 2.17 (m, 2H, CHMe₂), 2.03 (m, 2H, CHMe₂), 1.26 (dvt, J_{H-H} = J_{H-P} = 7.0 Hz, 6H, CHMe₂), 1.18 (dvt, J_{H-H} = J_{H-P} = 7.2 Hz, 6H, CHMe₂), 0.86 (dvt, J_{H-H} = J_{H-P} = 7.1 Hz, 6H, CHMe₂), 0.58 (dvt, J_{H-H} = J_{H-P} = 7.2 Hz, 6H, CHMe₂), -15.69 (br, 1H, Rh-H). ³¹P{¹H} NMR (202 MHz, C₆D₆) δ 71.6 (d, J_{P-Rh} = 130.2 Hz). ¹¹B{¹H} NMR (160 MHz, C₆D₆) δ 2.0. ¹³C{¹H} NMR (126 MHz, C₆D₆) δ 221.6 (s, free CO), 193.5 (br, Rh-B-C-N), 165.8 (br, B-*Phenyl*), 150.1 (s, *Pyridyl*), 141.0 (t, J_{P-C} = 21.7 Hz, P-*Phenyl*), 132.9 (s, *Pyridyl*), 132.2 (t, J_{P-C} = 9.1 Hz, *Phenyl*), 129.3 (s, *Phenyl*), 129.2 (s, *Phenyl*), 125.1 (t, J_{P-C} = 3.2 Hz, *Phenyl*), 125.0 (s, *Pyridyl*), 120.4 (s, *Pyridyl*), 30.1 (t, J_{P-C} = 10.1 Hz, CHMe₂), 29.2 (t, J_{P-C} = 15.1 Hz, CHMe₂), 20.2 (s, CHMe₂), 19.9 (t, J_{P-C} = 2.6 Hz, CHMe₂), 19.8 (t, J_{P-C} = 2.9 Hz, CHMe₂), 19.6 (s, CHMe₂). (Rh-CO signals were not

observed due to broadness). ATR-IR: ν_{CO} 1968 cm^{-1} Selected spectroscopic data for **V-3RhC**: ^1H NMR (500 MHz, C_6D_6) δ 7.67 (d, $J_{\text{H-H}} = 7.7$ Hz, 1H, *Pyridyl*), 7.32 (t, $J_{\text{H-H}} = 5.6$ Hz, 2H, *PBP-Phenyl*), 6.51 (t, $J_{\text{H-H}} = 7.5$ Hz, 1H, *Pyridyl*), 5.92 (t, $J_{\text{H-H}} = 6.5$ Hz, 1H, *Pyridyl*), 1.98 (m, 2H, *CHMe*₂), 0.93 (dvt, $J_{\text{H-H}} = J_{\text{H-P}} = 7.1$ Hz, 6H, *CHMe*₂), 0.40 (dvt, $J_{\text{H-H}} = J_{\text{H-P}} = 7.1$ Hz, 6H, *CHMe*₂). $^{-11.04}$ (dt, $J_{\text{H-P}} = 12.6$ Hz, $J_{\text{H-Rh}} = 10.4$ Hz, 1H, *Rh-H*). $^{31}\text{P}\{^1\text{H}\}$ NMR (202 MHz, C_6D_6) δ 78.8 (d, $J_{\text{P-Rh}} = 126.1$ Hz). Other signals overlapped with **V-3RhN**.

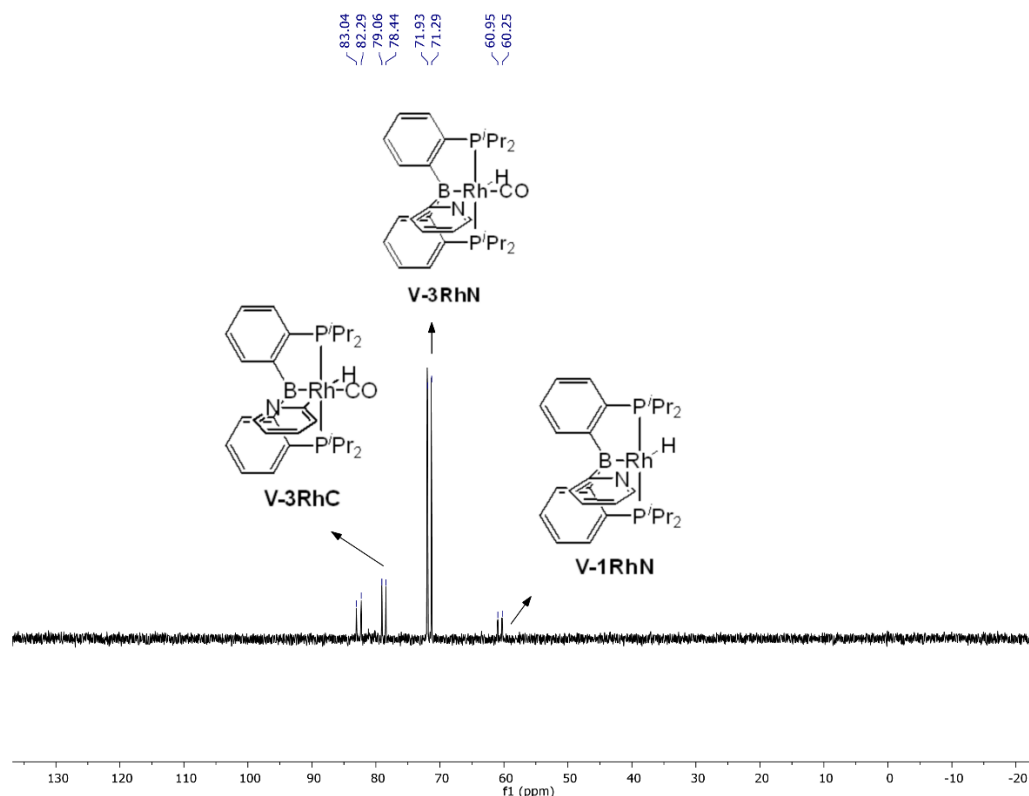
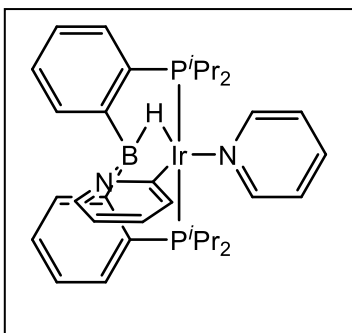


Figure V-9. $^{31}\text{P}\{^1\text{H}\}$ NMR (202 MHz, C_6D_6) spectrum recorded at room temperature after the reaction mixture were heated at 65 °C for 24 h. The sample contains a mixture of an unidentified complex, **V-3RhC**, **V-3RhN**, and **V-1RhN** at a ratio of 1:3:17:1



(PBP)Ir(Py)H(Py) (501). To **70** (0.10 mmol, 63 mg) in 2 mL toluene was added pyridine (9.0 μ L, 0.10 mmol) and sodium bis(trimethylsilyl)amide (19 mg, 0.10 mmol). After being heated at 45 $^{\circ}$ C for 12 h, $^{31}\text{P}\{^1\text{H}\}$ NMR spectrum were recorded, showing a mixture of three unidentified complexes. Additional pyridine (18 μ L, 0.10 mmol) were added, and the mixture was heated at 45 $^{\circ}$ C for 12 h. The reaction mixture was filtered through Celite, and volatiles were removed under vacuum. C_6D_6 were added and NMR spectra were recorded for characterization. ^1H NMR (500 MHz, C_6D_6) δ 8.97 (dt, $J_{\text{H-H}} = 1.6$ Hz, 4.4 Hz, 2H, PBP-Phenyl), 8.53 (d, $J_{\text{H-H}} = 7.5$ Hz, 2H, Ir-Pyridine), 7.85 (d, $J_{\text{H-H}} = 7.8$ Hz, 1H, Pyridyl), 7.30 (m, 5H, PBP-Phenyl & Pyridyl), 7.18 (m, 2H, PBP-Phenyl), 6.94 (tt, $J_{\text{H-H}} = 1.8$ Hz, 7.6 Hz, 1H, Ir-Pyridine), 6.72 (td, $J_{\text{H-H}} = 1.6$ Hz, 7.6 Hz, 1H, Pyridyl), 6.58 (ddd, $J_{\text{H-H}} = 1.5$ Hz, 4.5 Hz, 7.6 Hz, 2H, Ir-Pyridine), 5.93 (t, $J_{\text{H-H}} = 6.3$ Hz, 1H, Pyridyl), 2.48 (m, 2H, CHMe_2), 2.33 (m, 2H, CHMe_2), 1.24 (dvt, $J_{\text{H-H}} = J_{\text{H-P}} = 7.6$ Hz, 6H, CHMe_2), 1.09 (dvt, $J_{\text{H-H}} = J_{\text{H-P}} = 6.9$ Hz, 6H, CHMe_2), 0.98 (dvt, $J_{\text{H-H}} = J_{\text{H-P}} = 7.0$ Hz, 6H, CHMe_2), 0.62 (dvt, $J_{\text{H-H}} = J_{\text{H-P}} = 7.1$ Hz, 6H, CHMe_2), -7.17 (br, 1H, Ir-H). $^{31}\text{P}\{^1\text{H}\}$ NMR (202 MHz, C_6D_6) δ 50.0 (s). $^{11}\text{B}\{^1\text{H}\}$ NMR (128 MHz, C_6D_6) δ -7.4. $^{13}\text{C}\{^1\text{H}\}$ NMR (126 MHz, C_6D_6) δ 153.4 (s), 142.5 (t, $J_{\text{P-C}} = 3.2$ Hz), 139.3 (s), 136.4 (s), 134.8 (s), 131.7 (s), 129.6 (s), 129.2 (t, $J_{\text{P-C}} = 8.8$ Hz), 125.7 (t, $J_{\text{P-C}} = 3.4$ Hz), 123.7 (s), 117.9 (s), 113.4 (s), 30.6 (t, $J_{\text{P-C}} = 11.2$ Hz), 30.2 (t, $J_{\text{P-C}} = 17.2$ Hz), 20.2 (m, 2C), 19.9 (t, $J_{\text{P-C}} = 2.8$ Hz), 19.6 (s).

5.4.4 X-Ray Structural Determination Details.

V-1RhN, **CCDC 2014200**. A light yellow, multi-faceted block of suitable size ($0.46 \times 0.22 \times 0.16 \text{ mm}^3$) was selected from a representative sample of crystals of the same habit using an optical microscope and mounted onto a nylon loop. Low temperature (110 K) X-ray data were obtained on a Bruker APEXII CCD based diffractometer (Mo sealed X-ray tube, $K_{\alpha} = 0.71073 \text{ \AA}$). All diffractometer manipulations, including data collection, integration and scaling were carried out using the Bruker APEXII software.¹²² An absorption correction was applied using SADABS.¹²³ The space group was determined on the basis of systematic absences and intensity statistics and the structure was solved by direct methods and refined by full-matrix least squares on F^2 . The structure was solved in the monoclinic P $2_1/c$ space group using XS^{124, 127-129} (incorporated in Olex). All non-hydrogen atoms were refined with anisotropic thermal parameters. All hydrogen atoms were placed in idealized positions and refined using riding model with the exception of the hydrogen bound to rhodium which was located from the difference map. The structure was refined (weighted least squares refinement on F^2) and the final least-squares refinement converged. No additional symmetry was found using ADDSYM incorporated in PLATON program.¹⁶⁹

V-1RhNq, **CCDC 2014201**. A Leica MZ 7₅ microscope was used to identify a suitable yellow block with very well-defined faces with dimensions (max, intermediate, and min) $0.368 \times 0.36 \times 0.164 \text{ mm}^3$ from a representative sample of crystals of the same habit. The crystal mounted on a nylon loop was then placed in a cold nitrogen stream (Oxford) maintained at 110 K. A BRUKER APEX 2 X-ray (three-circle) diffractometer

was employed for crystal screening, unit cell determination, and data collection. The goniometer was controlled using the APEX2 software suite, v2008-6.0.²¹⁹ The sample was optically centered with the aid of a video camera such that no translations were observed as the crystal was rotated through all positions. The detector was set at 6.0 cm from the crystal sample (APEX2, 512x512 pixel). The X-ray radiation employed was generated from a Mo sealed X-ray tube ($K_{\alpha} = 0.70173\text{\AA}$ with a potential of 40 kV and a current of 40 mA). 60 data frames were taken at widths of 1.0° . These reflections were used in the auto-indexing procedure to determine the unit cell. A suitable cell was found and refined by nonlinear least squares and Bravais lattice procedures. The unit cell was verified by examination of the $h k l$ overlays on several frames of data. No super-cell or erroneous reflections were observed. After careful examination of the unit cell, an extended data collection procedure (4 sets) was initiated using omega scans. Integrated intensity information for each reflection was obtained by reduction of the data frames with the program APEX2.²¹⁹ The integration method employed a three-dimensional profiling algorithm and all data were corrected for Lorentz and polarization factors, as well as for crystal decay effects. Finally, the data was merged and scaled to produce a suitable data set. The absorption correction program SADABS¹²³ was employed to correct the data for absorption effects. Systematic reflection conditions and statistical tests of the data suggested the space group $P-1$. A solution was obtained readily using XT/XS in APEX2.^{124, 127-129, 219} Hydrogen atoms were placed in idealized positions and were set riding on the respective parent atoms. All non-hydrogen atoms were refined with anisotropic thermal parameters. Absence of additional symmetry and voids were

confirmed using PLATON (ADDSYM).¹⁶⁹ The structure was refined (weighted least squares refinement on F^2) to convergence.^{124, 127-130}

V-1IrCq, CCDC 2014205. A Leica MZ 7₅ microscope was used to identify an orange plate with very well-defined faces with dimensions (max, intermediate, and min) 0.528 x 0.213 x 0.046 mm³ from a representative sample of crystals of the same habit. The crystal mounted on a nylon loop was then placed in a cold nitrogen stream (Oxford) maintained at 110 K. A BRUKER APEX 2 Duo X-ray (three-circle) diffractometer was employed for crystal screening, unit cell determination, and data collection. The goniometer was controlled using the APEX3 software suite, v2017.3-0.²⁰⁰ The sample was optically centered with the aid of a video camera such that no translations were observed as the crystal was rotated through all positions. The detector (Bruker - PHOTON) was set at 6.0 cm from the crystal sample. The X-ray radiation employed was generated from a Mo sealed X-ray tube ($K_{\alpha} = 0.71073\text{\AA}$ with a potential of 40 kV and a current of 40 mA). 45 data frames were taken at widths of 1.0°. These reflections were used in the auto-indexing procedure to determine the unit cell. A suitable cell was found and refined by nonlinear least squares and Bravais lattice procedures. The unit cell was verified by examination of the $h k l$ overlays on several frames of data. No super-cell or erroneous reflections were observed. After careful examination of the unit cell, an extended data collection procedure (16 sets) was initiated using omega scans. Integrated intensity information for each reflection was obtained by reduction of the data frames with the program APEX3.²⁰⁰ The integration method employed a three-dimensional profiling algorithm and all data were corrected for Lorentz and polarization factors, as well as for

crystal decay effects. Finally, the data was merged and scaled to produce a suitable data set. The absorption correction program SADABS¹²³ was employed to correct the data for absorption effects. Systematic reflection conditions and statistical tests of the data suggested the space group *P*-1. A solution was obtained readily (*Z*=4; *Z'*=2) using XT/XS in APEX2.^{124, 127-129, 219} A molecule of toluene was found solvated (1/2 a molecule per Ir-complex). Hydrogen atoms were placed in idealized positions and were set riding on the respective parent atoms. All non-hydrogen atoms were refined with anisotropic thermal parameters. Elongated ellipsoids and nearby residual electron density peaks for C64 – C66 indicated disorder which was modeled between two positions with an occupancy ratio of 0.77:0.23. Appropriate restraints and constraints were added to keep the bond distances, angles, and thermal ellipsoids meaningful. Absence of additional symmetry and voids were confirmed using PLATON (ADDSYM).¹⁶⁹ The structure was refined (weighted least squares refinement on *F*²) to convergence.^{124, 127-130}

V-2RhC, CCDC 2014203. A Leica MZ 7₅ microscope was used to identify a suitable yellow block with very well-defined faces with dimensions (max, intermediate, and min) 0.222 x 0.19 x 0.182 mm³ from a representative sample of crystals of the same habit. The crystal mounted on a nylon loop was then placed in a cold nitrogen stream (Oxford) maintained at 110 K. A BRUKER APEX 2 X-ray (three-circle) diffractometer was employed for crystal screening, unit cell determination, and data collection. The goniometer was controlled using the APEX2 software suite, v2008-6.0.²¹⁹ The sample was optically centered with the aid of a video camera such that no translations were observed as the crystal was rotated through all positions. The detector was set at 6.0 cm from the

crystal sample (APEX2, 512x512 pixel). The X-ray radiation employed was generated from a Mo sealed X-ray tube ($K_{\alpha} = 0.70173\text{\AA}$ with a potential of 40 kV and a current of 40 mA). 60 data frames were taken at widths of 1.0° . These reflections were used in the auto-indexing procedure to determine the unit cell. A suitable cell was found and refined by nonlinear least squares and Bravais lattice procedures. The unit cell was verified by examination of the $h k l$ overlays on several frames of data. No super-cell or erroneous reflections were observed. After careful examination of the unit cell, an extended data collection procedure (4 sets) was initiated using omega scans. Integrated intensity information for each reflection was obtained by reduction of the data frames with the program APEX2.²¹⁹ The integration method employed a three-dimensional profiling algorithm and all data were corrected for Lorentz and polarization factors, as well as for crystal decay effects. Finally, the data was merged and scaled to produce a suitable data set. The absorption correction program SADABS¹²³ was employed to correct the data for absorption effects. Systematic reflection conditions and statistical tests of the data suggested the space group $P4_3$. A solution was obtained readily using XT/XS in APEX2.^{124, 127-129, 219} Hydrogen atoms were placed in idealized positions and were set riding on the respective parent atoms. All non-hydrogen atoms were refined with anisotropic thermal parameters. Elongated thermal ellipsoids on C27 and C28 suggested disorder, which was modeled successfully between two positions with an occupancy ratio of 0.42 to 0.58. Appropriate restraints were added to keep the bond distances, angles and thermal ellipsoids meaningful. Absence of additional symmetry and voids were confirmed

using PLATON (ADDSYM).¹⁶⁹ The structure was refined (weighted least squares refinement on F^2) to convergence.^{124, 127-130}

V-3RhN, CCDC 2014204. A Leica MZ 7₅ microscope was used to identify a suitable colorless block with very well-defined faces with dimensions (max, intermediate, and min) 0.774 x 0.706 x 0.429 mm³ from a representative sample of crystals of the same habit. The crystal mounted on a nylon loop was then placed in a cold nitrogen stream (Oxford) maintained at 110 K. A BRUKER APEX 2 Duo X-ray (three-circle) diffractometer was employed for crystal screening, unit cell determination, and data collection. The goniometer was controlled using the APEX3 software suite, v2017.3-0.²⁰⁰ The sample was optically centered with the aid of a video camera such that no translations were observed as the crystal was rotated through all positions. The detector was set at 6.0 cm from the crystal sample (APEX2, 512x512 pixel). The X-ray radiation employed was generated from a Mo sealed X-ray tube ($K_{\alpha} = 0.70173\text{\AA}$ with a potential of 40 kV and a current of 40 mA). 45 data frames were taken at widths of 1.0°. These reflections were used in the auto-indexing procedure to determine the unit cell. A suitable cell was found and refined by nonlinear least squares and Bravais lattice procedures. The unit cell was verified by examination of the $h k l$ overlays on several frames of data. No super-cell or erroneous reflections were observed. After careful examination of the unit cell, an extended data collection procedure (24 sets) was initiated using omega and phi scans. Integrated intensity information for each reflection was obtained by reduction of the data frames with the program APEX3.²⁰⁰ The integration method employed a three-dimensional profiling algorithm and all data were corrected for Lorentz and polarization

factors, as well as for crystal decay effects. Finally, the data was merged and scaled to produce a suitable data set. The absorption correction program SADABS¹²³ was employed to correct the data for absorption effects. Systematic reflection conditions and statistical tests of the data suggested the space group $P2_1/n$. A solution was obtained readily using XT/XS in APEX2.^{124, 127-129, 219} Hydrogen atoms were placed in idealized positions (the one connected to Rh was refined independently) and were set riding on the respective parent atoms. All non-hydrogen atoms were refined with anisotropic thermal parameters. Absence of additional symmetry and voids were confirmed using PLATON (ADDSYM).¹⁶⁹ The structure was refined (weighted least squares refinement on F^2) to convergence.^{124, 127-130}

ORTEP-3 for Windows and POV-Ray were employed for the final data presentation and structure plots.²²⁰

5.4.5 DFT Calculations.

The Gaussian suite of programs²²¹ was used for the ab initio electronic structure calculations. All structures were fully optimized by the B97D3²²² functional in the gas phase, and harmonic vibrational frequency calculations were performed to ensure that either a minimum was obtained. The Los Alamos basis set and the associated effective core potential (ECP) was used for Ru and Ir atoms, and an all-electron 6-31G(d) basis set was used for all the other atoms. Unless otherwise stated, the energies reported in this paper are Gibbs free energies under 298.15 K and 1 atm with solvent effect corrections.

The more recent natural orbitals for chemical valence (NOCV) analyses²²³ implemented as part of the ORCA program²²⁴ were applied to study the chemical bonds

in terms of the electron density rearrangement taking place upon bond formation at the B97D3/def2-TZVP level using the Extended Transition State (ETS) method of Ziegler.

The figures of NOCV deformation densities are generated by Multiwfn code.²²⁵

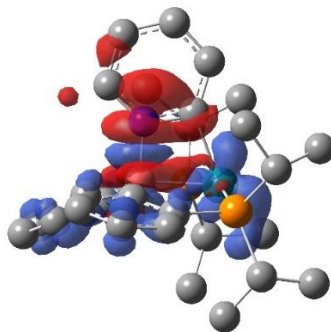
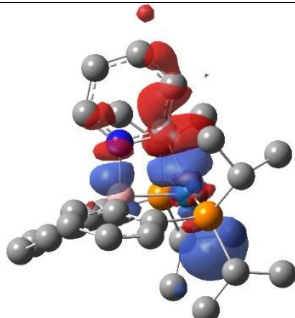
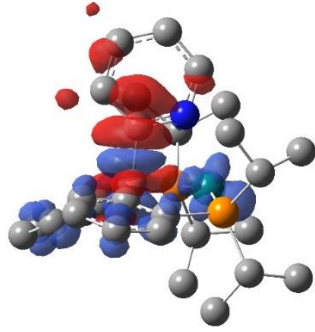
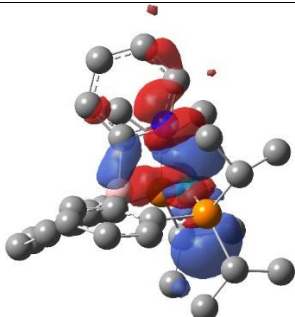
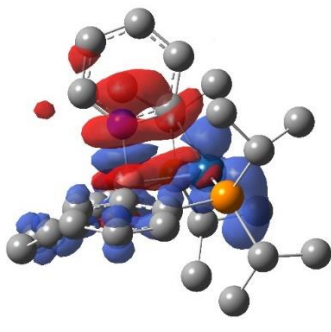
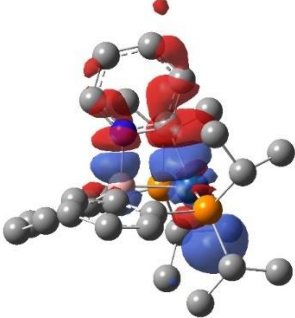
Table V-2. Absolute free energies and enthalpies in the gas phase at 298K and free energies and enthalpies for the M–C/M–N isomerizations (negative values favor the M–N isomer) calculated at the B97D3/LANL2DZ/6-31G(d) level in gas phase

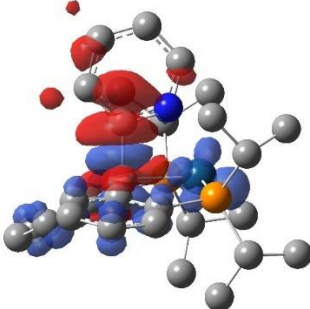
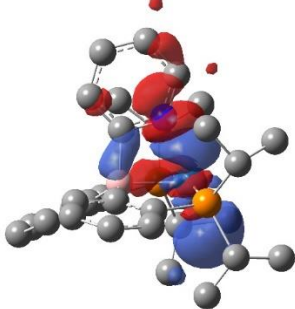
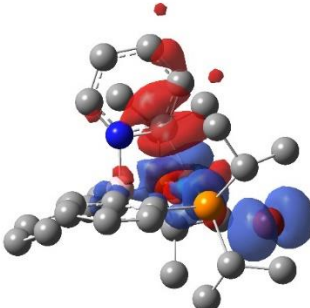
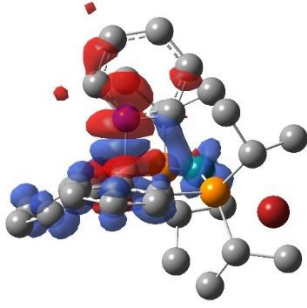
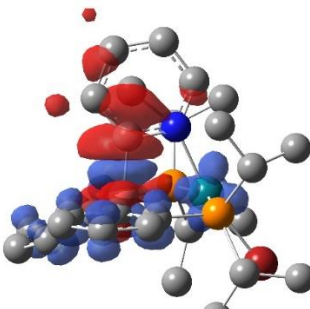
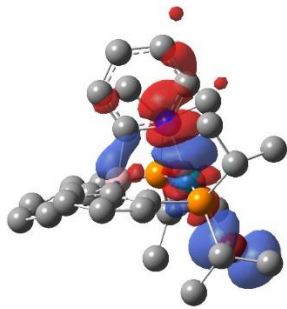
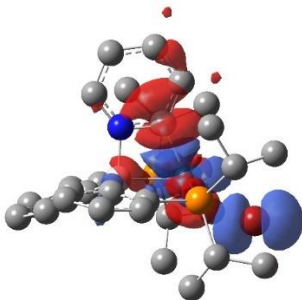
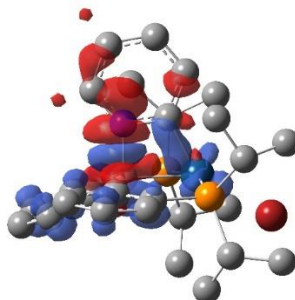
	Absolute values of Gibbs free energy (G) at 298 K (a. u.)	Absolute values of enthalpy (H) (a. u.)	$\Delta G_{\text{isomerization}}$ (kcal/mol)	$\Delta H_{\text{isomerization}}$ = (kcal/mol)
V-1RhC	-2000.592744	-2000.486785		
V-1RhN	-2000.599909	-2000.492665	-4.5	-3.7
V-1IrC	-1995.792319	-1995.686313		
V-1IrN	-1995.789668	-1995.681918	1.7	2.8
V-2RhC	-4572.779866	-4572.670542		
V-2RhN	-4572.762453	-4572.652586	10.9	11.3
V-2IrC	-4567.973024	-4567.863829		
V-2IrN	-4567.946079	-4567.836552	16.9	17.1
V-3RhC	-2113.872887	-2113.761183		
V-3RhN	-2113.875726	-2113.763486	-1.8	-1.4
V-3IrC	-2109.088223	-2108.977483		
V-3IrN	-2109.081008	-2108.969473	4.5	5.0
V-4RhC	-2113.847909	-2113.738511		
V-4RhN	-2113.84592	-2113.73573	1.2	1.7
V-4IrC	-2109.06682	-2108.958266		
V-4IrN	-2109.057584	-2108.948267	5.8	6.3

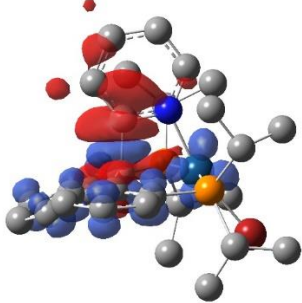
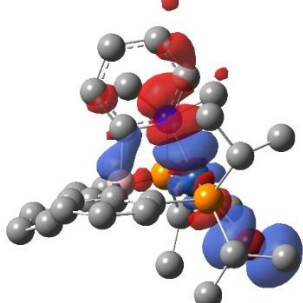
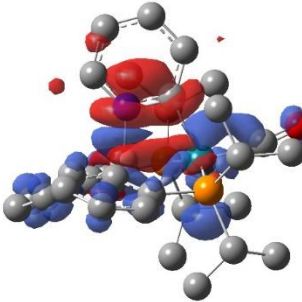
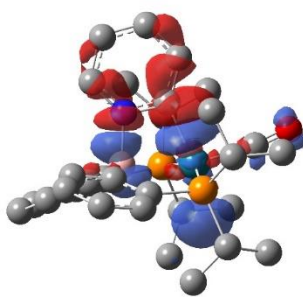
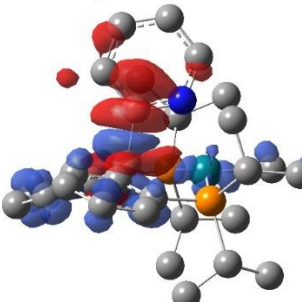
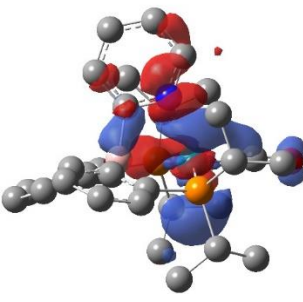
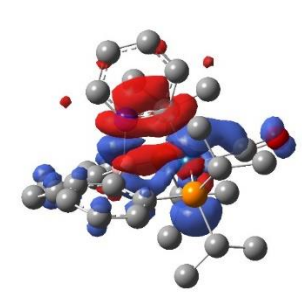
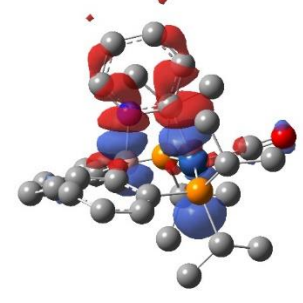
Table V-3. Wiberg bond indices calculated at the B97D3/LANL2DZ/6-31G(d) level of theory for Type V-1 to Type V-4 Rh and Ir complexes

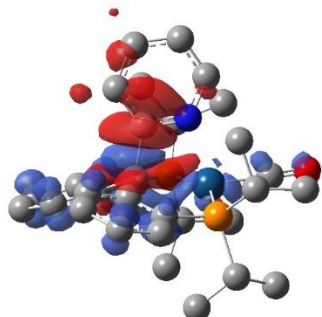
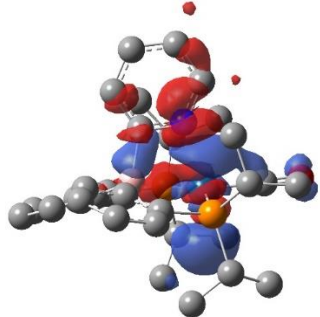
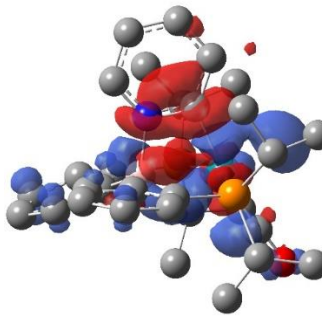
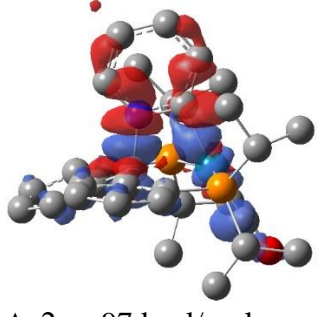
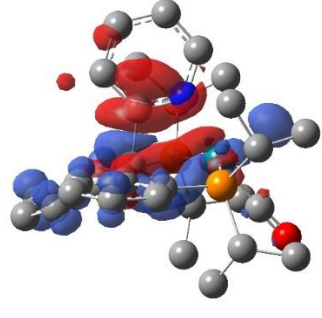
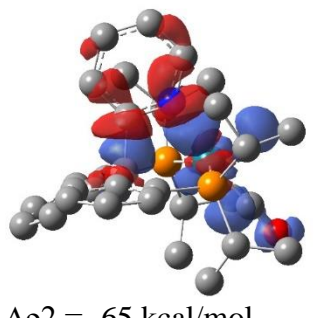
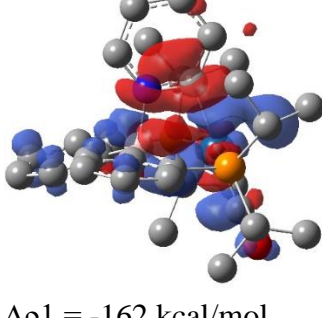
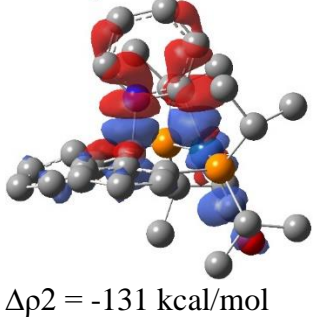
	Wiberg Bond Index			
	M-B	B-C/N	C-N	M-N/C
V-1RhC	0.58	0.59	1.23	0.59
V-1RhN	0.56	0.81	1.31	0.28
V-1IrC	0.66	0.59	1.22	0.67
V-1IrN	0.65	0.81	1.30	0.32
V-2RhC	0.52	0.58	1.24	0.75
V-2RhN	0.52	0.80	1.29	0.43
V-2IrC	0.60	0.57	1.23	0.83
V-2IrN	0.61	0.79	1.27	0.50
V-3RhC	0.51	0.59	1.26	0.65
V-3RhN	0.48	0.82	1.31	0.38
V-3IrC	0.59	0.59	1.25	0.73
V-3IrN	0.56	0.81	1.29	0.46
V-4RhC	0.49	0.58	1.27	0.68
V-4RhN	0.41	0.81	1.31	0.45
V-4IrC	0.58	0.57	1.27	0.72
V-4IrN	0.54	0.80	1.29	0.50

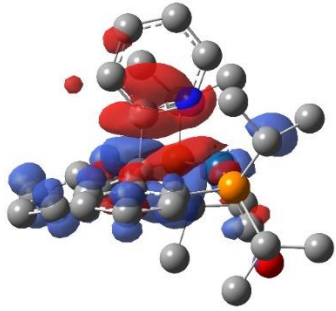
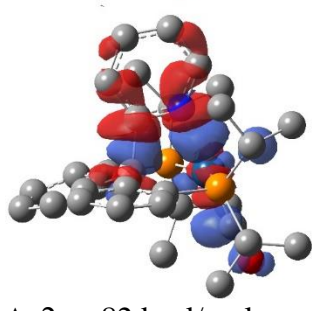
Table V-4. ETS-NOCV analysis of the interaction between 2-pyridyl anion and the formally positive charged rest of the molecule. The two largest decomposed NOCV contributions ($\Delta\rho_1$ and $\Delta\rho_2$) constructed with the density isosurface contour value of 0.002 are shown. Blue and red surfaces identify regions of electron density accumulation and depletion, respectively. It is clear the electrons “flow” from CN anion to metal cation

	Sum of decomposition energy by ETS-NOCV (kcal/mol)	The Two Major Components	
V-1RhC	-243.2	 $\Delta\rho_1 = -105$ kcal/mol	 $\Delta\rho_2 = -76$ kcal/mol
V-1RhN	-232.0	 $\Delta\rho_1 = -153$ kcal/mol	 $\Delta\rho_2 = -30$ kcal/mol
V-1IrC	-343.7	 $\Delta\rho_1 = -155$ kcal/mol	 $\Delta\rho_2 = -117$ kcal/mol

	Sum of decomposition energy by ETS-NOCV (kcal/mol)	The Two Major Components	
V-1IrN	-255.3	 $\Delta\rho_1 = -150$ kcal/mol	 $\Delta\rho_2 = -51$ kcal/mol
V-2RhC	-310.9	 $\Delta\rho_1 = -131$ kcal/mol	 $\Delta\rho_2 = -106$ kcal/mol
V-2RhN	-271.0	 $\Delta\rho_1 = -157$ kcal/mol	 $\Delta\rho_2 = -56$ kcal/mol
V-2IrC	-467.0	 $\Delta\rho_1 = -260$ kcal/mol	 $\Delta\rho_2 = -111$ kcal/mol

	Sum of decomposition energy by ETS-NOCV (kcal/mol)	The Two Major Components	
V-2IrN	-313.1	 $\Delta\rho_1 = -153 \text{ kcal/mol}$	 $\Delta\rho_2 = -96 \text{ kcal/mol}$
V-3RhC	-241.0	 $\Delta\rho_1 = -101 \text{ kcal/mol}$	 $\Delta\rho_2 = -83 \text{ kcal/mol}$
V-3RhN	-236.3	 $\Delta\rho_1 = -153 \text{ kcal/mol}$	 $\Delta\rho_2 = -36 \text{ kcal/mol}$
V-3IrC	-329.8	 $\Delta\rho_1 = -135 \text{ kcal/mol}$	 $\Delta\rho_2 = -129 \text{ kcal/mol}$

	Sum of decomposition energy by ETS-NOCV (kcal/mol)	The Two Major Components	
V-3IrN	-259.6	 $\Delta\rho_1 = -148$ kcal/mol	 $\Delta\rho_2 = -58$ kcal/mol
V-4RhC	-282.6	 $\Delta\rho_1 = -125$ kcal/mol	 $\Delta\rho_2 = -97$ kcal/mol
V-4RhN	-274.6	 $\Delta\rho_1 = -159$ kcal/mol	 $\Delta\rho_2 = -65$ kcal/mol
V-4IrC	-366.9	 $\Delta\rho_1 = -162$ kcal/mol	 $\Delta\rho_2 = -131$ kcal/mol

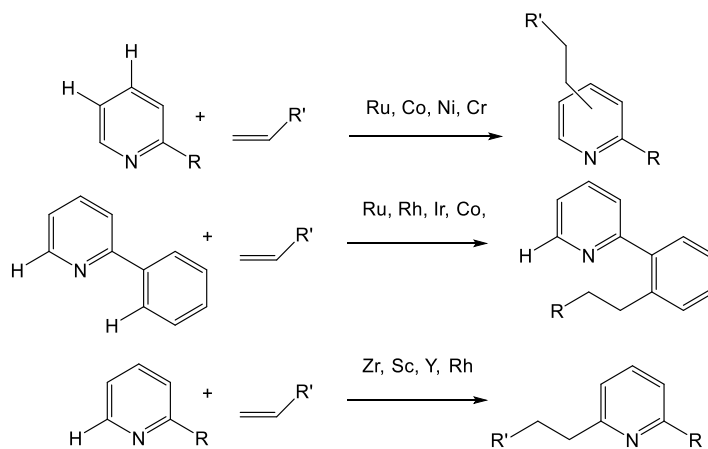
	Sum of decomposition energy by ETS-NOCV (kcal/mol)	The Two Major Components	
V-4IrN	-297.1	 <p data-bbox="711 722 980 756">$\Delta\rho_1 = -154$ kcal/mol</p>	 <p data-bbox="1068 701 1321 735">$\Delta\rho_2 = -82$ kcal/mol</p>

CHAPTER VI

ORTHO-SELECTIVE C-H NORBORNONYLATION OF PYRIDINES

6.1 Introduction

Pyridines are common motifs in a lot of materials and pharmaceuticals. Thus, the development of selective functionalization of pyridines is significant.²⁰¹⁻²⁰² Developing methods for synthesizing ortho alkylated pyridines has attracted increasing interest because it could offer synthetic method for later stage functionalization of drug candidates.^{203, 205-211} Olefins hydroarylation is an atom economic way to achieve alkylation of arene substrates and some transition metal catalyzed C–H alkylation of pyridines were reported previously²²⁶⁻²²⁹. As the pyridyl group was usually utilized as a directing group in some cases^{107, 109-110, 230-233}, the functionalization of the ortho position of pyridine was achieved with early transition metals²³⁴⁻²³⁵, rare earth catalysts^{203, 236}, or Rh catalysts^{29, 114, 117}.



Scheme VI-1. Transition metal catalyzed hydroarylation of olefins by substrates with pyridyl groups

We previously reported the selective ortho C–H activation by diarylboryl based (PBP)Ir complexes³⁷, and this reactivity was also observed with our diarylboryl based (PBP)Rh complexes (See details in section V). This ligand cooperative selective C–H activation was also mediated by Nakao’s (PAIP)Rh complex, which catalyzed ortho alkylation of pyridine.²⁹ In their case, only pyridine, 2- and 3-picoline were investigated as pyridines substrates. Here, we tested the ortho alkylation of pyridines with different substrate scopes, catalyzed by our (PBP)Rh complexes, resulting in different C–H selectivity.

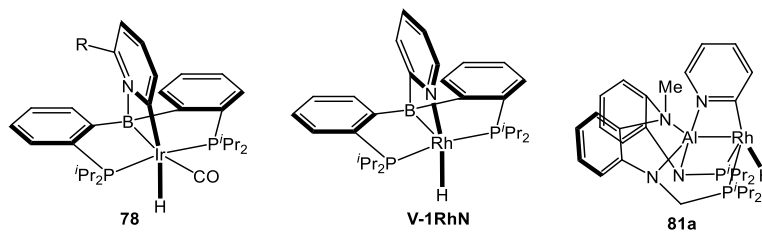


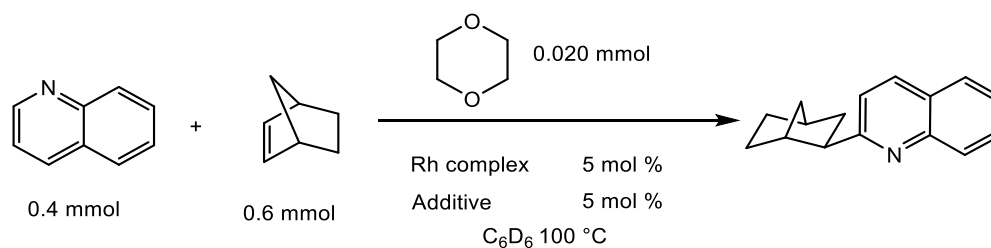
Figure VI-1. C–H activation of pyridine by (PBP)Ir, (PBP)Rh, and (PAIP)Rh.

6.2 Result and Discussion.

We first investigated the ethylation of quinoline catalyzed by our (PBP)Rh precursor **V-1RhNq** (20 mol%). After heating at 100 °C for 84 hours, 95% of quinoline was consumed to form 2-ethylquinoline, indicating a selective ortho alkylation of quinoline. Ethylene was refilled every 12 h to maintain constant pressure, and the conversion was monitored by ¹H NMR spectroscopy. After examining different olefin substrates (see details in section 6.4), we discovered that ortho alkylation of quinoline by norbornene catalyzed with **V-1RhNq** (5 mol%) was accomplished (99% conversion to exo-2-norbornylquinoline) after heating at 100 °C for 96 h.

Control experiments were set based on Table VI-1. Rh pincer complexes with aryl center donor or amino center donor did not catalyze this norbornylation (Trial 1 - 3). (Rh(COD)Cl)₂ itself did not catalyze this reaction, and no reactivity was observed with NaEt₃BH as additive and PPh₃ as supporting ligand (Trial 4 - 5). Analogous (PBP)Ir complex **V-IrCq** does not catalyze this reaction (Trial 6). Besides **V-RhNq**, (PBP)RhHCl (**69**) also result in 73% conversion with ⁿBuLi additive (Trial 7 - 8).

Table VI-1. Ortho selective norbornylation of quinoline catalyzed by different metals with additives



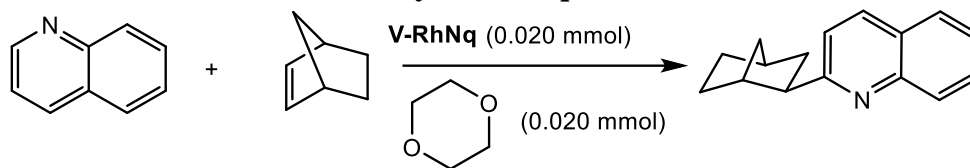
	Rh complex	Additive	Conversion
1	(POCOP)RhHCl	NaEt ₃ BH	0%
2	(PCP)RhHCl	NaEt ₃ BH	0%
3	(PNP)RhH ₂	/	0%
4	(Rh(COD)Cl) ₂	/	0%
5	(Rh(COD)Cl) ₂	NaEt ₃ BH + 2PPh ₃	0%
6	V-IrCq	/	0%
7	V-RhNq	/	99% ^a
8	69	ⁿ BuLi	73% ^b

a. This reaction was heated at 100 °C for 96 h, b. This reaction was heated at 125 °C for 24 h

Next, we tested how the concentration of each substrate would affect the reactivity (Table VI-2). As the catalyst **V-RhNq** would decompose in reactive solvents such as dichloromethane, DMF and DMSO, only dioxane, methylcyclohexane and toluene were used as the solvent, and they seem to have little effect on the conversion (Trial 1 - 3).

Increasing the concentration of norbornene to 2 equiv. resulted in a higher conversion (Trial 2, 5, 4). However, an increased amount of quinoline inhibited this catalysis (Trial 3, 6). A higher temperature resulted in 99% conversion of quinoline to 2-norbornylquinoline, but the decomposition of catalyst to free ligand and unknown Rh complexes also occurred faster (Trial 2, 7, 8).

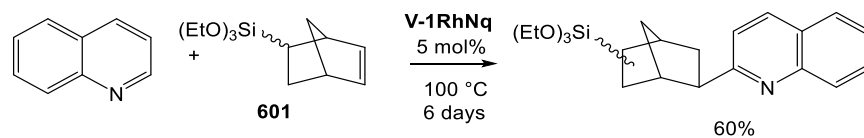
Table VI-2. Ortho selective norbornylation of quinoline



	Quinoline (mmol)	Norbornene (mmol)	Temperature (°C)	Solvent (0.40 mL)	Conversion
1	0.4	0.8	100	dioxane	47%
2	0.4	0.8	100	methylcyclohexane	65%
3	0.4	0.8	100	toluene	53%
4	0.4	1.6	100	methylcyclohexane	65%
5	0.4	0.4	100	methylcyclohexane	24%
6	0.8	0.8	100	methylcyclohexane	29%
7	0.4	0.8	125	methylcyclohexane	94%
8	0.4	0.8	150	methylcyclohexane	99% ^a

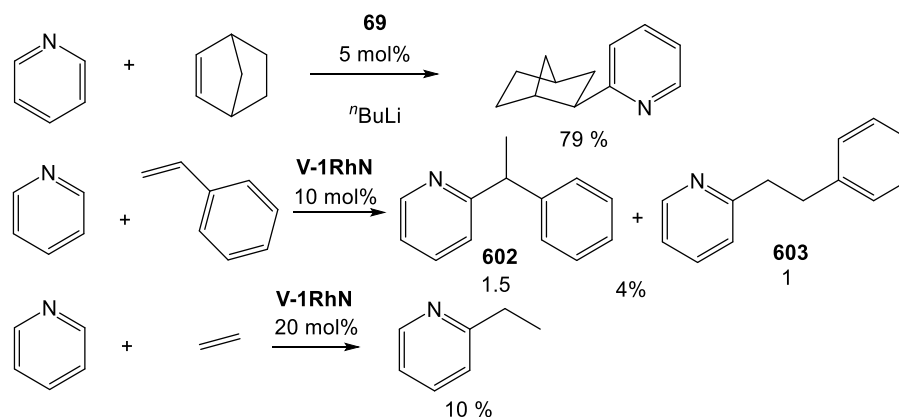
a. Based on $^{31}\text{P}\{^1\text{H}\}$ NMR spectra, the catalysts were decomposed completely to form free $\text{PB}^{\text{R}}\text{P}$ ligand and some inactivate Rh complexes.

Next, we move on to examine more substrate scopes (See section 6.4.5 and 6.4.6 for details). Different olefin substrates were examined. 1-hexene, 2,5 dihydrofuran, result in the isomerization of olefin. Neohexene, styrene and 2,3,4,5,6-pentafluorostyrene result in less than 2% conversion to the ortho alkylated product. A norbornene derivative **601** resulted in 60 % conversion to isomers of ortho alkylated products (Scheme VI-2).



Scheme VI-2. Ortho norbornylation of quinoline to generate different isomers

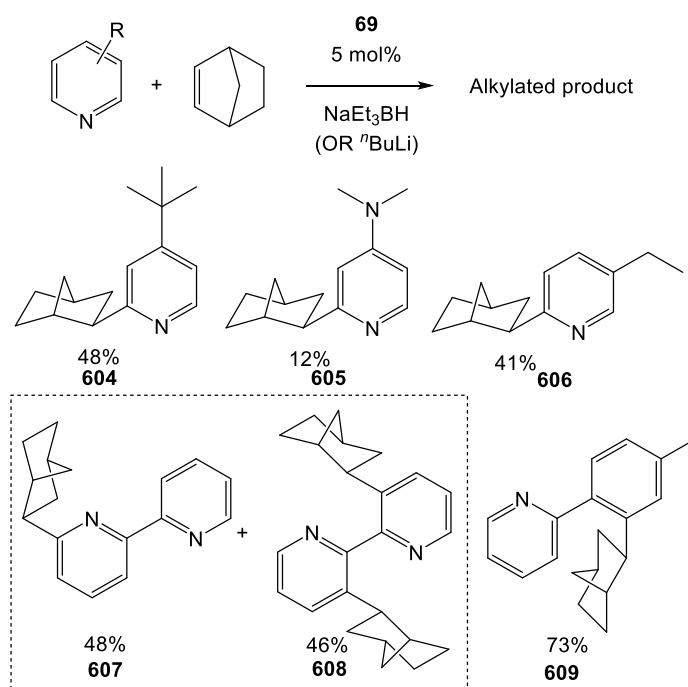
As pyridine was believed to be a challenging substrate since it could easily poison the metal center, we tested the alkylation of pyridine by our catalysts (Scheme VI-3). Ortho norbornylation of pyridine happened slower than quinoline, which reach to 79% conversion after heating at 125 °C for a week. With an increased amount of catalyst loading, ortho alkylation of pyridine with styrene catalyzed by **V-1RhN** resulted in 4% conversion to two isomers (**602** : **603** = 1 : 1.5). The generation of 2-ethylpyridine was catalyzed by 20 mol% **V-1RhN**. Although only 10% conversion was observed after heating at 125 C for 48 h, active catalysts was still observed by $^{31}\text{P}\{^1\text{H}\}$ NMR.



Scheme VI-3. Ortho alkylation of pyridine

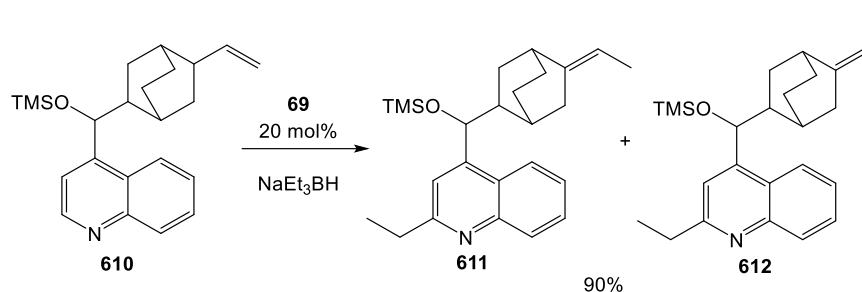
Finally, more substrates with pyridyl group were examined (Scheme VI-4). Among which, 4-tert-butylpyridine, 4-dimethylaminopyridine were norbornylated at C2 position (**604** - **605**). Interestingly, the norbornylation of 3-ethylpyridine happened at C6 position

and the C2 norbornylated product was not observed by ^1H NMR. The norbornylation of 2,2'-bipyridine at 100 °C for a week resulted 94% conversion into both mono functionalized product (**607**, 48%) and bi functionalized product (**608**, 46%).¹¹² The norbornylation of 2-tolylpyridine happened at tolyl group (**609**) after heating at 100 °C for 16 h, which seems to indicate that a traditional metal directed C–H alkylation occurred faster than the desired C2 alkylation directed by the PBP supporting ligand.



Scheme VI-4. Norbornylation of substrates containing pyridyl group

We also examined ethylation of a more challenged substrate: **610** catalyzed by our (PBP)Rh system (Scheme VI-5). After heating at 125 °C for 24h, 90% of **610** was consumed to form **611** and **612** (1 : 1.6), which indicated the ortho ethylation happened together with isomerization of terminal vinyl group.



Scheme VI-5. Ortho ethylation of 610 by (PBP)Rh to generate 611 and 612

6.3 Conclusion

In conclusion, (PBP)RhHCl catalyzed C–H alkylation of pyridines. The selectivity varied from different substrates. For substrates such as pyridine, quinoline, 4-tert-butylpyridine, 4-dimethylaminopyridine, and 3-ethylpyridine, the norbornylation happened at the ortho position. However, for 2-tolylpyridine, the norbornylation happened on the tolyl group. More study will be performed to understand the mechanism and to modify the catalyst.

6.4 Experimental Section

6.4.1 General Considerations

Unless specified otherwise, all manipulations were performed under an Ar atmosphere using standard Schlenk line or glovebox techniques. Toluene and pentane were dried and deoxygenated (by purging) using a solvent purification system (Innovative Technology Pure Solv MD-5 Solvent Purification System) and stored over molecular sieves in an Ar-filled glove box. C₆D₆ and toluene-d₈ was dried over NaK/Ph₂CO/18-crown-6, distilled and stored over molecular sieves in an Ar-filled glovebox. Pyridine derivatives and cyclohexene were dried over CaH₂, vacuum transferred and stored over

molecular sieves in an Ar-filled glove box. (PBP)RhHCl (**69**), (PBP)RhQuH (**V-RhNq**), (PBP)RhPyH (**V-RhN**), (PBP)IrQuH (**V-1IrCq**) were prepared via literature procedures. All other chemicals were used as received from commercial vendors.

6.4.2 Physical Methods

NMR spectra were recorded on Mercury 300 (^1H NMR, 299.952 MHz; ^{31}P NMR, 121.422 MHz), Bruker 400MHz (^{11}B NMR, 128.185 MHz, ^1H NMR, 399.535 MHz; ^{31}P NMR, 161.734 MHz) and Varian Inova 500 (^1H NMR, 499.703 MHz; ^{13}C NMR, 125.697 MHz; ^{31}P NMR, 202.265 MHz) spectrometer. Chemical shifts are reported in δ (ppm). For ^1H and ^{13}C NMR spectra, the residual solvent peak was used as an internal reference (^1H NMR: δ 7.16 for C_6D_6 , ^{13}C NMR: δ 128.06 for C_6D_6). ^{11}B NMR spectra were referenced externally with BF_3 etherate at δ 0. ^{31}P NMR spectra were referenced externally with 85% phosphoric acid at δ 0.

6.4.3 In Situ Observation of Ortho-selective Quinoline Ethylation and Nobornylation

Ortho C–H ethylation of quinoline to form 2-ethylquinoline. In a J. Young tube, quinoline (0.10 mmol, 12 μL), (PBP)RhQuH (**V-1RhNq**) (0.020 mmol, 13 mg), 1,4 dioxane (0.020 mmol, 0.10 mL, 0.20 M solution in C_6D_6) were added to C_6D_6 (0.40 mL). 1 atm of ethylene was introduced to the tube after three times of freeze-pump-thaw. The reaction mixture was heated at 100 $^\circ\text{C}$, and ethylene was refilled every 12 h to maintain a constant pressure. After 84 h, 95% of quinoline was consumed to form 2-ethylquinoline. (calculated by ^1H NMR spectrum with 1,2 dioxane as internal standard. (The NMR data for 2-ethylquinoline matched the data that were reported.)²⁰³

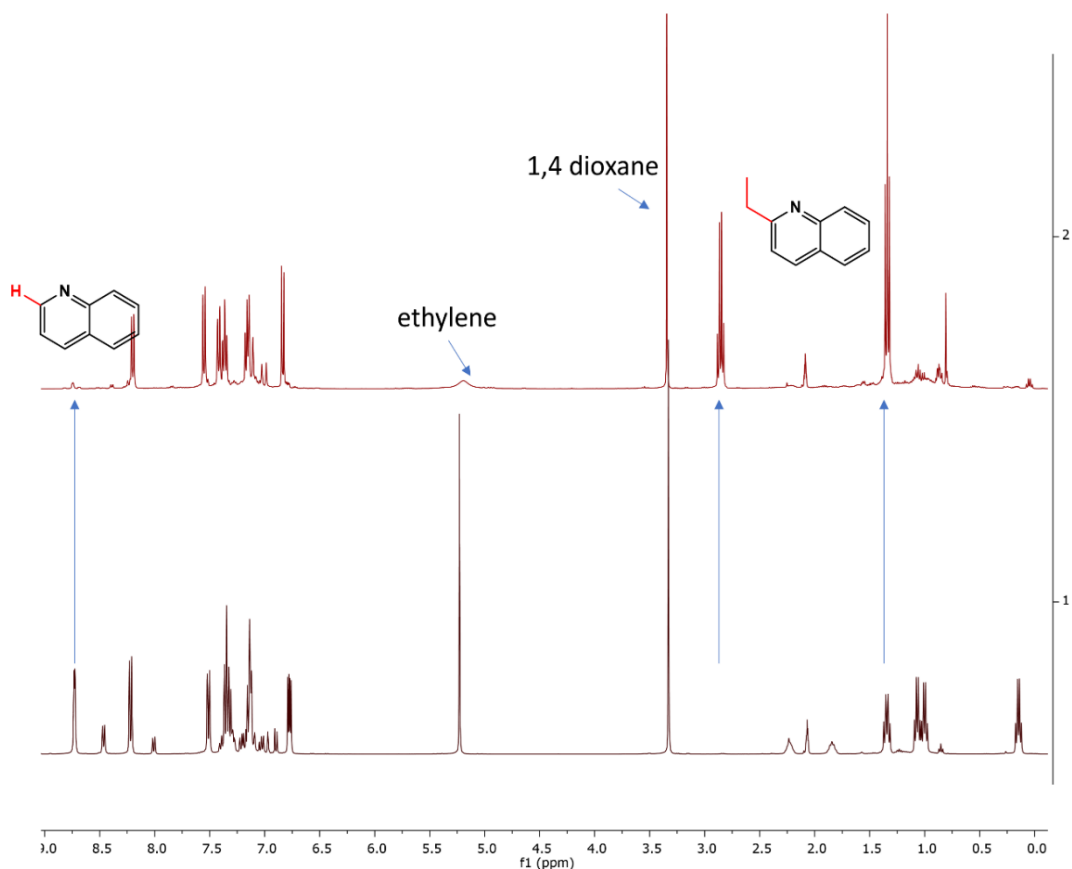
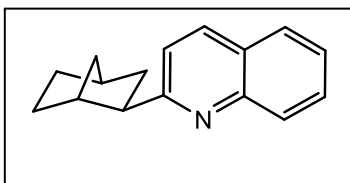


Figure VI-2. Bottom. ^1H NMR spectrum for reaction mixture of quinoline, **V-1RhNq** ethylene, 1,4-dioxane and before heating. **Top.** ^1H NMR spectrum for the same mixture after heating at 100 °C for 84 h



Ortho C–H alkylation of quinoline to form 2-

norbornylquinoline. In a J. Young tube, quinoline (0.40 mmol, 48 μL), norbornene (0.80 mmol, 76 mg), 1,2 dioxane

(0.020 mmol, 0.10 mL, 0.20 M solution in C_6D_6) and **V-1RhNq** (0.020 mmol, 13 mg) were added to 0.40 mL C_6D_6 . The reaction mixture was heated at 100 °C and ^1H NMR spectra were record every 48 h. After 96 h, 99% quinoline was consumed to form 2-norbornylquinoline. The resulting mixture was passed through Celite, followed by

purification with column chromatography (Ethyl Acetate: Hexane: 1:50), yielding a colorless liquid (57 mg, 64%). ^1H NMR (400 MHz, C_6D_6) δ 8.26 (d, $J_{\text{H-H}} = 8.4$ Hz, 1H), 7.57 (d, $J_{\text{H-H}} = 8.5$ Hz, 1H), 7.45 (d, $J_{\text{H-H}} = 8.1$ Hz, 1H), 7.37 (ddd, $J_{\text{H-H}} = 8.3$ Hz, 7.0 Hz, 1.4 Hz, 1H), 7.17 (m, 1H), 6.92 (d, $J_{\text{H-H}} = 8.5$ Hz, 1H), 2.89 (dd, $J_{\text{H-H}} = 8.7$ Hz, 5.3 Hz, 1H), 2.66 (m, 1H), 2.56 (s, 1H), 2.38 (s, 1H), 1.97 (d, $J_{\text{H-H}} = 9.5$ Hz, 1H), 1.57 (m, 3H), 1.33 (m, 1H), 1.25 (m, 1H), 1.11 (d, $J_{\text{H-H}} = 9.5$ Hz, 1H). $^{13}\text{C}\{^1\text{H}\}$ NMR (101 MHz, C_6D_6) δ 165.7 (s), 148.4 (s), 135.7 (s), 130.1 (s), 129.2 (s), 127.6 (s), 127.1 (s), 125.7 (s), 121.9 (s), 50.5 (s), 43.8 (s), 37.2 (s), 36.0 (s), 36.0 (s), 30.7 (s), 29.7 (s). HR MS (ESI+): Found 224.1429 $[\text{M}+\text{H}]^+$, calcd. for $\text{C}_{16}\text{H}_{18}\text{N}^+$: 224.1434.

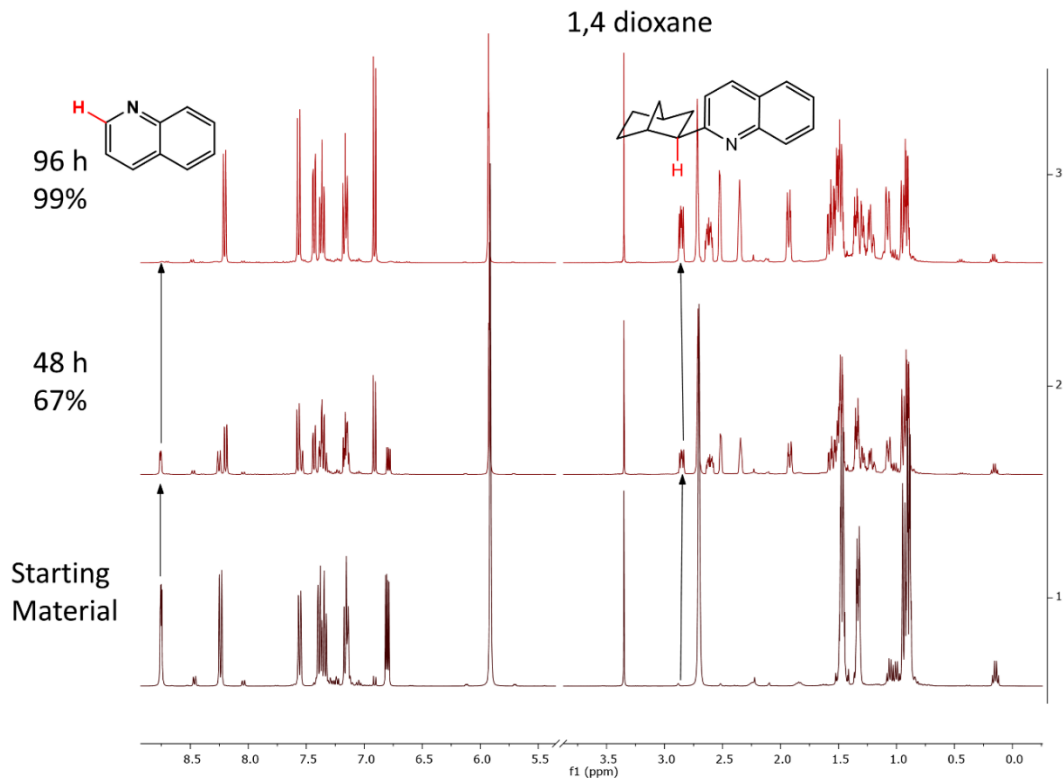


Figure VI-3. Bottom. ^1H NMR spectrum for reaction mixture of quinoline, norbornene, 1,4-dioxane and V-1RhNq before heating. **Middle.** ^1H NMR spectrum

for reaction mixture of quinoline, norbornene, 1,4-dioxane and V-1RhNq after heating at 100 °C for 48 h. Top. ¹H NMR spectrum for the same mixture after heating at 100 °C for 96 h

6.4.4 Details for Condition Optimization

Control experiments for ortho selective norbornylation of quinoline. In a J. Young tube, quinoline (0.40 mmol, 48 μ L), norbornene (0.60 mmol, 56 mg), 1,2 dioxane (0.020 mmol, 0.10 mL, 0.20 M solution in C₆D₆), metal complex, and additive based on Table VI-1 were added to 0.40 mL C₆D₆. The reaction mixture was heated at 100 °C for 48 h. Only reaction with (PBP)Rh complexes as catalysts had desired product observed.

Different conditions for ortho selective norbornylation of quinoline. In 8 mL vials, quinoline, norbornene and V-RhNq (0.020 mmol, 13 mg) were added to 0.40 mL solvent with stir bars. The vials were capped by PTFE screw caps and the reaction mixtures were heated at indicated temperature for 24 hours. Volatiles were removed under vacuum and mesitylene (0.40 mL, 0.050 M in C₆D₆, 0.020 mmol) was added as internal standard to determine conversion by ¹H NMR spectra. In general, solvent effect is not obvious for this reaction. Higher temperature and longer time are required for better conversion. The major decomposition was the releasing of PB^RP ligand from Rh center to form inactive Rh metal complexes.

6.4.5 Substrate Scopes

Ortho C–H ethylation of pyridine to form 2-ethylpyridine. In a J. Young tube, (PBP)RhPyH (V-1RhN) (0.020 mmol, 100 μ L, 0.20 M in C₆D₆), pyridine (0.10 mmol, 8.0 μ L), 1,4-dioxane (0.020 mmol, 100 μ L, 0.20 M in C₆D₆) were added to 0.20 mL C₆D₆.

1 atm of ethylene was introduced to the tube after 3 times of freeze-pump-thaw. The reaction mixture was heated at 125 °C for 48 h, 10% of pyridine was consumed to form 2-ethylpyridine. (Calculated by ^1H NMR spectrum with 1,2 dioxane as internal standard. The NMR data for 2-ethylpyridine matched the data that were reported.)²³⁷

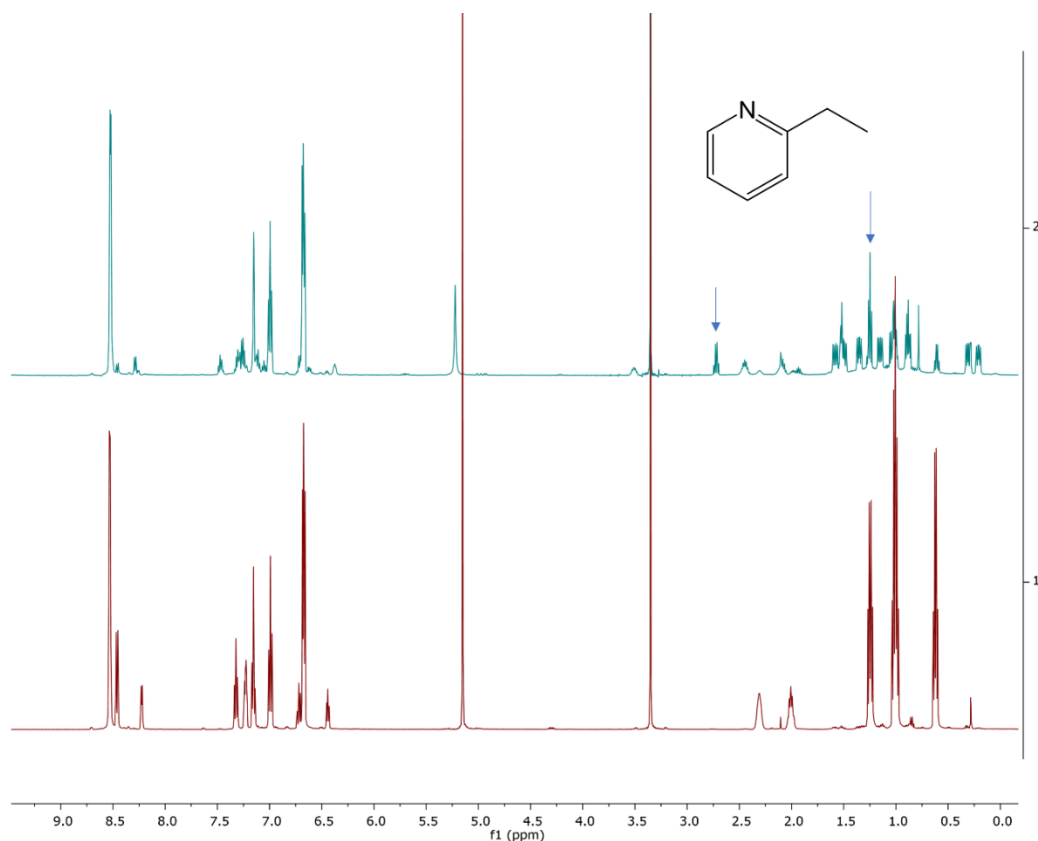


Figure VI-4. Bottom. ^1H NMR spectrum for reaction mixture of pyridine, ethylene, 1,4-dioxane and V-1RhN before heating. **Top.** ^1H NMR spectrum for the same mixture after heating at 125 °C for 48 h.

Ortho C-H alkylation of pyridine to form 2-(α -methylbenzyl)pyridine and 2-(2-phenylethyl)pyridine. In a J. Young tube, V-1RhN (0.020 mmol, 100 μL , 0.20 M in C_6D_6), pyridine (0.20 mmol, 16 μL), styrene (0.20 mmol, 23 μL) and 1,4-dioxane (0.020

mmol, 100 μL , 0.20 M in C_6D_6) were added to 0.20 mL C_6D_6 . The reaction mixture was heated at 100 $^\circ\text{C}$ for 20 h, 4% of pyridine was consumed to form 2-(α -methylbenzyl)pyridine (**602**) and 2-(2-phenylethyl)pyridine (**603**) (1.5 : 1). (Calculated by ^1H NMR spectrum with 1,2 dioxane as internal standard. The NMR data for **602** and **603** matched the data that were reported.)²³⁸⁻²³⁹

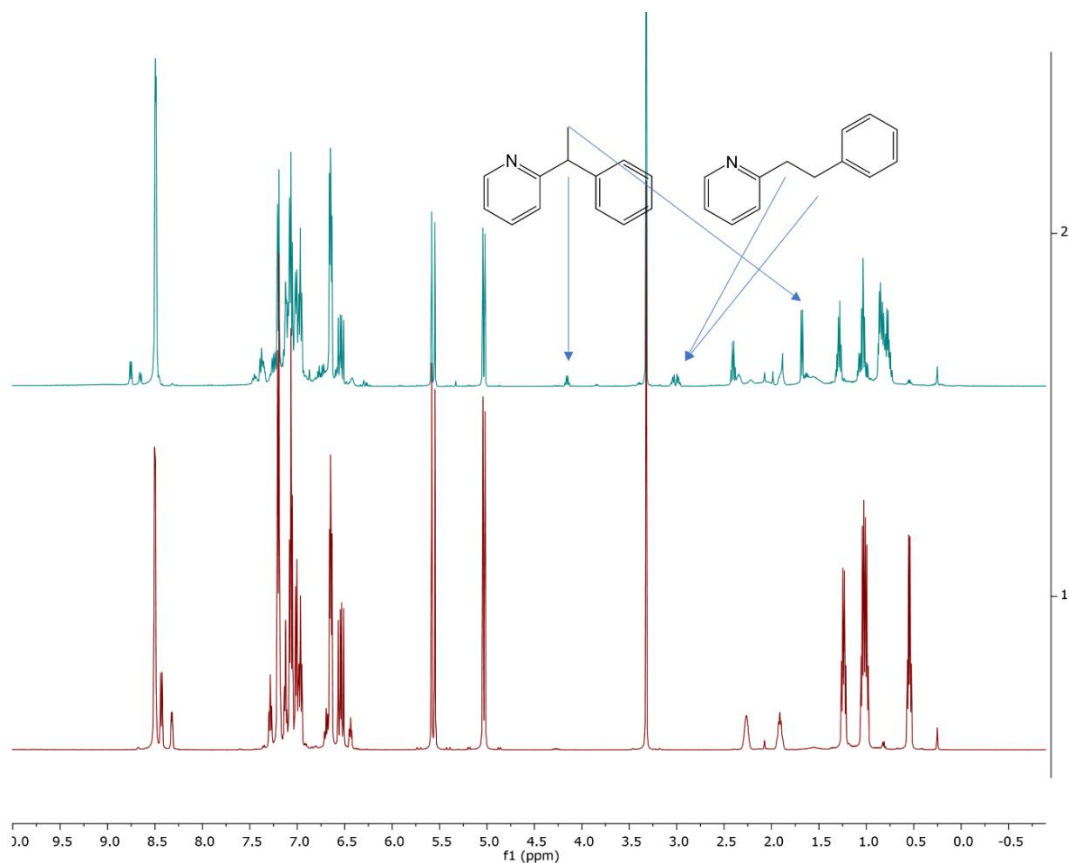


Figure VI-5. Bottom. ^1H NMR spectrum for reaction mixture of pyridine, styrene, 1,4-dioxane and (PBP)RhPyH before heating. **Top.** ^1H NMR spectrum for the same mixture after heating at 100 $^\circ\text{C}$ for 20 h

General procedure 1 for alkylation of quinoline with V-1RhNq. In J. Young tubes, V-1RhNq (0.020 mmol, 100 μL , 0.20 M in C_6D_6), quinoline (0.40 mmol, 48 μL), olefin

(0.80 mmol) and 1,4-dioxane (0.020 mmol, 100 μ L, 0.20 M in C_6D_6) were added to 0.20 mL C_6D_6 . The reaction mixtures were heated at indicated temperature for indicated time. The resulting products were analyzed by 1H NMR spectrum.

Quinoline + 2,3,4,5,6-pentafluorostyrene. After heating at 100 $^{\circ}C$ for 20 h, trace amount of the desired product was observed by 1H NMR spectrum.

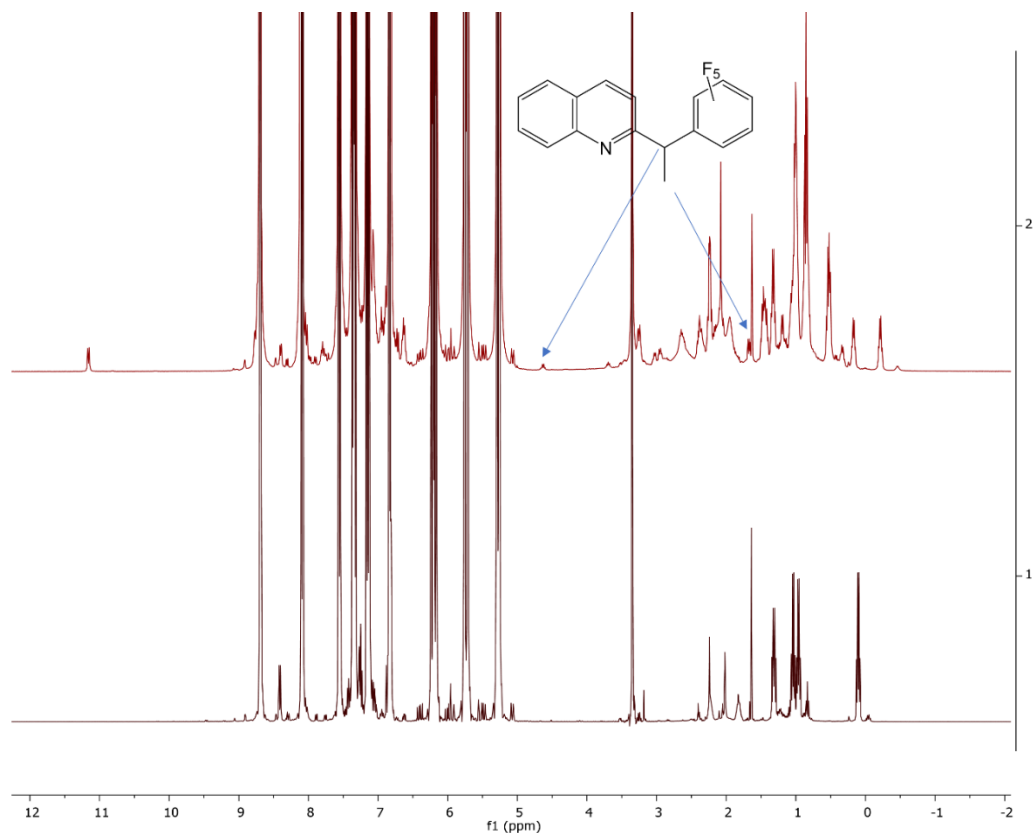


Figure VI-6. Bottom. 1H NMR spectrum for reaction mixture of quinoline, 2,3,4,5,6-pentafluorostyrene, 1,4-dioxane and V-1RhNq before heating. **Top.** 1H NMR spectrum for the same mixture after heating at 100 $^{\circ}C$ for 20 h

Quinoline + 5-bicyclo[2.2.1]hept-2-enyl(triethoxy)silane. After heating at 100 $^{\circ}C$ for 132 h, 60% of quinoline was consumed to form the desired products, which exist as a

mixture of different isomers. The C–H of the carbon connected to the ortho position of quinoline has a unique chemical shift (~ 3 ppm) and appears as a doublet of doublet on ^1H NMR spectrum. Three different signals were observed within that range in the ^1H NMR spectrum of the resulting mixture, which indicated that at least three different isomers were generated.

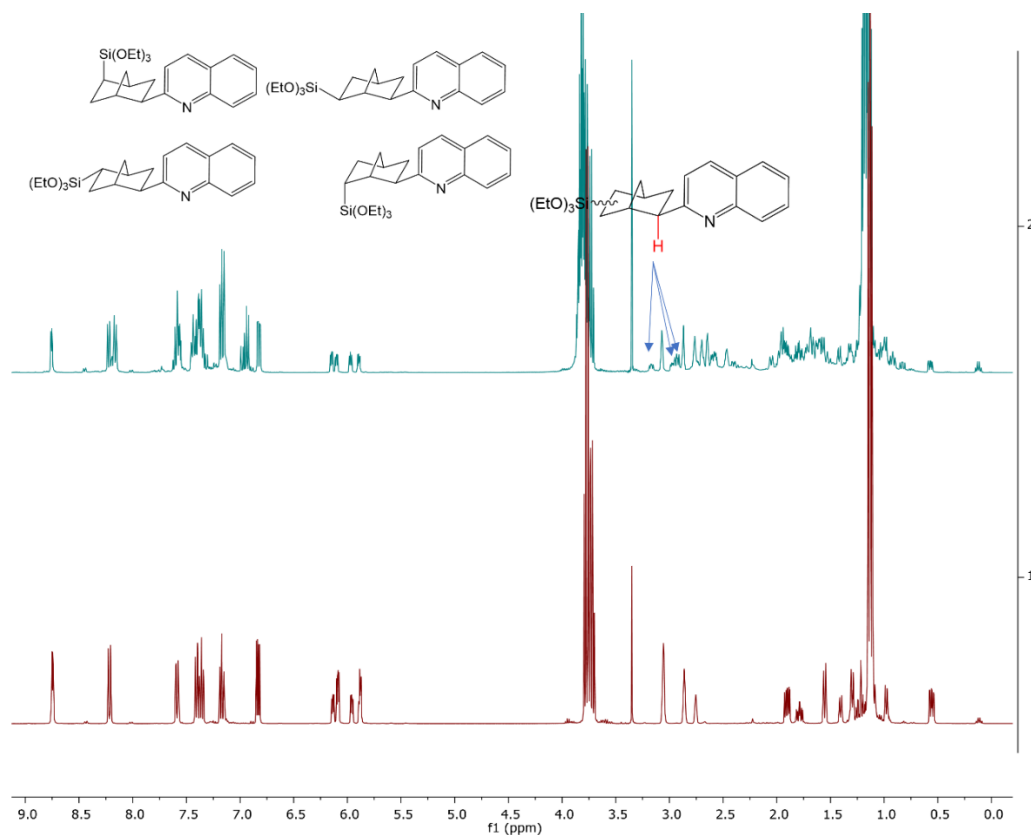


Figure VI-7. Bottom. ^1H NMR spectrum for reaction mixture of quinoline, 5-bicyclo[2.2.1]hept-2-enyl(triethoxy)silane, 1,4-dioxane and V-1RhNq before heating. **Top.** ^1H NMR spectrum for the same mixture after heating at 100 °C for 132 h

General procedure 2 for alkylation of quinoline with V-1RhNq. In 8 ml vials, V-1RhNq (0.020 mmol, 12.6 mg), quinoline (0.40 mmol, 48 μL), olefins (0.80 mmol) were added to 0.40 mL methylcyclohexane. The vials were heated at indicated temperature for

indicated time. The volatiles were removed and mesitylene (0.020 mmol, 0.40 mL, 0.050 M in C₆D₆) were added as internal standard to analyze the resulting product by ¹H NMR spectrum.

Quinoline + neohexene. After heating at 125 °C for 24 h, less than 1% of quinoline was consumed to form 2-(3,3-dimethylbutyl)quinoline. Further heating at 150 °C for 24 h lead to 6% conversion to 2-(3,3-dimethylbutyl)quinoline.

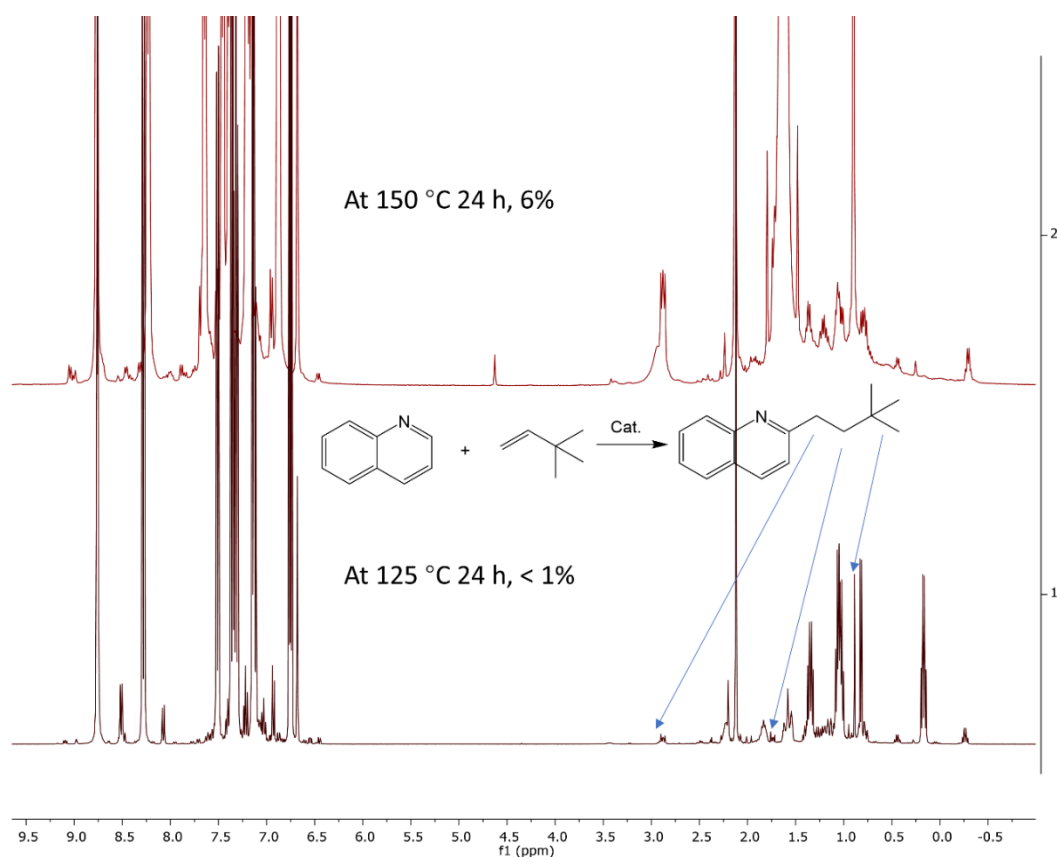


Figure VI-8. Bottom. ¹H NMR spectrum for the reaction mixture after heating the reaction at 125 °C for 24 h. **Top.** ¹H NMR spectrum for the reaction mixture after heating the reaction at 150 °C for 24 h

Quinoline + styrene. After heating at 125 °C for 24 h, 2% of quinoline was consumed to form 2-(1-phenylethyl)quinoline.

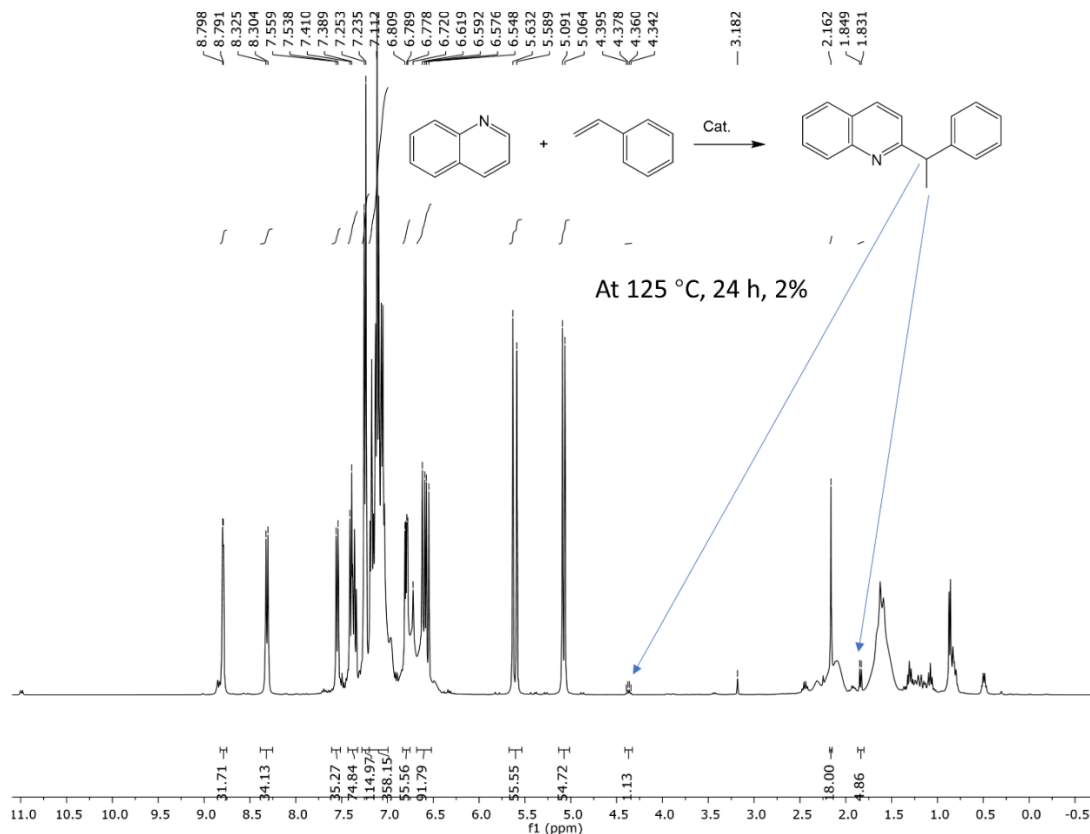


Figure VI-9. ¹H NMR spectrum for the reaction mixture after heating the reaction at 125 °C for 24 h

Ortho C–H ethylation of o-(trimethylsilyl)cinchonine (610). In a 50 mL Teflon screw-capped round-bottomed Schleck flask, **69** (0.040 mmol, 21 mg) and NaEt₃BH (0.040 mmol, 40 μL, 1.0 M in toluene) were added to 1.0 mL of methylcyclohexane. After stirring at room temperature for 5 min, o-(trimethylsilyl)cinchonine (73 mg, 0.20 mmol) was added. After 3 times of freeze-pump-thaw, 1 atm of ethylene was added. After heating at 125 °C for 24 h, volatiles were removed under vacuum and mesitylene (0.40 mL, 0.020

mmol, 0.050 M in C₆D₆) was added. ¹H NMR spectrum was recorded to monitor the resulting product. 90% **610** were consumed to form the ethylated products **611** and **612**.

The terminal vinyl group was isomerized to internal alkenes.

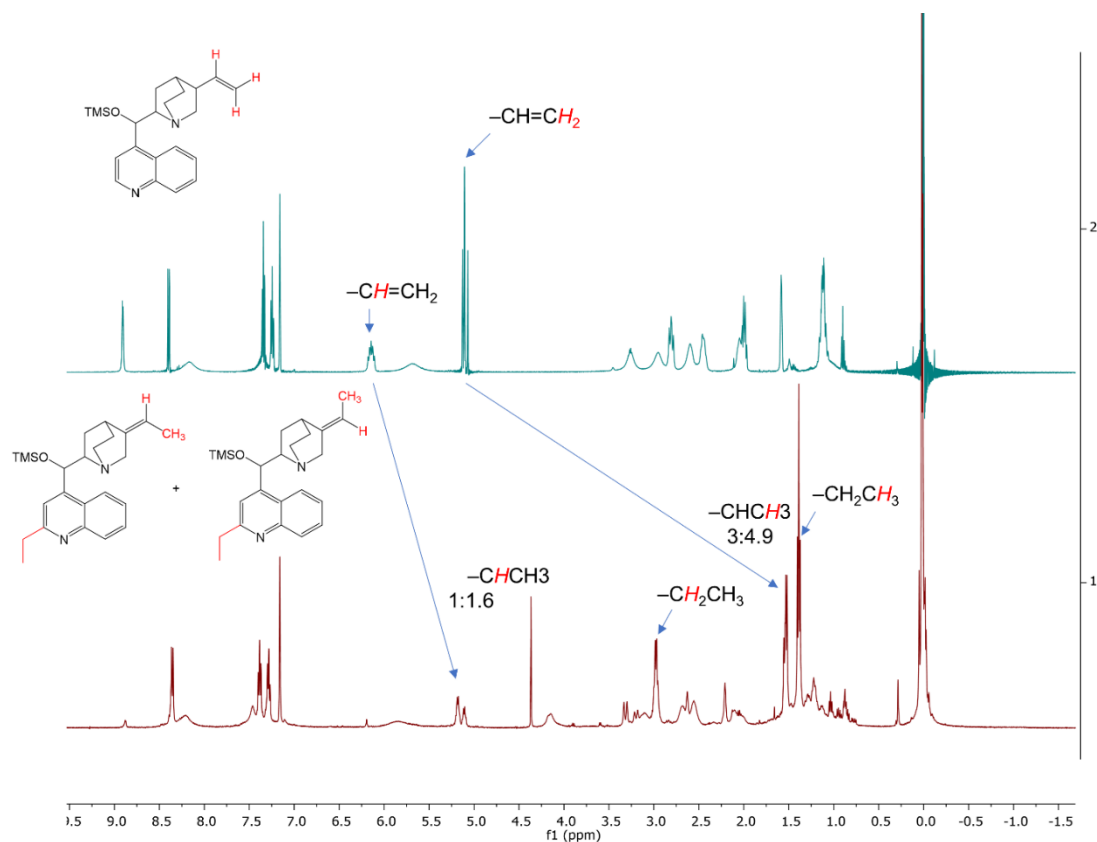


Figure VI-10. Bottom. ¹H NMR spectrum for the reaction mixture after heating at 125 °C for 24 h. **Top.** ¹H NMR spectrum for pure o-(trimethylsilyl)cinchonine

General procedure 1 for alkylation of pyridines with 69. In 8 ml vials, **69** (0.02 mmol, 11 mg), NaEt₃BH (0.020 mmol, 20 μL, 1.0 M in toluene) were mixed. After stirring at r. t. for 5 min, volatiles were removed under vacuum. Pyridines (0.40 mmol), norbornene (0.80 mmol, 76 mg) and methylcyclohexane (0.40 mL) were added to the vials. After heating at 125 °C for 24 h, volatiles were removed and mesitylene (0.020

mmol, 0.40 mL, 0.050 M in C₆D₆) was added as internal standard to analyze the resulting product by ¹H NMR spectrum.

4-tert-butylpyridine + norbornene. After heating at 125 °C for 24 h, 48% of 4-tert-butylpyridine was converted to the desired product **604**.

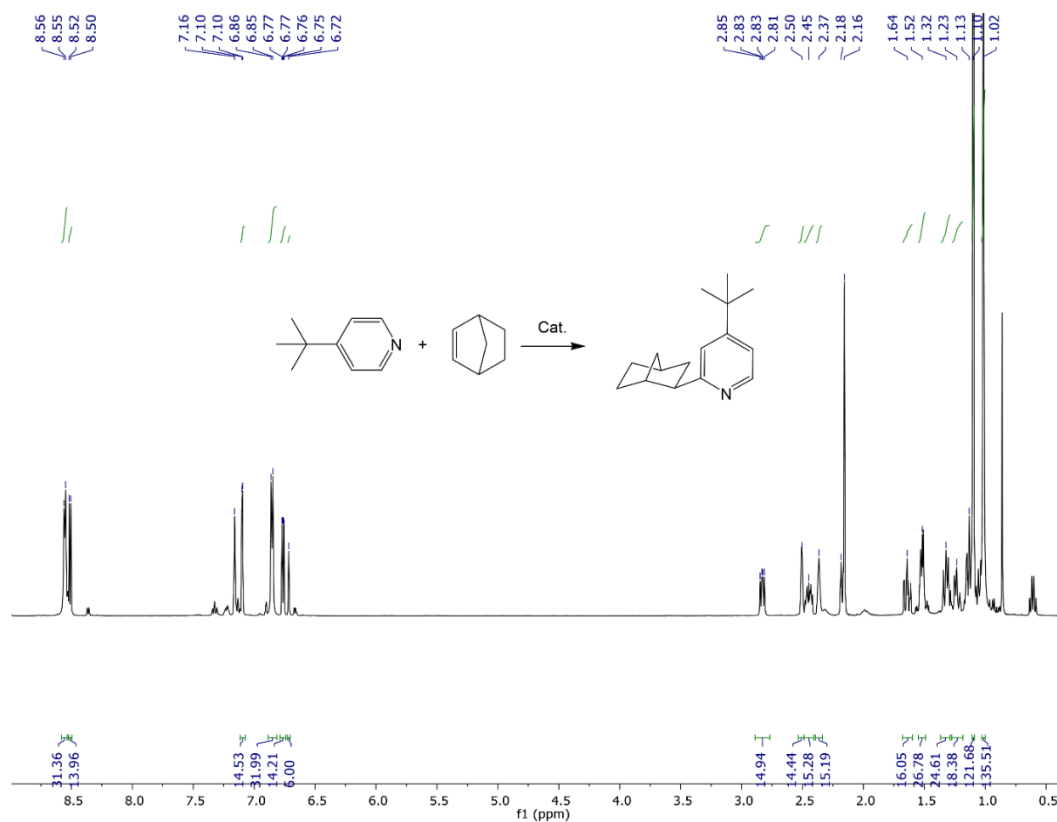


Figure VI-11. ¹H NMR spectrum for the reaction mixture after heating at 125 °C for 24 h

4-dimethylaminopyridine + norbornene. After heating at 125 °C for 24 h, 12 % of 4-dimethylaminopyridine was converted to the desired product **605**.

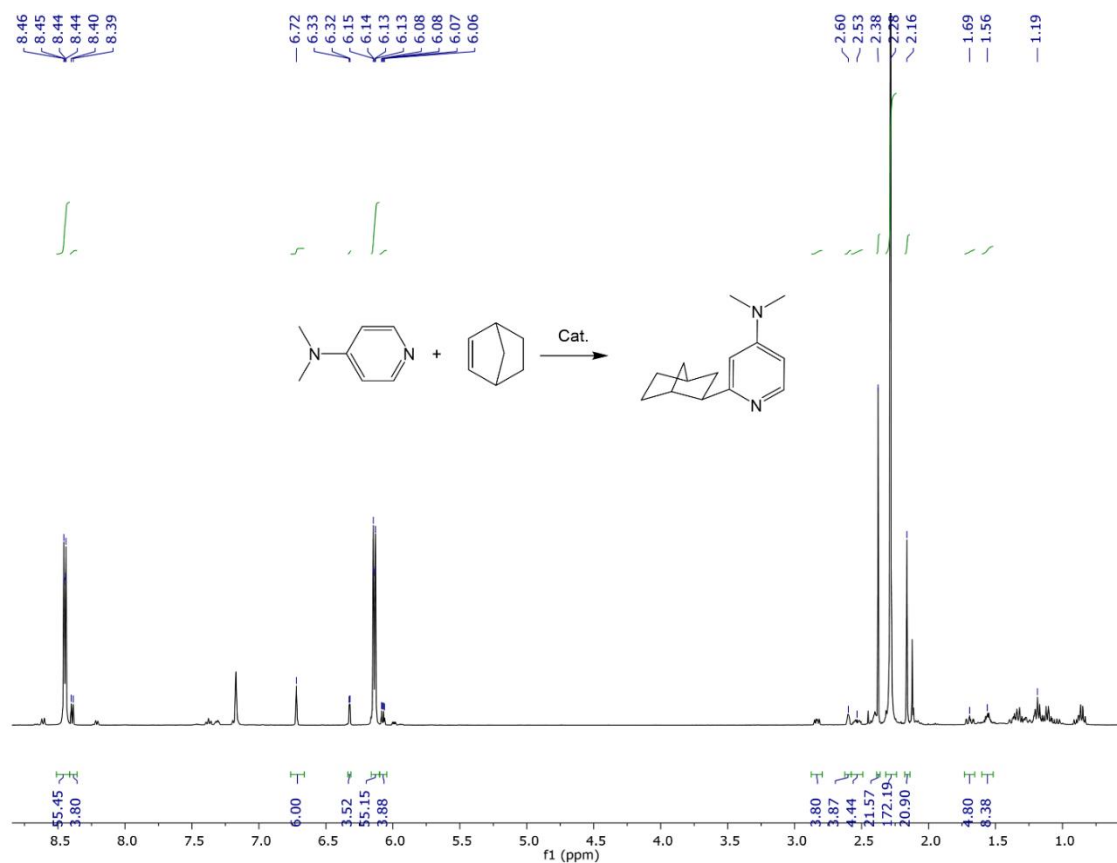


Figure VI-12. ¹H NMR spectrum for the reaction mixture after heating the at 125 ° C for 24 h

General procedure 2 for alkylation of pyridines with 69. In J. Young tubes, **69** (0.020 mmol, 100 μ L, 0.20 M in toluene- d_8), ⁿBuLi (8.0 μ L, 2.5 M in hexane), pyridines (0.40 mmol) and olefin (0.80 mmol) were added to 0.20 mL toluene- d_8 . The reaction mixtures were heated at 125 °C for a week and ¹H NMR spectra were recorded to monitor the conversion.

Pyridine + norbornene. After heating at 125 °C for a week, 79% of pyridine was converted to 2-norbornylpyridine.

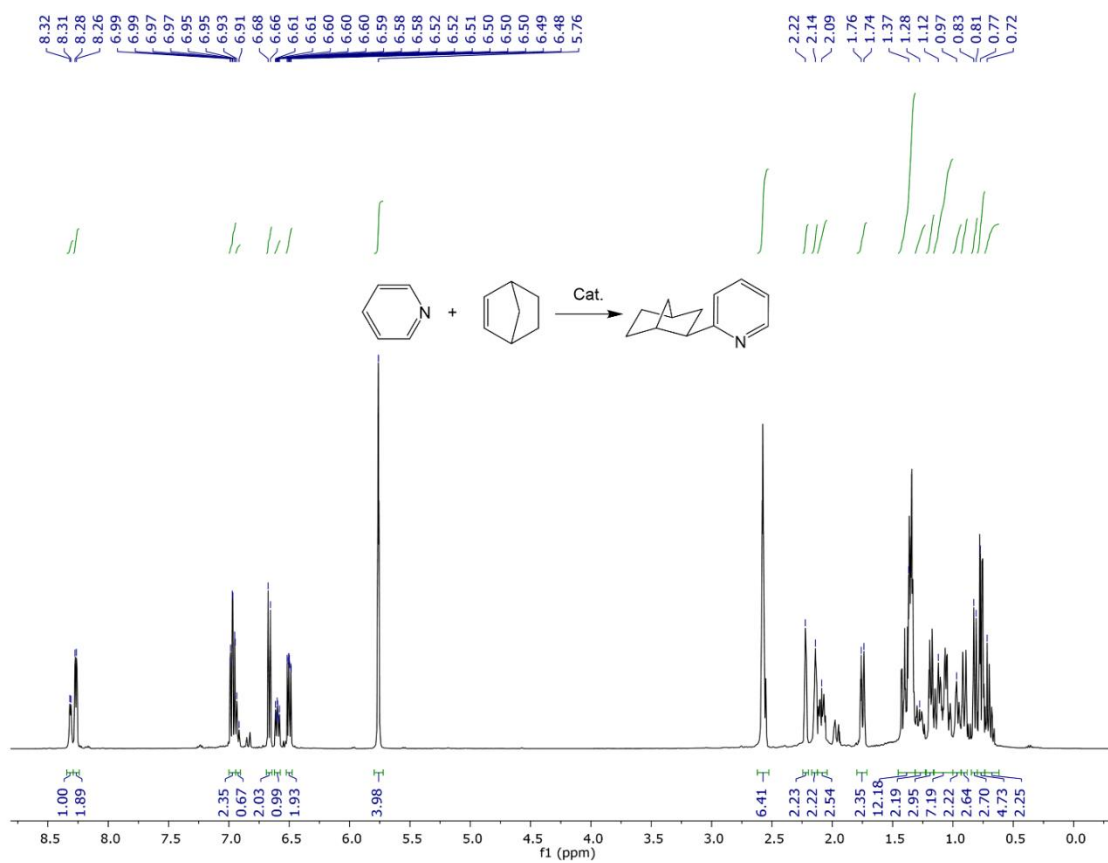


Figure VI-13. ^1H NMR spectrum for the reaction mixture after heating at 125 °C for a week

3-ethylpyridine + norbornene. After heating at 125 °C for a week, 41 % of 3-ethylpyridine was converted to 2-norbornyl-4-ethylpyridine (**606**).

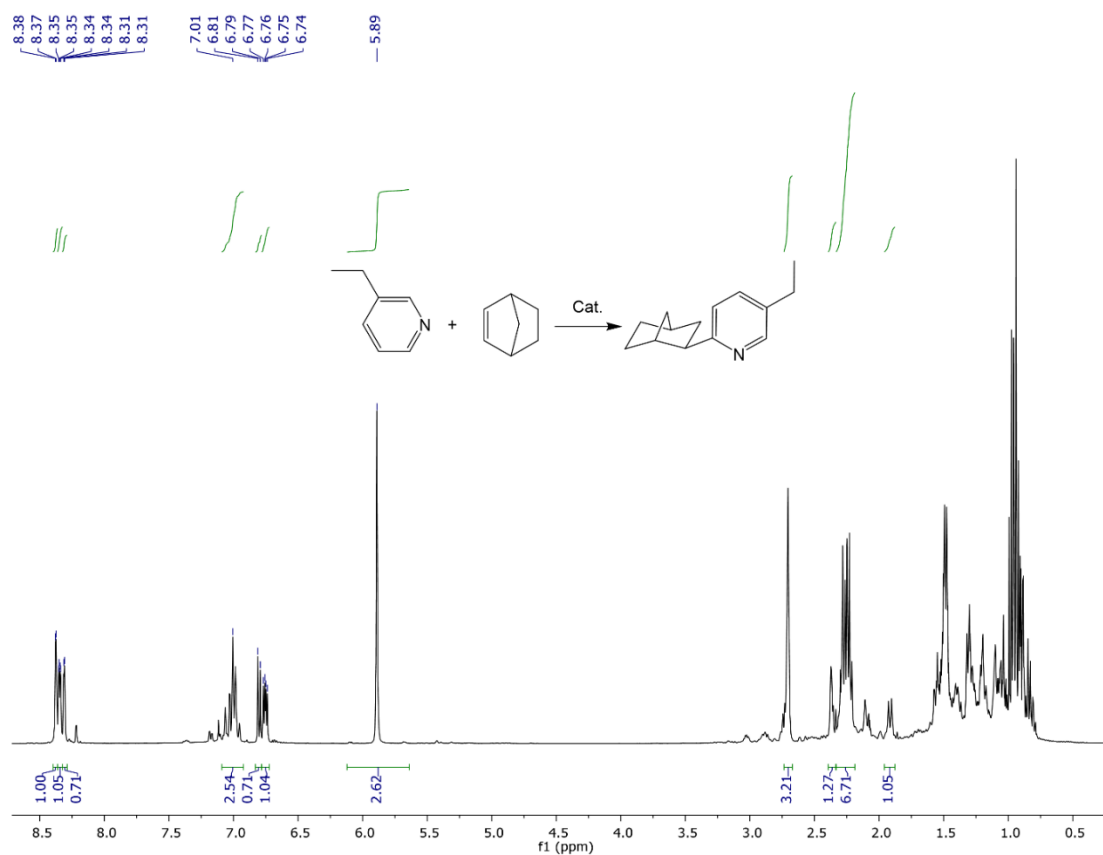


Figure VI-14. ^1H NMR spectrum for the reaction mixture after heating at 125 °C for a week

6.4.6 Unsuccessful Substrates and Side Reactions Analysis

General procedure for unsuccessful attempts of pyridines alkylation with V-1RhNq.

In J. Young tubes, **V-1RhNq** (0.020 mmol, 13 mg), Quinoline (0.40 mmol, 48 μL), olefin (0.80 mmol), 1,4-dioxane (0.020 mmol, 100 μL , 0.20 M in C_6D_6) were added to 0.30 mL C_6D_6 . The reaction mixtures were heated at indicated temperature for indicated time. The resulting products were analyzed by ^1H NMR spectra.

Quinoline + 1-hexene. After heating at 100 °C for 40 h, 1-hexene was isomerized to a mixture of internal hexenes.

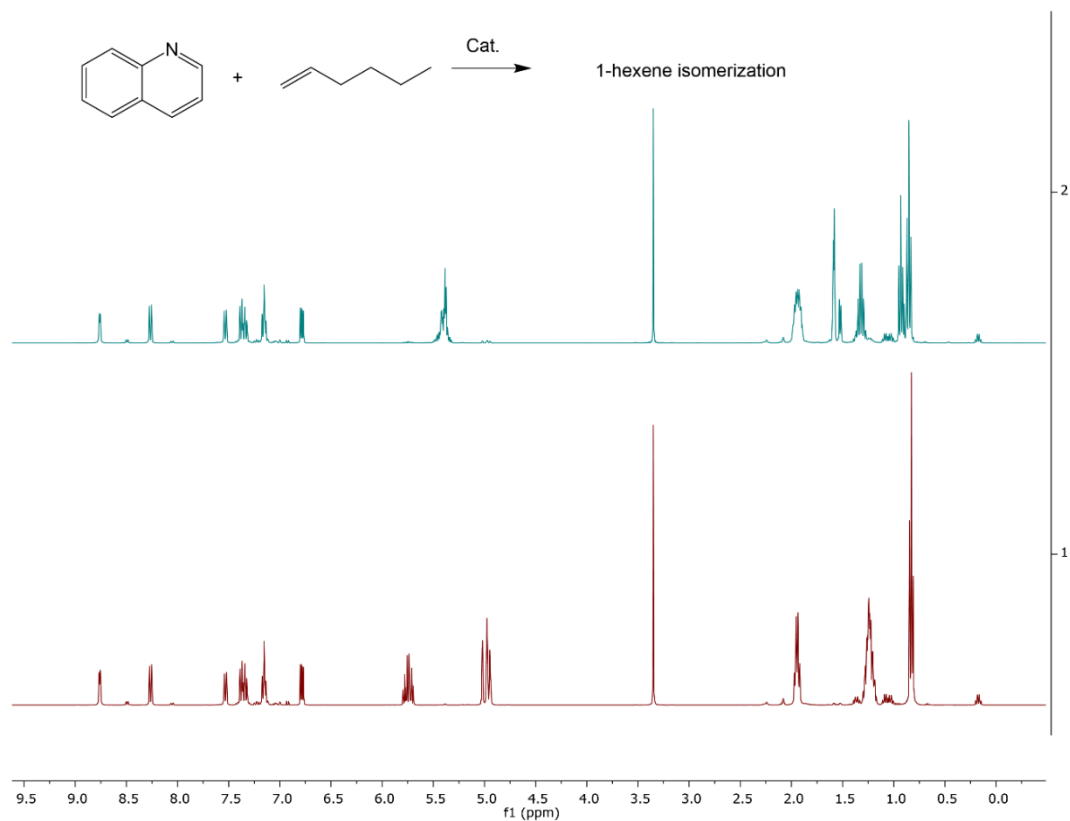


Figure VI-15. Bottom. ¹H NMR spectrum for quinoline, 1-hexene, 1,4-dioxane and V-1RhNq in C₆D₆. **Top.** ¹H NMR spectrum for the reaction mixture after heating at 100 °C for 40 h

Quinoline + 2,5-Dihydrofuran. After heating at 100 °C for 20 h, 2,5-dihydrofuran isomerization happened to form 2,3-dihydrofuran.

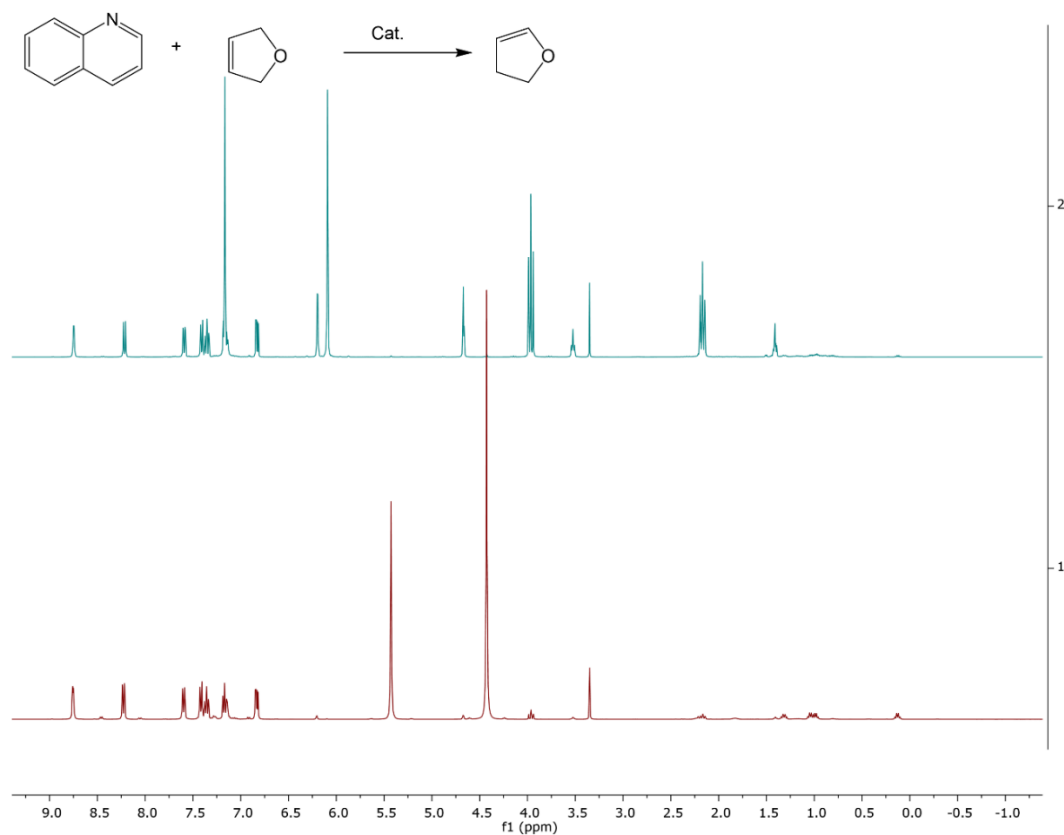


Figure VI-16. Bottom. ^1H NMR spectrum for quinoline, 2,5-dihydrofuran, 1,4-dioxane and V-1RhNq in C_6D_6 . **Top.** ^1H NMR spectrum for the reaction mixture after heating at 100 °C for 20 h

General procedure for unsuccessful attempts of pyridines alkylation with 69. In J. Young tubes, **69** (0.020 mmol, 11 mg) and NaEt_3BH (0.020 mmol, 20 μL 1.0 M in toluene) were added in 0.40 mL toluene. After mixing at room temperature for 5 min, volatiles were removed under vacuum to remove the BEt_3 that was generated. Pyridines (0.40 mmol), norbornene (0.80 mmol, 76 mg) and 1,4 dioxane (0.020 mmol, 100 μL , 0.20 M in C_6D_6) and C_6D_6 were added, and the resulting mixture were heated at indicated

temperature for indicated time. ^1H NMR were recorded to monitor the generation of products.

2,2'-bipyridine + norbornene. After heating at 100 °C for a week, 94% of 2,2'-bipyridine was consumed to form 48% mono functionalized 2,2'-bipyridine (**607**) and 46% bi functionalized 2,2'-bipyridine (**608**).

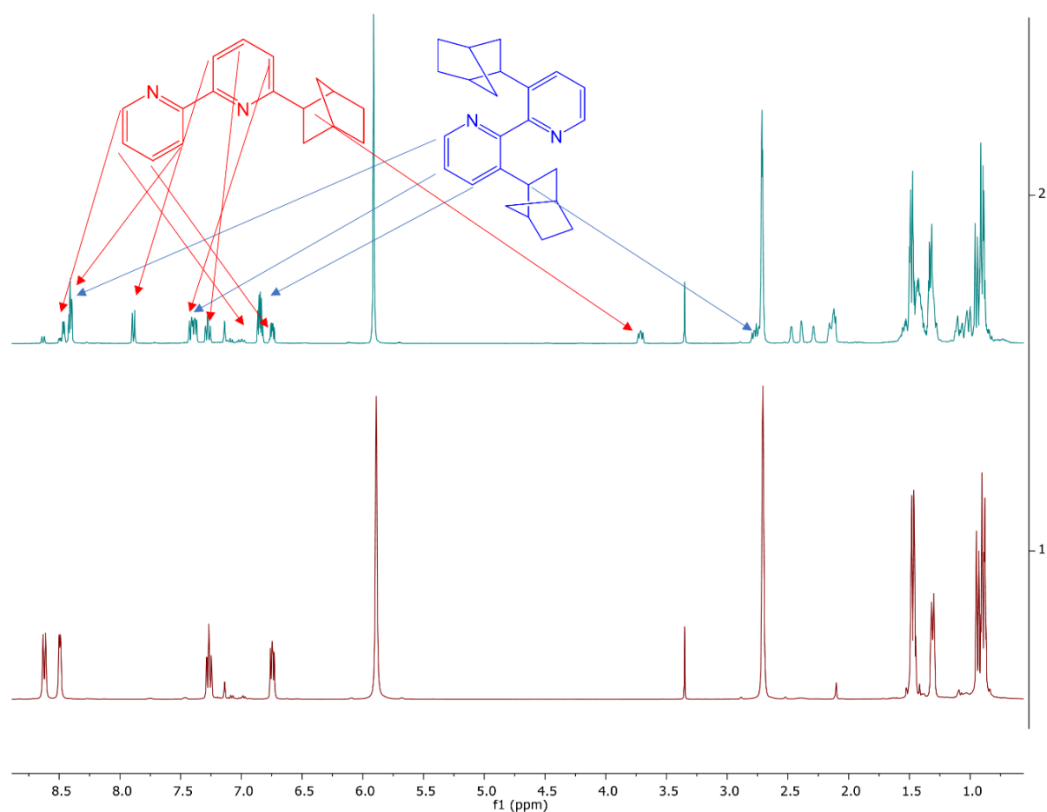


Figure VI-17. Bottom. ^1H NMR spectrum for 2,2'-bipyridine, norbornene, 1,4-dioxane and $[(\text{PBP})\text{RhH}_2]$ in C_6D_6 . **Top.** ^1H NMR spectrum for the reaction mixture after heating at 100 °C for a week

2-tolylpyridine + norbornene. After heating at 100 °C for 16 h, 73% of 2-tolylpyridine was consumed to form **609**.

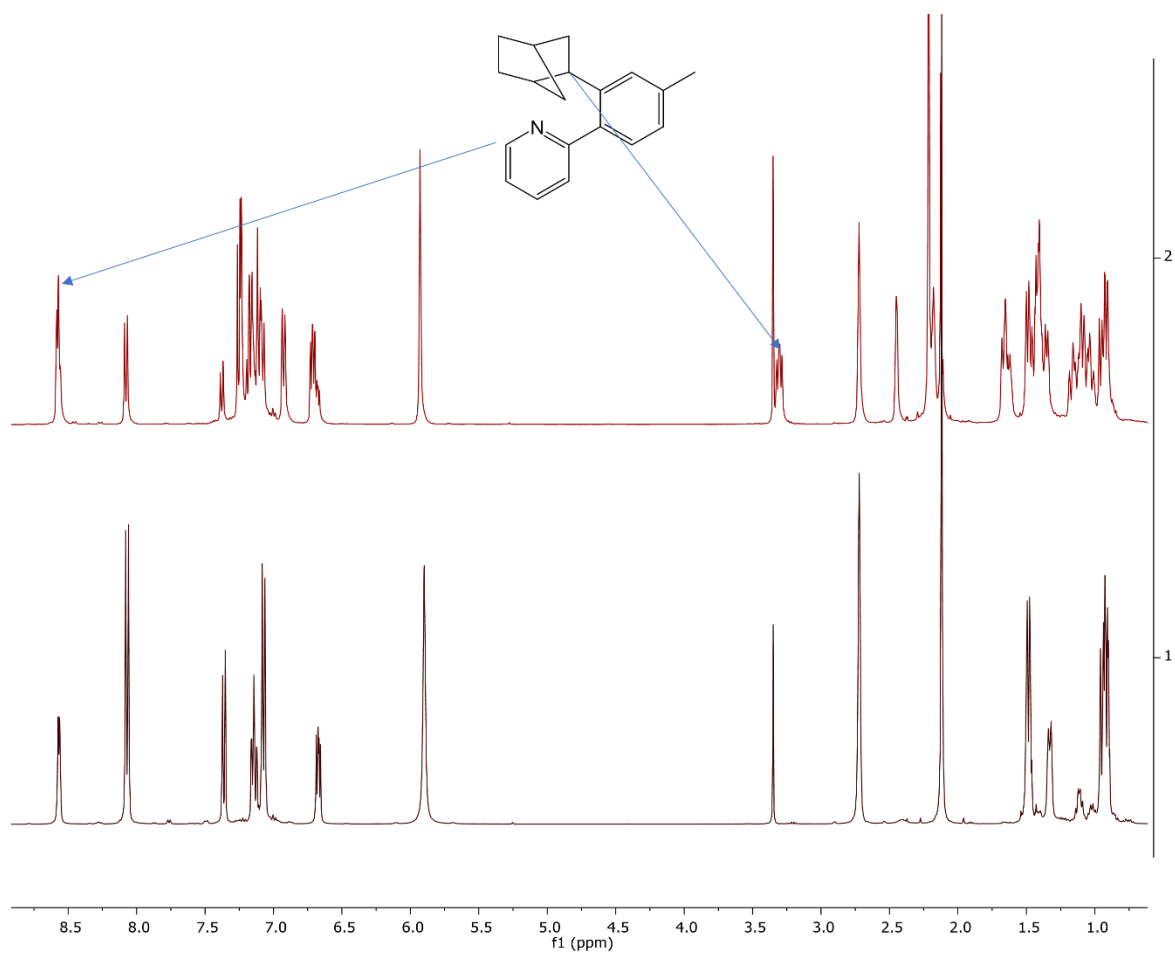
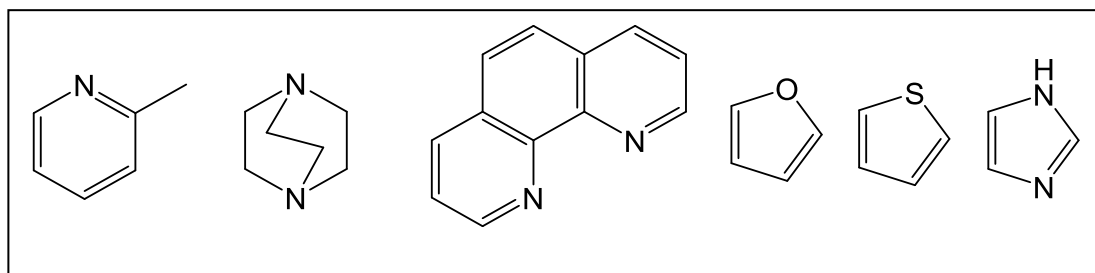
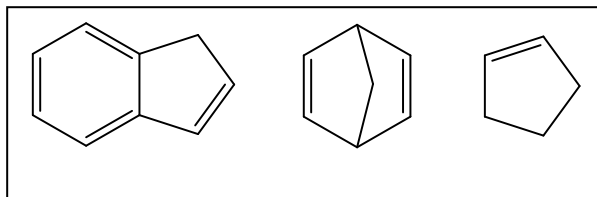


Figure VI-18. Bottom. ^1H NMR spectrum for 2-tolylpyridine, norbornene, 1,4-dioxane and $[(\text{PBP})\text{RhH}_2]$ in C_6D_6 . **Top.** ^1H NMR spectrum for the reaction mixture after heating at $100\text{ }^\circ\text{C}$ for 16 h

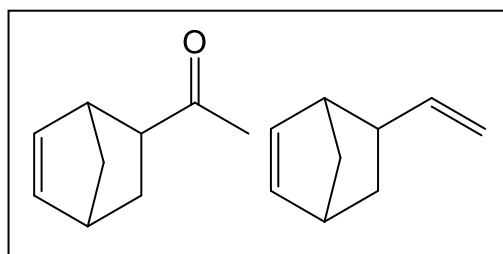
Other unsuccessful heterocyclic substrates (only starting materials were observed by ^1H NMR spectra recorded after heating).



Other unsuccessful olefin substrates (only starting materials were observed by ^1H NMR spectra recorded after heating).



Other unsuccessful olefin substrates (Only decompositions of olefins were observed by ^1H NMR spectra recorded after heating).



CHAPTER VII

SUMMARY

Silver halide complexes of $P^{iPr}B^{Ph}P$ were prepared and characterized. With AgF, the borane abstracts fluoride, resulting in a zwitterionic complex, which was characterized by NMR spectroscopy and X-ray crystallography. With AgCl/Br/I, the halide stays coordinated to Ag. The resulting complexes contain a borane moiety, but the spectroscopic and structural evidence points to a weak interaction between B and Ag. This interaction's weakness contrasts with the observations in the analogous AuCl and CuCl complexes reported by Bourissou et al. earlier. Still, the Au > Cu > Ag trend for the strength of interaction with a Z-type borane among the coinage metals appears to be general.

(PBP)Ir complexes were synthesized and reported earlier in 2016. Boryl participated H–X bond cleavages were examined by reacting the previously reported (PBP)Ir(CO)₂ with substrates that possess H–X bond. Water, methanol, ethanol, cyclohexanol, phenols, benzoic acid, and triethylamine trihydrofluoride added the O–H and F–H units across the Ir–B bond, resulting in dicarbonyl complexes with Ir–H and B–O/F bond. Thermolysis of (PBP)Ir(CO)₂ with *n*-butylamine resulted in a monocarbonyl product. Mechanistic experiments indicated that the reaction with ROH substrates and triethylamine trihydrofluoride proceeds by initial protonation of Ir. However, for amines, the reaction appears to require coordination of the Lewis basic nitrogen to Lewis acidic boron center. We also examined reactions of (PBP)Ir complexes with ethylene. (PBP)IrH₄, (PBP)IrH₂(CO), and (PBP)Ir(CO)₂ activated ethylene C–H bond to form unique products

that have the elements of ethylene incorporated into the molecules and result in B–C bonds. This outcome differs from those typical ethylene activations by other pincer Ir complexes, which formed ethylene adducts or Ir vinyl hydride complexes. (PBP)IrH₄ reacted with four equivalents of ethylene to form two equivalents of ethane and a (PBP)Ir metal complex that possesses an Ir hydride, an Ir-bound ethylene, and a vinyl group that binds to boron. Both (PBP)IrH₂(CO) and (PBP)Ir(CO)₂ reacted with ethylene to form a bridging ethylidene on the Ir–B unit, with no replacement of the original ligands. These reactions demonstrate that the boryl donor is not merely an electronically unique central donor with Lewis acidic properties. It also participates in the activation of C–H bonds by the metal center and forms B–C bond in the product.

Transition metal catalyzed selective C–H functionalization is a promising strategy for organic synthesis. One efficient method to obtain regioselectivity is utilizing weak interactions between catalysts and substrates. Previously, we reported that (PBP)Ir(CO)₂ activated ortho C–H of pyridines selectively by forming non-covalent bonds between Lewis acidic boron and Lewis basic pyridines. This reaction resulted in the formation of (PBP)Ir(Py)H(CO), an iridium pyridyl hydride complex with B–N coordination and Ir–C bond. To explore pyridine activation by (PBP)Rh system, we obtained the product of pyridine selective C–H activation reaction by (PBP)Rh. It resulted in the formation of (PB^{Py}P)RhH, a N–Rh coordinated rhodium complex with a borane ligand generated by B–C bond formation. Compared to the Ir complex with carbonyl ligand, the Rh complex without carbonyl ligand showed reverse connectivity. To further investigate this isomerization reaction between C-bound metal complexes and N-bound metal complexes,

we also synthesized (PBP)IrQuH, (PB^{Py}P)RhH(CO), (PBP)IrQuBr, and (PBP)RhPyBr. With the assistance of DFT calculation, we assumed that the main factor controlling the thermodynamics of this isomerization reaction should be the quality of the M–C bond. The synthesized (PBP)Rh complexes catalyzed C–H alkylation of pyridines. The selectivity varied from different substrates. For substrates such as pyridine, quinoline, 4-tert-butylpyridine, 4-dimethylaminopyridine, and 3-ethylpyridine, the norbornylation happened at the ortho position and the exo products formed selectively. However, for 2-tolylpyridine, norbornylation happened on the tolyl group. Both linear and branched products were observed, and isomerization was observed. However, a moderate yield was observed only when norbornene and ethylene were used as alkenes.

REFERENCES

- (1) Zassinovich, G., Mestroni, G., Gladiali, S., *Chem. Rev.* **1992**, *92*, 1051.
- (2) Susse, L., Stoltz, B. M., *Chem. Rev.* **2021**, *121*, 4084.
- (3) Garrou, P. E., *Chem. Rev.* **1985**, *85*, 171.
- (4) Crabtree, R. H., *Chem. Rev.* **2012**, *112*, 1536.
- (5) Morales-Morales, D., Jensen, C. G., *The chemistry of pincer compounds*, Elsevier, **2011**.
- (6) Peris, E., Crabtree, R. H., *Chem. Soc. Rev.* **2018**, *47*, 1959.
- (7) Moulton, C. J., Shaw, B. L., *J. Chem. Soc., Dalton Trans.* **1976**, 1020.
- (8) Gunanathan, C., Milstein, D., *Chem. Rev.* **2014**, *114*, 12024.
- (9) Gunanathan, C., Milstein, D., *Science* **2013**, *341*.
- (10) Selander, N., Szabó, K. J., *Chem. Rev.* **2011**, *111*, 2048.
- (11) Choi, J., MacArthur, A. H. R., Brookhart, M., Goldman, A. S., *Chem. Rev.* **2011**, *111*, 1761.
- (12) Van der Boom, M. E., Milstein, D., *Chem. Rev.* **2003**, *103*, 1759.
- (13) Van Koten, G., Milstein, D., *Organometallic pincer chemistry, Vol. 40*, Springer, **2012**.
- (14) Szabo, K. J., Wendt, O. F., *Pincer and pincer-type complexes: applications in organic synthesis and catalysis*, John Wiley & Sons, **2014**.
- (15) Ren, P., Pike, S. D., Pernik, I., Weller, A. S., Willis, M. C., *Organometallics* **2015**, *34*, 711.

- (16) Zhou, X., Malakar, S., Zhou, T., Murugesan, S., Huang, C., Emge, T. J., Krogh-Jespersen, K., Goldman, A. S., *ACS Catalysis* **2019**, *9*, 4072.
- (17) Shih, W.-C., Ozerov, O. V., *Organometallics* **2015**, *34*, 4591.
- (18) Fan, L., Foxman, B. M., Ozerov, O. V., *Organometallics* **2004**, *23*, 326.
- (19) Pérez-García, P. M., Darù, A., Scheerder, A. R., Lutz, M., Harvey, J. N., Moret, M.-E., *Organometallics* **2020**, *39*, 1139.
- (20) Mazzeo, M., Strianese, M., Kühn, O., Peters, J. C., *Dalton Trans.* **2011**, *40*, 9026.
- (21) Qi, X., Zhao, H., Sun, H., Li, X., Fuhr, O., Fenske, D., *New J. Chem.* **2018**, *42*, 16583.
- (22) Langer, R., Leitus, G., Ben-David, Y., Milstein, D., *Angew. Chem. Int. Ed.* **2011**, *50*, 2120.
- (23) Morales-Morales, D., Grause, C., Kasaoka, K., Redón, R. o., Cramer, R. E., Jensen, C. M., *Inorg. Chim. Acta* **2000**, *300-302*, 958.
- (24) Zhang, J., Foley, B. J., Bhuvanesh, N., Zhou, J., Janzen, D. E., Whited, M. T., Ozerov, O. V., *Organometallics* **2018**, *37*, 3956.
- (25) Dong, Y., Zhang, P., Fan, Q., Du, X., Xie, S., Sun, H., Li, X., Fuhr, O., Fenske, D., *Inorg. Chem.* **2020**, *59*, 16489.
- (26) Ritter, F., John, L., Schindler, T., Schroers, J. P., Teeuwen, S., Tauchert, M. E., *Chemistry – A European Journal* **2020**, *26*, 13436.
- (27) Shih, W.-C., Gu, W., MacInnis, M. C., Timpa, S. D., Bhuvanesh, N., Zhou, J., Ozerov, O. V., *J. Am. Chem. Soc.* **2016**, *138*, 2086.
- (28) Saito, T., Hara, N., Nakao, Y., *Chem. Lett.* **2017**, *46*, 1247.

- (29) Hara, N., Saito, T., Semba, K., Kuriakose, N., Zheng, H., Sakaki, S., Nakao, Y., *J. Am. Chem. Soc.* **2018**, *140*, 7070.
- (30) Miloserdov, F. M., Isaac, C. J., Beck, M. L., Burnage, A. L., Farmer, J. C. B., Macgregor, S. A., Mahon, M. F., Whittlesey, M. K., *Inorg. Chem.* **2020**, *59*, 15606.
- (31) Li, Q.-Z., Hara, N., Nakao, Y., Sakaki, S., *Inorg. Chem.* **2020**, *59*, 15862.
- (32) Takaya, J., Iwasawa, N., *J. Am. Chem. Soc.* **2017**, *139*, 6074.
- (33) Zhu, C., Takaya, J., Iwasawa, N., *Org. Lett.* **2015**, *17*, 1814.
- (34) Yang, H., Gabbai, F. P., *J. Am. Chem. Soc.* **2014**, *136*, 10866.
- (35) Amgoune, A., Bourissou, D., *Chem. Commun. (Camb.)* **2011**, *47*, 859.
- (36) Braunschweig, H., Dewhurst, R. D., Schneider, A., *Chem. Rev.* **2010**, *110*, 3924.
- (37) Shih, W.-C., Ozerov, O. V., *J. Am. Chem. Soc.* **2017**, *139*, 17297.
- (38) Hill, A. F., Owen, G. R., White, A. J., Williams, D. J., *Angew. Chem.* **1999**, *111*, 2920.
- (39) Bontemps, S., Bouhadir, G., Dyer, P. W., Miqueu, K., Bourissou, D., *Inorg. Chem.* **2007**, *46*, 5149.
- (40) Bontemps, S., Bouhadir, G., Gu, W., Mercy, M., Chen, C.-H., Foxman, B. M., Maron, L., Ozerov, O. V., Bourissou, D., *Angew. Chem. Int. Ed.* **2008**, *47*, 1481.
- (41) Sircoglou, M., Bontemps, S., Bouhadir, G., Saffon, N., Miqueu, K., Gu, W., Mercy, M., Chen, C.-H., Foxman, B. M., Maron, L., Ozerov, O. V., Bourissou, D., *J. Am. Chem. Soc.* **2008**, *130*, 16729.
- (42) Moret, M.-E., Zhang, L., Peters, J. C., *J. Am. Chem. Soc.* **2013**, *135*, 3792.
- (43) Suess, D. L. M., Tsay, C., Peters, J. C., *J. Am. Chem. Soc.* **2012**, *134*, 14158.

- (44) Del Castillo, T. J., Thompson, N. B., Suess, D. L. M., Ung, G., Peters, J. C., *Inorg. Chem.* **2015**, *54*, 9256.
- (45) Kameo, H., Hashimoto, Y., Nakazawa, H., *Organometallics* **2012**, *31*, 3155.
- (46) Kameo, H., Hashimoto, Y., Nakazawa, H., *Organometallics* **2012**, *31*, 4251.
- (47) Moret, M.-E., Peters, J. C., *Angew. Chem. Int. Ed.* **2011**, *50*, 2063.
- (48) Thompson, N. B., Green, M. T., Peters, J. C., *J. Am. Chem. Soc.* **2017**, *139*, 15312.
- (49) Anderson, J. S., Moret, M.-E., Peters, J. C., *J. Am. Chem. Soc.* **2013**, *135*, 534.
- (50) Moret, M.-E., Peters, J. C., *J. Am. Chem. Soc.* **2011**, *133*, 18118.
- (51) Chalkley, M. J., Peters, J. C., *Angew. Chem. Int. Ed.* **2016**, *55*, 11995.
- (52) Anderson, J. S., Cutsail, G. E., Rittle, J., Connor, B. A., Gunderson, W. A., Zhang, L., Hoffman, B. M., Peters, J. C., *J. Am. Chem. Soc.* **2015**, *137*, 7803.
- (53) Deegan, M. M., Peters, J. C., *J. Am. Chem. Soc.* **2017**, *139*, 2561.
- (54) Deegan, M. M., Peters, J. C., *Chem. Sci.* **2018**, *9*, 6264.
- (55) Fong, H., Moret, M.-E., Lee, Y., Peters, J. C., *Organometallics* **2013**, *32*, 3053.
- (56) Nesbit, M. A., Oyala, P. H., Peters, J. C., *J. Am. Chem. Soc.* **2019**, *141*, 8116.
- (57) Thompson, N. B., Oyala, P. H., Dong, H. T., Chalkley, M. J., Zhao, J., Alp, E. E., Hu, M., Lehnert, N., Peters, J. C., *Inorg. Chem.* **2019**, *58*, 3535.
- (58) Cao, Y., Shih, W.-C., Bhuvanesh, N., Ozerov, O. V., *Dalton Trans.* **2019**, *48*, 9959.
- (59) Sircoglou, M., Bontemps, S., Mercy, M., Saffon, N., Takahashi, M., Bouhadir, G., Maron, L., Bourissou, D., *Angew. Chem. Int. Ed.* **2007**, *46*, 8583.

- (60) Inagaki, F., Matsumoto, C., Okada, Y., Maruyama, N., Mukai, C., *Angew. Chem. Int. Ed.* **2015**, *54*, 818.
- (61) Inagaki, F., Nakazawa, K., Maeda, K., Koseki, T., Mukai, C., *Organometallics* **2017**, *36*, 3005.
- (62) Bontemps, S., Sircoglou, M., Bouhadir, G., Puschmann, H., Howard, J. A. K., Dyer, P. W., Miqueu, K., Bourissou, D., *Chemistry – A European Journal* **2008**, *14*, 731.
- (63) Schindler, T., Lux, M., Peters, M., Scharf, L. T., Osseili, H., Maron, L., Tauchert, M. E., *Organometallics* **2015**, *34*, 1978.
- (64) Steinhoff, P., Tauchert, M. E., *Beilstein J. Org. Chem.* **2016**, *12*, 1573.
- (65) Kameo, H., Yamamoto, J., Asada, A., Nakazawa, H., Matsuzaka, H., Bourissou, D., *Angew. Chem. Int. Ed.* **2019**, *58*, 18783.
- (66) Boudjelel, M., Sadek, O., Mallet-Ladeira, S., García-Rodeja, Y., Sosa Carrizo, E. D., Miqueu, K., Bouhadir, G., Bourissou, D., *ACS Catalysis* **2021**, *11*, 3822.
- (67) Bontemps, S., Gornitzka, H., Bouhadir, G., Miqueu, K., Bourissou, D., *Angew. Chem. Int. Ed.* **2006**, *45*, 1611.
- (68) Conifer, C. M., Law, D. J., Sunley, G. J., White, A. J. P., Britovsek, G. J. P., *Organometallics* **2011**, *30*, 4060.
- (69) Shih, W.-C., Gu, W., MacInnis, M. C., Herbert, D. E., Ozerov, O. V., *Organometallics* **2017**, *36*, 1718.
- (70) Kameo, H., Nakazawa, H., *Organometallics* **2012**, *31*, 7476.
- (71) Suess, D. L. M., Peters, J. C., *J. Am. Chem. Soc.* **2013**, *135*, 12580.

- (72) Sircoglou, M., Bontemps, S., Mercy, M., Miqueu, K., Ladeira, S., Saffon, N., Maron, L., Bouhadir, G., Bourissou, D., *Inorg. Chem.* **2010**, *49*, 3983.
- (73) Harman, W. H., Peters, J. C., *J. Am. Chem. Soc.* **2012**, *134*, 5080.
- (74) Harman, W. H., Lin, T.-P., Peters, J. C., *Angew. Chem. Int. Ed.* **2014**, *53*, 1081.
- (75) Nesbit, M. A., Suess, D. L. M., Peters, J. C., *Organometallics* **2015**, *34*, 4741.
- (76) Suess, D. L. M., Peters, J. C., *J. Am. Chem. Soc.* **2013**, *135*, 4938.
- (77) Boone, M. P., Stephan, D. W., *J. Am. Chem. Soc.* **2013**, *135*, 8508.
- (78) Schuhknecht, D., Ritter, F., Tauchert, M. E., *Chem. Commun. (Camb.)* **2016**, *52*, 11823.
- (79) Spokoyny, A. M., Reuter, M. G., Stern, C. L., Ratner, M. A., Seideman, T., Mirkin, C. A., *J. Am. Chem. Soc.* **2009**, *131*, 9482.
- (80) El-Zaria, M. E., Arai, H., Nakamura, H., *Inorg. Chem.* **2011**, *50*, 4149.
- (81) Eleazer, B. J., Smith, M. D., Peryshkov, D. V., *J. Organomet. Chem.* **2017**, *829*, 42.
- (82) Eleazer, B. J., Smith, M. D., Popov, A. A., Peryshkov, D. V., *J. Am. Chem. Soc.* **2016**, *138*, 10531.
- (83) Segawa, Y., Yamashita, M., Nozaki, K., *J. Am. Chem. Soc.* **2009**, *131*, 9201.
- (84) Lin, T.-P., Peters, J. C., *J. Am. Chem. Soc.* **2014**, *136*, 13672.
- (85) Curado, N., Maya, C., López-Serrano, J., Rodríguez, A., *Chem. Commun. (Camb.)* **2014**, *50*, 15718.
- (86) Ríos, P., Curado, N., López-Serrano, J., Rodríguez, A., *Chem. Commun. (Camb.)* **2016**, *52*, 2114.

- (87) Ríos, P., Rodríguez, A., López-Serrano, J., *ACS Catalysis* **2016**, *6*, 5715.
- (88) Ríos, P., Borge, J., Fernández de Córdova, F., Sciortino, G., Lledós, A., Rodríguez, A., *Chem. Sci.* **2021**, *12*, 2540.
- (89) Ding, Y., Ma, Q.-Q., Kang, J., Zhang, J., Li, S., Chen, X., *Dalton Trans.* **2019**, *48*, 17633.
- (90) Ogawa, H., Yamashita, M., *Dalton Trans.* **2013**, *42*, 625.
- (91) Lin, T.-P., Peters, J. C., *J. Am. Chem. Soc.* **2013**, *135*, 15310.
- (92) Hasegawa, M., Segawa, Y., Yamashita, M., Nozaki, K., *Angew. Chem. Int. Ed.* **2012**, *51*, 6956.
- (93) Masuda, Y., Hasegawa, M., Yamashita, M., Nozaki, K., Ishida, N., Murakami, M., *J. Am. Chem. Soc.* **2013**, *135*, 7142.
- (94) Fang, F., Chang, J., Zhang, J., Chen, X., *Catal. Lett.* **2021**.
- (95) Hill, A. F., Lee, S. B., Park, J., Shang, R., Willis, A. C., *Organometallics* **2010**, *29*, 5661.
- (96) Hill, A. F., McQueen, C. M. A., *Organometallics* **2014**, *33*, 1977.
- (97) Miyada, T., Yamashita, M., *Organometallics* **2013**, *32*, 5281.
- (98) Miyada, T., Huang Kwan, E., Yamashita, M., *Organometallics* **2014**, *33*, 6760.
- (99) McQueen, C. M. A., Hill, A. F., Sharma, M., Singh, S. K., Ward, J. S., Willis, A. C., Young, R. D., *Polyhedron* **2016**, *120*, 185.
- (100) Kwan, E. H., Kawai, Y. J., Kamakura, S., Yamashita, M., *Dalton Trans.* **2016**, *45*, 15931.
- (101) Kwan, E. H., Ogawa, H., Yamashita, M., *ChemCatChem* **2017**, *9*, 2457.

- (102) Shih, W.-C., Ozerov, O. V., *Organometallics* **2017**, *36*, 228.
- (103) Dong, Z., Ren, Z., Thompson, S. J., Xu, Y., Dong, G., *Chem. Rev.* **2017**, *117*, 9333.
- (104) Yang, L., Huang, H., *Chem. Rev.* **2015**, *115*, 3468.
- (105) Colby, D. A., Bergman, R. G., Ellman, J. A., *Chem. Rev.* **2010**, *110*, 624.
- (106) Wang, D., Dong, B., Wang, Y., Qian, J., Zhu, J., Zhao, Y., Shi, Z., *Nat. Commun.* **2019**, *10*, 3539.
- (107) Lim, Y.-G., Kim, Y. H., Kang, J.-B., *J. Chem. Soc., Chem. Commun.* **1994**, 2267.
- (108) Lim, Y.-G., Kang, J.-B., Kim, Y. H., *Journal of the Chemical Society, Perkin Transactions I* **1996**, 2201.
- (109) Kakiuchi, F., Le Gendre, P., Yamada, A., Ohtaki, H., Murai, S., *Tetrahedron: Asymmetry* **2000**, *11*, 2647.
- (110) Shibata, T., Takayasu, S., Yuzawa, S., Otani, T., *Org. Lett.* **2012**, *14*, 5106.
- (111) Rubio-Pérez, L., Iglesias, M., Castarlenas, R., Polo, V., Pérez-Torrente, J. J., Oro, L. A., *ChemCatChem* **2014**, *6*, 3192.
- (112) Kwak, J., Ohk, Y., Jung, Y., Chang, S., *J. Am. Chem. Soc.* **2012**, *134*, 17778.
- (113) Rej, S., Chatani, N., *ACS Catalysis* **2018**, *8*, 6699.
- (114) Lewis, J. C., Bergman, R. G., Ellman, J. A., *J. Am. Chem. Soc.* **2007**, *129*, 5332.
- (115) Esteruelas, M. A., Fernández-Alvarez, F. J., Oñate, E., *J. Am. Chem. Soc.* **2006**, *128*, 13044.
- (116) Alvarez, E., Conejero, S., Paneque, M., Petronilho, A., Poveda, M. L., Serrano, O., Carmona, E., *J. Am. Chem. Soc.* **2006**, *128*, 13060.
- (117) Yotphan, S., Bergman, R. G., Ellman, J. A., *Org. Lett.* **2010**, *12*, 2978.

- (118) Jones, J. S., Gabbai, F. P., *Acc. Chem. Res.* **2016**, *49*, 857.
- (119) Kameo, H., Nakazawa, H., *Chemistry – An Asian Journal* **2013**, *8*, 1720.
- (120) Anderson, J. S., Rittle, J., Peters, J. C., *Nature* **2013**, *501*, 84.
- (121) Inagaki, F., Maeda, K., Nakazawa, K., Mukai, C., *Eur. J. Org. Chem.* **2018**, *2018*, 2972.
- (122) APEX2, Version 2 User Manual, M86-E01078, Bruker Analytical X-ray Systems, Madison, WI, June 2006.
- (123) Sheldrick, G., “*SADABS (version 2008/1): Program for Absorption Correction for Data from Area Detector Frames*”, University of Göttingen, 2008.
- (124) Sheldrick, G., *Acta Cryst. A* **2008**, *64*, 112.
- (125) Spek, A., “*PLATON, A Multipurpose Crystallographic Tool.*”, Utrecht University: Utrecht, The Netherlands, 1998.
- (126) Spek, A., *Acta Cryst. C* **2015**, *71*, 9.
- (127) Sheldrick, G., *Acta Cryst. A* **2015**, *71*, 3.
- (128) Sheldrick, G., *Acta Cryst. C* **2015**, *71*, 3.
- (129) XT, XS, BRUKER AXS Inc., 5465 East Cheryl Parkway, Madison, WI 53711-5373 USA.
- (130) Dolomanov, O. V., Bourhis, L. J., Gildea, R. J., Howard, J. A. K., Puschmann, H., *J. Appl. Crystallogr.* **2009**, *42*, 339.
- (131) Milstein, D., *Philosophical Transactions of the Royal Society A: Mathematical, Physical and Engineering Sciences* **2015**, *373*, 20140189.
- (132) Khusnutdinova, J. R., Milstein, D., *Angew. Chem. Int. Ed.* **2015**, *54*, 12236.

- (133) Bielinski, E. A., Lagaditis, P. O., Zhang, Y., Mercado, B. Q., Würtele, C., Bernskoetter, W. H., Hazari, N., Schneider, S., *J. Am. Chem. Soc.* **2014**, *136*, 10234.
- (134) Askevold, B., Roesky, H. W., Schneider, S., *ChemCatChem* **2012**, *4*, 307.
- (135) Grützmacher, H., *Angew. Chem. Int. Ed.* **2008**, *47*, 1814.
- (136) Wang, D., Astruc, D., *Chem. Rev.* **2015**, *115*, 6621.
- (137) DeMott, J. C., Bhuvanesh, N., Ozerov, O. V., *Chem. Sci.* **2013**, *4*, 642.
- (138) Stephan, D. W., *Science* **2016**, *354*, aaf7229.
- (139) Flynn, S. R., Wass, D. F., *ACS Catalysis* **2013**, *3*, 2574.
- (140) Fryzuk, M. D., MacNeil, P. A., *Organometallics* **1983**, *2*, 682.
- (141) Owen, G. R., *Chem. Commun. (Camb.)* **2016**, *52*, 10712.
- (142) Vollmer, M. V., Xie, J., Cammarota, R. C., Young Jr., V. G., Bill, E., Gagliardi, L., Lu, C. C., *Angew. Chem. Int. Ed.* **2018**, *57*, 7815.
- (143) Bouhadir, G., Bourissou, D., *Chem. Soc. Rev.* **2016**, *45*, 1065.
- (144) Kiernicki, J. J., Zeller, M., Szymczak, N. K., *J. Am. Chem. Soc.* **2017**, *139*, 18194.
- (145) Cowie, B. E., Emslie, D. J. H., *Chemistry - A European Journal* **2014**, *20*, 16899.
- (146) Rickard, C. E. F., Roper, W. R., Williamson, A., Wright, L. J., *Organometallics* **2002**, *21*, 1714.
- (147) Braunschweig, H., Matz, F., Radacki, K., Schneider, A., *Organometallics* **2010**, *29*, 3457.
- (148) Lee, C.-I., DeMott, J. C., Pell, C. J., Christopher, A., Zhou, J., Bhuvanesh, N., Ozerov, O. V., *Chem. Sci.* **2015**, *6*, 6572.

- (149) Ishiyama, T., Takagi, J., Ishida, K., Miyaura, N., Anastasi, N. R., Hartwig, J. F., *J. Am. Chem. Soc.* **2002**, *124*, 390.
- (150) Press, L. P., Kosanovich, A. J., McCulloch, B. J., Ozerov, O. V., *J. Am. Chem. Soc.* **2016**, *138*, 9487.
- (151) Urban, M., Durka, K., Jankowski, P., Serwatowski, J., Luliński, S., *The Journal of Organic Chemistry* **2017**, *82*, 8234.
- (152) Zhang, N., Wang, C., Zou, G., Tang, J., *J. Organomet. Chem.* **2017**, *842*, 54.
- (153) Rami Reddy, E., Trivedi, R., Giribabu, L., Sridhar, B., Pranay kumar, K., Srinivasa Rao, M., Sarma, A. V. S., *Eur. J. Inorg. Chem.* **2013**, *2013*, 5311.
- (154) Cook, K. S., Piers, W. E., Hayes, P. G., Parvez, M., *Organometallics* **2002**, *21*, 2422.
- (155) Kolpin, K. B., Emslie, D. J. H., *Angew. Chem. Int. Ed.* **2010**, *49*, 2716.
- (156) Kohrt, S., Kehr, G., Daniliuc, C. G., Rojas, R. S., Rieger, B., Troll, C., Erker, G., *Organometallics* **2016**, *35*, 2689.
- (157) Himmel, D., Krossing, I., Schnepf, A., *Angew. Chem. Int. Ed.* **2014**, *53*, 370.
- (158) Morgan, E., MacLean, D. F., McDonald, R., Turculet, L., *J. Am. Chem. Soc.* **2009**, *131*, 14234.
- (159) Meiners, J., Scheibel, M. G., Lemée-Cailleau, M.-H., Mason, S. A., Boeddinghaus, M. B., Fässler, T. F., Herdtweck, E., Khusniyarov, M. M., Schneider, S., *Angew. Chem. Int. Ed.* **2011**, *50*, 8184.
- (160) Askevold, B., Friedrich, A., Buchner, M. R., Lewall, B., Filippou, A. C., Herdtweck, E., Schneider, S., *J. Organomet. Chem.* **2013**, *744*, 35.

- (161) Fryzuk, M. D., MacNeil, P. A., Rettig, S. J., *J. Am. Chem. Soc.* **1985**, *107*, 6708.
- (162) Wan, K. Y., Roelfes, F., Lough, A. J., Hahn, F. E., Morris, R. H., *Organometallics* **2018**, *37*, 491.
- (163) Chen, H. J., Hong Xiang Teo, R., Li, Y., Pullarkat, S. A., Leung, P.-H., *Organometallics* **2018**, *37*, 99.
- (164) Meiners, J., Friedrich, A., Herdtweck, E., Schneider, S., *Organometallics* **2009**, *28*, 6331.
- (165) Gao, H., Gao, Y., Wang, C., Hu, D., Xie, Z., Liu, L., Yang, B., Ma, Y., *ACS Appl. Mater. Interfaces* **2018**, *10*, 14956.
- (166) Taniguchi, T., Wang, J., Irle, S., Yamaguchi, S., *Dalton Trans.* **2013**, *42*, 620.
- (167) Findlater, M., Bernskoetter, W. H., Brookhart, M., *J. Am. Chem. Soc.* **2010**, *132*, 4534.
- (168) Abdur-Rashid, K., Fong, T. P., Greaves, B., Gusev, D. G., Hinman, J. G., Landau, S. E., Lough, A. J., Morris, R. H., *J. Am. Chem. Soc.* **2000**, *122*, 9155.
- (169) Spek, A., *J. Appl. Crystallogr.* **2003**, *36*, 7.
- (170) Schrock, R. R., Hoveyda, A. H., *Angew. Chem. Int. Ed.* **2003**, *42*, 4592.
- (171) Straub, B. F., Wiley Online Library, **2010**.
- (172) Chen, C., *Nat. Rev. Chem.* **2018**, *2*, 6.
- (173) Verendel, J. J., Pàmies, O., Diéguez, M., Andersson, P. G., *Chem. Rev.* **2014**, *114*, 2130.
- (174) Kumar, A., Bhatti, T. M., Goldman, A. S., *Chem. Rev.* **2017**, *117*, 12357.
- (175) Franke, R., Selent, D., Börner, A., *Chem. Rev.* **2012**, *112*, 5675.

- (176) Ogba, O. M., Warner, N. C., O'Leary, D. J., Grubbs, R. H., *Chem. Soc. Rev.* **2018**, *47*, 4510.
- (177) Hartwig, J. F., *Organotransition metal chemistry: from bonding to catalysis*, University Science Books, **2010**.
- (178) Renkema, K. B., Kissin, Y. V., Goldman, A. S., *J. Am. Chem. Soc.* **2003**, *125*, 7770.
- (179) Stoutland, P. O., Bergman, R. G., *J. Am. Chem. Soc.* **1985**, *107*, 4581.
- (180) Schrock, R. R., Shih, K.-Y., Dobbs, D. A., Davis, W. M., *J. Am. Chem. Soc.* **1995**, *117*, 6609.
- (181) Hirsekorn, K. F., Veige, A. S., Marshak, M. P., Koldobskaya, Y., Wolczanski, P. T., Cundari, T. R., Lobkovsky, E. B., *J. Am. Chem. Soc.* **2005**, *127*, 4809.
- (182) Ozerov, O. V., Watson, L. A., Pink, M., Caulton, K. G., *J. Am. Chem. Soc.* **2003**, *125*, 9604.
- (183) Ozerov, O. V., Huffman, J. C., Watson, L. A., Caulton, K. G., *Organometallics* **2003**, *22*, 2539.
- (184) Ozerov, O. V., Watson, L. A., Pink, M., Caulton, K. G., *J. Am. Chem. Soc.* **2004**, *126*, 6363.
- (185) Coalter, J. N., Spivak, G. J., Gérard, H., Clot, E., Davidson, E. R., Eisenstein, O., Caulton, K. G., *J. Am. Chem. Soc.* **1998**, *120*, 9388.
- (186) Spokoyny, A. M., Reuter, M. G., Stern, C. L., Ratner, M. A., Seideman, T., Mirkin, C. A., *J. Am. Chem. Soc.* **2009**, *131*, 9482.

- (187) Eleazer, B. J., Smith, M. D., Popov, A. A., Peryshkov, D. V., *J. Am. Chem. Soc.* **2016**, *138*, 10531.
- (188) Obligacion, J. V., Chirik, P. J., *Nat. Rev. Chem.* **2018**, *2*, 15.
- (189) Mkhaliid, I. A. I., Barnard, J. H., Marder, T. B., Murphy, J. M., Hartwig, J. F., *Chem. Rev.* **2010**, *110*, 890.
- (190) Addison, A. W., Rao, T. N., Reedijk, J., van Rijn, J., Verschoor, G. C., *J. Chem. Soc., Dalton Trans.* **1984**, 1349.
- (191) Hui, Z., Watanabe, T., Tobita, H., *Organometallics* **2017**, *36*, 4816.
- (192) Emslie, D. J. H., Cowie, B. E., Kolpin, K. B., *Dalton Trans.* **2012**, *41*, 1101.
- (193) Cordero, B., Gómez, V., Platero-Prats, A. E., Revés, M., Echeverría, J., Cremades, E., Barragán, F., Alvarez, S., *Dalton Trans.* **2008**, 2832.
- (194) Cao, Y., Shih, W.-C., Ozerov, O. V., *Organometallics* **2019**, *38*, 4076.
- (195) Baker, R. T., Calabrese, J. C., Westcott, S. A., Nguyen, P., Marder, T. B., *J. Am. Chem. Soc.* **1993**, *115*, 4367.
- (196) Dang, L., Zhao, H., Lin, Z., Marder, T. B., *Organometallics* **2007**, *26*, 2824.
- (197) Laitar, D. S., Tsui, E. Y., Sadighi, J. P., *Organometallics* **2006**, *25*, 2405.
- (198) Clark, G. R., Irvine, G. J., Roper, W. R., Wright, L. J., *Organometallics* **1997**, *16*, 5499.
- (199) Iverson, C. N., Smith, M. R., *Organometallics* **1996**, *15*, 5155.
- (200) *APEX3 "Program for Data Collection on Area Detectors" BRUKER AXS Inc., 5465 East Cheryl Parkway, Madison, WI 53711-5373 USA.*
- (201) Murakami, K., Yamada, S., Kaneda, T., Itami, K., *Chem. Rev.* **2017**, *117*, 9302.

- (202) Nakao, Y., *Synthesis* **2011**, 2011, 3209.
- (203) Guan, B.-T., Hou, Z., *J. Am. Chem. Soc.* **2011**, 133, 18086.
- (204) Tran, G., Hesp, K. D., Mascitti, V., Ellman, J. A., *Angew. Chem.* **2017**, 129, 5993.
- (205) Do, H.-Q., Daugulis, O., *J. Am. Chem. Soc.* **2011**, 133, 13577.
- (206) Berman, A. M., Lewis, J. C., Bergman, R. G., Ellman, J. A., *J. Am. Chem. Soc.* **2008**, 130, 14926.
- (207) Li, M., Hua, R., *Tetrahedron Lett.* **2009**, 50, 1478.
- (208) Seiple, I. B., Su, S., Rodriguez, R. A., Gianatassio, R., Fujiwara, Y., Sobel, A. L., Baran, P. S., *J. Am. Chem. Soc.* **2010**, 132, 13194.
- (209) Wen, J., Qin, S., Ma, L.-F., Dong, L., Zhang, J., Liu, S.-S., Duan, Y.-S., Chen, S.-Y., Hu, C.-W., Yu, X.-Q., *Org. Lett.* **2010**, 12, 2694.
- (210) Tobisu, M., Hyodo, I., Chatani, N., *J. Am. Chem. Soc.* **2009**, 131, 12070.
- (211) Yin, C., Zhong, K., Li, W., Yang, X., Sun, R., Zhang, C., Zheng, X., Yuan, M., Li, R., Lan, Y., Fu, H., Chen, H., *Adv. Synth. Catal.* **2018**, 360, 3990.
- (212) Snieckus, V., *Chem. Rev.* **1990**, 90, 879.
- (213) Murai, S., Kakiuchi, F., Sekine, S., Tanaka, Y., Kamatani, A., Sonoda, M., Chatani, N., *Nature* **1993**, 366, 529.
- (214) Lyons, T. W., Sanford, M. S., *Chem. Rev.* **2010**, 110, 1147.
- (215) Zhang, M., Zhang, Y., Jie, X., Zhao, H., Li, G., Su, W., *Organic Chemistry Frontiers* **2014**, 1, 843.
- (216) He, J., Wasa, M., Chan, K. S. L., Shao, Q., Yu, J.-Q., *Chem. Rev.* **2017**, 117, 8754.

- (217) Fujii, I., Semba, K., Li, Q.-Z., Sakaki, S., Nakao, Y., *J. Am. Chem. Soc.* **2020**, *142*, 11647.
- (218) Riehl, J. F., Jean, Y., Eisenstein, O., Pelissier, M., *Organometallics* **1992**, *11*, 729.
- (219) APEX2 “Program for Data Collection on Area Detectors”, BRUKER AXS Inc., 5465 East Cheryl Parkway, Madison, WI 53711-5373 USA.
- (220) Farrugia, L., *J. Appl. Crystallogr.* **2012**, *45*, 849.
- (221) Frisch, M. J., Trucks, G. W., Schlegel, H. B., Scuseria, G. E., Robb, M. A., Cheeseman, J. R., Scalmani, G., Barone, V., Mennucci, B., Petersson, G. A., Nakatsuji, H., Caricato, M., Li, X., Hratchian, H. P., Izmaylov, A. F., Bloino, J., Zheng, G., Sonnenberg, J. L., Hada, M., Ehara, M., Toyota, K., Fukuda, R., Hasegawa, J., Ishida, M., Nakajima, T., Honda, Y., Kitao, O., Nakai, H., Vreven, T., Montgomery, Jr. J. A., Peralta, J. E., Ogliaro, F., Bearpark, M., Heyd, J. J., Brothers, E., Kudin, K. N., Staroverov, V. N., Kobayashi, R., Normand, J., , Raghavachari, K., Rendell, A., Burant, J. C., Iyengar, S. S., Tomasi, J., Cossi, M., Rega, N., Millam, N. J., Klene, M., Knox, J. E., Cross, J. B., Bakken, V., Adamo, C., Jaramillo, J., Gomperts, R., Stratmann, R. E., Yazyev, O., Austin, A. J., Cammi, R., Pomelli, C., Ochterski, J. W., Martin, R. L., Morokuma, K., Zakrzewski, V. G., Voth, G. A., Salvador, P., Dannenberg, J. J., Dapprich, S., Daniels, A. D., Farkas, Ö., Foresman, J. B., Ortiz, J. V., Cioslowski, J. & Fox, D. J. Revision D.01 ed.; Gaussian, Inc.: Wallingford, CT, 2009.
- (222) Grimme, S., Ehrlich, S., Goerigk, L., *J. Comput. Chem.* **2011**, *32*, 1456.
- (223) Mitoraj, M. P., Michalak, A., Ziegler, T., *J. Chem. Theory Comput.* **2009**, *5*, 962.

- (224) Neese, F., *WIREs Computational Molecular Science* **2018**, 8, e1327.
- (225) Lu, T., Chen, F., *J. Comput. Chem.* **2012**, 33, 580.
- (226) Grigg, R., Savic, V., *Tetrahedron Lett.* **1997**, 38, 5737.
- (227) Andou, T., Saga, Y., Komai, H., Matsunaga, S., Kanai, M., *Angew. Chem. Int. Ed.* **2013**, 52, 3213.
- (228) Nakao, Y., Yamada, Y., Kashihara, N., Hiyama, T., *J. Am. Chem. Soc.* **2010**, 132, 13666.
- (229) Li, Y., Deng, G., Zeng, X., *Organometallics* **2016**, 35, 747.
- (230) Kozhushkov, S. I., Yufit, D. S., Ackermann, L., *Org. Lett.* **2008**, 10, 3409.
- (231) Kim, J., Park, S.-W., Baik, M.-H., Chang, S., *J. Am. Chem. Soc.* **2015**, 137, 13448.
- (232) Gao, K., Yoshikai, N., *J. Am. Chem. Soc.* **2011**, 133, 400.
- (233) Ebe, Y., Nishimura, T., *J. Am. Chem. Soc.* **2015**, 137, 5899.
- (234) Rodewald, S., Jordan, R. F., *J. Am. Chem. Soc.* **1994**, 116, 4491.
- (235) Jordan, R. F., Taylor, D. F., *J. Am. Chem. Soc.* **1989**, 111, 778.
- (236) Song, G., O, W. W. N., Hou, Z., *J. Am. Chem. Soc.* **2014**, 136, 12209.
- (237) Ott, J. C., Blasius, C. K., Wadepohl, H., Gade, L. H., *Inorg. Chem.* **2018**, 57, 3183.
- (238) Meng, N., Yu, W., Suzuki, T., Chen, M., Qi, Z., Hu, B., Bao, J., Debenham, J. S., Mazzola, R., Duffy, J. L., *The Journal of Organic Chemistry* **2021**, 86, 5560.
- (239) Obora, Y., Ogawa, S., Yamamoto, N., *The Journal of Organic Chemistry* **2012**, 77, 9429.

APPENDIX A

OTHER RELATED (PBP)IR AND (PBP)RH COMPLEXES

(PBP)IrQuH₂Bpin. In a J. Young tube, (PBP)IrQuH (0.020 mmol, 14 mg) was mixed with HBpin (0.020 mmol, 20 μ L, 1.0 M in C₆D₆) in C₆D₆, and the NMR spectra of the resulting product were recorded for characterization. ¹H NMR (499 MHz, C₆D₆) δ 9.12 (d, J = 8.4 Hz, 1H, *Quinoly*l), 8.80 (d, J = 7.3 Hz, 2H, *Phenyl*), 8.51 (d, J = 8.6 Hz, 1H, *Quinoly*l), 7.30 (t, J = 7.5 Hz, 2H, *Phenyl*), 7.27 (m, 2H, *Phenyl*), 7.12 (t, J = 7.2 Hz, 1H, *Quinoly*l), 7.04 (m, 4H, *Phenyl* & *Quinoly*l), 6.74 (t, J = 7.4 Hz, 1H, *Quinoly*l), 2.38 (m, 2H, *CHMe*₂), 2.18 (m, 2H, *CHMe*₂), 1.47 (dvt, J = 7.4 Hz, 6H, *CHMe*₂), 1.25 (br, 12H), 1.08 (dvt, J = 7.3 Hz, 6H, *CHMe*₂), 1.01 (s, 1H, *H-Bpin*), 0.87 (dvt, J = 7.0 Hz, 6H, *CHMe*₂), 0.45 (dvt, J = 7.1 Hz, 6H, *CHMe*₂), -6.35 (br, 1H, Ir–H–B). ³¹P{¹H} NMR (202 MHz, C₆D₆) δ 42.6 (s).

(PBP)IrQuH₂(Phenylacetylenyl). In a J. Young tube, (PBP)IrQuH (0.020 mmol, 14 mg) was mixed with Phenylacetylene (0.020 mmol, 20 μ L, 1.0 M in C₆D₆) in C₆D₆, and the NMR spectra of the resulting product were recorded for characterization. ¹H NMR (499 MHz, C₆D₆) δ 9.02 (d, J = 8.4 Hz, 1H, *Quinoly*l), 8.76 (d, J = 7.5 Hz, 2H, *Phenyl*), 8.36 (d, J = 8.5 Hz, 1H, *Quinoly*l), 7.81 (dd, J = 8.0, 1.1 Hz, 2H, *Phenyl*), 7.28 (m, 4H), 7.13 (m, 2H), 7.08 (m, 3H), 7.01 (m, 3H), 6.75 (t, J = 7.4 Hz, 1H, *Quinoly*l), 2.22 (m, 2H, *CHMe*₂), 2.10 (m, 2H, *CHMe*₂), 1.51 (dvt, J = 7.1 Hz, 6H, *CHMe*₂), 1.34 (dvt, J = 7.1 Hz, 6H, *CHMe*₂), 0.87 (dvt, J = 7.1 Hz, 6H, *CHMe*₂), 0.51 (dvt, J = 7.3 Hz, 6H, *CHMe*₂), -

9.29 (br, 1H, Ir–H–B), -12.66 (t, $J = 16.5$ Hz, 1H, Ir–H). $^{31}\text{P}\{^1\text{H}\}$ NMR (202 MHz, C_6D_6) δ 31.3 (s). $^{11}\text{B}\{^1\text{H}\}$ NMR (128 MHz, C_6D_6) δ 5.9 (br).

(PBP)IrQuH₂(Si(OTMS)₂Me). In a J. Young tube, (PBP)IrQuH (0.020 mmol, 14 mg) was mixed with 1,1,1,3,5,5,5-Heptamethyltrisiloxane (0.020 mmol, 20 μL , 1.0 M in C_6D_6) in C_6D_6 , and the NMR spectra of the resulting product were recorded for characterization. ^1H NMR (499 MHz, C_6D_6) δ 8.77 (d, $J = 7.5$ Hz, 2H, *Phenyl*), 8.58 (d, $J = 8.5$ Hz, 1H, *Quinoly*l), 8.49 (d, $J = 8.7$ Hz, 1H, *Quinoly*l), 7.32 (m, 2H, *Phenyl*), 7.28 (t, $J = 7.4$ Hz, 2H, *Phenyl*), 7.13 (t, $J = 7.5$ Hz, 1H, *Quinoly*l), 7.08 (t, $J = 8.3$ Hz, 2H, *Phenyl*), 7.02 (t, $J = 7.5$ Hz, 2H, *Quinoly*l), 6.78 (m, t, $J = 7.15$ Hz, 1H, *Quinoly*l), 3.05 (m, 2H, *CHMe*₂), 2.28 (s, 2H, *CHMe*₂), 1.38 (dvt, $J = 7.1$ Hz, 6H, *CHMe*₂), 0.99 (dvt, $J = 6.5$ Hz, 6H, *CHMe*₂), 0.81 (dvt, $J = 7.1$ Hz, 6H, *CHMe*₂), 0.40 (br, 21H), 0.11 (dvt, $J = 7.4$ Hz, 6H, *CHMe*₂), -7.25 (br, 1H, Ir–H–B), -14.39 (br, 1H, Ir–H). $^{31}\text{P}\{^1\text{H}\}$ NMR (202 MHz, C_6D_6) δ 32.8. $^{11}\text{B}\{^1\text{H}\}$ NMR (128 MHz, C_6D_6) δ 1.5 (br).

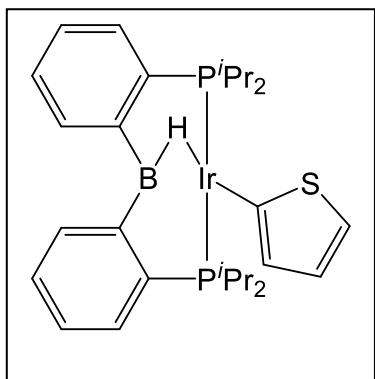
(PBP)IrH₃Bpin. In a J. Young tube, (PBP)IrHCl (0.020 mmol, 13 mg) was mixed with NaEt₃BH (0.020 mmol, 20 μL , 1.0 M in toluene) in toluene, and volatiles were removed after 5 min stirring. HBpin (0.020 mmol, 20 μL , 1.0 M in C_6D_6) was added, and the NMR spectra of the resulting product were recorded for characterization. ^1H NMR (499 MHz, C_6D_6) δ 8.66 (d, $J = 7.5$ Hz, 2H, *Phenyl*), 7.51 (s, 2H, *Phenyl*), 7.32 (t, $J = 7.4$ Hz, 2H, *Phenyl*), 7.13 (t, $J = 7.4$ Hz, 2H, *Phenyl*), 3.36 (m, 2H, *CHMe*₂), 2.31 (m, 2H, *CHMe*₂), 1.45 (dvt, $J = 7.2$ Hz, 6H, *CHMe*₂), 1.25 (dvt, $J = 6.6$ Hz, 6H, *CHMe*₂), 1.17 (s, 12H, Bpin), 0.98 (dvt, $J = 7.5$ Hz, 6H, *CHMe*₂), 0.82 (dvt, $J = 7.6$ Hz, 6H, *CHMe*₂), -4.10 (br, 1H, Ir–

H-B), -5.65 (br, 1H, Ir-*H*-B), -13.57 (t, *J* = 11.3 Hz, 1H, Ir-*H*). $^{31}\text{P}\{^1\text{H}\}$ NMR (202 MHz, C_6D_6) δ 59.4 (s).

(PBP)RhQuH₂(SPh). In a J. Young tube, (PBP)RhQuH (0.020 mmol, 13 mg) was mixed with Thiophene (0.020 mmol, 20 μL , 1.0 M in C_6D_6) in C_6D_6 , and the NMR spectra of the resulting product were recorded for characterization. ^1H NMR (499 MHz, C_6D_6) δ 9.95 (d, *J* = 8.7 Hz, 1H, *Quinolyl*), 8.54 (d, *J* = 7.5 Hz, 2H, *Phenyl*), 8.19 (d, *J* = 7.3 Hz, 2H, *Phenyl*), 7.57 (t, *J* = 7.7 Hz, 1H, *Quinolyl*), 7.38 (t, *J* = 7.4 Hz, 2H, *Phenyl*), 7.17 (m, 5H, *Phenyl* & *Quinolyl*), 7.09 (d, *J* = 8.1 Hz, 1H, *Quinolyl*), 7.06 (t, *J* = 7.5 Hz, 2H, *Phenyl*), 7.03 (t, *J* = 7.5 Hz, 1H, *Phenyl*), 6.96 (t, *J* = 7.3 Hz, 1H, *Quinolyl*), 6.80 (d, *J* = 8.4 Hz, 1H, *Quinolyl*), 2.41 (s, 2H, *CHMe*₂), 2.24 (s, 2H, *CHMe*₂), 1.23 (m, 12H, *CHMe*₂), 0.96 (dvt, *J* = 6.9 Hz, 6H, *CHMe*₂), 0.29 (dvt, *J* = 7.3 Hz, 6H, *CHMe*₂), -9.97 (s, 0H), -16.63 (q, *J* = 13.0, 12.6 Hz, 1H). $^{31}\text{P}\{^1\text{H}\}$ NMR (202 MHz, C_6D_6) δ 52.72 (d, *J* = 99.6 Hz). $^{11}\text{B}\{^1\text{H}\}$ NMR (128 MHz, C_6D_6) δ -8.99.

APPENDIX B

THIOPHENE BORYLATION REACTIONS AND SOME RELATED TESTS



(PBP)IrH(Thienyl). Method I: (PBP)IrHCl (0.10 g, 0.16 mmol), NaHMDS (0.29 mL, 0.16 mmol, 0.60 M in toluene) and thiophene (13 μ L, 0.16 mmol) were mixed in 5 ml toluene and stirred for 12 h, resulting in a red solution. The mixture was passed through Celite, and volatiles were removed under vacuum. Recrystallization failed in toluene/pentane or pure pentane. NMR spectroscopic data indicated the generation of **(PBP)IrH(Thienyl)** as the major product. **Method II:** (PBP)IrHCl (13 mg, 0.020 mmol), NaEt₃BH (20 μ L, 0.020 mmol, 1.0 M in toluene) and thiophene (20 μ L, 0.020 mmol, 1.0 M in C₆D₆) were mixed in 0.4 ml C₆D₆ and heated at 50 °C for 12 h, resulting in a red solution. The mixture was passed through Celite, and volatiles were removed under vacuum. C₆D₆ was added to confirm the formation of **(PBP)IrH(Thienyl)** as the major product. ¹H NMR (400 MHz, C₆D₆) δ 8.45 (d, J = 7.3 Hz, 2H), 7.77 (d, J = 4.7 Hz, 1H), 7.42 (dd, J = 4.6, 3.2 Hz, 1H), 7.35 (m, 2H), 7.21 (t, J = 7.1 Hz, 2H), 7.15 (m, 2H), 6.83 (d, J = 2.7 Hz, 1H), 2.61 (m, 4H), 1.27 (dvt, J = 7.5 Hz, 6H), 1.06 (dvt, J = 7.3 Hz, 6H), 0.96 (dvt, J = 6.7 Hz, 6H), 0.88 (dvt, J = 7.3 Hz, 6H), -12.80 (t, J = 8.4 Hz, 1H). ³¹P{¹H} NMR (162 MHz, C₆D₆) δ 57.3 (s). ¹¹B{¹H} NMR (128 MHz, C₆D₆) δ 57.8 (br).

Borylation of thiophene. In J. Young tubes, thiophene (80 μ L, 1.0 mmol) were mixed with HBpin (0.31 mL, 2.1 mmol) and the indicated catalyst precursor (0.020 mmol) with

hydrogen acceptor (2.0 mmol). After heating at 100 °C for the indicated time, the conversion was calculated by ¹H NMR.

Table VII-1. ortho borylation of thiophene and 2-bromo thiophene catalyzed by Ir metal catalysts

	Catalyst	Additive	Hydrogen acceptor	Time	Conversion ^c
1	(PBP)IrH(Thienyl) ^a	/	Cyclohexene	20 h	100%
2	(PBP)IrH(Thienyl) ^b	/	Cyclohexene	20 h	6%
3	(PBP)IrH ₃ Bpin	/	Cyclohexene	20 h	3%
4	(PBP)IrH ₃ Bpin	HMDS	Cyclohexene	20 h	3%
5	(PBP)IrH ₃ Bpin	NaHMDS	Cyclohexene	20 h	3%
6	(PBP)IrHCl	NaHMDS	Cyclohexene	6 h	97%
7	(PBP)IrHCl	NaEt ₃ BH	Cyclohexene	20 h	3%
8	(PBP)IrHCl	NaHMDS	1-hexene	4 h	7% ^d
9	(POCOP)Ir(TBE)	/	Cyclohexene	5 h	12%
10	(POCOP)Ir(TBE)	/	1-hexene	3 h	32% ^e

a. (PBP)IrH(Thienyl) prepared by method I. b. (PBP)IrH(Thienyl) prepared by method II. c. 2-Thiopheneboronic acid pinacol ester and 2,5-bis-thiopheneboronic acid pinacol ester were formed, and the conversion was calculated by the consumption of thiophene. d. HBpin and 1-hexene were consumed completely to form hydroboration products. e. Borylation of benzene and hydroboration of 1-hexene were also observed in products.

Interactions between NaHMDS and (PBP)IrHCl/Br. In J. Young tubes, (PBP)IrHCl (13 mg, 0.020 mmol) or (PBP)IrHBr (13 mg, 0.020 mmol) was mixed with NaHMDS (33 μL, 0.020 mmol, 0.60 M in toluene) in 0.4 mL C₆D₆. ¹H NMR were recorded (Figure VII-1), showing interactions between NaHMDS and (PBP)IrHCl/Br.

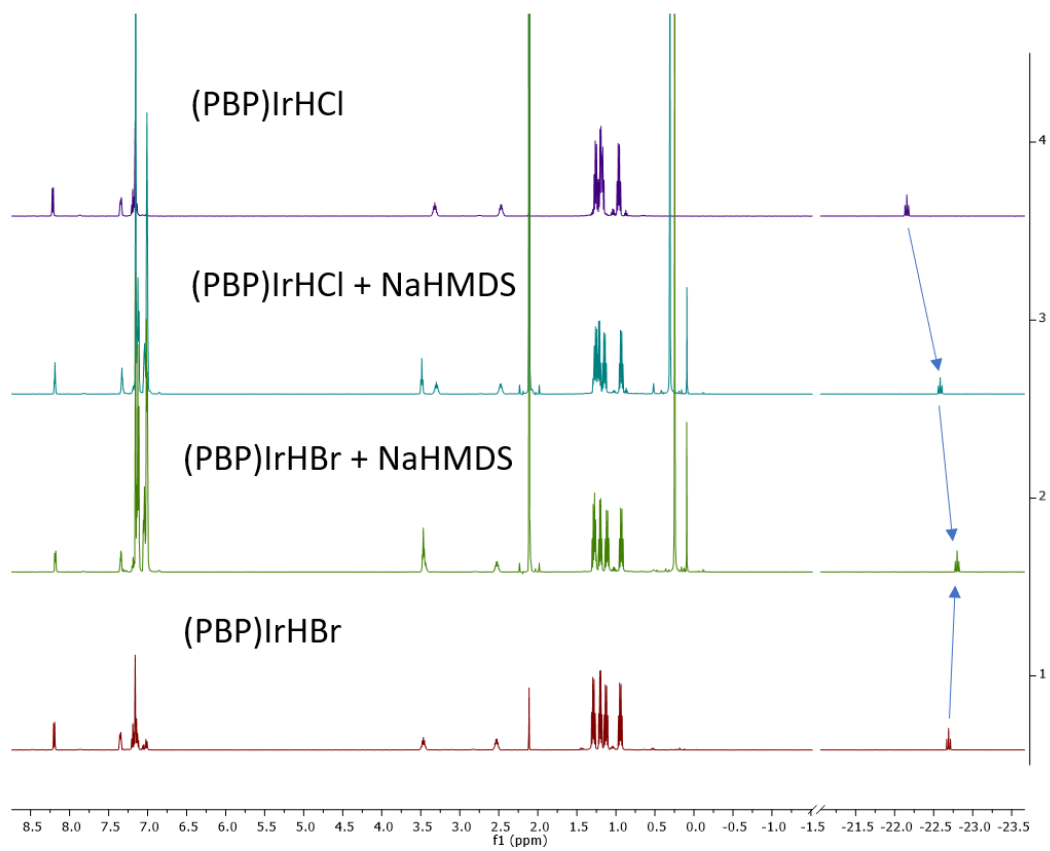
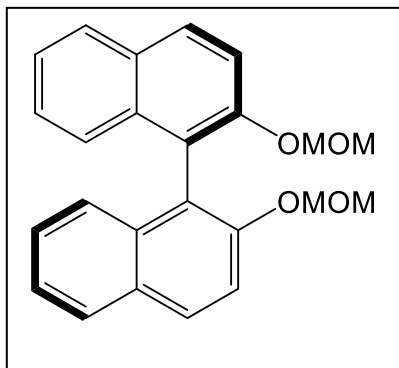


Figure VII-1. Interactions between NaHMDS and (PBP)IrHCl/Br

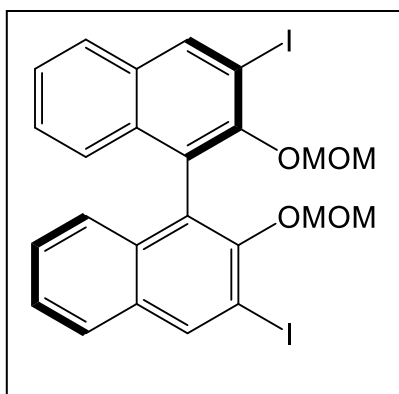
APPENDIX C

SYNTHESIS OF BINOL LIGAND AND ATTEMPTED METALATIONS WITH NIOBIUM AND TANTALUM



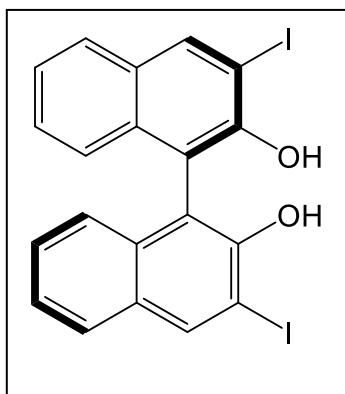
BINOL-OMOM. To a suspension of KH (0.28 g, 7.0 mmol) in THF was added a solution of (R)-(+)-1,1'-bi(2-naphthol) (0.50 g, 1.8 mmol in 20 mL THF) in an ice bath under argon. After H₂ evolution ceased (stirring for an hour), large amount of solid was generated. Chloromethyl methyl ether (0.28 ml, 3.7 mmol) was

added, resulted in light yellow solution. After stirring at room temperature for 12 h, the mixture become light yellow with white solid. All volatiles were removed under vacuum, and 45 mL toluene was added. The mixture was filtered through C elite and toluene was removed under vacuum to give **BINOL-OMOM** as a white solid (0.59 g, 91%). ¹H NMR (400 MHz, C₆D₆) δ 7.75 (d, *J* = 9.1 Hz, 2H), 7.71 (d, *J* = 8.2 Hz, 2H), 7.62 (d, *J* = 9.0 Hz, 2H), 7.41 (d, *J* = 8.5 Hz, 2H), 7.17 (m, 2H), 7.04 (t, *J* = 7.6 Hz, 2H), 4.80 (d, *J* = 6.9 Hz, 2H), 4.72 (d, *J* = 6.8 Hz, 2H), 2.92 (s, 6H). ¹³C{¹H} NMR (101 MHz, C₆D₆) δ 154.0 (s), 135.4 (s), 131.0 (s), 130.3 (s), 129.9 (s), 127.3 (s), 126.7 (s), 124.9 (s), 122.3 (s), 117.9 (s), 95.6 (s), 56.1 (s)



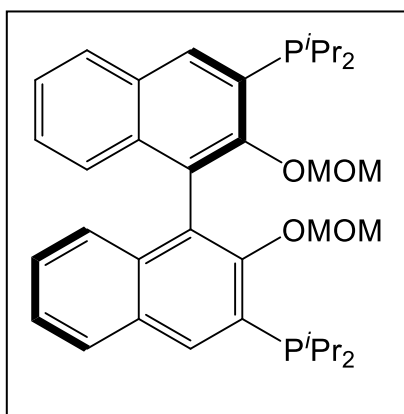
BINOL-OMOM-I₂. At -78 °C, 0.85 mL nBuLi (2.5 M in hexane, 2.1 mmol) was added dropwisely to a solution of **BINOL-OMOM** (0.20 g in 10 ml Et₂O, 0.53 mmol) under argon. The resulting solution was gradually warmed up to room temperature and kept stirring for 3 hours. Large amount of light brown solid was observed.

The resulting mixture was brought to -78 °C again and I₂ (0.60 g, 2.4 mmol) was added with argon flow. The resulting mixture was stirred at room temperature for 12 hours and resulted in an orange solution with no solid. It was quenched by Na₂S₂O₃, extracted by ethyl acetate. The organic layer was washed with brine and dried over Na₂SO₄. Volatiles were removed under vacuum and the crude product was used for the next step without further purification. ¹H NMR (400 MHz, C₆D₆) δ 8.34 (s, 2H), 7.37 (d, *J* = 7.8 Hz, 2H), 7.16 (m, 2H), 7.06 (t, *J* = 7.2 Hz 2H), 6.91 (t, *J* = 7.2 Hz 2H), 4.81 (d, *J* = 4.7 Hz, 2H), 4.67 (d, *J* = 4.8 Hz, 2H), 2.46 (s, 6H).



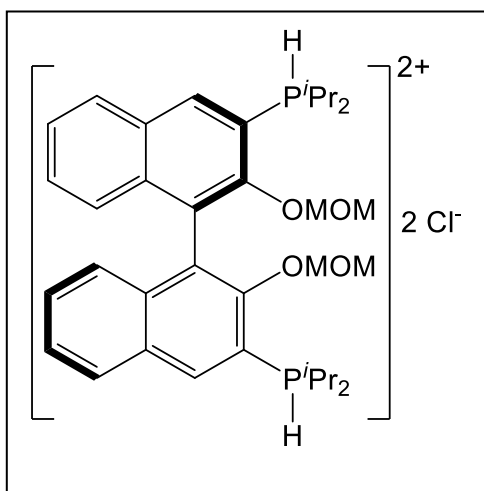
BINOL-I₂. To a **BINOL-OMOM-I₂** solution (0.20 g in 10 mL THF, 0.32 mmol) was added HCl (1.3 mL, 2.6 mmol, 2N in ether). The mixture was stirred at 50 °C for 12 h. All volatiles were removed under vacuum, and the resulting product was recrystallized in THF/pentane 1:3, yielding a white solid (0.13 g, 74%). ¹H NMR (400 MHz, C₆D₆) δ 8.24

(s, 2H), 7.35 (d, *J* = 7.9 Hz, 2H), 7.04 – 6.94 (m, 4H), 6.88 (t, *J* = 7.9 Hz, 2H), 5.87 (s, 2H).



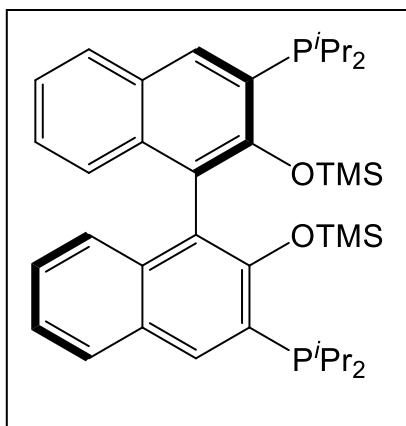
BINOL-OMOM- P^iPr_2 . At $-35\text{ }^\circ\text{C}$, 2.2 mL nBuLi (2.5 M in hexane, 5.4 mmol) was added dropwisely to a **BINOL-OMOM** solution (1.0 g in 20 mL Et_2O , 2.7 mmol). After stirring at room temperature for 1 hour, a dark green solution with brown solid was formed. To the mixture was added 7 mL THF, and the mixture was

brought to $-35\text{ }^\circ\text{C}$ by the freezer. CIP^iPr_2 (0.87 mL, 5.4 mmol) was added dropwisely, and the solution turned to light yellow after stirring at room temperature for 12 hours. Volatiles were removed under vacuum and the resulting solid was dissolved in toluene and passed through Celite. Toluene was removed under vacuum and the crude product was used for the next step without further purification. ^1H NMR (499 MHz, C_6D_6) δ 7.99 (d, $J = 2.3$ Hz, 2H), 7.74 (d, $J = 8.2$ Hz, 2H), 7.46 (d, $J = 8.5$ Hz, 2H), 7.20 (t, $J = 7.5$ Hz, 2H), 7.05 (t, $J = 8.2$ Hz, 2H), 5.11 (d, $J = 5.4$ Hz, 2H), 4.99 (d, $J = 5.4$ Hz, 2H), 2.18 (m, 4H), 1.25 (dd, $J = 13.9, 6.9$ Hz, 6H), 1.21 (dd, $J = 14.0, 6.8$ Hz, 6H), 1.11 (dd, $J = 12.5, 6.8$ Hz, 6H), 1.01 (dd, $J = 11.0, 6.9$ Hz, 6H). $^{31}\text{P}\{^1\text{H}\}$ NMR (202 MHz, C_6D_6) δ -2.8 (s).



BINOL-OMOM- HP^iPr_2 . HCl (11 mL, 21.6 mmol, 2N in ether) was added to the crude product of **BINOL-OMOM- P^iPr_2** (1.8 g, ~ 2.7 mmol). After stirring at $65\text{ }^\circ\text{C}$ for 48 hours, all volatiles were removed under vacuum and the resulting solid was recrystallized in methanol/ Et_2O 1: 10 to yield a transparent crystal (1.4 g, 79%). ^1H NMR

(400 MHz, Methanol- d_4) δ 8.75 (d, $J = 13.1$ Hz, 2H), 8.19 (d, $J = 7.2$ Hz, 2H), 7.53 (m, 4H), 7.08 (d, $J = 9.2$ Hz, 2H), 5.23 (d, $J = 1.7$ Hz, 3H, H-D exchanged with methanol- d_4), 3.27 (m, 4H), 1.75 – 1.08 (m, 24H). $^{31}\text{P}\{^1\text{H}\}$ NMR (162 MHz, Methanol- d_4) δ 38.8 (s, P-H), 37.5 (m, P-D).



BINOL-OTMS- P^iPr_2 . KH (0.40 g, 10 mmol) was stirred in a solution of **BINOL-OMOM- HP^iPr_2** (0.59 g in 20 mL THF, 1.0 mmol) and NEt_3 (1.4 mL, 10 mmol) for 12 hours. TMSCl (1.3 mL, 10 mmol) was added to the mixture. After stirring at room temperature for 12 hours, all volatiles were removed under vacuum and the

resulting solid was recrystallized in THF/pentane 1:5, yielding a white solid (0.50 g, 75%). ^1H NMR (400 MHz, C_6D_6) δ 7.93 (s, 2H), 7.77 (d, $J = 8.1$ Hz, 2H), 7.31 (d, $J = 8.5$ Hz, 2H), 7.18 (m, 2H), 6.99 (t, $J = 7.3$ Hz, 2H), 2.28 (m, 2H), 2.05 (m, 2H), 1.26 (dd, $J = 13.1$, 7.3 Hz, 6H), 1.20 (dd, $J = 13.1$, 6.7 Hz, 6H), 1.17 (dd, $J = 13.2$, 6.3 Hz, 6H), 1.11 – 1.03 (m, 6H), -0.07 (s, 18H). $^{31}\text{P}\{^1\text{H}\}$ NMR (162 MHz, C_6D_6) δ -7.7 (s). $^{13}\text{C}\{^1\text{H}\}$ NMR (101 MHz, C_6D_6) δ 156.1 (d, $J = 19.9$ Hz), 135.7 (s), 133.6 (d, $J = 2.6$ Hz), 130.0 (s), 129.8 (s), 129.6 (s), 126.8 (s), 126.4 (s), 124.2 (s), 123.8 (m), 24.8 (d, $J = 17.2$ Hz), 21.0 (d, $J = 12.8$ Hz), 20.4 (d, $J = 17.5$ Hz), 19.7 (d, $J = 11.3$ Hz), 19.5 (d, $J = 1.3$ Hz), 17.9 (d, $J = 4.1$ Hz), 1.4 (d, $J = 8.3$ Hz).

Table VII-2. Summary of metalation attempts: NbCl₅ + BINOL-OTMS-PⁱPr₂.

	Solvent	Container	Condition	Observation	Spectroscopic details
1	C ₆ D ₆	J. Young tube	r. t.	Red solution and dark red oil & dark red solid	³¹ P{ ¹ H} NMR signals: 38.9 ppm/ 33.6 ppm/ -7.2 ppm/ -7.7 ppm/ -7.9 ppm ratio: 17:13:13:54:3 Amount of TMSCl generated: 32%
2	C ₆ D ₆	J. Young tube	70 °C	Same as 1	Same as 1
3	C ₆ D ₆	J. Young tube	Remove volatiles and heat at 70 °C	Same as 1	Same as 1
4	C ₆ D ₆	J. Young tube	100 °C	Brown solid and light red solution	¹ H NMR signals: OTMS signal disappeared. Paramagnetic signals appeared.
5	toluene	Schleck flask	stir at r. t. for 12 hours Remove volatiles and redissolve in C ₆ D ₆	Red solution and dark red oil	³¹ P{ ¹ H} NMR signals: 38.9 ppm/ 33.6 ppm/ -7.2 ppm/ -7.7 ppm/ -7.9 ppm ratio: 16:11:11:60:3 Amount of TMSCl generated: 30%
6	C ₆ D ₁₂	J. Young tube	stir at r. t. 1 day & 1 week	Purple solution initially. Large amount of red solid formed and became light red solution	³¹ P{ ¹ H} NMR signals: 30.2 ppm/ -7.3 ppm/ -7.7 ppm Ratio after 1 day: 7 : 7 : 86 Ratio after 1 week: 7 : 7 : 86 Amount of TMSCl generated: 12.5% / 13 %
7	pentane	Schleck flask	Remove volatiles every 1h.	Same as 6	³¹ P{ ¹ H} NMR spectra only observed ligand

APPENDIX D

LIST OF PUBLICATIONS RESULTING FROM THE WORK DESCRIBED IN THE DISSERTATION

- (1) Cao, Y.; Shih, W.-C.; Bhuvanesh, N. S.; Zhou, J.; Ozerov, O. V., CN vs NC Isomerism in Bridging Pyridyls Arising from C-H Activation of Pyridine by Rh and Ir Complexes of a Boryl-Centered PBP Ligand. Submitted.
 - (2) Cao, Y.; Shih, W.-C.; Bhuvanesh, N. S.; Ozerov, O. V., Reversible Addition of Ethylene to a Pincer-Based Boryl-Iridium Unit with the Formation of a Bridging Ethylidene. *Chem. Sci.* **2020**, *11*, 10998-11002.
 - (3) Cao, Y.; Shih, W.-C.; Ozerov, O. V., Addition of O–H, N–H, and F–H Bonds across a Boryl–Iridium Unit. *Organometallics* **2019**, *38*, 4076-4081.
 - (4) Cao, Y.; Shih, W.-C.; Bhuvanesh, N.; Ozerov, O. V., Silver halide complexes of a borane/bis(phosphine) ligand. *Dalton Trans.* **2019**, *48*, 9959-9961.
-